

DOCTORAL THESIS

Mathematical Modelling of
Three Phase Squirrel Cage
Induction Motor and Related
Signal Processing for Fault
Diagnostics

Bilal Asad

TALLINN UNIVERSITY OF TECHNOLOGY
DOCTORAL THESIS
40/2021

Mathematical Modelling of Three Phase Squirrel Cage Induction Motor and Related Signal Processing for Fault Diagnostics

BILAL ASAD



TALLINN UNIVERSITY OF TECHNOLOGY

School of Engineering

Department of Electrical Power Engineering and Mechatronics

This dissertation was accepted for the defense of the degree 28/06/2021

Supervisor:

Dr. Toomas Vaimann
School of Engineering
Tallinn University of Technology
Tallinn, Estonia

Co-supervisors:

Prof. Dr. Anouar Belahcen
School of Electrical Engineering
Aalto University
Espoo, Finland

Prof. Dr. Ants Kallaste
School of Engineering
Tallinn University of Technology
Tallinn, Estonia

Opponents:

Prof. Dr. Jose A. Antonino-Daviu
Department of Electrical Engineering
Polytechnic University of Valencia, Spain

Dr. Konstantinos N. Gyftakis
Department of Electronics and Electrical Engineering
The University of Edinburgh, UK

Defense of the thesis: 27/08/2021, Tallinn

Declaration:

Hereby I declare that this doctoral thesis, my original investigation and achievement, submitted for the doctoral degree at Tallinn University of Technology and at Aalto University has not been submitted for doctoral or equivalent academic degree.

Bilal Asad

signature



European Union
European Regional
Development Fund



Investing
in your future

Copyright: Bilal Asad, 2021

ISSN 2585-6898 (publication)

ISBN 978-9949-83-726-7 (publication)

ISSN 2585-6901 (PDF)

ISBN 978-9949-83-727-4 (PDF)

Printed by Spin Press

TALLINNA TEHNIKAÜLIKOOL
DOKTORITÖÖ
40/2021

**Kolmefaasilise lühisrootoriga
asünkroonmootori matemaatiline
modelleerimine ning lähtuv
rikkediagnostiline signaalitöötlus**

BILAL ASAD



Mathematical Modelling of Three Phase Squirrel Cage Induction Motor and Related Signal Processing for Fault Diagnostics

Bilal Asad

A doctoral dissertation conducted under a convention for the joint supervision of thesis at Aalto University (Finland) and Tallinn University of Technology (Estonia) for the degree of Doctor of Science (Technology) at Aalto University, to be defended with the permission of the Aalto University School of Electrical Engineering and for the degree of Doctor of Philosophy (Electrical Power Engineering and Mechatronics) to be defended with the permission of Tallinn University of Technology, at a public examination held at Auditorium NRG-131, Tallinn University of Technology and remotely through “<https://zoom.us/j/95915675538?pwd=MVE3SXBkUVhEV3Rxa0ZFt3JjN0tvZz09>”, 291646, on 27 August 2021 at 14:00.

Aalto University
School of Electrical Engineering
Department of Electrical Engineering and Automation

Supervising professor

Prof. Dr. Anouar Belahcen, Department of Electrical Engineering and Automation, Aalto University, Espoo, Finland

Co-supervisor

Dr. Toomas Vaimann, Department of Electrical Power Engineering and Mechatronics, Tallinn University of Technology, Estonia

Thesis advisor

Prof. Dr. Ants Kallaste, Department of Electrical Power Engineering and Mechatronics, Tallinn University of Technology, Estonia

Preliminary examiners

Prof. Dr. Jose A. Antonino-Daviu, Department of Electrical Engineering, Polytechnic University of Valencia, Spain

Dr. Konstantinos N. Gyftakis, Department of Electronics and Electrical Engineering, The University of Edinburgh, UK

Opponents

Prof. Dr. Jose A. Antonino-Daviu, Department of Electrical Engineering, Polytechnic University of Valencia, Spain

Prof. Dr. Lucia Frosini, Department of Industrial and Information Engineering, University of Pavia, Italy

Aalto University publication series

DOCTORAL DISSERTATION DD87 / 2021

© 2021 Bilal Asad

ISBN 978-952-64-0427-1

ISBN 978-952-64-0428-8 (pdf)

ISSN-L 1799-4934

ISSN 1799-4934 (printed)

ISSN 1799-4942 (pdf)

<http://urn.fi/URN:ISBN:978-952-64-0428-8>

Author

Bilal Asad

Name of the doctoral dissertation

Mathematical Modelling of Three Phase Squirrel Cage Induction Motor and Related Signal Processing for Fault Diagnostics

Publisher School of Engineering**Unit** Department of Electrical Engineering and Mechatronics**Series** Aalto University publication series DOCTORAL DISSERTATION**Field of research** Electrical Engineering, Electrical Machines**Date of the defence** 27 August 2021☐ **Monograph**☒ **Article dissertation**☐ **Essay dissertation****Abstract**

This thesis aims to study different analytical methods to model a squirrel cage induction motor, which should have minimal simulation time than the corresponding finite element method (FEM) based models. The purpose of doing so is to develop a model suitable to simulate all major faults and be used for advanced model-dependent fault diagnostic algorithms, such as parameters estimation and inverse problem theory. This thesis's second key objective is to study various signal-processing techniques for their pros and cons to detect fault at the embryonic stage and investigate the entire current harmonic spectrum of induction motors both in transient and steady-state regions. Thus, the motor under healthy and broken rotor bar (BRB) conditions are simulated, and experimental measurements are investigated for validation.

The dynamic d-q model with the inclusion of non-linear magnetization inductance was considered as a starting point. This model helps understand the machine's basic concepts because of its comprehensiveness and ability to produce compact equations, which can be used for drives as general and in observers and state estimators as particular. However, this model was found to be less suitable to simulate machine faults because of the considered approximations.

To address the d-q model limitations, the winding function analysis (WFA) based model was prepared. In this model, the analytical equations to calculate various inductances, resistances, currents, fluxes, torque, and speed are derived for the motor under investigation. These equations were simulated in MATLAB, giving results near to the practical measurements. The model is suitable for implementing some faults, such as BRB and broken end rings. Still, the consideration of constant air gap makes it less ideal for the implementation of eccentricity and saturation-related faults. Moreover, the spatial harmonics, which are very important for fault diagnostics and sensor-less speed estimation, cannot be simulated. Those approximations can be reduced with Fourier summation of higher-order harmonics (winding) and Taylor series to include inverse air gap functions but at the cost of the self-defined number and amplitude of harmonics.

To get more realistic results, the modified winding function analysis (MWFA) based model was prepared to ensure that all winding functions and air gap were defined as a function of stator and rotor individual and respective angles. The geometry of stator and rotor slots is considered to calculate the leakage inductances and various resistances. The self and mutual inductances

between rotor and stator are computed with a stepping rotor. The results at each rotor position are saved in offline 3D lookup tables. During the online simulation, all pre-saved matrices are used as a rotor position function using their index value, and the performance parameters, such as currents, fluxes, torque, and speed, are calculated. The FEM and hybrid FEM-analytical models of the machine under investigation are prepared using commercial software to validate the results. The comparison of results shows an excellent agreement with a minimal simulation time and least ill-posedness for the proposed model compared to the corresponding FEM model.

Both analytical and hybrid FEM-analytical models are divided into online, offline portions and compatible for the solution on cluster computation. Their division in the online and offline portions reduces the complexity and gives the model the freedom to simulate faults in the online portion without doing unnecessary offline calculations again. Moreover, the compatibility with cluster computation is excellent for exploiting distributed computational resources such as cloud computation, an integral part of industry 4.0 standards.

Towards the signal processing side, the fast Fourier transform (FFT) and wavelet transform (WT) are used extensively to study the steady-state and transient regime signals. The infinite impulse response (IIR) based digital filters are used to improve the motor's current spectrum's legibility. In this way, the total harmonics are segregated according to their cause of production. Moreover, the spectrum of current simulated from the proposed model is compared with that simulated using the FEM model and the test rig measurements. The comparison is made until a wide bandwidth of frequencies for further validation of the proposed model.

Moreover, the WFA based model is also investigated during the transient regime by doing the time-frequency analysis of the stator current. The recovered non-stationary signal's pattern is in good agreement with the one obtained from the practical measurements. The specific fault-related pattern during the transient interval can further enhance the model's effectiveness.

Keywords Analytical models, electrical machines, induction motors, fault diagnostics, condition monitoring, numerical modelling, finite element method, signal processing, cluster computation

ISBN (printed) 978-952-64-0427-1		ISBN (pdf) 978-952-64-0428-8
ISSN-L 1799-4934	ISSN (printed) 1799-4934	ISSN (pdf) 1799-4942
Location of publisher Finland	Location of printing Estonia	Year 2021

urn <http://urn.fi/URN:ISBN:978-952-64-0428-8>

Contents

List of Publications	11
Author's Contribution to the Publications	13
Abbreviations	15
Symbols	16
1 Introduction	19
1.1 Importance of electrical machines.....	19
1.1.1 Types and importance.....	19
1.1.2 Contribution to energy consumption.....	20
1.2 Fault diagnostics and its importance at the embryonic stage	20
1.2.1 Importance of early detection	20
1.2.2 Faults and contribution.....	21
1.3 The modeling of electrical machines	22
1.3.1 The analytical models.....	22
1.3.2 The finite element method (FEM) based models.....	23
1.4 Objectives and scope of the thesis.....	23
1.5 Scientific contributions	25
2 State of the art	28
2.1 The modeling techniques.....	28
2.2 The SQIM fault representing frequencies	32
2.3 The fault diagnostics techniques.....	34
3 The modeling of induction motors.....	38
3.1 The dynamic d-q models	38
3.1.1 Two-axis theory.....	38
3.1.2 Equivalent model of motor	39
3.1.3 The state-space model	39
3.1.4 Results	41
3.1.5 Attributes of two-axis theory-based models	41
3.2 The winding function-based model	43
3.2.1 Introduction	43
a) Block diagram for implementation	43
b) Block diagram for simulation	44
3.2.2 Mathematical modeling	45
a) The analytical equations	45
b) Resistances calculations.....	47
c) Leakage inductances	48
d) Inductances.....	50
I. Stator self-inductance	50
II. Stator mutual inductances	52
III. Rotor to rotor self and mutual inductances.....	53
IV. Stator to rotor mutual inductances	54
3.2.3 Torque and speed	55
3.2.4 Results	56
3.2.5 Attributes of WFA	57

3.3 The modified winding function-based model	58
3.3.1 Introduction	58
a) Inductances calculation using MWFA	59
b) Air gap calculation	60
c) Stator and rotor winding functions	61
3.3.2 Results	62
a) Inductances	62
b) Inductance derivatives	63
c) Torque and speed	63
d) Stator currents	64
e) Rotor currents	65
3.4 Finite Element Method (FEM) in comparison with MWFA	66
3.4.1 Introduction	66
3.4.2 Broken bars simulation in FEM and proposed model	67
3.4.3 Simulations	67
3.4.4 Attributes of MWFA	70
3.5 The compatibility with cluster computation	71
3.5.1 Introduction	71
a) Cluster formation	71
b) Implementation strategy	72
4 The test rig and the spectrum analysis	74
4.1 Measurement Setup	74
4.1.1 Case 1	74
4.1.2 Case 2	75
4.2 The spectrum analysis of stationary and non-stationary signals	75
4.3 The segregation of motor current harmonics	77
4.3.1 The winding and space harmonics	77
4.3.2 The supply fed harmonics	77
4.3.3 The fault-based harmonics	78
4.4 Spectrum analysis in the steady-state regime	78
4.5 Spectrum analysis in the transient regime	81
a) Legibility improvement by extending the transient time	81
b) Legibility improvement by attenuating the fundamental component	85
5 Conclusions and future work	88
5.1 Conclusions and the summary of the work	88
5.2 Future works	89
References	91
Acknowledgements	97
Abstract	98
Kokkuvõte	100
Appendix	103
Curriculum vitae	247
Elulookirjeldus	249

List of Publications

The list of author's publications, based on which the thesis has been prepared:

- I **Asad, B.**; Vaimann, T.; Belahcen, A.; Kallaste, A.; Rassõlkin, A.; Ghafarokhi, P. S.; Kudelina, K. "Transient Modeling and Recovery of non-Stationary Fault Signature for Condition Monitoring of Induction Motors," Appl. Sci., vol. 11 (6), 2806, Mar. 2021.
- II **Asad, B.**; Vaimann, T.; Belahcen, A.; Kallaste, A.; Rassõlkin, A.; Iqbal, M. N. "The Cluster Computation-Based Hybrid FEM–Analytical Model of Induction Motor for Fault Diagnostics," Appl. Sci., vol. 10 (21), 7572, Oct. 2020.
- III **Asad, B.**; Vaimann, T.; Belahcen, A.; Kallaste, A.; Rassõlkin, A.; Heidari, H. "The Low Voltage Start-up Test of Induction Motor for the Detection of Broken Bars," International conference on electrical machines (ICEM 2020), Gothenburg, Sweden, August 23-26. IEEE, pp. 1481–1487.
- IV **B. Asad**, T. Vaimann, A. Belahcen, A. Kallaste, A. Rassõlkin, M. Naveed Iqbal, "Modified Winding Function-based Model of Squirrel Cage Induction Motor for Fault Diagnostics," IET Electric Power Applications, vol. 14 (9), pp. 1722–1734, May 2020.
- V **B. Asad**, T. Vaimann, A. Belahcen, A. Kallaste, A. Rassõlkin, M. Naveed Iqbal, "Broken rotor bar fault detection of the grid and inverter fed induction motor by effective attenuation of the fundamental component," IET Electric Power Applications, vol. 13 (12), pp. 2005–2014, Dec. 2019.
- VI **B. Asad**, T. Vaimann, A. Kallaste, A. Rassõlkin, A. Belahcen, M. Naveed Iqbal, "Improving Legibility of Motor Current Spectrum for Broken Rotor Bars Fault Diagnostics," Electrical, Control, and Communication Engineering, vol. 15 (1), pp. 1–8, Sep. 2019.
- VII **B. Asad**, T. Vaimann, A. Kallaste, A. Rassõlkin, A. Belahcen, "A Survey of Broken Rotor Bar Fault Diagnostic Methods of Induction Motor," Electrical, Control and Communication Engineering, vol. 14 (2), pp. 117–124, Mar. 2019.
- VIII **B. Asad**, T. Vaimann, A. Kallaste, A. Rassõlkin, A. Belahcen, "Review of Electrical Machine Diagnostic Methods Applicability in the Perspective of Industry 4.0," Electrical, Control, and Communication Engineering, vol. 14 (2), pp. 108–116, Mar. 2019.
- IX **B. Asad**, T. Vaimann, A. Belahcen, A. Kallaste, A. Rassõlkin, "Rotor Fault Diagnostic of Inverter Fed Induction Motor Using Frequency Analysis," 12th IEEE International Symposium on Diagnostics for Electric Machines, Power Electronics and Drives (SDEMPED) Toulouse, France, 2019, pp. 127–133.
- X **B. Asad**, T. Vaimann, A. Belahcen, A. Kallaste, A. Rassõlkin, "Winding Function-Based Analytical Model of Squirrel Cage Induction Motor for Fault Diagnostics," 26th International Workshop on Electric Drives: Improvement in Efficiency of Electric Drives (IWED), Mar. 2019, pp. 1–6.
- XI **B. Asad**, T. Vaimann, A. Belahcen, A. Kallaste, "Broken Rotor Bar Fault Diagnostic of Inverter Fed Induction Motor Using FFT, Hilbert and Park's Vector Approach," IEEE XXIIIrd International Conference on Electrical Machines (ICEM'2018) Alexandroupoli - Greece September 3-6, 2018, pp. 2352–2358.

- XII **B. Asad**, T. Vaimann, A. Rassölkin, A. Belahcen, “Dynamic State-Space Model-Based Analysis of a Three-Phase Induction Motor Using Nonlinear Magnetization Inductance,” IEEE 19th International Scientific Conference on Electric Power Engineering (EPE) Brno, Czech Republic, June 2018, pp. 260–265.

Author's Contribution to the Publications

Publication I: "Transient Modeling and Recovery of non-Stationary Fault Signature for Condition Monitoring of Induction Motors".

The author prepared the mathematical model of an induction motor, implemented it in the simulation environment, performed laboratory experiments for practical measurements, prepared the signal processing-based diagnostic algorithms, and wrote the manuscript.

Publication II: "The Cluster Computation-Based Hybrid FEM–Analytical Model of Induction Motor for Fault Diagnostics".

The author designed the simulation model compatible with cluster computation, performed laboratory experiments for practical measurements, prepared the signal processing-based validating algorithm, and wrote the manuscript.

Publication III: "The Low Voltage Start-up Test of Induction Motor for the Detection of Broken Bars".

The author performed laboratory experiments for practical measurements, prepared the signal processing-based diagnostic algorithm, and wrote the manuscript. The author presented the work at the conference.

Publication IV: "Modified Winding Function-based Model of Squirrel Cage Induction Motor for Fault Diagnostics".

The author prepared the mathematical model of the induction motor, implemented it in the simulation environment, performed laboratory experiments for practical measurements, prepared the signal processing-based validating algorithm, and wrote the manuscript.

Publication V: "Broken rotor bar fault detection of the grid and inverter fed induction motor by effective attenuation of the fundamental component".

The author performed laboratory experiments for practical measurements, prepared the signal processing-based diagnostic algorithm, and wrote the manuscript.

Publication VI: "Improving Legibility of Motor Current Spectrum for Broken Rotor Bars Fault Diagnostics".

The author performed laboratory experiments for practical measurements, prepared the signal processing-based diagnostic algorithm, and wrote the manuscript.

Publication VII: "A Survey of Broken Rotor Bar Fault Diagnostic Methods of Induction Motor".

The author did the literature survey for the state-of-the-art techniques being used for fault diagnosis of induction machines. The author wrote the manuscript.

Publication VIII: “Review of Electrical Machine Diagnostic Methods Applicability in the Perspective of Industry 4.0”.

The author did the literature survey for the techniques being used for fault diagnosis of induction machines. The author wrote the manuscript.

Publication IX: “Rotor Fault Diagnostic of Inverter Fed Induction Motor Using Frequency Analysis”.

The author performed laboratory experiments for practical measurements, prepared the signal processing-based diagnostic algorithm, and wrote the manuscript. The author presented the work at the conference.

Publication X: “Winding Function-Based Analytical Model of Squirrel Cage Induction Motor for Fault Diagnostics”.

The author prepared the mathematical model of the induction motor and presented the work at a conference.

Publication XI: “Broken Rotor Bar Fault Diagnostic of Inverter Fed Induction Motor Using FFT, Hilbert and Park’s Vector Approach”.

The author performed laboratory experiments for practical measurements, prepared various signal processing-based diagnostic algorithms. The author wrote the paper and presented the work at a conference.

Publication XII: “Dynamic State-Space Model-Based Analysis of a Three-Phase Induction Motor Using Nonlinear Magnetization Inductance”.

The author prepared the mathematical model of the induction motor, wrote the paper, and presented the work at a conference.

Abbreviations

BRB	Broken rotor bars
DTFT	Discrete-time Fourier transform
ESA	Effective slot area
EPRI	Electric power research institute
FF	Filling factor
FFT	Fast Fourier transform
FEM	Finite element method
IEEE	Institute of Electrical and Electronics Engineers
IAS	Industrial applications society
IIR	Infinite impulse response
MCC	Multiple coupled circuits
MWFA	Modified winding function analysis
MCSA	Motor current signature analysis
PM	Permanent magnet
SA	Slot area
STFT	Short-time Fourier transform
SQIM	Squirrel cage induction motor
WFA	Winding function analysis

Symbols

a	Number of parallel paths, Phase a
A	Magnetic vector potential
Ac	Conductor cross-sectional area
b_d	Bearing ball's diameter
B_f	Friction coefficient
B	Magnetic flux density
D	Displacement current
D_s	Stator's inner diameter
D_r	Rotor's outer diameter
dL_f	Inductance matrix derivative
E	Electric field strength
f_s	Supply frequency
f_{br}	Broken bar frequencies
f_{bb}	Bearing fault frequencies
f_r	Rotor frequency
f_{bbo}	Bearing outer race fault frequencies
f_{bbi}	Bearing inner race fault frequencies
g	Air gap
H	Magnetic field strength
$invL_f$	The inverse of the inductance matrix
i_{ds}^s	Stator's direct axis current in the stationary frame of reference
i_{qs}^s	Stator's quadrature axis current in the stationary frame of reference
I_s	Stator current vector (i_{as} , i_{bs} , i_{cs})
I_r	Rotor currents matrix (i_{r1} , i_{r2} i_{rn})
J	Current density
k	Harmonic order
K_p	Pitch factor
K_d	Distribution factor
K_s	Skewing factor
l	The effective length of stator or rotor core
l_{av}	Average turn length
l_{bar}	Rotor bar length
L_g	Air gap leakage inductance
L_l	Leakage inductance
L_q	Slot leakage inductance
L_t	Tooth tip leakage inductance
L_{ew}	End winding leakage inductance
L_{sq}	Skew leakage inductance

L_{ring}	End ring leakage inductance
L_m	The magnetization inductance
L_r	Rotor's per phase inductance referred to the primary side
l_s	Stator slot length
L_s	Stator's phase inductance
L_{sl}	Stator leakage inductance
L_e	End ring leakage inductance
L_b	Rotor bar inductance
L_{ss}	Stator-stator inductances
L_{rr}	Rotor-rotor inductances
L_{rl}	Rotor leakage inductance
L_{sr}	Stator-rotor inductances
L_{rs}	Rotor-stator inductances
L_f	Overall inductance matrix
l_{ew}	End winding length
m	A positive integer, number of stator phases
n_b	Number of rotor bars
n_{bb}	Number of bearing balls
n_d	Dynamic eccentricity
N_s	The effective number of stator's turns per phase
N_t	Total number of turns per phase
p	Number of poles
P	Number of pole pairs
p_d	Bearing pitch
Q_s	Number of stator slots
q, Q_{pp}	Number of slots per pole and phase
R_r	Rotor's per phase resistance referred to the primary side
\mathbf{R}_r	Rotor resistance matrix ($R_{r1}, R_{r2}, \dots, R_{rm}$)
R_s	Stator's phase resistance
\mathbf{R}_s	Stator resistance matrix (R_{as}, R_{bs}, R_{cs})
r_e	The resistance of the end ring sector between two consecutive bars
r_{et}	Rotor end ring resistance
r, r_g	Average air gap radius
ρ	Resistivity
s	Slip, arc length between two consecutive rotor bars
σ_δ	Leakage factor
σ	Electric conductivity
τ_p	Pole pitch
T_e	Generated torque
T_L	Loading torque

v_s	Supply fed harmonics
ν	Magnetic reluctivity of the material
V_{ds}^s	Stator's d-axis supply voltage in the stationary frame of reference
V_{qs}^s	Stator's q-axis supply voltage in the stationary frame of reference
\mathbf{V}_s	Stator voltage vector (V_{as}, V_{bs}, V_{cs})
W_{ew}	End winding span
W	The average coil span
ω_m	Mechanical speed
ω_s	Synchronous speed
Z_q	Number of conductors per slot
α_r	Arc angle between two consecutive rotor bars
β	Positive constant
$g^{-1}(\varphi, \vartheta)$	Inverse air gap function with respect to rotor and stator position
$L_{ij}(\vartheta)$	Phase i and j mutual inductance concerning rotor angle θ
$\lambda_u, \lambda_{ew}, \lambda_{lew}$	Permeance factors
μ_o	Permeability of free space
$n_i(\varphi, \vartheta)$	The turn function wrt rotor and stator position
$N_i(\varphi, \vartheta)$	The winding function wrt rotor and stator position
ϑ	Angle
ϑ_b	The angle between bearing ball and race
ϑ_e	Electrical angle
ϑ_r	Rotor position
$P(\varphi, \vartheta)$	Inverse air gap permeance function
φ_{ds}^s	Stator's direct axis flux in the stationary frame of reference
φ_{qs}^s	Stator's quadratic axis flux in the stationary frame of reference
$\boldsymbol{\varphi}_s$	Stator flux vector ($\boldsymbol{\varphi}_{sa}, \boldsymbol{\varphi}_{sb}, \boldsymbol{\varphi}_{sc}$)
$\boldsymbol{\varphi}_r$	Rotor flux vector ($\boldsymbol{\varphi}_{r1}, \boldsymbol{\varphi}_{r2}, \dots, \boldsymbol{\varphi}_{rn}$)

1 Introduction

1.1 Importance of electrical machines

1.1.1 Types and importance

In almost every domain of industrial and domestic life, electrical machines are playing a vital role. They act as the working horse in several applications, such as fans, pumps, washing machines, traction, textile mills, process industries, ship thrust systems, robots, conveyor belts, electricity generators, etc. [IX]. The wide range of their applications increases the importance of their better performance towards torque, power density, speed range, efficiency, broad constant power operating capability, reliability, robustness for changing load, less impact on power quality, better controllability, low cost, etc. The main classification of electrical machines is presented in Table 1.1.

Table 1.1. The most common types of electrical machines.

Machine	Types		Attributes
DC	Wound field <ul style="list-style-type: none"> • Series • Shunt • Compound • Separately excited PM field		<ul style="list-style-type: none"> • High starting torque • Simple control • Good speed regulation • Commutator problems • Complex structure
AC	Induction <ul style="list-style-type: none"> • Cage rotor • Wound rotor <p>The mentioned attributes are well suited for cage-type induction machines, however in case of wound rotor machines the slip ring related issues increase the complexities. For example, the wound-rotor induction machines are comparatively less robust, simple and reliable etc.</p>		<ul style="list-style-type: none"> • Simple • Rugged • Robust • Reliable • Easy maintenance • Comparative difficult modeling and control due to a variety of slip dependent variables.
	Synchronous <ul style="list-style-type: none"> • Reluctance rotor • PM rotor <ul style="list-style-type: none"> ➤ Surface-mounted PM ➤ Interior PM • Wound rotor <ul style="list-style-type: none"> ➤ Salient ➤ Non-salient 	Synchronous	<ul style="list-style-type: none"> • Easy speed control • Power factor regulator • More complex than induction • Wider air gap • Low losses

	<ul style="list-style-type: none"> • Permanent magnet brushless AC (PM-BLAC) SynRM • Permanent magnet brushless DC (PM-BLDC) 		<ul style="list-style-type: none"> • Mandatory starter • Low starting torque
	Doubly salient <ul style="list-style-type: none"> • Switched reluctance (SR) • Stator PM (Stepper) <ul style="list-style-type: none"> ➤ Doubly salient PM (DSPM) ➤ Flux reversal PM (FRPM) ➤ Flux switched PM (FSPM) ➤ Flux controllable PM (FCPM) 		
	Special Axial flux Hysteresis Variable reluctance PM <ul style="list-style-type: none"> • Vernier PM • Transversal flux PM (TF PM) 		<ul style="list-style-type: none"> • A variety of applications • Different shapes and sizes • Low power applications

The wide acceptance of induction motors is due to various benefits such as, low cost, simple and rugged structure, easy maintenance, and good torque per weight ratio.

1.1.2 Contribution to energy consumption

Electrical motors are the biggest consumer of electricity worldwide. A detailed energy consumption analysis and the importance of preventive maintenance can be studied in [1][VI]. In this paper, the author claimed that motor systems consume about 59% of all electricity generated in the United States, with its distribution in various sectors is presented. This proportion can differ slightly depending upon the industries in different countries. Moreover, the utilization of electrical machines in modern society is increasing day by day in electric vehicles to reduce carbon footprint and lessen the dependency on fossil fuels.

1.2 Fault diagnostics and its importance at the embryonic stage

1.2.1 Importance of early detection

Since the machines are associated with mechanically moving parts, they are always subject to failures. The induction motors' faults are usually degenerative; hence, their detection at the developing stage is crucial to avoid catastrophic situations. No doubt, the motor's failure will affect the reliability of operation, economy, and motor's life itself [IX]. The author in [1] analyzed a paperboard plant with 485 motors having two operating production lines with an average downtime cost of \$6375 per hour and concluded that preventive maintenance program costs \$73 900 per year and gives a total saving of \$569 360 per year having a payback period of as short as 1.6 months. The average downtime

cost and a comparison of rewind versus recondition are described in detail in [VII]. It can be concluded that early fault diagnostic and preventive maintenance increase the machine's life and make the system more reliable, giving better financial results. The predictive maintenance techniques can detect the fault at the developing stage without instigating unnecessary preventive techniques on all machines. Hence, the scheduled overhauling of all machines does not remain necessary anymore.

1.2.2 Faults and contribution

A variety of faults found in literature can be broadly classified into four significant categories, i.e., supply related, machine-related electrical and mechanical, thermal, and external or environmental, as presented in Table 1.2. Almost all faults are intertwined with each other. For example, cooling failure can cause insulation degradation, which can lead to inter-turn short circuit faults. The short circuits will increase the non-uniformity of the air gap flux distribution, increasing the unnecessary magnetic stresses on the rotor side.

Table 1.2. Categories of most common faults, types, and diagnostic methods for cage induction machines.

Category	Types	Location of the faults	Common diagnostic/preventive /predictive methods
Supply (grid, inverter)	<ul style="list-style-type: none"> • Unbalanced supply voltage • Over or under voltage • Phase reversal • Earth fault • Inverter related 	Mainly stator	<ul style="list-style-type: none"> • Sensors with relays & switches • Signal processing of various observables • Model dependent techniques
Electrical Mechanical	<ul style="list-style-type: none"> • Inter-turn short circuit fault and insulation degradation • Broken rotor bar • Broken end rings • Eccentricity fault • Bearing fault • Rotor winding failure • Shaft and load misalignment 	Both stator and rotor	<ul style="list-style-type: none"> • Signal processing of a variety of observables • Model dependent techniques
Thermal	<ul style="list-style-type: none"> • Inadequate cooling due to several reasons such as blockage of cooling channels or spray nozzles and faulty external fans, etc. • Ambient temperature 	Both stator and rotor	<ul style="list-style-type: none"> • Local or global temperature measurements • Thermal imaging
Environmental	<ul style="list-style-type: none"> • External moisture • Vibrations due to the bad foundation, etc. 	Both	<ul style="list-style-type: none"> • Sensors and protective devices • Signal processing of a variety of parameters

In cage induction machines, supply-related faults are mainly associated with the stator side. They can be easily detected and controlled using simple protective devices by monitoring supply voltage and current quality if the faults are mature (above threshold). However, detecting faults at the developing stage needs careful monitoring of the global or local parameters.

The machine-specific electrical and mechanical faults make a significant proportion of general faults, and they are degenerative, i.e., they tend to increase with time. The mechanical faults, particularly bearing associated faults, make the most significant proportion of overall faults. According to IEEE-IAS and electrical power research institute (EPRI) standards, the detailed distribution of faults in medium voltage induction motors is shown in Figure 1.1 [2]. In very large machines, the percentage fault distribution may vary. Mainly the bearing-fault percentage decreases significantly as mostly sleeve bearings are used in those machines.

Though these kinds of fault divisions are not easy to make because of the varying types of machines and their working environment, they give a glimpse of the most significant failures in induction motors. The bearing and stator-associated faults make more than 50% contribution to the general faults in both standards. A more detailed division of the faults contribution in various voltage machines can be found in [3][4].

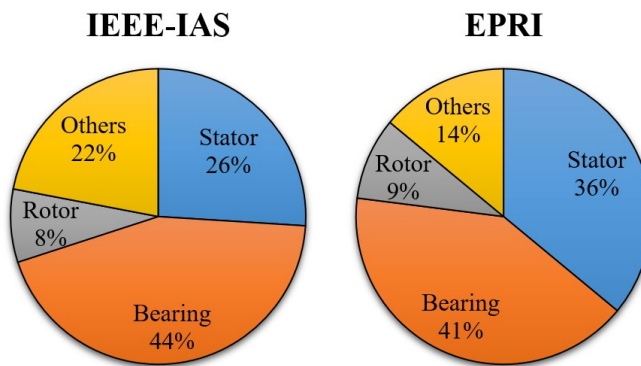


Figure 1.1. The percentage faults contribution in medium voltage induction machines according to IEEE and EPRI standards.

1.3 The modeling of electrical machines

For a reliable design of an electrical machine, its mathematical model's importance cannot be ignored. The same is true for advanced model-dependent fault diagnostic techniques. These techniques may include estimating design parameters in various ways, hardware in the loop, inverse problem theory, and other iteration-based algorithms. The importance of the mathematical models becomes manifold for reliable drive systems and state observers. The wide variety of modeling techniques available in literature can be broadly classified into analytical and numerical.

1.3.1 The analytical models

In the analytical models, the machines are represented with differential equations. The most common analytical technique is two-axis theory-based models (d-q), where the three phases are transformed into two equivalent orthogonal phases. Moreover, the air gap is removed by referring, rotor parameters on the stator side or stator parameters on

the rotor side. This approach reduces the complexity and number of equations. The drives and state observers depend upon these models because they are more straightforward and comprehensive. The biggest drawback of these models is that they are based on approximations. It is hard to include some practicalities, such as the non-sinusoidal distribution of windings, the practical air gap with slotting effects, material nonlinearities, non-symmetry, etc. Although these models have proved their importance in the field of motor drives, they are less suitable for design and fault diagnostic algorithms. However, some authors used those models to simulate faults but at the cost of complicated changes in the motor's equivalent circuit.

The multiple coupled circuit (MCC) based models are gaining heightened popularity in fault diagnostics these days. The prevalent types include winding function analysis (WFA) and modified winding function analysis (MWFA) based models. Using these techniques, the more practical aspects, such as non-uniform air gap, actual stator, and rotor winding functions, and almost all kinds of faults, including saturation effect, can be simulated.

The magnetic reluctance-based models can also be seen in literature, giving similar results as MCC but at the cost of increased complexity. This is because the entire geometry needs to be represented with reluctances, which end up with the matrices of immense dimensions. This complexity cannot be avoided using symmetry because the machine is no longer symmetrical for fault diagnostics.

The other analytical models, such as generalized harmonic, Concordia transformation-based, voltage behind reluctance, and convolution theorem-based models, are also available in the literature [IV].

1.3.2 The finite element method (FEM) based models

The finite element method is a numerical method used to solve partial differential equations or boundary value problems. This technique is used extensively to solve significant engineering problems related to heat flow, fluid dynamics, structural analysis, electromagnetic analysis, mass transport, etc. In this method, any system's geometry is divided into small elements represented by nodes making mesh. The partial differential equations are solved for each node to get the final answer. Although these techniques are much more accurate than analytical methods and can handle almost all kinds of practical aspects of the machine, but at the cost of increased complexity. This complexity is in the sense of an increased number of equations requiring more processing power and memory to save intermediate results. This is the biggest drawback of these techniques, making them less suitable for online, drive and fault diagnostic algorithms. Moreover, the resultant massive matrices having many singularities make the solution of inverse mapping non-unique and unstable. However, researchers are trying to reduce the simulation time using several approximate methods such as model order reduction, symmetry exploitation, and hybrid analytical-FEM models. Still, they are much more complex and less suitable for condition monitoring algorithms. A detailed comparison of these techniques with the help of an appropriate number of references is discussed in the subsequent chapter [IV].

1.4 Objectives and scope of the thesis

This thesis aims to study different analytical methods to model a squirrel cage induction motor, which should have minimal simulation time than the corresponding finite element method (FEM) based models. The purpose of doing so is to develop a model suitable to simulate all major faults and well-suited for advanced model-dependent fault

diagnostic algorithms, such as parameter estimation and inverse problem theory. This thesis's second prime objective is to study various signal-processing techniques for their pros and cons to detect fault at the nascent stage and investigate the entire current harmonic spectrum of induction motors in transient and steady-state regions. Thus, the motor under healthy and broken rotor bar (BRB) conditions are simulated, and experimental measurements are investigated for validation.

The dynamic d-q model with the inclusion of non-linear magnetization inductance was considered as a starting point. This model helps understand the machine's basic concepts because of its comprehensiveness and ability to produce compact equations, which can be used for drives as general and in observers and state estimators as particular. However, this model was less suitable to simulate machine faults because of the considered approximations.

To address the d-q model limitations, the winding function analysis (WFA) based model was prepared. In this model, the analytical equations to calculate various inductances, resistances, currents, fluxes, torque, and speed are derived for the motor under investigation. These equations were simulated in MATLAB, giving results near to the practical measurements. The model is suitable for implementing some faults, such as BRB and broken end rings. Still, the consideration of constant air gap makes it less ideal for the implementation of eccentricity and saturation-related faults.

Moreover, the spatial harmonics, which are very important for fault diagnostics and sensor-less speed estimation, cannot be simulated. However, those approximations can be removed by using Fourier summations for handling non-sinusoidal winding distribution and Taylor series to implement inverse air gap function. It will lead to the approximations such as; the self-defined number and the amplitude of the harmonics and the number of Taylor series terms.

To get more realistic results, the modified winding function analysis (MWFA) based model was prepared to ensure that all winding functions and air gap were defined as a function of stator and rotor individual and respective angles. The geometry of stator and rotor slots is considered to calculate the leakage inductances and various resistances. The self and mutual inductances between rotor and stator are computed with a stepping rotor. The results at each rotor position are saved in offline 3D lookup tables. During the online simulation, all pre-saved matrices are used as a rotor position function using their index value, and the performance parameters, such as currents, fluxes, torque, and speed, are calculated. To validate the results, the FEM model of the machine under investigation is prepared using commercial software. The comparison of results shows an excellent agreement with a minimal simulation time for the proposed model compared to the corresponding FEM model [IV]. The matrix dimensions of the proposed model are minimal compared to the corresponding FEM models. It can be considered as least ill-posed, making it an excellent candidate to implement inverse problem theory. The inverse problem theory is the mapping of observables to the unknown, and ill-posedness is the measure of the uniqueness and the stability of inverse map solutions.

Towards the signal processing side, the fast Fourier transform (FFT) and wavelet transform (WT) are used extensively to study the steady-state and transient regime signals. The infinite impulse response (IIR) based digital filters are used to improve the motor's current spectrum's legibility. Moreover, the frequency spectrums with the decent resolution are achieved by eliminating the starting and ending fractional cycles, data interpolation, counting the integral number of cycles by zero-order detection, etc. In this way, the total harmonics are segregated according to their cause of production.

Moreover, the spectrum of current simulated from the proposed model is compared with that simulated using the FEM model and the test rig measurements. The comparison is made until a wide bandwidth of frequencies for further validation of the proposed model.

Moreover, the proposed model is also investigated during the transient regime by doing the time-frequency analysis. The recovered non-stationary signal is in good agreement with the one obtained from the practical measurement. During the transient interval, the specific fault-related pattern can further enhance the model's effectiveness, as presented in [1]. It is proposed that the contour plots with specific confidence intervals can give better differentiation among fault and inherent eccentricity-based patterns.

1.5 Scientific contributions

Scientific Novelty

- In the modified winding function-based model, all parameters, such as winding and air gap functions, are defined as conditional analytical expressions to calculate inductances offline. In most of the literature, these functions are defined as a summation of various harmonics using the Fourier series technique. This limits the number of harmonics, while in the proposed model, all harmonics are automatically considered while calculating the performance parameters.
- The division of the model into offline and online sections makes it more suitable for fault diagnostic techniques. This gives the freedom to simulate the faults (such as BRB) in the online section without doing unnecessary offline calculations again, which reduces the simulation time considerably. However, in FEM-based models, the entire model needs to be simulated for every new faulty scenario.
- The conversion of the integral-based winding function formula into the mean value equation reduces the computational complexity and the integration's constant related problems.
- The proposed model is made compatible with the cluster computation. It can further reduce the simulation time if necessary.
- A hybrid FEM-analytical model compatible with a cluster of parallel processors is prepared, and simulation time reduction is discussed. Although it takes considerable simulation time even on multiple processors compared to the proposed MWFA mode, it is suitable for validation of results.
- The compatibility of both models with cluster computation makes them feasible to exploit distributed computational resources such as cloud computation, which is vital to industry 4.0 standards.
- An algorithm to improve spectral resolution by decreasing spectral leakage is proposed on the signal processing side. It can improve the spectrum's legibility even at the low sampling frequency by data interpolation and counting integer number of cycles. This has a good impact on reducing the complexity and cost of data acquisition devices and makes a pavement for remote sensors.
- It is shown that in direct torque control (DTC) mode, the drive's controller directly impacts stator current. It attenuates the fault-based harmonics in the current to reduce torque and speed ripples. As a result, it reduces the current

distortion due to rotor asymmetries. The controller changes current by changing voltage, making it a potential candidate for fault diagnostics rather than current.

- The transient time is extended to improve the resolution of the time-frequency response of current under non-stationary conditions. This time can be extended using some high inertia load or variable transformer, as in most literature. This technique needs the machine to be removed from the workplace, interrupting the process for a long time. However, the rotor's self-inertia is exploited here for this purpose. To do so, the motor's power is reduced by dropping the voltage below its nominal value. In this way, no external load is needed for doing the condition monitoring test. An industrial inverter is programmed to get variable voltage with a constant frequency while driving the motor in scalar control mode with zero acceleration and deceleration time.
- Despite having various approximations, the WFA model is used effectively to get similar time-frequency pattern during the transient regime as it was in the experimental measurement. It makes the model suitable for the diagnostic algorithms depending upon the transient interval, mainly for broken bars and end rings. The model is also suitable for defining theoretical fault-based patterns and studying the impact of fault on various observables.
- Non-linear magnetization inductance is considered in the d-q model of the induction motor, which can be similarly used in other analytical models. Moreover, the proposed model gives the freedom to include material magnetic behavior in the form of a B-H curve lookup table or modulation of the air gap permeance function.

Practical novelty

The following is the laboratory-based practical setup-related information.

- The development of a test rig where two similar machines are connected back to back, on the same mechanical foundation. One machine is used for testing the rotors with faults, while the other machine is used as a loading motor. This mechanism gives better slip controllability. Two similar test rigs with different machines are tested for better understandings.
- Industrial inverters are used for testing healthy and faulty machines. This fact makes the proposed signal processing-based diagnostic algorithms feasible for industries.
- The industrial inverters under different control mechanisms such as scalar and direct torque control (DTC) are used to investigate the presence of inverter-fed harmonics and the drive controller's influence.
- The segregation of various harmonics is achieved by considering the grid-fed motor's current spectrum as a benchmark signal. These measurements are taken by supplying the motor with grid voltage using a variable transformer.
- For current analysis in the transient regime, the rotor's inertia is used to extend the non-stationary signal rather than external high inertia load or variable transformer. This is achieved by reducing the voltage using an industrial inverter while maintaining constant frequency.

Moreover, the research work can help implement advanced novel diagnostic algorithms in the industry in the following ways that can be considered as futuristic in this field.

- The proposed model can be used as a part of advanced model-dependent fault diagnostic algorithms because of reduced computational complexity and minimal simulation time.
- Because the model is least ill-posed, it can be used for inverse problem theory-based diagnostic algorithms.
- As the model has offline and online portions, once the offline calculations are done using cluster computation (optional), the online portion can be easily handled by the onboard processors. Moreover, the online portion gives the freedom to simulate various faults without doing all the calculations again.
- The compatibility of the model for cluster computation makes it feasible for utilizing distributed computational resources, e.g., cloud computation as in industry 4.0 standards.
- The model can train artificial intelligence-based diagnostic algorithms with a variety of single and composite faults.
- The selection of appropriate signals for fault diagnosis is of crucial importance. It is proved that the current, speed, and torque can give wrong results if the machine is under DTC control mode.
- The use of the rotor's inertia to extend the transient time by reducing the applied voltage while maintaining constant frequency in scalar control mode is proposed. It minimizes the need for high inertia external load, and the industrial inverters can perform the test quite easily.

2 State of the art

2.1 The modeling techniques

Since the advanced fault diagnostic techniques depend on the motor's model, it should be a good replica of the actual system and should be able to simulate various faults in the motor. The more accurate the model of the motor is, the better the diagnostic would be. Mostly the faults are degenerative, giving a limited time window for maintenance. Hence the model-dependent algorithm should be fast and sensitive enough to detect the faults at a very early stage. Also, the model should have as few approximations as possible. Various kinds of motor modeling techniques available in the literature can be divided into two main streams: analytical and numerical. The most common methods, along with their attributes, are summarized in Table 2.1 [IV].

The two-axis theory (d-q) based models are prevalent in literature. The detailed dynamic analysis of wound-rotor induction motor under balanced and unbalanced conditions in various reference frames can be found in [5], while a similar kind of research without the unbalances is available in [6]. In [5], the authors used the d-q model in conjunction with coupled magnetic circuit theory to consider the rotor winding's actual non-sinusoidal distribution. The d-q modeling-based analysis of broken rotor bars is presented in [7]-[8], where the authors transformed the rotor d-q currents into n-loop currents in each iteration. In [8], the authors used d-q modeling to represent an unbalanced three-phase motor having a stator open circuit with the equivalent unbalanced two-phase motor to present a new fault-tolerant vector control method. The transient model for the analysis of stator turn faults is presented in [9].

These models are simple to understand, comprehensive, suitable for dynamic analysis, and better for drive systems, but they have various simplifications, making them less attractive for the field of fault diagnostics. These simplifications include sinusoidal distribution of stator and rotor windings, although they can be converted to the actual windings but at the cost of increased complexity [IV]. Since the rotor side parameters are referred to as the stator side or vice versa, the changing air gap cannot be considered, eliminating spatial harmonics, which are very important for fault diagnostics. All inductances are regarded as constant, eliminating their dependence on the rotor position and the non-linearities of magnetic material. Moreover, the proximity and skin effects are neglected.

The multiple coupled circuit (MCC) theory can solve the previously mentioned problems as it allows modeling the unbalanced machine. The authors of [10] used winding function analysis (WFA) for modeling a three-phase squirrel cage induction motor (SQIM) with stator inter-turn short circuit fault. In [11], the authors used it to simulate SQIM with broken rotor bars. The analysis of various faults, such as stator phase disconnection, broken bars, and broken end rings, is presented in [12], while the approach was used for the analysis of adjustable speed drive applications in [13]-[14]. The authors of [15] used this technique to model a permanent magnet machine with a fractional slot concentrated winding.

In majority of WFA based papers, the air gap is considered as constant, which do not allow to simulate eccentricity faults, and the principal slot harmonics are potentially ignored. Moreover, the uniform air gap makes it challenging to deal with nonlinearities such as magnetic saturation using the WFA approach. The solution to those problems is

possible by using Fourier and Taylor series but at the cost of associated limitations. However, they can be effectively solved using the modified winding function analysis (MWFA) method. The slot openings of the stator and rotor can be considered by making the air gap a function of the stator and rotor position.

The authors in [16] extended the WFA based method to simulate electrical machines with a non-uniform air gap. The use of the MWFA to model the stator and rotor slot effects for speed sensor-less drive systems is presented in [17]. The static and dynamic eccentricities are shown in [18] and [19], respectively. Unlike [17], where the air gap permeance is approximated by cosine series functions, [20] used the actual stator and rotor slot opening functions and a medium magnetic equipotential surface to simulate the machine. By doing so, the authors obtained results very close to the ones obtained from FEM. The simulation time was further reduced by exploiting the rotor cage's symmetry, which is valid for the simulation of healthy symmetrical machines and is not true for faulty machines. The analytical models show their limitations while dealing with complex geometries, material properties, non-linearities, etc. However, these approximations have a negligible impact on diagnostic algorithms. But they are essential for designing problems.

The FEM has been extensively used in literature to tackle the mentioned problems. The authors in [21] used FEM to model an induction machine with the inclusion of eddy current and hysteresis in steel laminations. The magnetic field analysis of induction motors with cooling ducts is presented in [22]. The authors of [23] used this technique to study the vibrations in an induction motor with a 2D magnetic solution, coupled with a 3D mechanical model of the stator, to reduce the complexity. For the same purpose, the authors of [24] used a quasi-3D FEM to compute the magnetic forces acting on an induction machine's stator end windings. Although the FEM-based models are very close approximations of the actual systems, they present a high complexity level and unaffordable computation time, especially in real-time applications. Moreover, FEM-based models produce huge-sized matrices with a greater possibility of singularities. It hinders them from using inverse mappings because of non-unique and inconsistent results.

Since the motor becomes unsymmetrical under faulty conditions, the solution of complete geometry is necessary, causing an extensive increase in the number of mesh elements. Although modern-day computers are powerful, still the FEM-based models require considerable time for simulation, making them unsuitable for use in online diagnostic methods, such as inverse problem theory, hardware-in-the-loop environment, and online parameters estimation. The authors in [20] simulated the same machine with FEM and analytical method and concluded that the analytical approach could give approximately the same results but with considerably less computation time. The detailed comparative analysis is presented in [IV].

Table 2.1. The common modeling techniques with corresponding attributes.

Technique	Faults and applications	Attributes
<p>Two-axis theory</p> <ul style="list-style-type: none"> • d-q • Modified d-q 	<ul style="list-style-type: none"> • Drives • Dynamic analysis [25][26] • Broken rotor bars [7][8] • Broken end rings [7][8] • Stator open circuit [27] • Stator short circuit [9] 	<p>Pros:</p> <ul style="list-style-type: none"> • Simple • Comprehensive • Provides useful equations for parameters estimation • An excellent choice to learn making forward problems • Suitable for control and drives <p>Cons:</p> <ul style="list-style-type: none"> • No saturation • Absence of air gap • Sinusoidal stator winding • No inter-bar currents • No spatial harmonics • No eccentricity faults • No skin effects • Challenging to deal with asymmetries, which are inevitable with the fault
<p>Multiple coupled circuits (MCC)</p> <ul style="list-style-type: none"> • Winding function analysis (WFA) • Modified winding function analysis (MWFA) • Extended Modified winding function analysis (MWFA) 	<ul style="list-style-type: none"> • Broken rotor bars [11] • Broken end rings • Stator open circuit [12] • Stator short circuit [10] • Dynamic eccentricity [19] • Static eccentricity [18] • Corroded rotor bars 	<p>Pros:</p> <ul style="list-style-type: none"> • Non-uniform air gap • Practical winding functions • Saturation can be defined analytically • Various kind of faults can be simulated • Low computation time as compared to FEM • An excellent tradeoff between complexity and accuracy <p>Cons:</p> <ul style="list-style-type: none"> • Some geometrical constraints are difficult to handle, such as cooling ducts in the stator or rotor. However, their definition frequencies can be included analytically or by doing appropriate changes in the air-gap function.

<p>Magnetic coupling</p> <ul style="list-style-type: none"> • Magnetic reluctance method 	<ul style="list-style-type: none"> • Broken rotor bars [28] • Broken end rings [29] • Stator open circuit • Stator short circuit [28] • Dynamic eccentricity [30] • Static eccentricity [30] 	<p>Pros:</p> <ul style="list-style-type: none"> • Can include spatial dependencies • Computationally less intense than FEM but more than MCC • It can include geometry, material parameters to some extent, and winding distribution <p>Cons:</p> <ul style="list-style-type: none"> • Since all slots need to be modeled and the faulty machine is no longer symmetrical, the model becomes very complex for model-dependent diagnostic algorithms, i.e., inverse problem theory
<p>Others analytical</p> <ul style="list-style-type: none"> • Generalized harmonic analysis [31][32][33] • Concordia transformation [34] • Voltage behind reactance [35] • Convolution based [36] 	<ul style="list-style-type: none"> • Winding faults [19] • Losses and torque pulsation [33] • Stator short circuit and broken rotor bars [34][35] • Broken rotor bars [36] 	<p>Pros:</p> <ul style="list-style-type: none"> • Concordia transformation reduces the number of state variables. • The convolution-based method is fast and allows to handle various non-ideal parameters <p>Cons:</p> <ul style="list-style-type: none"> • The generalized harmonic analysis limits the number of harmonics taken into consideration • The inclusion of non-uniform air gap is not straightforward in two-axis theory-based models • Nonlinearities will increase the complexity of analytical equations in two-axis theory-based models • Concordia transform inherits the problems of d-q modeling • The convolution theorem inherits the drawbacks of FFT • The air gap in the convolution-based model is taken as constant

<p>Finite element analysis</p> <ul style="list-style-type: none"> • Static • Time-stepping • Quasi-static • 2D • 3D 	<ul style="list-style-type: none"> • Broken rotor bars [37][38] • Broken end rings [38] • Stator open circuit [39] • Stator short circuit [40] • Dynamic eccentricity [41] • Static eccentricity [42] 	<p>Pros:</p> <ul style="list-style-type: none"> • Complex geometries can be considered • Non-linearities, such as saturation, skinning effect, and non-idealities, can be considered • All kind of faults can be simulated • The combination of FEM and analytical modeling can be the right choice for complexity reduction <p>Cons:</p> <ul style="list-style-type: none"> • The computational complexity is the biggest problem and becomes worst in case of fault diagnostics where symmetry is no longer present. The problem becomes worst for 3D analysis. • Unsuitable for the hardware-in-the-loop environment and inverse problem theory • The 2D models do not allow to include the skew and cross-currents effect.
------------------------------------------------------------------------------------------------------------------------------------------------------------------------	-------------------------------------------------------------------------------------------------------------------------------------------------------------------------------------------------------------------------------------------------------------------	-------------------------------------------------------------------------------------------------------------------------------------------------------------------------------------------------------------------------------------------------------------------------------------------------------------------------------------------------------------------------------------------------------------------------------------------------------------------------------------------------------------------------------------------------------------------------------------------------------------------------------------------------------------------------------------------------------------------------------------------------------------------------------------------------------------------------

2.2 The SQIM fault representing frequencies

It is observed that each kind of fault modulates the motor's global signals such as current, torque, speed, and voltage in a specific manner leaving certain harmonics in them. The detection of those frequency components can lead to the fault even at the developing stage. The most common faults in induction machines and their current modulating frequencies are summarized in Table 2.2, with detailed descriptions available in [43]-[45].

Table 2.2. The fault signature frequencies for cage induction machines.

Fault	Modulating Frequencies	Where
Rotor winding asymmetries	$f_{asym} = f_s \pm 2ksf_s, \quad k = 1, 2, 3, \dots$	k : Harmonic order v : Supply fed harmonics f_s : Supply frequency
Broken rotor bars	$f_{BR1} = \left[\frac{k}{p}(1-s) \pm s \right] f_s, \quad \frac{k}{p} = 1, 3, 5, \dots$	f_{BR1} : Broken bar frequencies f_{bb} : Bearing fault frequencies $f_{i,o}$: Characteristic vibration frequencies
Bearing faults	$f_{bb} = f_s \pm m f_{i,o} $ $f_{i,o} = \frac{n_{bb}}{2} f_r \left[1 \pm \frac{b_d}{p_d} \cos \theta \right]$ For n_{bb} between 6-9, the above equation can be simplified as: $f_{bb o} = f_s \pm 0.4k n_{bb} f_r, \quad k = 1, 2, 3, \dots$ $f_{bb i} = f_s \pm 0.6k n_{bb} f_r, \quad k = 1, 2, 3, \dots$	m : Positive integer n_b : Number of rotor bars n_{bb} : Number of bearing balls n_d : Dynamic eccentricity (0 for static and 1,2,3.... for dynamic) f_r : Rotor frequency b_d : Bearing ball's diameter p_d : Bearing pitch $f_{bb o}$: Bearing outer race fault frequencies $f_{bb i}$: Bearing inner race fault frequencies
Eccentricity & PSH	$f_{ecce} = \left[(kn_b \pm n_d) \left(\frac{1-s}{P} \right) \pm v \right] f_s$ And for mixed eccentricity: $f_{ecce} = f_s \pm k f_r, \quad k = 1, 2, 3, \dots$	ϑ : The angle between bearing ball and race s : Slip p : Number of poles P : Number of pole pairs
Inter-turn short circuit	$f_{st} = f_s \left[\frac{m}{p}(1-s) \pm k \right], \quad k = 0, 1, 3, 5, \dots$	

There is a certain discrepancy among the authors that the frequencies shown by inter-turn short circuit in table 2.2 really depict the stator winding short circuits as they also appear in case of rotor asymmetries such as broken rotor bars, eccentricities and rotor misalignment etc. However, the authors in [44] claimed that, the formula clearly depicts the frequencies produced by the short circuits as well. Besides, the stator current analysis can also be used for the detection of bad coupling systems between machine and load [46].

2.3 The fault diagnostics techniques

The fault diagnostics of electrical machines at the embryonic stage are indispensable to avoid catastrophic situations, resulting in complete process failure and substantial economic loss. A variety of fault diagnostic techniques available in literature can be broadly classified into the following categories:

- Current analysis e.g., motor current signature analysis (MCSA)
- Vibration analysis
- Thermal analysis
- Acoustics analysis
- Electromagnetic field inference
- Infrared detection
- Stray flux detection

Almost all advanced condition-monitoring techniques directly or indirectly depend upon those methods.

Since electrical machines are complex systems, several parameters are associated with another; detecting the fault's exact cause is challenging. Much work has already been done in fault diagnostics, such as MCSA, vibration analysis, thermal analysis, electromagnetic field inference, etc., while MCSA is the most cited in the literature. MCSA's popularity is caused by its non-invasive nature, simplicity, and compatibility with several signal processing tools. Almost every condition monitoring algorithm depends upon signal processing techniques. The conventional signal processing methods, along with their attributes, are given in Table 2.3. The presented attributes give a more generic comparison in the sense of computational complexity. However, it may vary to some extent from case to case. A detailed application of those techniques during transient and steady-state intervals using various signals can be studied in [47]-[50].

Table 2.3. The primary signal processing techniques for fault diagnostics with their corresponding attributes.

Technique	Complexity	Attributes
DTFT	Low	<ul style="list-style-type: none"> • It can be used on a variety of signals • Works under the steady-state regime • Fails when the signal is non-stationary • An excellent choice if the fault is modulating the signal in a consistent way • It does not depend upon any modeling of the system • Aliasing and spectral leakage are common problems • It can be used for fault segregation • Challenging to implement under varying load conditions • Cannot give time-frequency analysis • Discontinuities in the signal can be erroneous • The choice of truncating window is crucial

STFT	Medium	<ul style="list-style-type: none"> • Can work under both steady-state and transient regime • Time-frequency representation is a key feature • The selection of the proper window is important • Heisenberg uncertainty is the problem for time and frequency resolution as compared to the wavelet transform • Increased complexity as compared to DTFT due to moving window • Inherits the problems of FFT
Wavelet	High	<ul style="list-style-type: none"> • Can work under both steady-state and transient regime • Better time-frequency resolution than STFT • The selection of the mother wavelet is important • Possess excellent filtering properties as compared to the corresponding DTFT • Heisenberg uncertainty is still the problem but less than that in STFT • More complicated than STFT in the sense of required computational power due to constantly moving mother wavelet with different scaling factors • CWT is much more computationally intense than corresponding DWT

Due to the inevitable inclusion of complex control algorithms and inverters, the diagnostic techniques do not remain straightforward [51]-[53]. The drawbacks become worst when there are multiple machine faults, making them almost impossible to be segregated. For example in [48], the authors presented that the rotor's air ducts can imitate broken bars and cause a false alarm.

The effective utilization of the machine's model for parameter estimation and fault diagnostic can give promising results that can diminish the earlier mentioned problems. The drawbacks of the model's complexity and required computational power are not a big issue, as the world is moving towards Industry 4.0 and cloud computation, which provides unlimited resources. In the field of inverse problem theory, hardware-in-the-loop, or parameters estimation, the motor's global parameters, such as speed, torque, or currents, can be used inversely to estimate the design parameters, such as inductances and resistances, etc. [54][IV]. With an increase in the complexity of motor structure and control mechanisms, more than one fault diagnostic techniques can be used all together to get maximum benefits.

The Park's vector-based methods can also be considered as a field of interest for fault diagnostics. The common variants of Park's vector method with their attributes are presented in Table 2.4 [VII].

Table 2.4. The Park's vector variants and attributes.

Technique	Mathematical Calculations	Memory Required	Attributes
Park's vector (MCSA) <ul style="list-style-type: none"> • Extended Park's vector • Double park's vector • Reduced modulus of extended Park's vector • Multiplier Park's vector 	Medium	Medium	<ul style="list-style-type: none"> • Noninvasive • Suitable to study various fault conditions • Easily implementable under stationary load conditions, however can be applied for varying loads but at the cost of increased complexity • The supply harmonics can reduce the legibility of results • The sampling rate can be reduced • It can be implemented on FPGA and DSP kits • Segregation of different faults is possible but challenging • Becomes more complex in case of inverter fed machines particularly DTC controlled machines

With the evolution of powerful computers and cloud computation, advanced diagnostic algorithms are becoming increasingly popular. Most of these techniques depend upon the system's mathematical model, which increases the complexity on the one hand, but reduces the limitations of conventional methods considerably. Some advanced techniques are presented in Table 2.5. The detailed description of most traditional and cutting-edge techniques is discussed in [VII]-[VIII]. Moreover, a very well-written state-of-the-art for conditioning monitoring of electrical machines and the future challenges can be found in [55].

Table 2.5. Some advanced emerging techniques.

Technique	Mathematical Calculations	Memory Required	Attributes
<ul style="list-style-type: none"> • Sliding mode observers • Datamining • Fuzzy Logic, Neuro-Fuzzy • Neural Network • Pattern recognition • Kalman Filter • Inverse problem theory • Digital Twin 	High	High	<ul style="list-style-type: none"> • Invasive and non-invasive • It can be used for faults segregation • No need for exact measurement of slip, high accuracy • Mostly model dependent • Model accuracy matters a lot • Sophisticated hardware required • Some techniques remain good with less sampling frequency • Long measurement time required for techniques like pattern recognition and machine learning • Extensive data under different faulty scenarios is required to train the AI-based techniques.

3 The modeling of induction motors

3.1 The dynamic d-q models

Induction machines work like a transformer with a rotating secondary winding. This rotating nature makes the machine parameters time and space-dependent. This dependency leads to the varying inductances as a function of the rotor's position, making the model complicated (for two-axis theory). To solve this complexity, R. H. Park (1920s), H.C. Stanley (1930s), and G. Krone proposed the solution by transforming stator variables to a winding, rotating with the rotor, rotor parameters to the stator side, and both rotor and stator variables to synchronously rotating frame of reference respectively [56]. In this way, the air gap can be eliminated, and both stator and rotor sides can be considered stationary to each other. Moreover, transforming the number of phases from one coordinate system to another coordinate system with a lower number of the axis can reduce the number of equations. In the following section, a simple d-q model is summarized, and its suitability for fault diagnostics is discussed at the end.

3.1.1 Two-axis theory

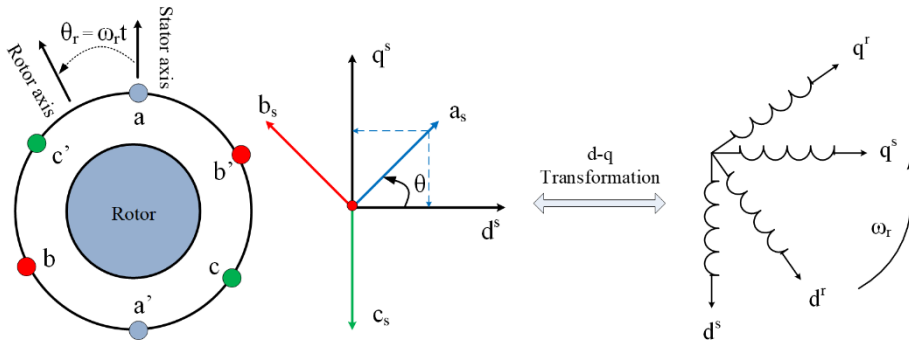


Figure 3.1. Three phases to two-phase transformation.

The three-phases (a_s - b_s - c_s) in a stationary frame of reference can be transformed into equivalent two phases both in stationary (d^s - q^s) or rotating (d^r - q^r) frames of references, as shown in Figure 3.1 where superscripts “r” and “s” represent rotor and stator associated phases respectively. This transformation reduces the number and complexity of motor representing equations. The frame of reference is stationary when the rotor parameters are transformed to the stator side. In this case, the model does not remain dependent upon the synchronous speed ($\omega_e=0$). While when both rotor and stator parameters are shifted to an arbitrary winding rotating at synchronous speed, the model is known to be in a synchronously rotating frame of reference, where ω_e is no longer zero. Similarly, both windings can be shifted to the rotor side, and the model is in the rotor frame of reference. For a better understanding, the motor's model in the static frame of reference is presented in the subsequent section.

3.1.2 Equivalent model of motor

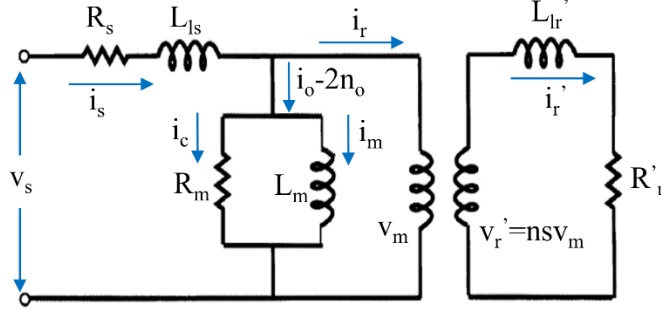


Figure 3.2. The equivalent circuit diagram of SQIM [56].

The per-phase equivalent circuit diagram of an induction motor is shown in Figure 3.2. Where R_s represents the per phase copper resistance, L_{ls} is the leakage inductance, L_m is the magnetization inductance, I_c and I_m are the working and magnetization components of no-load current, respectively, and I_r is the rotor reflected current. This model can be transformed into an equivalent d-q transformation-based T-model with the nonlinear magnetization inductance shown in Figure 3.3.

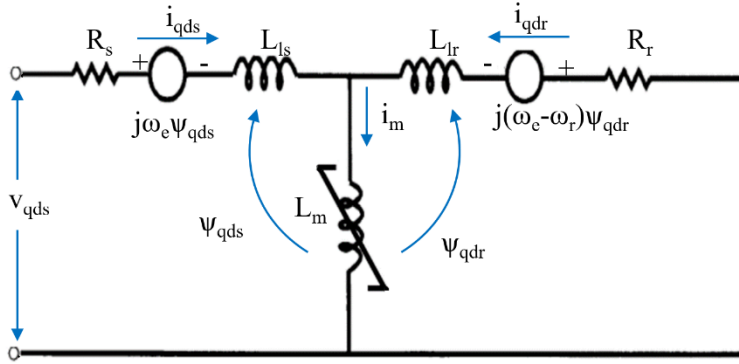


Figure 3.3. The equivalent circuit diagram with rotor parameters transformed towards the stator side and the inclusion of non-linear magnetization inductance [56].

3.1.3 The state-space model

The equivalent circuit's state-space model can be constructed easily to study and analyze the motor, using tools such as Eigenvalues, Root Locus, Bode Plot and output responses, etc. The basic state-space model can be defined as follows:

$$\begin{aligned} \dot{x} &= Ax + Bu \\ y &= Cx + Du \end{aligned} \quad (3.1)$$

Let the states " x " and the outputs " y " of the system under observation be:

$$x = [i_{ds}^s \quad i_{qs}^s \quad \varphi_{dr}^s \quad \varphi_{qr}^s], \quad (3.2)$$

$$y = [ids^s \quad iqs^s \quad 0 \quad 0], \quad (3.3)$$

The state-space model of a three-phase induction motor in a static frame of reference can be constructed as:

$$\begin{bmatrix} d(i_{ds}^s)/dt \\ d(i_{qs}^s)/dt \\ d(\phi_{dr}^s)/dt \\ d(\phi_{qr}^s)/dt \end{bmatrix} = \begin{bmatrix} -\frac{L_m^2 R_r + L_r^2 R_s}{\sigma L_s L_r^2} & 0 & \frac{L_m R_r}{\sigma L_s L_r^2} & \frac{L_m \omega_r}{\sigma L_s L_r} \\ 0 & -\frac{L_m^2 R_r + L_r^2 R_s}{\sigma L_s L_r^2} & -\frac{L_m \omega_r}{\sigma L_s L_r} & \frac{L_m R_r}{\sigma L_s L_r^2} \\ \frac{L_m R_r}{L_r} & 0 & -\frac{R_r}{L_r} & -\omega_r \\ 0 & \frac{L_m R_r}{L_r} & \omega_r & \frac{R_r}{L_r} \end{bmatrix} \begin{bmatrix} i_{ds}^s \\ i_{qs}^s \\ \phi_{dr}^s \\ \phi_{qr}^s \end{bmatrix} \quad (3.4)$$

$$+ \begin{bmatrix} \frac{1}{\sigma L_s} & 0 \\ 0 & \frac{1}{\sigma L_s} \\ 0 & 0 \\ 0 & 0 \end{bmatrix} \begin{bmatrix} V_{ds}^s & 0 & 0 & 0 \\ 0 & V_{qs}^s & 0 & 0 \end{bmatrix}$$

$$\begin{bmatrix} i_{ds}^s \\ i_{qs}^s \\ 0 \\ 0 \end{bmatrix} = \begin{bmatrix} 1 & 0 & 0 & 0 \\ 0 & 1 & 0 & 0 \end{bmatrix} \begin{bmatrix} i_{ds}^s \\ i_{qs}^s \\ \phi_{dr}^s \\ \phi_{qr}^s \end{bmatrix}, \quad (3.5)$$

$$\text{while } \sigma = 1 - \frac{L_m^2}{L_r L_s},$$

where L_m is the magnetization induction, which can be a constant or a nonlinear function of flux and current. The values of different design parameters for an 18-kW squirrel-cage induction motor are given in Table 3.1. These values are analytically calculated as discussed in the subsequent chapters. The saturation effect can be simulated by making the L_m a nonlinear flux and current function, as shown below [57]. The detailed implementation of the model and the non-linear magnetization inductance in Matlab/Simulink is presented in [XII].

$$i_m = \left(\frac{1 + \left(\left| \frac{\varphi_m}{\beta} \right| \right)^s}{L_m} \varphi_m \right), \quad (3.6)$$

where s and β are positive constants defining the saturation level.

3.1.4 Results

The dynamic d-q model allows studying the motor in both steady-state and transient regimes. The transformation of stator and rotor parameters to a common reference frame reduces the complexity of equations. The conversion of three phases to equivalent orthogonal two phases minimizes the number of equations resulting in a comprehensive model.

Figure 3.4 shows the results starting from an input three-phase voltage, which is first converted into two phases in the static frame of reference as in Figure 3.4 (a)-(b).

Figures 3.4 (c) and (d) show the simulated d-q currents of the stator and rotor in a synchronously rotating frame of reference, where the effect of load can be easily studied. The calculated stator d-q currents are transformed back to the three-phase system using inverse d-q transformation. The stator current and generated torque are presented in Figure 3.4 (e) and (f), respectively. The speed-torque curve is shown in Figure 3.5, where the motor's behavior in a steady-state and transient regime can be studied. These models are based on approximations, such as constant inductances, no slotting effects, no saturation, and sinusoidal distribution of stator and rotor windings. This makes them suitable for drive systems because of lower computation time but makes them unsuitable for fault diagnostics because the faults cannot be simulated using these symmetrical models.

Table 3.1. Parametric Values of the motor under investigation.

No.	Parameter	Symbol	Value
1	Stator per phase resistance	R_s	0.1500 Ω
2	Rotor resistance referred to the primary side	R_r	0.0546 Ω
3	Stator inductance	L_s	0.1229 H
4	Magnetization Inductance	L_m	0.1215 H
5	Rotor Inductance referred to the stator side	L_r	0.1215 H
6	Rotor moment of inertia	J	0.4 kg·m ²
7	Number of poles	p	4
8	Terminal voltage	V_{L-L}	333 V
9	Supply frequency	f_s	50 Hz
10	Friction coefficient	B_f	0.002 kg·m ² /sec ²

3.1.5 Attributes of two-axis theory-based models

Advantages

- Comprehensive
- Suitable for steady-state and transient analysis
- Useful for control and drives
- The fewer number of equations reduce the complexity
- Significantly short simulation time
- It shows an easy way for making forward models, mapping unknown to the observables

Limitations

- Incompatible for faults implementation without complex changes in the equivalent circuit diagram
- The removal of the air gap reduces its fault-related applications
- The spatial harmonics cannot be considered
- Mostly the wound rotor is considered, having three phases on it.
- Do not consider the position-varying nature of inductances
- It considers the motor as symmetrical, which is not in the case of a faulty machine.

Recommendations

- The winding function approach or finite element method (FEM) based modeling is necessary to study the system's actual behavior and simulate faults.

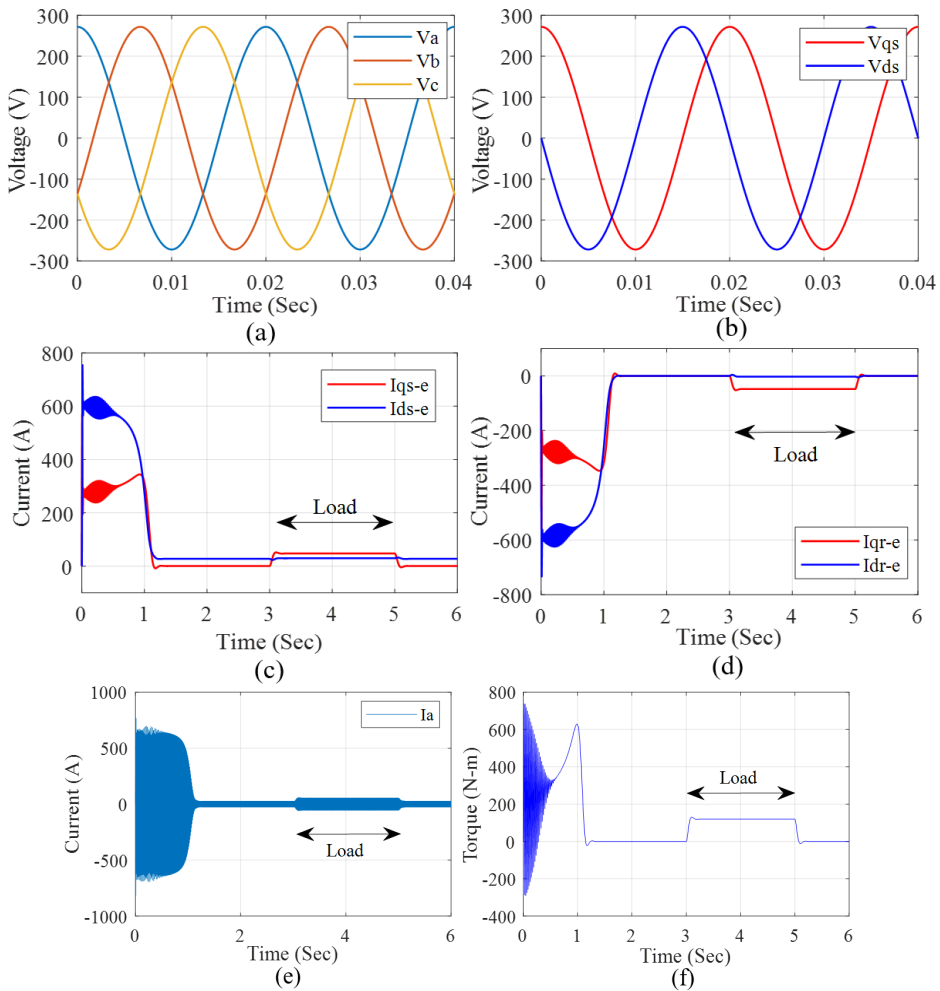


Figure 3.4. (a) The three-phase input voltage, (b) The equivalent two phases in the stationary frame of reference, (c) The simulated stator current in a synchronously rotating frame of reference, (d) The rotor's current in a synchronously rotating frame of reference, (e) The stator current, (f) The generated torque.

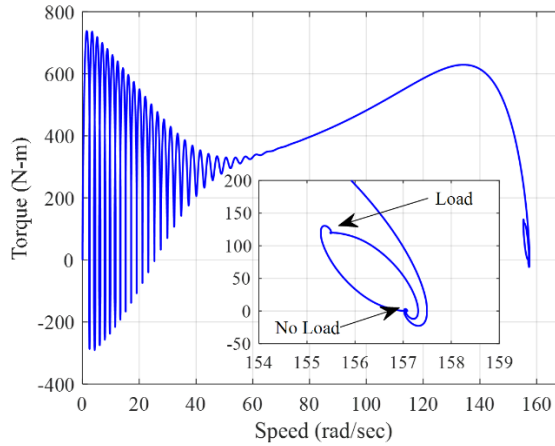


Figure 3.5. The speed-torque curve with a zoomed window representing the effect of load.

3.2 The winding function-based model

3.2.1 Introduction

The d-q modeling-related problems can be eradicated by considering the winding function-based models. In this approach, neither the stator nor the rotor parameters need to be transferred on either side to avoid an air gap. Instead, the stator windings, the rotor windings, and the air gap can be defined analytically and used to calculate various inductances and other motor performance parameters.

a) Block diagram for implementation

The induction motor is an intricate system where several parameters are interrelated with each other. It is recommended to follow a systematic way while making its mathematical model. The entire motor parameters can be divided into the rotor, stator, and mutual parameters to avoid complexity, as shown in Figure 3.6.

On the stator side, the electrical parameters, such as the number of phases, voltage, connection scheme, frequency, and the mechanical parameters, such as the number of slots, dimensions of the slot, and winding configuration, are taken as input and stator per phase resistances, and leakage inductances are calculated. The stator self and mutual inductances are computed using the winding function approach, as discussed in the subsequent section.

Similarly, the bar and end ring resistances and the leakage inductances are calculated on the rotor side based on the rotor slot's geometry. The self and mutual inductance among various rotor loops are computed using the winding function approach. For simplicity, the air gap is considered constant by neglecting the stator and rotor slot openings. They will be discussed in the modified winding function-based model section.

All inductances and resistances are calculated and saved in the form of matrices for ease of implementation. In the end, the performance parameters like torque, currents, speed, and rotor position are calculated. The rotor position is used in a feedback manner for the calculation of stator-rotor mutual inductances [X].

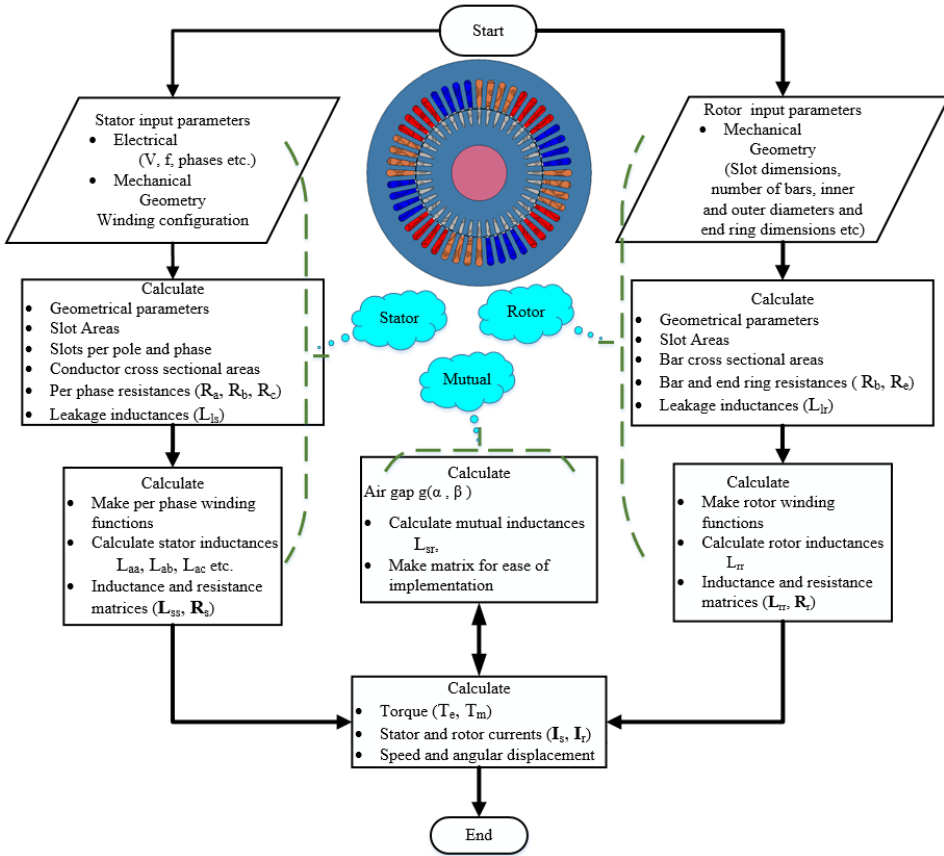


Figure 3.6. The block diagram describing the WFM implementation.

b) Block diagram for simulation

In MATLAB/Simulink, the model can be implemented with the help of two functions, responsible for calculating basic parameters, inductances, and their derivatives. One function calculates the constant values depending on the motor's geometry, such as an effective number of turns per slot and phase, leakage inductances, and resistances. The second function is used online to calculate different magnetizing inductances, currents, fluxes, torque, etc. using simple arithmetic operators, as shown in Figure 3.7. The description of the block diagram is as follows;

1. Function 1 is responsible for calculating constant parameters, as given in Table 3.2.
2. Function 2 is responsible for calculating the parameters, as shown in Table 3.3.
3. Simulink arithmetic operators to calculate
 - I. Stator currents
 - II. Rotor currents
 - III. Generated torque
 - IV. Rotor speed
 - V. Rotor position
4. Feedback rotor position back to step 2 to calculate inductances at the corresponding rotor position.

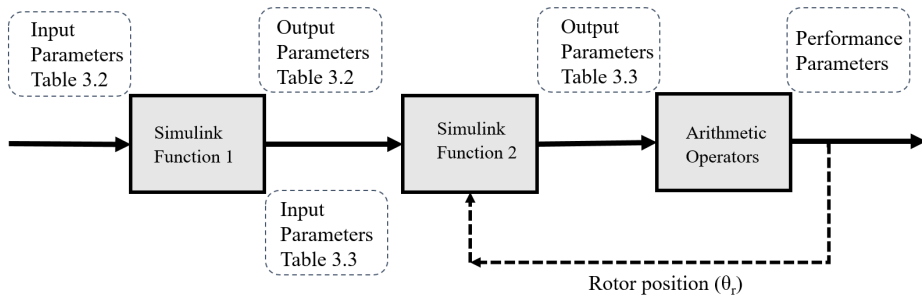


Figure 3.7. The implementation strategy in MATLAB/Simulink.

Table 3.2. The input and output parameters of function 1, shown in Figure 3.7.

No.	Input Parameters	Symbol	Output Parameters	symbol
1.	Stator slot dimensions	-	The effective number of turns per phase	N_s
2.	Rotor slot dimensions	-	Magnetization inductance	L_m
3.	Number of phases	m	Stator per phase resistance	R_s
4.	Number of stator slots	Q_s	Rotor bar resistance	R_r
5.	Number of rotor bars	n_b	Rotor end ring resistance	R_e
6.	rotor end ring dimensions	-	Stator leakage inductance	L_{ls}
7.	Stator inner diameter	D_s	Bar leakage inductance	L_b
8.	Rotor outer diameter	D_r	End ring leakage inductance	L_e
9.	Winding configuration	-		
10.	Machine's effective length	l		

Table 3.3. The input and output parameters of function 2, shown in Figure 3.7.

No	Input Parameters	Symbol	Output Parameters	symbol
1.	Per phase turns (effective)	N_s	Stator to stator inductances	L_{ss}
2.	Magnetization inductance	L_m	Stator to rotor inductances	L_{sr}
3.	Stator per phase resistance	R_s	Rotor to stator inductances	L_{rs}
4.	Rotor bar resistance	R_r	Rotor to rotor inductances	L_{rr}
5.	Rotor end ring resistance	r_e	Inductance matrix (overall)	L_f
6.	Stator leakage inductance	L_{ls}	Resistance matrix	R_f
7.	Rotor bar leakage inductance	L_b	inductance matrix Derivative	dL_f
8.	End ring leakage inductance	L_e	The inverse of the inductance matrix	$invL_f$
9.	Rotor position	ϑ_r		

3.2.2 Mathematical modeling

a) The analytical equations

According to the common reference frame definition, an ideal three-phase induction motor with a sinusoidal distributed stator winding and n_b rotor bars can be represented as shown in Figure 3.8 (a). The voltage equations for the stationary three-phase stator and rotating n phase rotor can be described as:

$$\mathbf{V}_s = \mathbf{I}_s \mathbf{R}_s + \frac{d}{dt} \boldsymbol{\varphi}_s, \quad (3.7)$$

$$\mathbf{0} = \mathbf{I}_r \mathbf{R}_r + \frac{d}{dt} \boldsymbol{\varphi}_r, \quad (3.8)$$

where \mathbf{V}_s , \mathbf{I}_s , \mathbf{I}_r , \mathbf{R}_s and \mathbf{R}_r are vectors containing stator three-phase voltage, stator and rotor currents, stator resistances, and rotor resistances.

In matrix form, these equations can be represented as:

$$\begin{bmatrix} v_{as} \\ v_{bs} \\ v_{cs} \end{bmatrix} = \begin{bmatrix} R_{as} & 0 & 0 \\ 0 & R_{bs} & 0 \\ 0 & 0 & R_{cs} \end{bmatrix} \begin{bmatrix} i_{as} \\ i_{bs} \\ i_{cs} \end{bmatrix} + \frac{d}{dt} \begin{bmatrix} \varphi_{as} \\ \varphi_{bs} \\ \varphi_{cs} \end{bmatrix}, \quad (3.9)$$

The equivalent circuit diagram of the rotor is shown in Figure 3.8 (b), for which the voltage equation is as follows;

$$\begin{bmatrix} 0 \\ 0 \\ 0 \\ \vdots \\ 0 \\ 0 \\ 0 \\ 0 \end{bmatrix} = \begin{bmatrix} 2(R_b + r_e) & -R_b & 0 & 0 & \dots & 0 & -R_b & -r_e \\ -R_b & 2(R_b + r_e) & -R_b & 0 & \dots & 0 & 0 & -r_e \\ 0 & -R_b & 2(R_b + r_e) & -R_b & \dots & 0 & 0 & -r_e \\ \vdots & \vdots & \vdots & \vdots & \ddots & \vdots & \vdots & \vdots \\ 0 & 0 & 0 & 0 & \dots & 2(R_b + r_e) & -R_b & -r_e \\ -R_b & 0 & 0 & 0 & \dots & -R_b & 2(R_b + r_e) & -r_e \\ -r_e & -r_e & -r_e & -r_e & \dots & -r_e & -r_e & n_b r_e \end{bmatrix} \begin{bmatrix} i_{r1} \\ i_{r2} \\ i_{r3} \\ \vdots \\ i_{r(n-1)} \\ i_{rn} \\ i_{re} \end{bmatrix} + \frac{d}{dt} \begin{bmatrix} \varphi_{r1} \\ \varphi_{r2} \\ \varphi_{r3} \\ \vdots \\ \varphi_{r(n-1)} \\ \varphi_{rn} \\ \varphi_{re} \end{bmatrix} \quad (3.10)$$

The flux equations can be written as:

$$\boldsymbol{\varphi}_s = \mathbf{L}_{ss} \mathbf{I}_s + \mathbf{L}_{sr} \mathbf{I}_r, \quad (3.11)$$

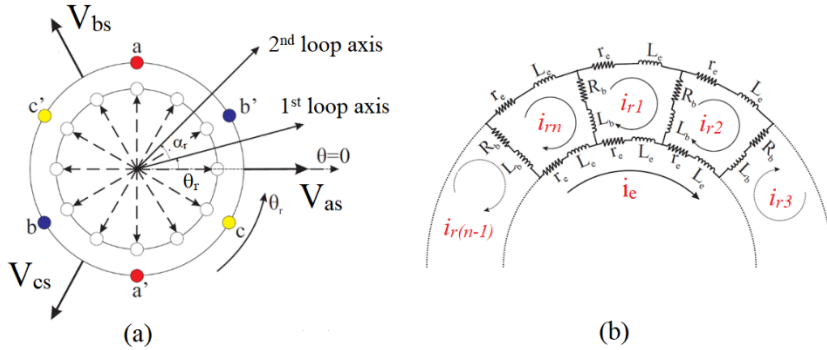


Figure 3.8. (a) The vector diagram of the motor where the vectors represent the stator and rotor phases, (b) The equivalent circuit diagram of the rotor cage.

where \mathbf{L}_{ss} and \mathbf{L}_{sr} are matrices containing stator and rotor self and mutual inductances, as shown below:

$$\mathbf{L}_{ss} = \begin{bmatrix} L_{aas} & L_{abs} & L_{acs} \\ L_{bas} & L_{bbs} & L_{bcs} \\ L_{cas} & L_{cbs} & L_{ccs} \end{bmatrix},$$

$$\mathbf{L}_{sr} = \begin{bmatrix} L_{ar1} & L_{ar2} & \dots & L_{ari} & \dots & L_{arn} & L_{are} \\ L_{br1} & L_{br2} & \dots & L_{bri} & \dots & L_{brn} & L_{bre} \\ L_{cr1} & L_{cr2} & \dots & L_{cri} & \dots & L_{crn} & L_{cre} \end{bmatrix},$$

$$\mathbf{L}_{sr} = \begin{bmatrix} L_{ar1} & L_{ar2} & \dots & L_{ari} & \dots & L_{arn} & 0 \\ L_{br1} & L_{br2} & \dots & L_{bri} & \dots & L_{brn} & 0 \\ L_{cr1} & L_{cr2} & \dots & L_{cri} & \dots & L_{crn} & 0 \end{bmatrix},$$

The subscripts a, b, c, and r represent entries related to the stator and rotor-associated phases.

Similarly, rotor fluxes can be represented as:

$$\boldsymbol{\varphi}_r = \mathbf{L}_{rs}\mathbf{I}_s + \mathbf{L}_{rr}\mathbf{I}_r = \mathbf{L}_{sr}^T\mathbf{I}_s + \mathbf{L}_{rr}\mathbf{I}_r, \quad (3.12)$$

$$\mathbf{L}_{rr} = \begin{bmatrix} L_{r1r1} & L_{r1r2} & \dots & L_{r1ri} & \dots & L_{r1rn} & L_{r1re} \\ L_{r2r1} & L_{r2r2} & \dots & L_{r2ri} & \dots & L_{r2rn} & L_{r2re} \\ \vdots & \vdots & \vdots & \vdots & \vdots & \vdots & \vdots \\ L_{rir1} & L_{rir2} & \dots & L_{riri} & \dots & L_{rirn} & L_{rire} \\ \vdots & \vdots & \vdots & \vdots & \vdots & \vdots & \vdots \\ L_{rnr1} & L_{rnr2} & \dots & L_{rnri} & \dots & L_{rnrn} & L_{rnre} \\ L_{rer1} & L_{rer2} & \dots & L_{reri} & \dots & L_{rern} & L_{rere} \end{bmatrix}.$$

Under the symmetrical condition, the last row and column, containing end ring resistance and mutual inductances, can be neglected because the net current in the end ring is zero, but it can lead to a problem of singularities in the simulation while taking the inverse of matrices. Moreover, they are necessary for the implementation of end ring-related faults.

b) Resistances calculations

The per-phase stator resistances can be calculated by considering the number of turns per phase, per turn resistance, and the length of a single turn, along with the number of parallel paths. The slot area and filling factor can help in this regard.

The following equations calculate the cross-sectional area of the conductor:

$$ASA = SA \times FF, \quad (3.13)$$

$$A_c = ASA / N_c, \quad (3.14)$$

where SA is a slot area, from where the effective slot area (ASA) can be calculated by multiplying it with the filling factor (FF), N_c is the number of conductors per slot, and A_c is the conductor cross-sectional area. The average length of a single turn (l_{av}) can be calculated using an analytical expression [58].

$$l_{av} \approx (2l + 2.4W + 0.1), \quad (3.15)$$

where l is the effective length of the machine, and W is the average coil span. The stator's per-phase DC resistance can be calculated as:

$$R_s = N_s \left(\frac{\rho l_{av}}{aAc} \right), \quad (3.16)$$

where N_s is the effective number of turns per phase, a is the number of parallel paths. N_s can be calculated as a function of the total number of series turns per phase (N_t) and winding factor ($K_w = K_p K_d K_s$) as described by the following equations:

$$N_s = K_p K_d K_s N_t, \quad (3.17)$$

where K_p , K_d , and K_s are pitch, distribution, and skewing factors, respectively, and can be calculated using the following formulas [58]:

$$K_p = \sin\left(v \frac{W \pi}{\tau_p 2}\right), \quad (3.18)$$

$$K_d = \frac{2 \sin\left(\frac{v \pi}{2 m}\right)}{\frac{Q_s}{mP} \sin\left(v \pi \frac{P}{Q_s}\right)}, \quad (3.19)$$

$$K_s = \frac{\sin\left(v \frac{s \pi}{2 \tau_p}\right)}{v \frac{s \pi}{2 \tau_p}}, \quad (3.20)$$

where v is v th harmonic, W is average coil span in meters, τ_p is pole pitch in meters, m is the number of stator phases, Q_s is the number of stator slots, P is the number of pole pairs, and s is arc length between two consecutive rotor bars.

The rotor bar and end ring resistances are calculated using the conventional resistivity formula. The resistance of the end ring sector (r_e) between two consecutive rotor bars is calculated by dividing the total end ring resistance (r_{et}) with the total number of rotor bars.

$$r_e = r_{et} / n_b. \quad (3.21)$$

c) Leakage inductances

In electrical machines, total flux can be divided into two parts, magnetization, and leakage flux. The magnetization flux (φ_m) is responsible for generating air gap flux linkage (ψ_m) between rotor and stator and participates in energy conversion. The leakage flux (φ_l) creates leakage flux linkage (ψ_l) and is associated with both stator and rotor as stator leakage flux (φ_{sl}) and rotor leakage flux (φ_{rl}). It is a common perception about leakage flux that it has a negative role in electrical machines due to an increase in the losses, which is not always true. This argument can be justified because the transient inductance of induction motors depends mainly on leakage inductances given by the following equation [X].

$$L'_s \cong L_{sl} + L_{rl} \quad (3.22)$$

These leakage inductances should be calculated carefully because any error in their calculation can lead to a wrong transient analysis of the motor. When this inductance is considered zero, both torque and speed become zero during the transient interval.

The leakage induction of a machine can be divided into air gap leakage inductance (L_g), slot leakage inductance (L_q), tooth tip leakage inductance (L_t), end winding leakage inductance (L_{ew}), and skew leakage inductance (L_{sq}), as shown by the following equation.

$$L_l = L_g + L_q + L_t + L_{ew} + L_{sq} \quad (3.23)$$

The asynchronous machines hold the following inequality.

$$L_{ew} > L_g > L_q > L_t > L_{sq} \quad (3.24)$$

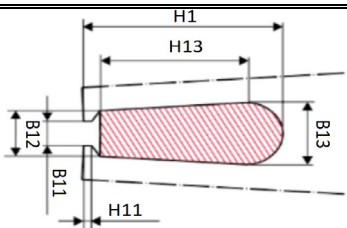
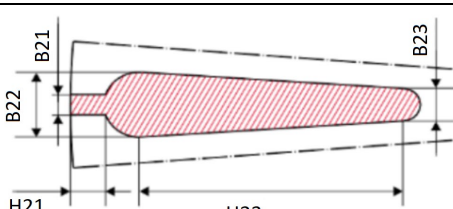
The analytical formulas to calculate those inductances are given below, whereas their detailed explanation can be found in [58]. The end winding leakage inductance can be calculated using the following formula.

$$L_{ew} = \frac{Q_s}{m} q \left(\frac{Z_q}{a} \right)^2 \mu_o l_w \lambda_w, \quad (3.25)$$

$$l_w \lambda_w = 2l_{ew} \lambda_{1ew} + W_{ew} \lambda_w. \quad (3.26)$$

where l_{ew} and W_{ew} are winding axial length outside of the stator and coil span, respectively. λ_{1ew} and λ_{ew} are the corresponding permeance factors which are 0.50 and 0.20 for motor under consideration, Q_s is the number of stator slots, Z_q is the number of conductors per slot, m is the number of stator phases, a is the number of parallel paths per phase and q is the number of slots per pole and phase.

Table 3.4. Slots dimensions of the machine under the investigation [IV].

Slot	Geometry	Dimensions (mm)
Sator		<ul style="list-style-type: none"> • B11 (2.8) • B12 (4) • B13 (6.8) • H1 (28.3) • H11 (0.7) • H13 (24)
Rotor		<ul style="list-style-type: none"> • B21 (1) • B22 (4.4) • B23 (2) • H21 (0.2) • H23 (12)

The slot leakage-inductance depends upon the geometry of the stator-slots and is calculated using the following formula.

$$L_q = \mu_o l \frac{Q_s}{m} \left(\frac{Z_q}{a} \right)^2 \lambda_u, \quad (3.27)$$

where λ_u is the permeance of the stator slot and can be calculated as:

$$\lambda_u = \frac{H_{13} + (B_{13}/2)}{3B_{13}} + \frac{H_{11}}{B_{11}} + \frac{H_1 - H_{11} - H_{13} - (B_{13}/2)}{B_{13} - B_{11}} \ln \frac{B_{13}}{B_{11}}, \quad (3.28)$$

where “H” and “B”s are dimensions of the slots, as shown in Table 3.4.

The air-gap leakage inductance is calculated using the following formula.

$$L_g = \sigma_\delta L_m, \quad (3.29)$$

where leakage factor σ_δ depends upon the number of the poles of the machine. It decreases with the increase in slots per pole and phase. For a 3 phase and 48-slot induction motor, the leakage factor is taken as 0.01 for four-pole and 0.0025 for two poles. The tooth tip and skewing leakage inductances are neglected, as they are negligible compared to end winding, slot, and air gap leakage inductances.

The end-ring leakage inductance of the rotor can be calculated as:

$$L_e = \mu_o \frac{nb}{3mP^2} \left((l_{bar} - l_s) + v \frac{\pi D_r}{2P} \right), \quad (3.30)$$

where $v = 0.36$ for two-pole and $v = 0.18$ for more than two-pole machines.

d) Inductances

I. Stator self-inductance

The self and mutual inductances associated with various coils are calculated using a conventional winding function approach [18][X].

$$L_{ij}(\theta) = \mu_o r l \int_0^{2\pi} g^{-1}(\varphi, \theta) N_i(\varphi, \theta) N_j(\varphi, \theta) d\theta, \quad (3.31)$$

where $L_{ij}(\theta)$ is the inductance between phases i and j at a specific rotor position, θ is the rotor's angular position to some reference point, φ is some point along the air gap with respect to the stator. $g^{-1}(\varphi, \theta)$ is the inverse air gap function, $N_i(\varphi, \theta)$ is the winding function of the i th coil. The winding function of any phase can be calculated as [59].

$$N_i(\varphi, \theta) = n_i(\varphi, \theta) - \langle n_i(\varphi, \theta) \rangle, \quad (3.32)$$

where $n_i(\varphi, \theta)$ is the turn function of the coil, which is spatially distributed along the stator or rotor surface and $\langle n_i(\varphi, \theta) \rangle$ is the average of this turn function. Since the shape of the turn function depends upon the reference point, it is advisable to make it so that it fulfills the even symmetry as in equation (3.33).

$$N_i(\theta^*) = N_i(-\theta^*), \quad (3.33)$$

$$\int_0^{2\pi} N_i(\theta^*) d\theta^* = 0, \quad (3.34)$$

where $\vartheta^* = 0$, is the unique angle for which $N_i(0)$ has a maximum value and ensures the function's even symmetry. However, this problem can be solved by transforming the integral-based winding function formula into the mean value equation described in the subsequent sections.

For a full pitch sinusoidal distributed stator winding, the per phase winding function can be represented by the following equation, as shown in Figure 3.9.

$$N_i(\theta_e) = \frac{N_s}{p} \cos(\theta_e), \quad (3.35)$$

N_s is the effective number of turns per phase in the stator, p is the number of poles and θ_e is the electrical angle.

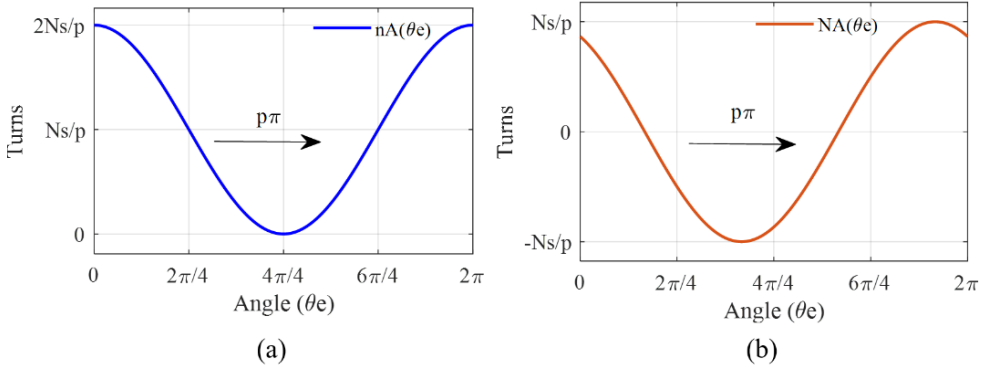


Figure 3.9. (a) The simplified turn function of the stator, (b) The corresponding winding function.

For a constant air gap, the magnetization inductance can be calculated as in (3.36). Whereas the magnetization inductance is the inductance of a single-phase without considering the rest of the phases plus its leakage inductance.

$$L_m = \frac{\mu_o r l}{g} \int_0^{p\pi} \left(\frac{N_s}{p} \cos(\theta_e) \right)^2 d\theta_e, \quad (3.36)$$

For even wave symmetry, the number of cycles can be reduced to half by multiplying the integral by 2.

$$L_m = \frac{\mu_o r l}{g} 2 \int_0^{p\pi/2} \left(\frac{N_s}{p} \cos(\theta_e) \right)^2 d\theta_e, \quad (3.37)$$

$$L_m = \frac{\mu_o r l}{g} \left(\frac{p}{2} \right) \left(\frac{N_s}{p} \right)^2 \pi, \quad (3.38)$$

With the same windings in all stator phases, all the rest of the phase's self-inductance can be considered the same and symmetrical.

$$L_{AA} = L_{BB} = L_{CC} = (L_m + L_{ls}), \quad (3.39)$$

II. Stator mutual inductances

Different stator phase windings are α ($2\pi/3$) electrical radians apart from each other, as shown in Figure 3.10. The mutual inductance can be calculated as follows.

$$L_{AB} = \frac{\mu_o r l}{g} \int_0^{p\pi} \left(\frac{N_A}{p} \cos(\theta_e) \frac{N_B}{p} \cos(\theta_e + \alpha) \right) d\theta_e, \quad (3.40)$$

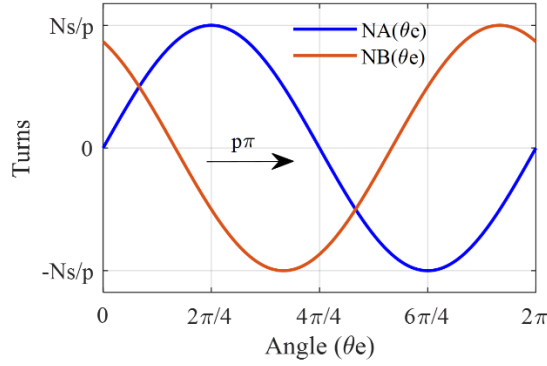


Figure 3.10. The corresponding winding function of two phases to calculate mutual inductances.

After integration and simplification:

$$L_{AB} = -\frac{\mu_o r l}{g} \frac{N_A N_B}{p} \frac{1}{4} \pi, \quad (3.41)$$

For ease of implementation, this equation can be converted as a function of magnetization inductance.

$$L_{AB} = -\frac{\mu_o r l}{g} \frac{N_A N_B}{p} \frac{1}{4} \pi = -\frac{L_m}{2}, \quad (3.42)$$

So, for a symmetrical three-phase system, the mutual inductances are half of the magnetization inductance with negative polarity.

$$L_{AB} = L_{BC} = L_{CA} = -\frac{L_m}{2}, \quad (3.43)$$

III. Rotor to rotor self and mutual inductances

The following conditional analytical function represents the turn function of one rotor loop.

$$n(\theta_e) = \begin{cases} 1, & \theta_i \leq \theta_e \leq \theta_i + \alpha_r \\ 0, & \theta_i > \theta_e > \theta_i + \alpha_r \end{cases}, \quad (3.44)$$

$$\langle n(\theta_e) \rangle = \frac{1}{p\pi} \int_{\theta_i}^{\theta_i + \alpha_r} 1. d\theta_e, \quad (3.45)$$

$$\langle n(\theta_e) \rangle = \frac{\alpha_r}{p\pi}, \quad (3.46)$$

where $\alpha_r = 2\pi/n_b$ is the angle between two consecutive rotor bars. The following equation shows the winding function of a single loop analytically shown in Figure 3.11.

$$N_r(\theta_e) = \begin{cases} -\frac{\alpha_r}{p\pi}, & 0 \leq \theta_e < \theta_i \\ 1 - \frac{\alpha_r}{p\pi}, & \theta_i \leq \theta_e \leq \theta_i + \alpha_r \\ -\frac{\alpha_r}{p\pi}, & \theta_i + \alpha_r < \theta_e \leq p\pi \end{cases}, \quad (3.47)$$

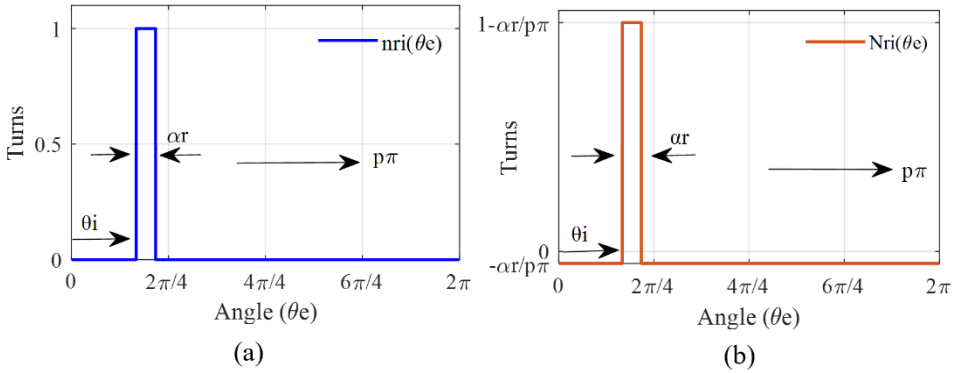


Figure 3.11. (a) The rotor turn function of a single loop, (b) The corresponding winding function.

The following equation shows how to calculate the self-inductance of the rotor's kth loop.

$$L_{rkk} = \frac{\mu_o r l}{g} \int_0^{p\pi} (N_r(\theta_e))^2 d\theta_e, \quad (3.48)$$

$$\begin{aligned} &= \frac{\mu_o r l}{g} \left[\int_0^{\theta_i} \left(-\frac{\alpha_r}{p\pi} \right)^2 d\theta_e + \int_{\theta_i}^{\theta_i + \alpha_r} \left(1 - \frac{\alpha_r}{p\pi} \right)^2 d\theta_e + \int_{\theta_i + \alpha_r}^{p\pi} \left(-\frac{\alpha_r}{p\pi} \right)^2 d\theta_e \right] \\ L_{rkk} &= \frac{\mu_o r l}{g} \left[\alpha_r - \left(\frac{\alpha_r^2}{p\pi} \right) \right] \\ L_{rkk} &= \frac{2p}{\pi} \left(\frac{1}{N_s} \right)^2 L_m \left[\alpha_r - \left(\frac{\alpha_r^2}{p\pi} \right) \right] \left(\frac{p}{2} \right). \end{aligned} \quad (3.49)$$

Similarly, the mutual inductance between any two-rotor loops can be calculated based on the winding functions shown in Figure 3.12 (a).

$$\begin{aligned} L_{rni} &= \frac{\mu_o r l}{g} \int_0^{p\pi} (N_{rn}(\theta_e))(N_{ri}(\theta_e)) d\theta_e, \quad (3.50) \\ &= \frac{\mu_o r l}{g} \left[\int_0^{\alpha_r} \left(1 - \frac{\alpha_r}{p\pi} \right) \left(-\frac{\alpha_r}{p\pi} \right) d\theta_e + \int_{\alpha_r}^{\theta_i} \left(-\frac{\alpha_r}{p\pi} \right)^2 d\theta_e \right. \\ &\quad \left. + \int_{\theta_i}^{\theta_i + \alpha_r} \left(1 - \frac{\alpha_r}{p\pi} \right) \left(-\frac{\alpha_r}{p\pi} \right) d\theta_e + \int_{\theta_i + \alpha_r}^{p\pi} \left(-\frac{\alpha_r}{p\pi} \right)^2 d\theta_e \right] \\ L_{rni} &= \frac{\mu_o r l}{g} \left[-\frac{\alpha_r^2}{p\pi} \right]. \end{aligned} \quad (3.51)$$

As discussed earlier, the conversion of the inductance expressions as a function of the magnetization inductances reduces the complexity during their implementation in the simulation program. Equation (3.51) can be transformed as follows:

$$L_{rni} = \left(\frac{1}{N_s} \right)^2 L_m \left[-\frac{2\alpha_r^2}{\pi^2} \right] \left(\frac{p}{2} \right), \quad (3.52)$$

$$L_{rni} = \frac{2p}{\pi} \left(\frac{1}{N_s} \right)^2 L_m \left[-\frac{\alpha_r^2}{p\pi} \right] \left(\frac{p}{2} \right), \quad (3.53)$$

IV. Stator to rotor mutual inductances

The mutual inductance between the rotor and stator is the function of the rotor's position and can be calculated using the stator and rotor winding functions, as shown in Figure 3.12 (b).

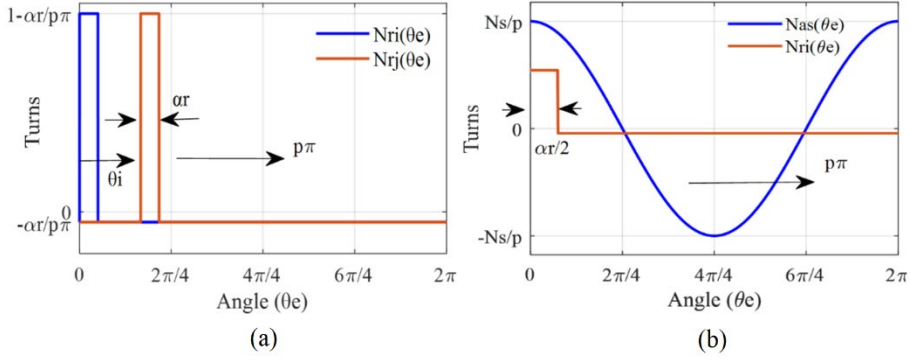


Figure 3.12. (a) The rotor winding functions of two loops to calculate mutual inductances, (b) The rotor and stator winding functions with even symmetry for the calculation of mutual inductances.

$$L_{asri} = \frac{\mu_o r l}{g} \int_0^{p\pi} (N_{as}(\theta_e))(N_{ri}(\theta_e))d\theta_e, \quad (3.54)$$

Even symmetry can be exploited to reduce the limit of integration. This can be done by multiplying the integration function by “p” while dividing the absolute limit with the same number.

$$L_{asri} = \frac{\mu_o r l N_s}{g p} p \left[\int_0^{\alpha_r/2} \left(1 - \frac{\alpha_r}{p\pi} \right) \cos(\theta_e) d\theta_e + \int_{\alpha_r/2}^{\pi} \left(-\frac{\alpha_r}{p\pi} \right) \cos(\theta_e) d\theta_e \right],$$

$$L_{asri} = \frac{\mu_o r l}{g} N_s [\sin(\alpha_r/2)], \quad (3.55)$$

$$L_{asri} = \frac{\sin(\alpha_r/2) 2p}{N_s \pi} L_m. \quad (3.56)$$

Since the rotor is rotating, the above equation can be represented in a general way as a rotor position function, as shown below.

$$L_{sri}(\theta_r) = \frac{\sin\left(\frac{\alpha_r}{2}\right) 2p}{N_s \pi} L_m \cos\left(\theta_r + (i-1)\alpha_r + \frac{\alpha_r}{2}\right), \quad (3.57)$$

The last term ($\alpha_r/2$) is for completing the angle skipped for symmetry, θ_r is the rotor position, and “i” represents the i^{th} rotor bar.

3.2.3 Torque and speed

The final equations in the form of matrices can be represented as:

$$\begin{bmatrix} V_s \\ 0 \end{bmatrix} = \begin{bmatrix} R_s & 0 \\ 0 & R_r \end{bmatrix} \begin{bmatrix} I_s \\ I_r \end{bmatrix} + \frac{d}{dt} \begin{bmatrix} L_{ss} & L_{sr} \\ L_{rs} & L_{rr} \end{bmatrix}, \quad (3.58)$$

From where currents can be calculated as:

$$\begin{bmatrix} I_s \\ I_r \end{bmatrix} = \begin{bmatrix} L_{ss} & L_{sr} \\ L_{rs} & L_{rr} \end{bmatrix}^{-1} \int \left[\begin{bmatrix} V_s \\ 0 \end{bmatrix} - \begin{bmatrix} R_s & 0 \\ 0 & R_r \end{bmatrix} \begin{bmatrix} I_s \\ I_r \end{bmatrix} \right] dt, \quad (3.59)$$

Since,

$$T_e = I_s^T \left(\frac{d}{d\theta} L_{rs} \right) I_r, \quad (3.60)$$

In the matrices form for a p pole machine:

$$T_e = \frac{1}{2} \left(\frac{p}{2} \right) \begin{bmatrix} I_s \\ I_r \end{bmatrix}^T \frac{d}{d\theta} \begin{bmatrix} L_{ss} & L_{sr} \\ L_{rs} & L_{rr} \end{bmatrix} \begin{bmatrix} I_s \\ I_r \end{bmatrix}, \quad (3.61)$$

$$T_e = \frac{1}{2} \left(\frac{p}{2} \right) \begin{bmatrix} I_s^T & I_r^T \end{bmatrix} \begin{bmatrix} 0 & \frac{d}{d\theta} L_{sr} \\ \frac{d}{d\theta} L_{rs} & 0 \end{bmatrix} \begin{bmatrix} I_s \\ I_r \end{bmatrix}, \quad (3.62)$$

$$T_e = \frac{1}{2} \left(\frac{p}{2} \right) \left(I_r^T \frac{d}{d\theta} L_{rs} I_s + I_s^T \frac{d}{d\theta} L_{sr} I_r \right), \quad (3.63)$$

where p is the number of poles while the derivative of L_{ss} and L_{rr} is zero as they are constant. Moreover, unlike equation (3.60), the equations (3.61)-(3.62) are divided by 2 to remove the effect of double terms as evident in (3.63). Finally, the rotor speed can be calculated using the following equation.

$$J \frac{d}{dt} \omega_m = T_e - T_L - B_f \omega_m, \quad (3.64)$$

where J is the moment of inertia of the rotor, ω_m is the rotor's angular velocity. T_e is the generated torque, T_L is the loading torque, B_f is the friction coefficient.

3.2.4 Results

Unlike two-axis theory-based models, the WFM-based model is adequate to simulate stator and rotor-related observables without the need for reference transformation. Figure 3.13 shows the dynamic analysis of motor for some global parameters under no-load and loaded conditions. The currents of the first fifteen rotor bars are shown in figure 3.13 (a). The rotor current's magnitude and frequency are the functions of slip, evident in Figure 3.13 (a). The magnitude of current increases considerably upon the application of load at time 6sec with the increase in frequency as a function of slip and supply frequency (sf_s). The stator currents are shown in Figure 3.13 (b), where the load effect is evident. The rotor speed is presented in Figure 3.13 (c), where the brown line shows the synchronous speed (157 rad/sec) for the four-pole machine, while the blue line represents the rotor's mechanical speed. The dynamic response of generated torque is given in Figure 13.3 (d). it shows a peak generated torque of 220N-m, while in the steady-state regime, it is the function of load. Under the no-load condition, it is minimal to produce a slight slip to overcome friction. The speed-torque curve is shown in Figure 3.14, where the shift of operating point from no-load to load and again back can be easily studied. The broken bar is simulated by increasing the resistance of relevant entries in

the rotor resistance matrix, as shown in equation (3.10); however, the detail is coming in the next section. In the faulty rotor, the speed and torque are no longer constant but start oscillating, as shown in Figure 3.14. In this model, the only harmonics are because of the faulty rotor while the rest of the harmonics are neglected for simplicity.

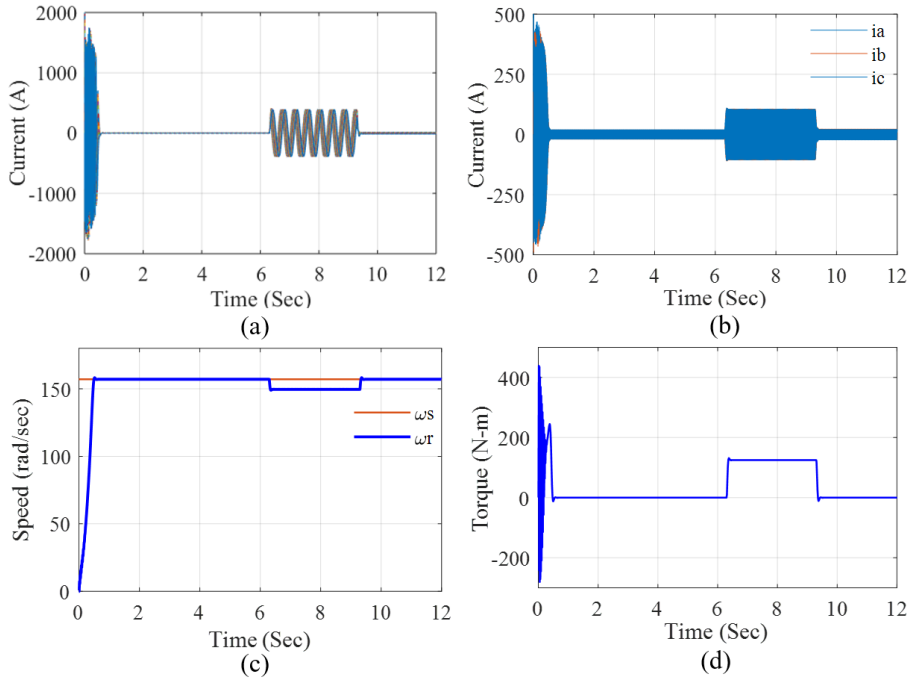


Figure 3.13. (a) The rotor currents of first 15 bars, (b) The stator currents under no-load and load conditions, (c) The rotor speed, (d) generated torque.

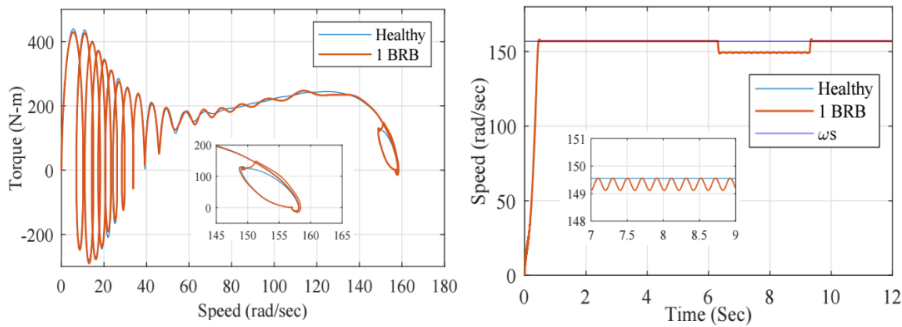


Figure 3.14. The speed-torque curve and rotor speed under healthy and one broken bar cases.

3.2.5 Attributes of WFA

Advantages

- Comprehensive
- Fast
- Least ill-posed due to small-sized matrices as compared to FEM or reluctance models
- Compatible for the simulation of the following faults

- Broken rotor bars and end rings
- Intern stator short-circuit faults
- Unbalanced power supplies

Compatible with

- Drives
- Hardware in the loop environment
- Parameters estimation
- Steady-state and transient analysis
- Design to some extent
- Inverse mapping from observables to the unknowns.

Limitations

- Sinusoidal stator winding distribution. However, it can be converted to the actual winding with the Fourier summation of various harmonics. However, it leads to the self-defined number of harmonics and their amplitudes.
- Constant air gap. The inverse air gap can be included using the Taylor series, but it will lead to the approximation as its solution leads to an infinite sum of higher-order terms.
- Not possible to simulate eccentricity fault with constant inverse air gap permeance function.
- The slotting effects of rotor and stator cannot be simulated accurately with constant inverse air gap permeance function.

Recommendations

- Modified winding function approach.

3.3 The modified winding function-based model

3.3.1 Introduction

The winding function theory has been extensively used in literature to model and analyze electrical machines summarized in the previous section in the form of premade equations suitable to simulate any SQIM. The authors in [60]-[64] are the pioneers of this field. They used it to model and analyzed two-phase induction motors, linear inductance motors, three-phase squirrel cage induction machines, and synchronous reluctance motors.

The authors in [16] have extended the winding function approach and made it suitable for implementing a non-uniform air gap. Using this modified winding function approach, the stator and rotor slots openings and eccentricity faults can be easily modeled. Unlike the analytical approximation as in [16] and [65], in the proposed model, the air gap permeance is calculated numerically by considering the slot openings as a function of rotor and stator angles. Moreover, the integration-based functions are reduced to the mean value function for complexity reduction. For more accurate results, the air gap center is not taken as constant but calculated as a mean function of stator and rotor air gap functions. The implementation strategy is shown in Figure 3.15, where the entire scheme is divided into online and offline calculation portions. In the offline portion, all inductances and resistances are calculated at different rotor positions, while in the online portion, the performance parameters are simulated [II],[IV].

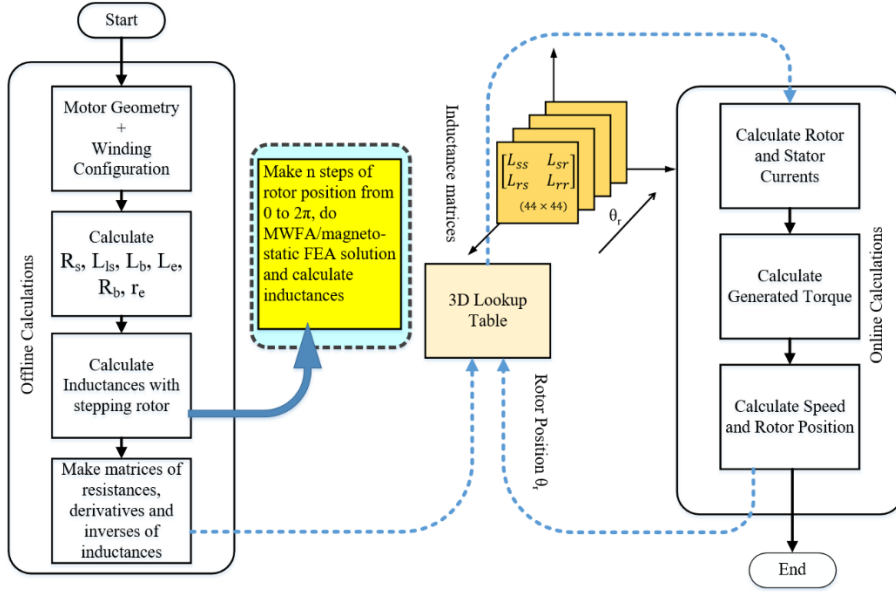


Figure 3.15. The flowchart diagram of modeling and simulation.

a) Inductances calculation using MWFA

Since the inductances are also dependent on the inverse air gap permeance P , which is not constant but is a function of stator and rotor slot openings, the (3.32) can be modified as [16].

$$N_i(\alpha) = \left(n_i(\alpha) - \frac{\langle P n_i \rangle}{\langle P \rangle} \right), \quad (3.65)$$

where $\langle f \rangle$ is the average or mean value as shown below:

$$\langle f \rangle = \frac{1}{2\pi} \int_0^{2\pi} f(\theta) \cdot d\theta, \quad (3.66)$$

For a p pole machine, the formula can be modified as follows, but the answer will remain the same because (2π) mechanical angle is equivalent to $(p\pi)$ electrical angle.

$$\langle f \rangle = \frac{1}{p\pi} \int_0^{p\pi} f(\theta_e) \cdot d\theta_e, \quad (3.67)$$

So, the Equ. (3.31) can be modified in electrical angle as follows:

$$L_{ij}(\theta_e) = \mu_o r l \int_0^{p\pi} P(\theta_e, \alpha) N_i(\theta_e, \alpha) n_j(\theta_e, \alpha) d\theta_e, \quad (3.68)$$

Which can be written as:

$$L_{ij}(\theta_e) = p\pi\mu_o r l \langle P(\theta_e, \alpha) N_i(\theta_e, \alpha) n_j(\theta_e, \alpha) d \rangle, \quad (3.69)$$

Or,

$$L_{ij}(\theta e) = p\pi\mu_o r l \left[\frac{\langle P(\theta e, \alpha) n_i(\theta e, \alpha) n_j(\theta e, \alpha) d \rangle - \langle P((\theta e, \alpha) n_i(\theta e, \alpha) \rangle \langle P((\theta e, \alpha) n_j((\theta e, \alpha) \rangle}{\langle P((\theta e, \alpha) \rangle} \right], \quad (3.70)$$

$$L_{ij}(\theta e) = p\pi\mu_o l \langle r_g((\theta e, \alpha) P((\theta e, \alpha) N_i((\theta e, \alpha) n_j((\theta e, \alpha) \rangle, \quad (3.71)$$

b) Air gap calculation

The inverse air gap permeance P can be defined as:

$$P(\theta e, \alpha) = \frac{1}{g_s(\theta e) + g_r(\theta e, \alpha)}, \quad (3.72)$$

where $g_s(\vartheta_e)$, $g_r(\vartheta_e, \alpha)$, $(g_s(\vartheta_e) + g_r(\vartheta_e, \alpha))$ and $P(\vartheta_e, \alpha)$ are air gaps associated with the stator, rotor, equivalent and inverse air gap permeance functions in stator frame of reference respectively. Moreover, ϑ_e is the stator's electrical angle from any fixed reference point, and α is the rotor angle in the stator reference frame.

The stator and rotor-linked air gaps are calculated by taking the center of the machine's air gap as a reference line. In this way, the total air gap can be divided into the stator and rotor-associated air gaps. The slot opening without any conductor of winding on the stator side is used to change the air gap as a function of the stator's electrical angle. This change is in the form of an increase in the air gap, equivalent to the slot opening height without winding. Similarly, rotor bar depth is used to change the rotor's associated air gap. Both air gaps are added together to get the equivalent air gap at each rotor position. These air gap functions for one stator and rotor slot can be defined as follows [IV]:

$$g_s(\theta e) = \begin{cases} r_g + h_{11}, & 0 \leq \theta e \leq B_{11} \\ r_g, & B_{11} < \theta e \leq (B_{11} + B_{tt}) \end{cases}, \quad (3.73)$$

$$g_r(\theta e, \alpha) = \begin{cases} r_g + h_{21}, & 0 \leq \theta e \leq B_{21} \\ r_g, & B_{21} < \theta e \leq (B_{11} + B_{rt}) \end{cases}, \quad (3.74)$$

where B_{11} , B_{tt} , B_{21} , B_{rt} , h_{11} , h_{21} , r_g are the width (in terms of angle) of the stator slot opening, stator tooth tip, rotor slot opening, rotor tooth tip, stator slot depth without winding, the rotor bar depth, and the height of air gap center respectively as given in Table 3.4. Figure 3.16 (a)-(b) shows the stator and rotor-associated air gaps until (2π) electrical angle, which is equivalent to half of the mechanical geometry since the machine is four-pole. The net air gap with its inverse function at a specific position is also shown in Figure 3.16 (c)-(d), where the distinguished (extended) lines are representing the points where rotor and stator slot openings overlap with each other. r_g is the average air gap radius and can be calculated as:

$$r_g = \frac{(D_s - D_r)}{4}, \quad (3.75)$$

For the inclusion of the effect of rotor and stator slots openings, the above equation can be modified as follows:

$$r_g(\theta e, \alpha) = r_g + \frac{(g_s(\theta e) + g_r(\theta e, \alpha))}{2}, \quad (3.76)$$

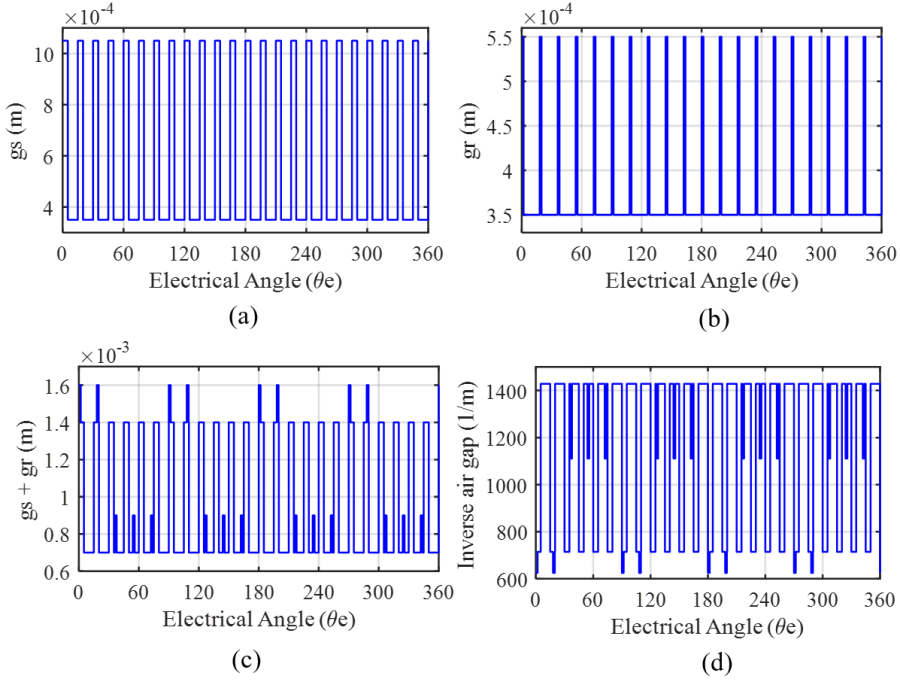


Figure 3.16. The air gap function of (a) the stator (g_s), (b) the rotor (g_r), (c) the net equivalent ($g_s + g_r$), and (d) the inverse air gap function at a specific rotor position.

c) Stator and rotor winding functions

The turn function of the stator phase 'a' can be defined as a conditional analytical expression, as given below.

$$n_{as}(\theta) = \begin{cases} Z_q * i, & i = 1:1:Q_{pp} \\ Q_{pp} * Z_q, & i = (Q_{pp} + 1):1:3 * Q_{pp} \\ Z_q(Q_{pp} - i), & i = (3 * Q_{pp} + 1):1:4 * Q_{pp} \\ 0, & i = (4 * Q_{pp} + 1):1:2 * Q_s/p \end{cases}, \quad (3.77)$$

Z_q is the number of conductors per stator slot, Q_{pp} is the number of slots per pole and phase, Q_s is the total number of stator slots, and i is the integer. This conditional analytical function can be used to generate the turn function of the stator. The remaining two-turn functions can be produced by shifting it to $(2\pi/3)$ and $(4\pi/3)$, respectively. In this case study, there are 17 conductors per slot and 4 slots per pole and phase.

As discussed previously, the corresponding winding function can be calculated by subtracting the respective mean value from the turn function. The stator and rotor

winding functions are shown in Figure 3.17. The rotor turn and winding functions are discussed in detail in the previous section.

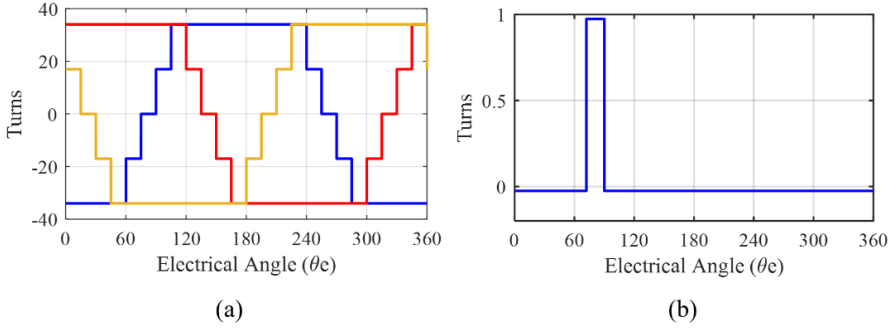


Figure 3.17. The winding functions (a) a three-phase stator, (b) one loop of the rotor.

3.3.2 Results

a) Inductances

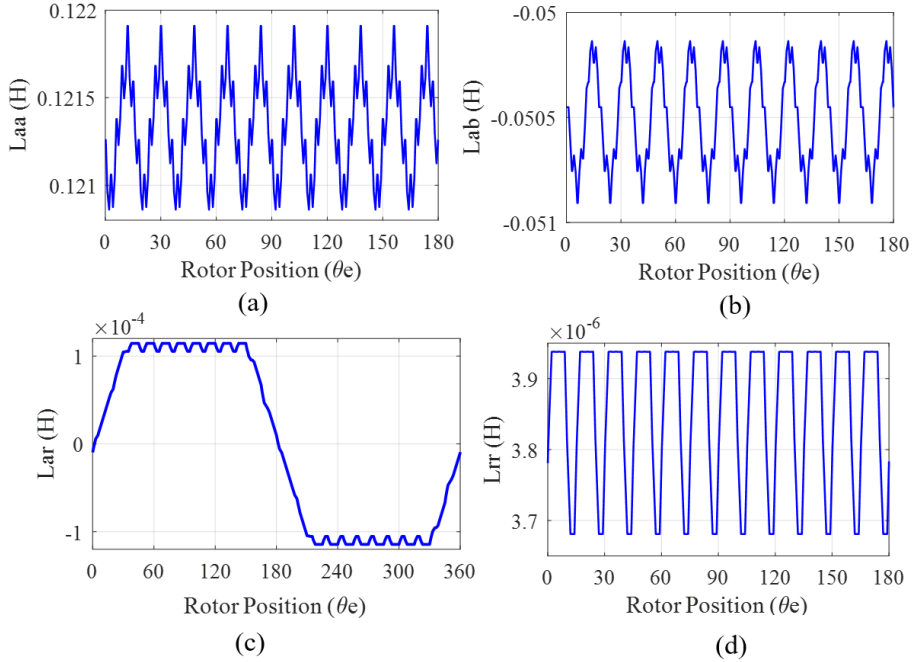


Figure 3.18. The calculated inductances, (a) stator to stator self (L_{aa}), (b) stator to stator mutual (L_{ab}), (c) stator to the rotor (L_{ar}), and (d) rotor to rotor (L_{rr}) concerning the rotor position.

The stator and rotor's self and mutual inductances are no longer constant but are the rotor position's functions. Similarly, stator and rotor mutual inductances are no more pure sinusoids but contain the winding and slotting harmonic's impact. Various self and mutual inductances as a function of rotor position are shown in Figure 3.18, where the effect of slot openings is evident. The rotor position is in electrical degrees, which is 360 degrees per pole pair.

b) Inductance derivatives

Figure 3.19 shows the derivatives of the stator and rotor inductance profiles. Unlike the WFA based model, the derivatives of self-inductance are no longer zero because of the changing inductance profiles as a function of the rotor position. The rate of change or derivative, increases with the increased change in the corresponding inductance.

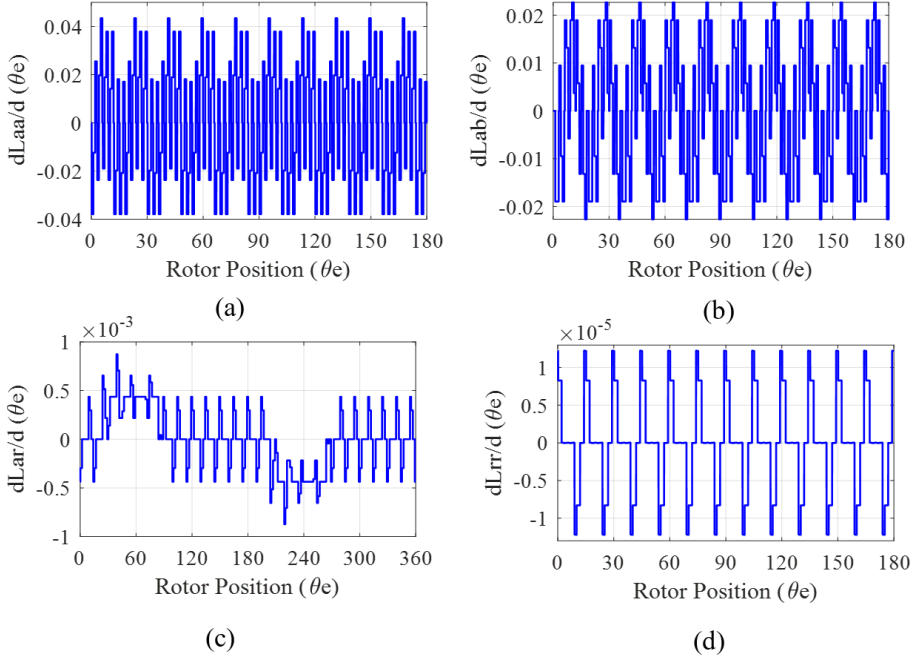


Figure 3.19. The derivative of the (a) stator to stator self (L_{aa}), (b) stator to stator mutual (L_{ab}), (c) stator to the rotor (L_{ar}), and (d) rotor to rotor (L_{rr}) with respect to the rotor position.

c) Torque and speed

The rotor speed and the generated torque both in the steady-state and transient regime are shown in Figure 3.20 and Figure 3.21, respectively.

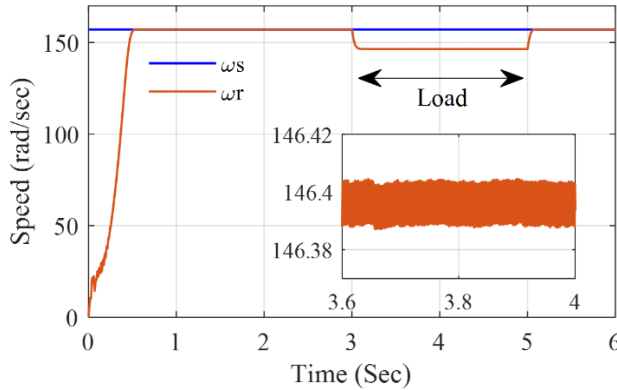


Figure 3.20. The rotor speed.

The effect of spatial harmonics is significant under load conditions, as shown in the zoomed window. This is due to the relation between the slip and slotting frequency components. Under loading conditions, the slip increase is visible as a difference between synchronous speed (ω_s) and rotor speed (ω_r) in Figure 3.20. This increase in slip increases the amplitude of rotor frequencies with a resultant increase in the torque and speed ripples.

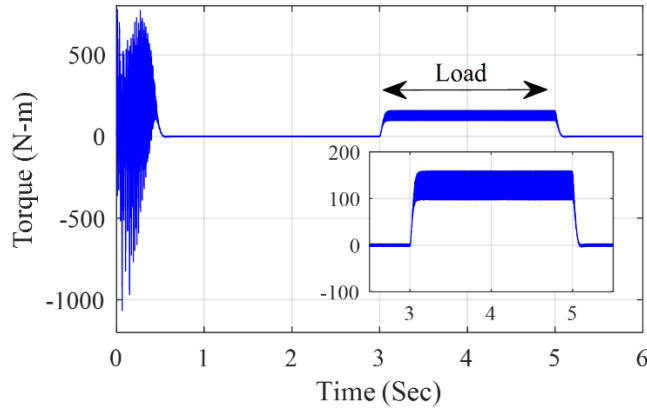


Figure 3.21. The generated torque.

d) Stator currents

Figure 3.22 (a) shows the dynamic response of the stator's current under the transient and steady-state regime. The current is not pure sinusoidal but contains the winding and spatial harmonics shown in Figure 3.22(b).

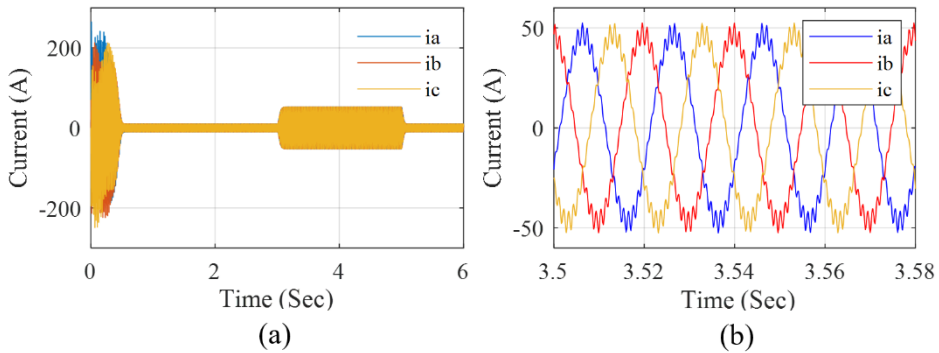


Figure 3.22. (a) Stator's current dynamic response, (b) Stator's current at a load of 125N-m.

e) Rotor currents

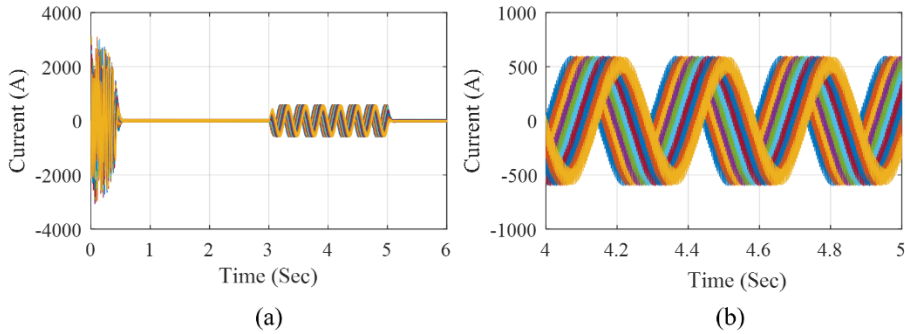


Figure 3.23. (a) Current of first ten rotor bars, (b) rotor bars current at rated load.

According to the induction motor's fundamental working principle, the generated voltage and current in rotor bars depend upon the changing flux linkage. This rate of change of flux depends upon the slip, which is the function of load. Figure 3.23 (a) depicts the dependence of the rotor current's magnitude and frequency on load. The current of each rotor bar is shifted because of the mechanical separation between two consecutive bars. Other than the fundamental rotor frequency component, these bar currents also contain spatial harmonics, as shown in Figure 3.23 (b). The 180 degrees phase shift between the currents of rotor bars under two consecutive poles, as shown in Figure 3.24 (b), further proves the model's validity. The change in the rotor bar current at the load application is visible in Figure 3.24 (a). During the no-load condition, the frequency of the fundamental component is minimal because of low slip. However, the low amplitude high-frequency components are present in the current, as shown in the zoomed window. Those components are because of the asynchronously rotating magnetic field due to high-frequency spatial components. When the load is applied at 3 Sec, the fundamental component increases both in amplitude and frequency.

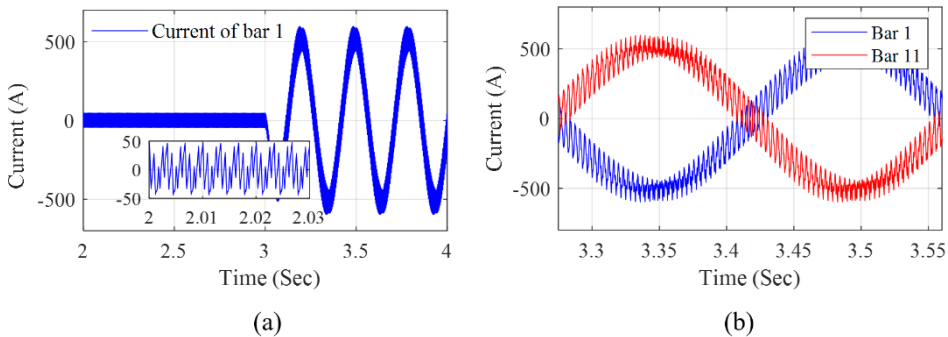


Figure 3.24. (a) Change in bar current at the application of load at 3sec, (b) The currents of rotor bars at one pole pitch.

3.4 Finite Element Method (FEM) in comparison with MWFA

3.4.1 Introduction

The finite element method (FEM) is a numerical technique to solve partial differential equations or boundary value problems. FEM divides any large system into n-small parts called finite elements. Each finite element is represented with an adequate number of nodes. The solution of all those nodes leads towards the overall solution to the problem. With the increase in computational power, numerical models such as FEM are gaining more and more popularity in the field of modeling and simulations. Those models are good approximations of an actual system, as they consider all possible parameters, but at the cost of complexity, long computational time, and ill-posedness. The numerical model of the induction motor relies on Maxwell's equations:

$$\nabla \times E = -\frac{\partial B}{\partial t}, \quad (3.78)$$

$$\nabla \times H = J + \frac{\partial D}{\partial t}, \quad (3.79)$$

$$H = \nu B, \quad (3.80)$$

$$J = \sigma E, \quad (3.81)$$

where E is the electric field strength, B is the magnetic flux density, D is displacement current, H is the magnetic field strength, J is the current density, ν is the magnetic reluctivity of material and σ is its electric conductivity.

By assuming that the magnetic field lies in an x-y plane, varies sinusoidally in time, and induces currents in the z-direction, the vector potential A distributes in the machine according to the following equation [66]:

$$\frac{\partial}{\partial x} \left(\frac{1}{\mu} \right) \frac{\partial A}{\partial x} + \frac{\partial}{\partial y} \left(\frac{1}{\mu} \right) \frac{\partial A}{\partial y} - s \frac{\partial}{\partial t} (\sigma A) + J = 0, \quad (3.82)$$

Suppose the rotor and stator laminations' conductivity is considered zero, and the reluctivity of conducting regions is equivalent to a vacuum. In that case, the electric scalar potential and voltage equation of a conductor can be represented as [67][68]:

$$\nabla \varphi = -\frac{u}{l} e_z, \quad (3.83)$$

$$u = iR + R \oint \sigma \frac{\partial A_z}{\partial t} \cdot ds, \quad (3.84)$$

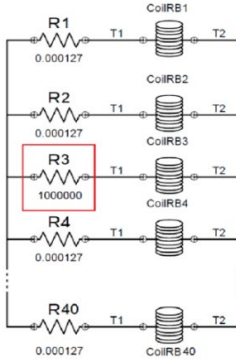
where u is the voltage over the conductor of length l , i is current, R is the dc-resistance. Almost all FEM based software rely on Maxwell equations for the solution of an electromagnetic problem. Some results that are simulated using FEM and proposed model is presented in the following section while their detailed description is in the next chapter.

3.4.2 Broken bars simulation in FEM and proposed model

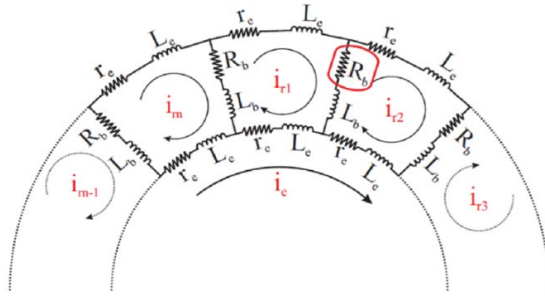
The broken bars are simulated by adding a series resistance of 1 MΩ in-circuit editor of FEM in a commercial software (Infolytica) with a considerable number of mesh elements with additional resistance and reactance for the compensation of the end windings [III],[IV]. The same is done by increasing the resistance of the bar-related entries in the resistance matrix of the proposed model (Figure 3.25), which is made using the equivalent rotor circuit model, as shown in Figure 3.26 (a)-(b). The broken bars can be imitated by replacing the bar with air. But it can lead to the problems such as the partially broken bars cannot be simulated; also, the ideal infinite air electrical resistance cannot be adjusted in the analytical resistance matrix. Since the inductances do not depend upon the rotor bar's resistance, they do not need to be calculated again. Changing the resistance matrix's respective elements can simulate the broken bar scenarios, further reducing the simulation time as inductances do not need to be calculated again (unlike commercial FEM).

$$R_{rr} = \begin{bmatrix} 2(R_b + r_e) & -R_b & 0 & 0 & \dots & 0 & \dots & 0 & -R_b & -r_e \\ -R_b & 2(R_b + r_e) & -R_b & 0 & \dots & 0 & \dots & 0 & 0 & -r_e \\ 0 & -R_b & 2(R_b + r_e) & -R_b & \dots & 0 & \dots & 0 & 0 & -r_e \\ \vdots & \vdots & \vdots & \vdots & \vdots & \vdots & \vdots & \vdots & \vdots & \vdots \\ 0 & 0 & 0 & 0 & \dots & 0 & \dots & 2(R_b + r_e) & -R_b & -r_e \\ -R_b & 0 & 0 & 0 & \dots & 0 & \dots & -R_b & 2(R_b + r_e) & -r_e \\ -r_e & -r_e & -r_e & -r_e & \dots & -r_e & \dots & -r_e & -r_e & n_b r_e \end{bmatrix}$$

Figure 3.25. The rotor resistance matrix with broken bar-related entries shown in red.



(a)



(b)

Figure 3.26. (a) The broken bar approximation in Infolytica circuit editor, (b) The cage structure, and the broken bar simulation in the proposed model.

3.4.3 Simulations

The FEM-based simulation of a three-phase induction motor with the parameters given in Tables 3.1 and 3.4 is performed under healthy, one, and two broken rotor bar conditions. Since the simulation is performed using 2D field analysis, the ignored end windings are compensated by adding additional resistances and inductances in series with coils. The per-phase stator coils are series and parallel connections of copper

strands making current density uniformly distributed. The simulation is performed at rated load under constant speed. The flux distribution under healthy and two broken rotor bar conditions is shown in figure 3.27 (a)-(b).

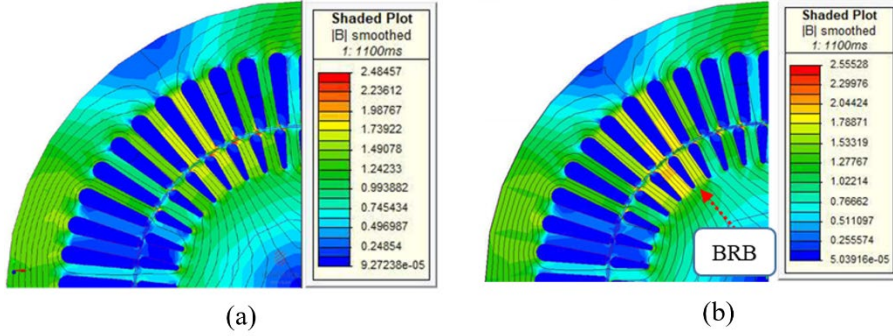


Figure 3.27. (a) Flux distribution under healthy condition, (b) The flux distribution under one broken rotor bar condition.

It is evident that the flux density increases across broken bars, putting the adjacent bars under increased magnetic stress [V][VI][X][68]. The increase in the neighboring bars' current makes the machine vulnerable to harm more bars in time if the fault is not timely diagnosed and repaired.

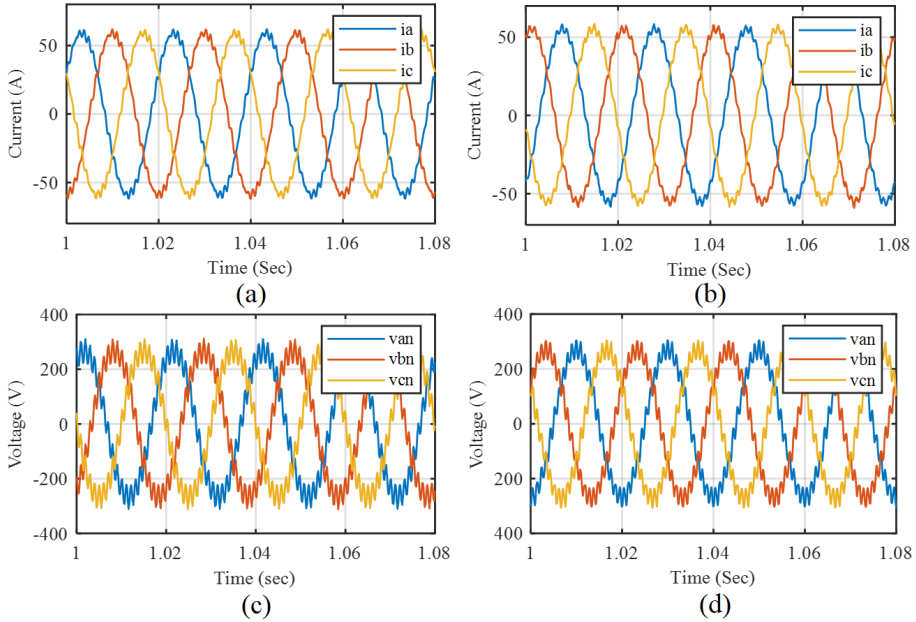


Figure 3.28. (a) The line currents simulated using FEM software, (b) The line currents simulated using the proposed model, (c) The phase voltage calculated using FEM software, (d) The simulated phase voltage using the proposed model.

Figure 3.28 shows the motor's current and phase voltage simulated using FEM and the proposed MWFA model under rated load conditions. In the FEM model, the results are taken with a stepping rotor having a step size of 0.033 ms for two seconds with 5328 mesh elements. The current seems distorted because of time and slot harmonics. The simulation results taken from the proposed model with the same sampling frequency show a good agreement with the results simulated using FEM but with a considerably reduced simulation time given in Table 3.5.

This similarity is because of the inclusion of all potential harmonics' sources, such as the non-sinusoidal distribution of stator and rotor windings and the slotting effects. These calculations are done at rated load (125Nm). Further validation is performed using spectrum analysis and is given in the subsequent chapter.

The simulated speed under healthy and broken rotor bar cases is shown in Figure 3.29. These simulations are done at rated slip (0.066), where the similarity of results is visible. In both FEM (left) and proposed model (right), the speed oscillation increases with the number of broken bars. The generated torque also possesses a minimal difference.

Table 3.5. Comparison of simulation time.

Model	Computer Specs.	Simulation time
MWFA [IV]	Intel(R) Core (TM) i7-7500 CPU	3 minutes
Hybrid with cluster computation [II]		4 hrs
FEM		12 hrs (1-time step / 0.72 Sec)

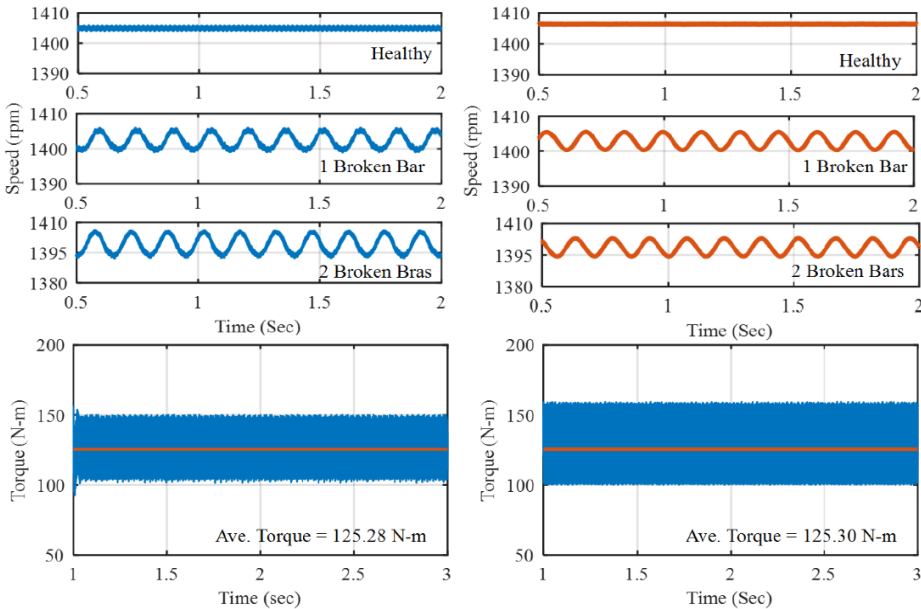


Figure 3.29. The speed and torque simulated using FEM software (left) and the proposed model (right).

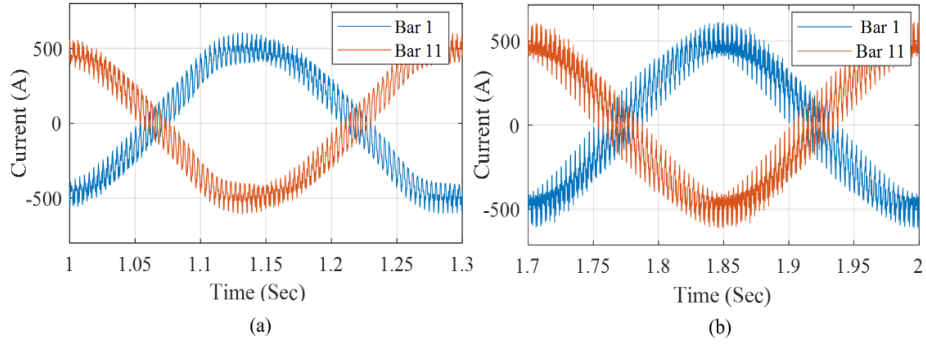


Figure 3.30. (a) The current in rotor bars placed at one pole pitch (FEM), (b) The current in bars at one pole pitch calculated using the proposed model.

The currents in the rotor bars placed at one pole pitch are shifted at an angle of 180 degrees in both FEM and the proposed model, as shown in Figure 3.30 (a)-(b).

3.4.4 Attributes of MWFA

From the results and discussion following attributes can be concluded:

- Unlike most of the work cited previously, where only low-order harmonics are considered in the form of Fourier summation of certain sinusoids with a specific frequency and amplitude. In the proposed model, the actual stator and rotor winding functions are defined in conditional analytical expressions. This approach makes the model independent of the selective number of frequency components and does not limit the spectrum bandwidth.
- The air gap is made as a function of rotor and stator slot openings, including spatial harmonics. Moreover, the inclusion of the air gap as a function of stator and rotor angles makes the model suitable for implementing air gap-related faults, such as eccentricity.
- The inclusion of rotor slot harmonics makes the model suitable for sensor-less speed drive systems. The principal slotting components can be studied and utilized for the estimation of slip.
- The principal slotting harmonics (PSH) have less spectral leakage than the fundamental component, making them a potential candidate for fault detection, even under fewer load conditions. The fault-based frequency components developing near PSH are less vulnerable to be buried under them as it happens near the fundamental component.
- The separate modeling (offline) and simulation parts (online) can further reduce the complexity and calculation time. Once the inductances are calculated, most of the faults can be simulated by making corresponding online environment changes without doing offline calculations again.
- The compatibility of the model with cluster computation makes it suitable to exploit distributed computational resources such as cloud computation. By doing so, the simulation time can be further reduced to a range of seconds [11].
- The model is so generic that most of the fault types, such as broken rotor bars, static and dynamic eccentricity, and stator short circuits, can be simulated.

- In comparison with FEM, the minimal simulation time makes the model suitable for advanced diagnostic algorithms, such as iterations-based estimation of design parameters, hardware-in the- loop, inverse problem theory, and other model-based diagnostic procedures.
- The model is also suitable for the iterative optimization of various design parameters, such as winding functions, slot openings, air gap, etc. The achieved results are in good agreement with the ones taken from the FEM model and laboratory measurements. The detailed comparison is presented in the next chapter.
- As the matrices are very small in dimension as compared to the FEM-based matrices, the solution of inverse mapping can be least ill-posed by producing stable and unique solutions.

3.5 The compatibility with cluster computation

3.5.1 Introduction

As the world moves towards industry 4.0 standards and cloud computation, computational resources are becoming unlimited. These resources can be in the form of software applications, processing power, and data storage. All these resources are essential for big data-based advanced diagnostic techniques such as machine learning [69], deep learning [70], parallel autonomous mining [71], image processing [72], online wireless monitoring through smart sensors [73], and neural networks [74][75][76], etc. The basic building blocks of cloud computation are infrastructure as a service (IaaS), platform as a service (PaaS), and software as a service (SaaS). Those building blocks can be utilized for ample data storage, costume software development, and computer application utilization, respectively [11].

To further reduce simulation time of the proposed analytical and hybrid FEM-analytical, the concept of parallel processing by utilizing the cluster of computers can be exploited. Unlike most of the researches where the simulation speed of the models is increased either by exploiting the symmetry (which is not valid in the case of faulty machines) or by data interpolation using the model order reduction [77][78][79]. The proposed model is compatible for division among several processors working together to solve the problem and send back the results to the client machine. All inductances are calculated by the proposed analytical model or by magneto-static solution (hybrid FEM-analytical) of the machine at several rotor positions. The calculated inductances are saved in the 3D lookup table as a function of the rotor position, as shown by the offline portion in Figure 3.15. The online portion will remain the same for the simulation of observables.

a) Cluster formation

Parallel computing is a form of concurrent computing where several workouts can be performed in overlapping periods. Generally, any significant problem can be divided into n-small problems, which can be solved simultaneously. Unlike traditional serial programs, the divided problem segments should be independent of each other to run on different processors, and the solutions can be combined on the client machine at the end. The general schematic diagram of distributed parallel computation is shown in Figure 3.31.

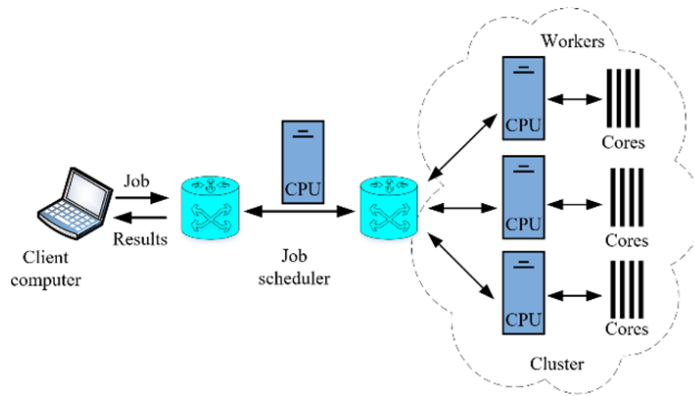


Figure 3.31. The cluster formation and utilization for parallel processing.

The client machines, job scheduler, WIFI or LAN network, and the worker processors are the core parts of the distributed cloud computation. The job scheduler's function is to divide and distribute the segments of the bigger problem into cluster computers. The cluster computers can further divide their portion among their cores in the same manner.

b) Implementation strategy

Since the solution at a distinct rotor position is independent of the solution at subsequent rotor positions, the total “n” rotor steps can be divided into various segments. The proposed analytical or FEM based magneto-static problems of different rotor position sectors such as, $(0 \rightarrow \theta_i)$, $(\theta_i \rightarrow \theta_j)$, ..., $(\theta_n \rightarrow \theta_{n+1})$, $(\theta_{n+1} \rightarrow 2\pi)$ can be divided among the workers for parallel processing. All the nested loops in the proposed algorithms are prepared so that the solution of each step is independent of the solution of subsequent rotor steps [11].

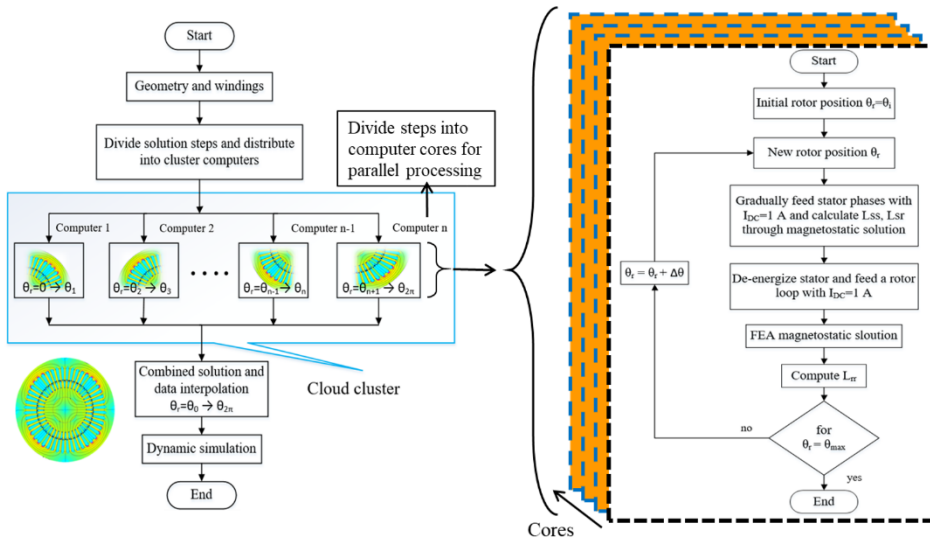


Figure 3.32. The division of rotor steps among various computers and their cores for parallel computation and the procedure of inductance calculation using FEM-based magneto-static solution.

Figure 3.32 shows the implementation strategy. The client computer in Figure 3.32 (a) divides the n rotor positions into groups. Every group is assigned to a computer where it is further divided among its cores. The inductances can be solved for corresponding rotor positions using the proposed analytical model or using magneto static solutions, as in Figure 3.32 (b). The calculated parameters will send back to the client machine, where they will be saved in the 3D lookup tables and used by the online portion. By doing so, the simulation time shall be reduced considerably. The detailed description of the model with results and discussion is presented in [11].

4 The test rig and the spectrum analysis

4.1 Measurement Setup

For experiments and measurements, two test rigs with different motors are prepared. Each measurement setup consists of two identical motors with the parameters given in Tables 4.1 and 4.2. One machine is under investigation while the other is acting as a load. Both machines are mounted on the same mechanical base and coupled through their shafts, as shown in Figure 4.1 and Figure 4.2. The loading machine is fed through the inverters to improve its controllability for various load levels. Grid and industrial inverter working under different control mechanisms feed the machine under investigation. The stator currents and voltages are measured using the Dewetron transient recorder. The measured signals' sampling frequency is 10 kHz for the grid and 100 kHz for inverter fed cases, and the measurement time is 70 seconds, giving an excellent resolution of the frequency spectrum.

4.1.1 Case 1

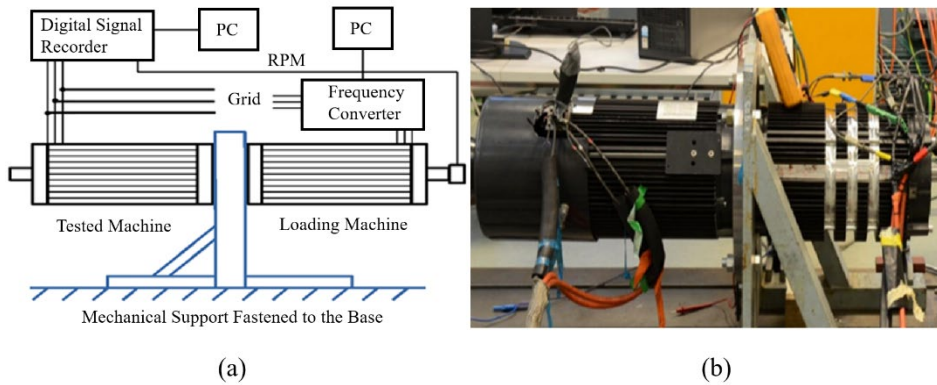


Figure 4.1. (a) The block diagram, (b) The experimental measurement setup.

Table 4.1. The specifications of motor 1.

Parameter	Symbol	Value
Number of poles	p	4
Number of phases	ϕ	3
Connection	Y- Δ	Star
Stator slots	Q_s	48; non-skewed
Rotor slots	N_b	40; skewed
Terminal voltage	V	333V@50 Hz
Rated slip	S	0.0667
Rated power	P_r	18 kW@50 Hz

4.1.2 Case 2

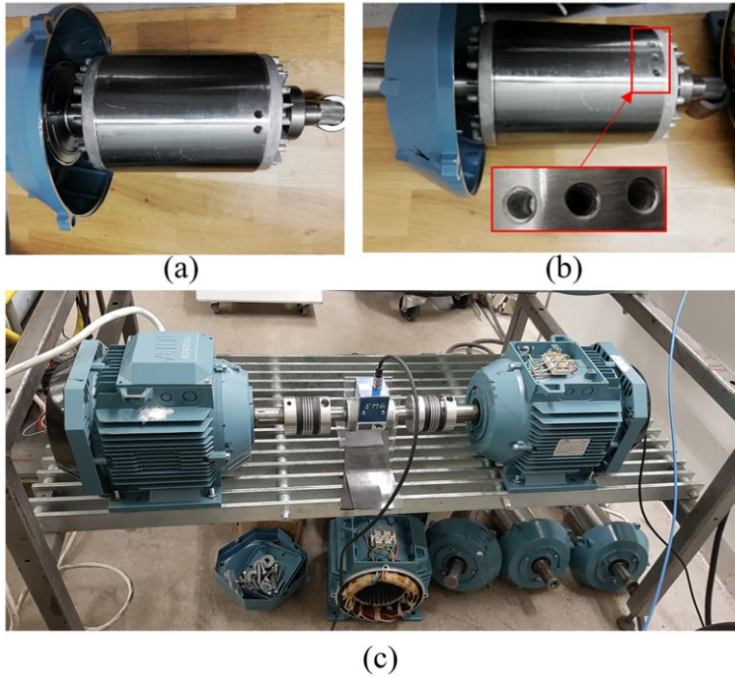


Figure 4.2. (a) The rotor with two broken bars, (b) The rotor with three broken bars, (c) The test bench with loading motor on the right side and test motor on the left side.

Table 4.2. The specifications of motor 2.

Parameter	Symbol	Value
Number of poles	p	4
Number of phases	ϕ	3
Connection	-	Delta
Stator slots	Q_s	36; non-skewed
Rotor bars	N_b	28; skewed
Rated voltage	V	400V@50 Hz
Rated current	I	15.3A
Rated power	P_r	7.5 kW @ 50 Hz

4.2 The spectrum analysis of stationary and non-stationary signals

Regarding frequency-time relation, the motor's global signals such as voltage and current can be broadly classified into stationary and non-stationary signals. In stationary signals, the frequency components do not change their value across the entire signal. The signal under the steady-state regime is the best example of stationary signals, particularly if the machine is grid-fed. These signals are easy to handle, and simple DTFT is enough to determine the components if necessary. The stationary signals sometimes do not possess enough information about faults in them. For example, suppose the motor is working under no-load or more minor load conditions. In that case, the faulty signals potentially

hide under the frequency lobe of the fundamental component, and it is tough to detect them. The same is true if the motor is being fed by some drive system whose close loop control system attenuates them to reduce the torque and speed ripples. These problems can be avoided by doing the signal analysis under the transient regime. In the transient regime, most of the signals are non-stationary. It means that the frequency components change their value across the course of the transient period. The non-stationary signals cannot be handled using simple DTFT, but the time-frequency analysis becomes essential. So the selection of appropriate techniques out of the basic signal processing algorithms mentioned in Table 2.3 is crucial. These signal processing tools under various conditions can be found in [VII, VIII]. Moreover, the basic flowchart for improving the resolution by reducing fractional starting and ending cycles, DC offset, and the low sampling frequency is shown in Figure 4.3.

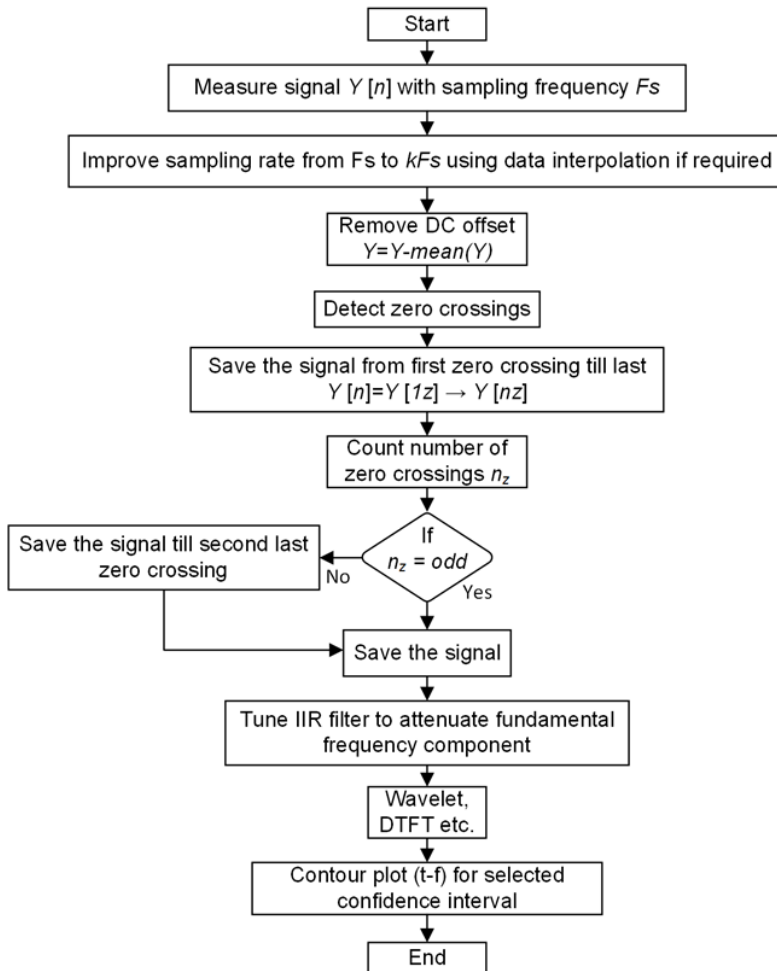


Figure 4.3. The flowchart diagram for resolution improvement.

4.3 The segregation of motor current harmonics

The majority of MCSA based fault diagnostic techniques depend upon the segregation of frequency components in the spectrum of signals such as current, voltage, torque, speed or vibration, etc. In currents and induced voltages, which directly affect speed and torque, the primary sources of harmonics are presented below.

4.3.1 The winding and space harmonics

Unlike ideal induction machines, where the stator and rotor windings are supposed to be sinusoidally distributed, it is not valid in practical machines. There are various types of stator winding configurations in practical machines, and the rotor also has a cage structure. The slots' openings both on the stator and rotor side are another cause of harmonics. This happens because the air gap does not remain uniform but becomes the rotor position's function, as described in the previous chapter.

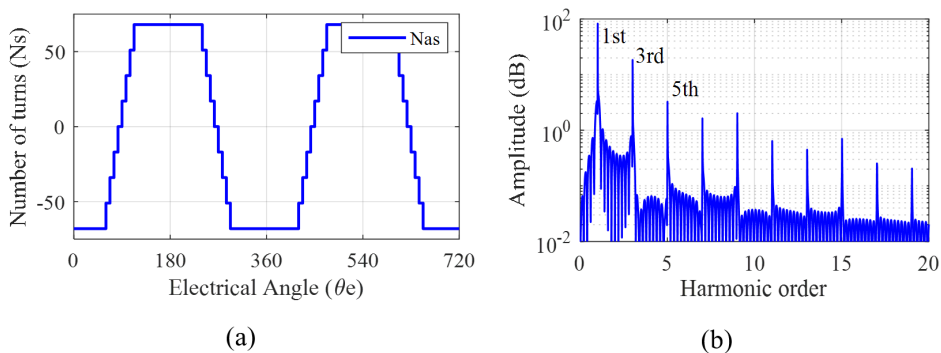


Figure 4.4. (a) The stator winding function, (b) The corresponding frequency spectrum.

These reasons give rise to harmonics called winding and spatial harmonics. The most prominent spatial harmonics are the rotor or principal slotting harmonics. Although these harmonics have drawbacks as they increase the speed and torque ripples, they can be used constructively for fault diagnostics. Being weak in amplitude, these harmonics have less spectral leakage than the fundamental component having less capability to bury the faulty frequency components beneath them. The frequency analysis of stator winding in Figure 4.4 (a)-(b) shows various other harmonics in the spectrum along with the fundamental component.

4.3.2 The supply fed harmonics

The supply is the potential source of harmonics that should be considered effectively while segregating the spectrum's frequency components. In the case of electrical machines, the use of frequency converters is increasing day by day. The inverters produce a voltage, which is the approximation to the sinusoidal wave shape. The grid and industrial inverter-based measured voltage and their corresponding spectrum with the attenuated fundamental component are shown in Figure 4.5.

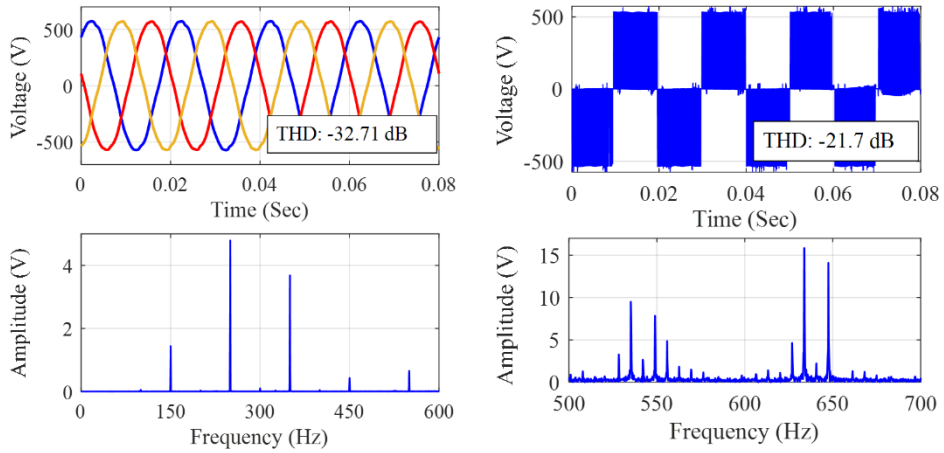


Figure 4.5. The grid voltage with the corresponding spectrum (left), the industrial inverter voltage with the corresponding spectrum (right).

The grid voltage harmonics depend upon the quality of the power network. However, mainly it contains the odd multiples of the fundamental component. In the inverter-fed voltage, the total harmonic distortion is much higher than that of the grid. It makes the detection of small amplitude fault-based frequency components challenging using simple diagnostic algorithms.

4.3.3 The fault-based harmonics

Almost every fault in the induction motors leaves specific frequencies in the current spectrum, changing the torque and speed accordingly. Due to the machine's cylindrical structure and rotating nature, the rotor-related electrical or mechanical faults tend to modulate the stator current and voltage with frequency dependent upon the rotor speed or slip, as described in Table 2.2. Those frequency components spread throughout the spectrum, while the most potent members are near the fundamental supply frequency component. Although the higher-order faulty components are weak in amplitude, they are less vulnerable to spectral leakage. This is due to the less powerful winding and supply-based components beside them. The causes of fault-based harmonics may also include inherent asymmetries, magnetic material saturation and the impact of supply based higher order harmonics on electrical properties of the windings.

4.4 Spectrum analysis in the steady-state regime

During the steady-state interval, the frequency components are stationary; hence they can be easily detected using simple DTFT analysis. The frequency spectrum of motor current simulated using the FEM, the proposed analytical model, and the test rig measurement under healthy conditions is shown in Figures 4.6-4.7 [IV, V, VI].

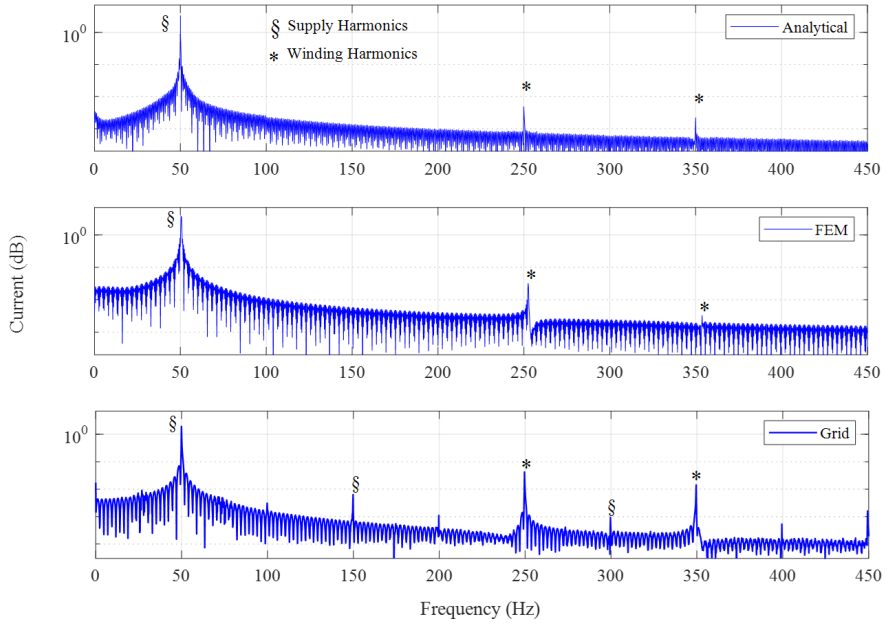


Figure 4.6. The frequency spectrum of stator current simulated using the proposed model, FEM, and practical measurements from top to bottom from 0- 450 Hz (motor 1).

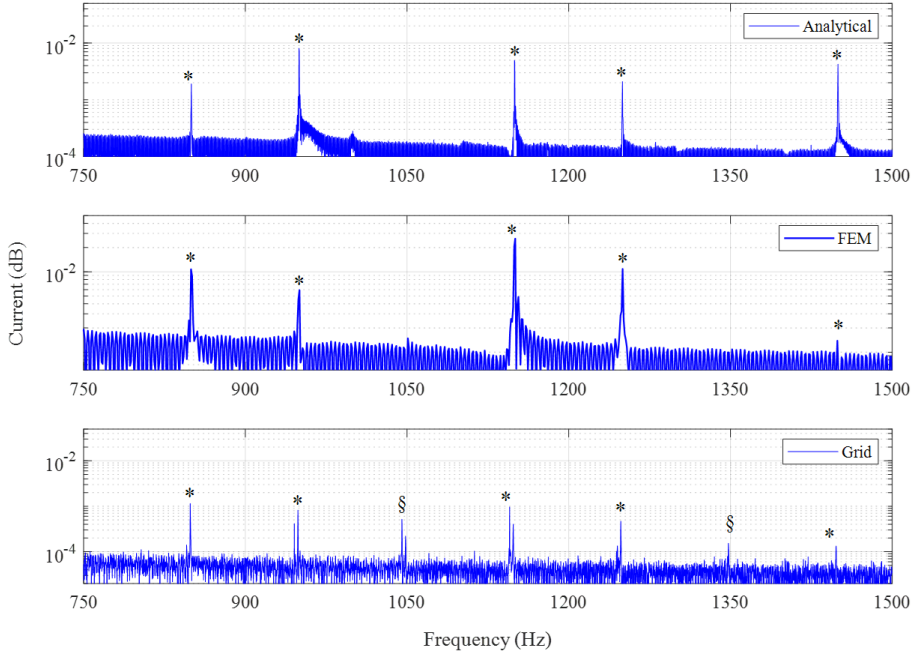


Figure 4.7. The frequency spectrum of stator current simulated using the proposed model, FEM, and practical measurements from top to bottom from 750 Hz to 1500 Hz (motor 1).

The entire current spectrum in all three cases is in good agreement. The frequency bandwidth from 0 Hz to 450 Hz mainly consists of supply and winding harmonics. In the case of FEM and the proposed MWFA model, the supply harmonic is the fundamental component because of the ideal source. In grid fed machine, some odd multiples of the fundamental component can be seen along with some inherent eccentricity-based harmonics. Similarly, the bandwidth from 750 Hz to 1500 Hz consists of prominent winding harmonics in all three cases.

Compared to the simulation, the practical rotor slotting harmonics are small in amplitude because the rotor bars are skewed. The skew angle is equal to one stator slot pitch. As the bars are skewed, the inductance profile becomes much smoother with reduced peak-to-peak ripple value, resulting in the attenuation of winding harmonics. The development and movement of those components with load are given in Table 4.3 and Figure 4.8.

Table 4.3. The rotor slot harmonics (RSH) in the case of motor 1.

Slip	Theoretical RSH1	Theoretical RSH2	RSH1 (Hz)	RSH2 (Hz)	RSH1 (A)	RSH2 (A)
0.0030	947	1047	946.7	1046.8	0.00042	0.0005
0.035	915	1015	914.76	1014.76	0.00185	0.0008
0.05	900	1000	899.2	999.2	0.0021	0.0007

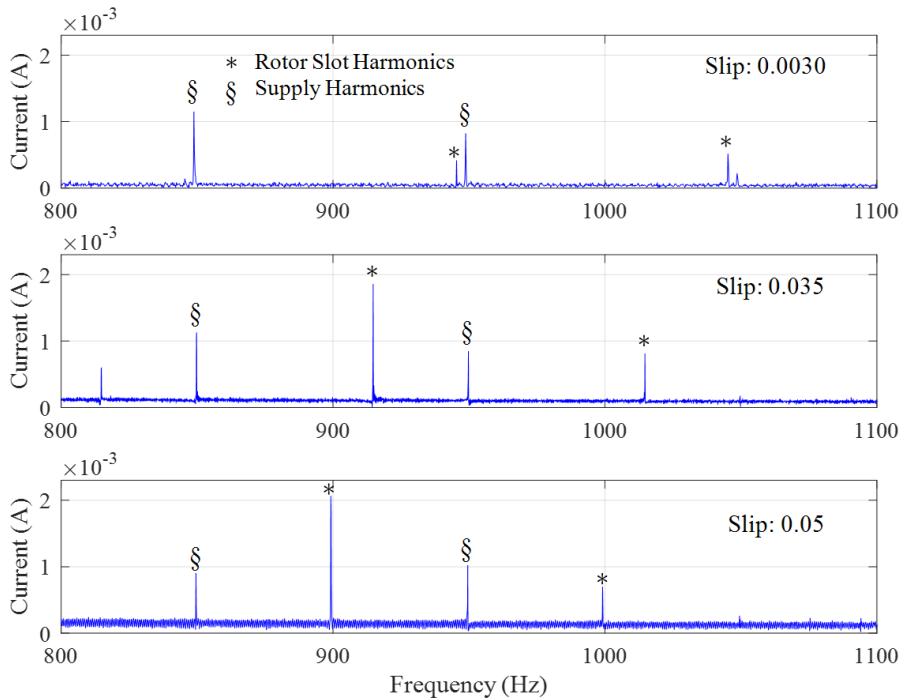


Figure 4.8. The development and movement of RSH (motor 1).

It is relatively easy to differentiate among the frequencies if they are limited in number, as discussed earlier. However, in the case of inverter-fed motors, this differentiation becomes very tedious. This is because of two main reasons: the tremendous number of

harmonics coming from the supply side, and the second is the drive controller's impact if it is working in the closed-loop system. The results presented in Figures 4.6-4.7 are based on no-load simulations and measurements, while the detailed studies in several other cases are presented in [IV, V, VI].

4.5 Spectrum analysis in the transient regime

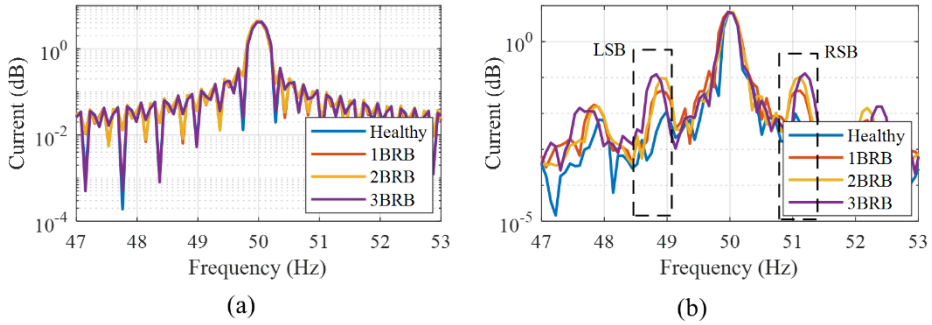


Figure 4.9. (a) The frequency spectrum of healthy and broken bar motors under no-load conditions, (b) The frequency spectrum of healthy and broken bar motors under rated-load conditions (motor 2).

The fault diagnosis of induction machines using steady-state signals possesses some limitations. In steady-state signals, faulty frequency components' detection becomes very challenging under no load or low load conditions because of the low slip. Figure 4.9 (a)-(b) shows the motor's frequency spectrum under no-load and rated load conditions. The broken bars are no longer detectable under the no-load state, which creates a challenge for the diagnostic algorithm. Other than the drawbacks while the machine is working under low slip conditions, the steady-state signal-related problems may also include the possibility of false indications caused by cooling ducts, broken outer bars in double cage rotors, rotor magnetic anisotropy, etc.

These problems can be solved by working under transient intervals, where the frequency components show very interesting results. This is because of the continuously changing slip from maximum to minimum in that interval. However, there are some difficulties dealing with that interval; first, at rated conditions, the transient interval time is minimal, leading to low frequency resolution. Secondly, since the signal is non-stationary, it cannot be handled using DTFT, but the time-frequency analysis becomes essential.

a) Legibility improvement by extending the transient time

The critical parameter for better time-frequency resolution is the sampling frequency and the measurement length of the signal. If the motor's start-up time is minimal, it will lead to no practical information about its condition. The transient time can be increased by using a large inertia load. However, this approach requires the motor to be removed from the production line, making the test practically impossible. However, the rotor's inertia can be exploited for the same purpose by decreasing the applied voltage and the motor's power. This technique increases the simplicity of the test, as no external load is needed. The presence of an industrial inverter in almost all working environments increases the feasibility of tests. In the industrial inverter case, the variable voltage at a constant frequency can be achieved by changing the rated parameters. Since the

voltage/Hz ratio in the scalar control remains constant, by changing the rated frequency with constant rated voltage, the output voltage can be varied, as shown in Table 4.4. Moreover, the acceleration and deceleration time should be equal to zero to avoid the drive controller's influence on the transient interval.

Table 4.4. The setting of the industrial inverter to achieve the desired voltage.

V_{rated} (V)	f_{rated} (Hz)	V/Hz	f_{set} (Hz)	V_{out} (V)
300	300	1	50	50
300	150	2	50	100
300	100	3	50	150
300	75	4	50	200
300	60	5	50	250
300	50	6	50	300

Since the prominent non-stationary signal bandwidth is from 0 to 50 Hz, the higher-order spatial and time harmonics become less significant. Although they also make similar time-frequency patterns, they are fragile compared to the pattern made by LHS and RHS components. It makes the simplified winding function-based model suitable for study and usage in advanced model-dependent diagnostic algorithms. The simplified model can also be used to draw theoretical fault-based patterns for better understanding. The simulated transient current at 10, 15, 25, and 100 percent of rated voltage is shown in Figure 4.10.

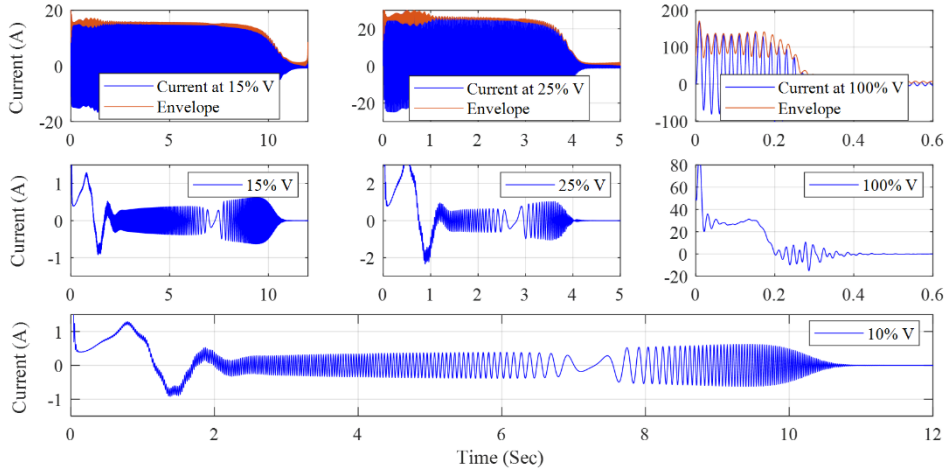


Figure 4.10. The motor's simulated startup currents at different voltage levels (top row), the recovered non-stationary signal (middle row), the non-stationary signal at 10% of the rated voltage (bottom).

The length of the transient interval increases with the decrease in the supply voltage. The non-stationary signal is recovered by attenuating the fundamental component with the help of a band-stop IIR filter.

Figure 4.11 shows the time-frequency analysis of the recovered non-stationary signal using the wavelet approach. The fault-based "V" shaped pattern becomes legible at 10% of the rated load while it is not present under nominal conditions. The fault pattern

becomes more legible by using filter and contour plots together. The contour plot shows the areas with a 95% of the confidence interval. With rated voltage, total power is confined in the region till 0.5 sec without any pattern as in Figure 11(b). In contrast, the pattern becomes visible with extended time, as in Figure 11(d). The detailed analysis of simulation and practical results with appropriate, relevant references can be studied in [1].

An infinite impulse response (IIR) filter with a band stop range from 49.99Hz to 50.01Hz is used for the fundamental component's attenuation. The IIR filter is tuned because of its better transition interval with fewer pass band ripples. While time-frequency analysis of the recovered non-stationary signal is done using wavelet approach with "Bump" mother wavelet. The Bump wavelet produces tighter frequency variance and broader time variance. However, its time and frequency localizations can be improved by properly tuning its parameters. The detailed mathematical description of this mother wavelet is accessible in [80].

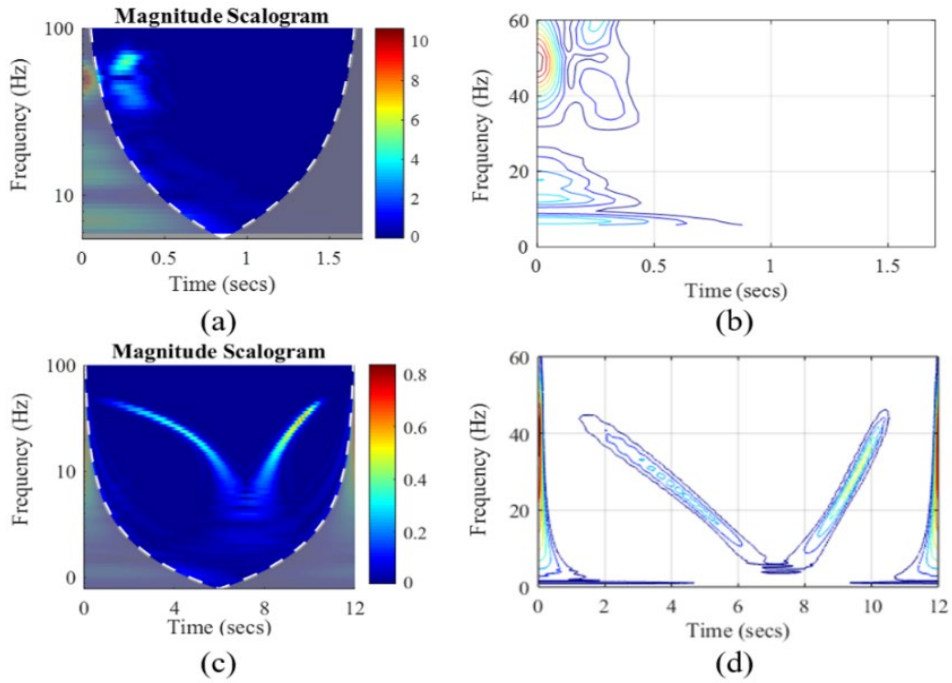


Figure 4.11. The time-frequency pattern of simulated current with two broken bars at (a) rated supply voltage, (b) contour pattern (c) 10% of the nominal voltage, (d) contour pattern for better legibility with a 95% confidence interval (motor 2).

Figure 4.12. shows the measured transient current at various voltage levels under two broken bar conditions. The recovered non-stationary signals contain all harmonics except the fundamental component, attenuated by the band-stop filter.

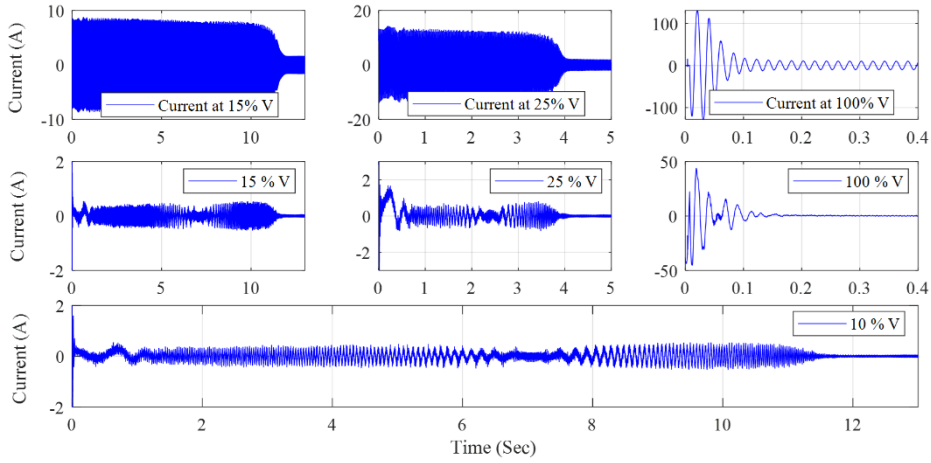


Figure 4.12. The motor's startup currents measured at different voltage levels (top row), the corresponding recovered non-stationary signals (middle row), and the non-stationary signal at 10% of the rated voltage representing the changing frequency pattern (bottom) (motor 2).

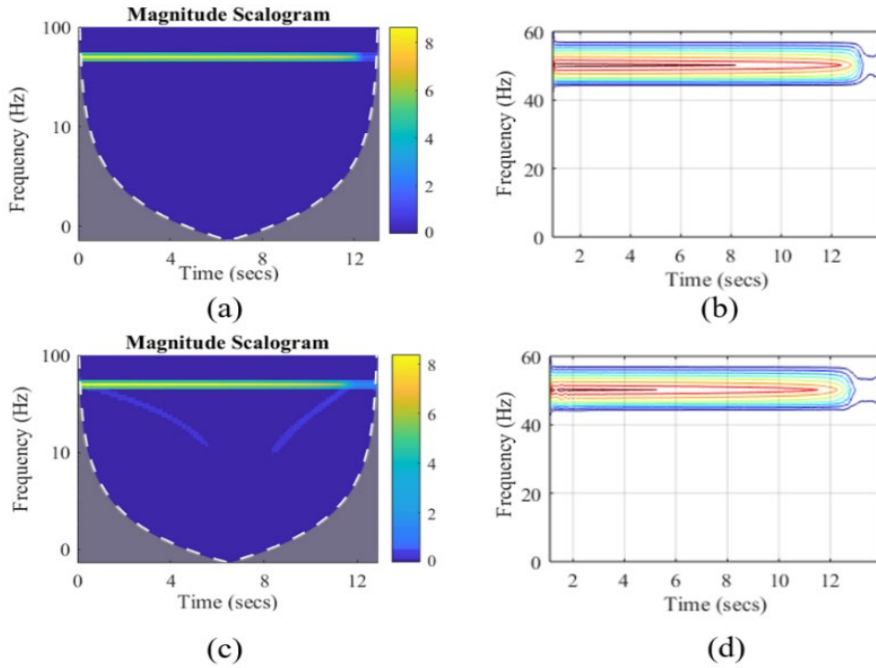


Figure 4.13. The results, based on the measurements taken at 10% of the rated supply voltage (a) The time-frequency response of healthy motor's phase current in transient regime, (b) The respective contour plot with a 95% confidence interval. (c) The time-frequency response of faulty motor's phase current in transient regime, (d) The respective contour plot with a 95% confidence interval (motor 2).

The time-frequency analysis of the motor's transient current at 10% of the nominal voltage under healthy and two broken bar cases is presented in Figure 4.13. The fault-based pattern is not visible in the presence of the fundamental component. Moreover,

the contour plot also misses the weak fault pattern as the maximum spectral power density is in the region made by the fundamental component.

b) Legibility improvement by attenuating the fundamental component

It is well-known that the fault representing frequencies are very weak in amplitude than the fundamental component. It decreases their visibility, which can be improved by removing the fundamental component out of the signal. This can be achieved using various digital filters such as Hilbert transform, Notch filter, or infinite impulse response (IIR) band-stop filters. The IIR filters can attenuate the fundamental component with the most negligible impact on the sideband frequencies because of its sharp transition band and low passband ripples. The current time-frequency spectrum of a healthy motor after the attenuation of the fundamental component with the band-stop IIR filter is shown in Figure 4.14.

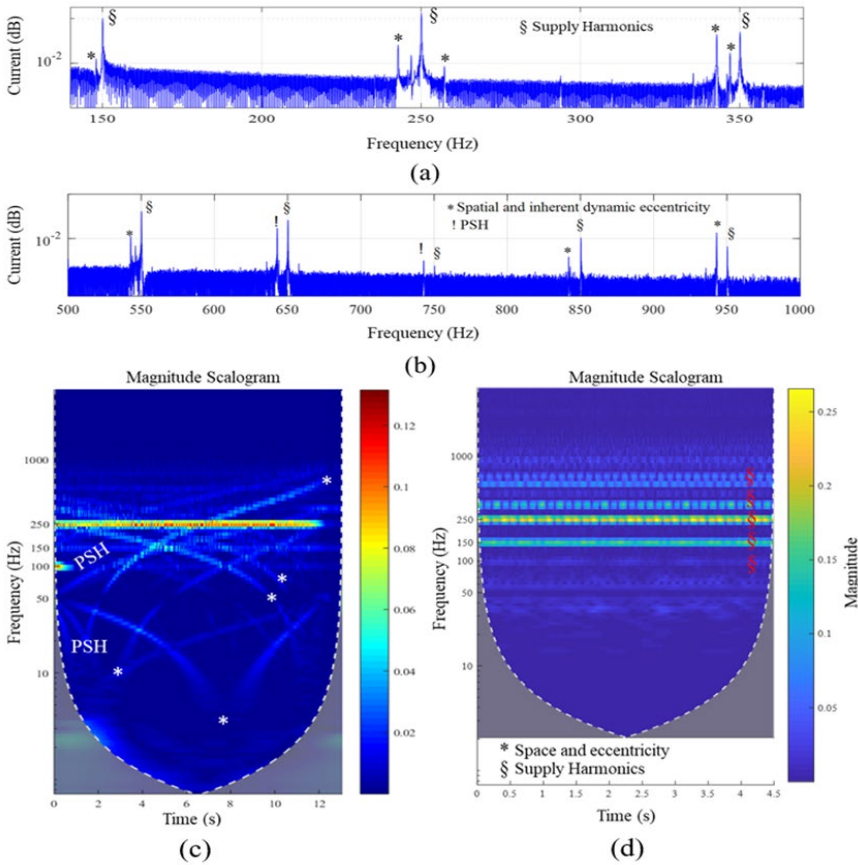


Figure 4.14. The generation of spatial harmonics in stator current. (a) Under steady-state regime with 50% of the rated load in the bandwidth of 100-400 Hz, (b) Under steady-state regime with 50% of the rated load in the bandwidth of 500-1000 Hz, (c) The development of time-frequency patterns due to the space harmonics, (d) The time-frequency spectrum under steady-state regime under 50% of rated load (motor 2).

Those patterns are because of the inherent eccentricity and the rotor slotting harmonics. All those harmonics are presented both in the transient and steady-state regimes. Their proper segregation is essential to avoid false fault alarms, as in the

transient region, they make similar patterns as rotor faults do. The broken rotor bar-based harmonics become much more substantial than inherent eccentricity at some fault level. Figure 4.15 shows the development of fault patterns in healthy, 1 BRB, and 2 BRB cases, respectively. Moreover, the current envelope shows the measurement time of the stator current in the transient interval.

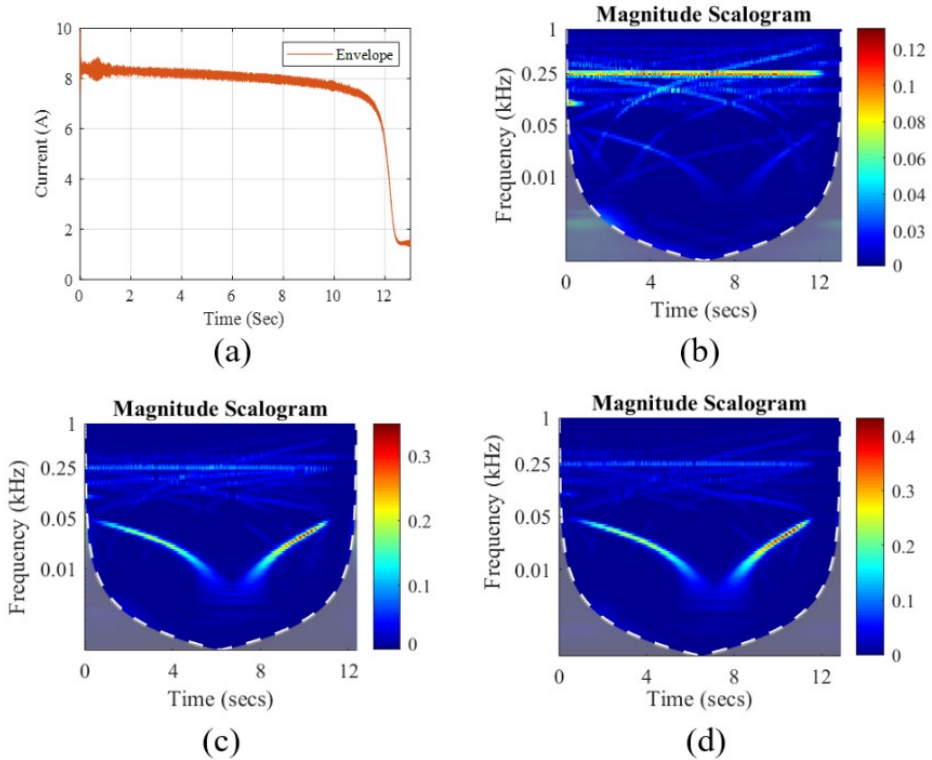


Figure 4.15. The results based on the measurements taken at 10% of the rated supply voltage (a) The envelope of motor's phase current in transient regime, (b) Time-frequency spectrum in the healthy case with an attenuated fundamental component, (c) Time-frequency spectrum in case of 1 broken bar with the attenuated fundamental component, (d) Time-frequency spectrum in case of 2 broken bar with an attenuated fundamental component (motor 2).

The contour lines representing the areas with specific amplitude of the frequency components can be used for better legibility of fault based patterns. The selected amplitude level is known as scaling, which can also be used as a quantitative indicator of the fault. It can help differentiate between fault-based patterns and the pattern based on inherent eccentricity to avoid false alarms. In this particular study, a confidence interval of 95% is considered for the contour plot.

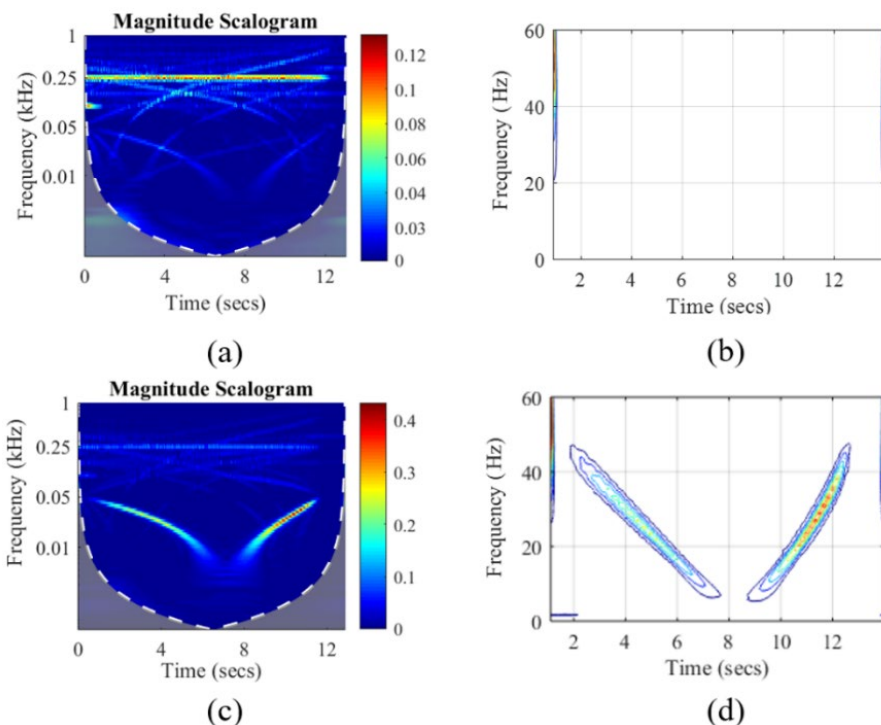


Figure 4.16. (a) The time-frequency plot of the healthy motor with 10% of rated voltage, (b) The time-frequency contour plot with a 95% confidence interval, (c) The time-frequency plot 1 BRB motor with 10% of rated voltage, (d) The corresponding contour plot with a 95% confidence interval (motor 2).

The time-frequency analysis of healthy and 1BRB based motor's transient current with the attenuated fundamental component is shown in Figure 4.16. The corresponding contour plot gives a better legible spectrum after neglecting the weaker spatial harmonics. The contour plot shows the region with maximum spectral power density, which can be achieved by selecting the regions with appropriate confidence intervals. In the absence of the fundamental component, the fault-based frequencies are the most potent components compared to winding and spatial harmonics; the contour region confines itself around the fault representing regions [1].

5 Conclusions and future work

This chapter concludes the outcomes of this research work for the proposed objectives. Moreover, some advancements in this field as future work are also suggested at the end.

5.1 Conclusions and the summary of the work

The main objectives of this work are twofold. The first is to make the squirrel cage induction motor's various models suitable for its analysis, condition monitoring, and fault diagnostics. The second is to investigate motor's current spectrum using multiple signal processing techniques suitable for fault detection under the transient and steady state regimes.

On the modeling side, the main emphases are given to the fact that the model should be fast, less complex in the perspective of ill-posedness, and should be able to simulate the most common faults. Moreover, the model should be suitable for advanced model-dependent diagnostic algorithms such as inverse problem theory and hardware in the loop environment.

To achieve the goals, the two-axis theory-based model (d-q) was considered as a starting point. This model is straightforward, comprehensive, and perfect for dynamic analysis of the motor under investigation. The approximations such as constant inductances, no air gap, and the approximate three-phase wound rotor make this model less beneficial for the fault simulations without a considerable increase in the equivalent circuit's complexity. However, the material's non-linear behavior is simulated using a second-order non-linear function of magnetization current and flux, compatible with the other models.

The winding function-based model was prepared as a next step to reduce the number of considered approximations in the d-q model. Various inductance analytical expressions are derived in this model, based on the constant air gap, sinusoidal stator winding functions, and the actual rotor loops. The derivation of the inductance analytical expressions as a function of the rotor position increases the simulation's speed drastically. Moreover, all rotor loop's consideration makes the model suitable for simulating all rotor bar currents and various broken bar and end ring faults. This model is an excellent selection for the broken rotor bars faults detection under the transient regime. It does not consider higher-order spatial and time harmonics, which increases the model's complexity unnecessarily. However, considering the constant air gap and sinusoidal stator winding distribution makes this model unsuitable for the simulation of eccentricity and stator short circuit failures without a considerable increase in complexity. The winding distribution-related approximation can be resolved by considering the summation of higher-order harmonics with the help of Fourier series. At the same time, a practical air gap can be considered using the Taylor series. However, both solutions can lead to the limitations of the self-defined number of harmonics and their amplitude.

To resolve those issues, the modified winding function-based model is proposed next. In that model, the winding function and the air gap are defined as conditional analytical expressions. These analytical expressions are the function of the rotor reference position. Moreover, the motor's mechanical geometry is considered to calculate various parameters, such as phase resistances and leakage inductances. The integration-based winding function formula was reduced to a mean value function, which considerably reduces the model's complexity and the integration's constant related issues. It also

reduces the problems of integration constant. Moreover, the entire model is divided into two portions. Several inductances and resistances are calculated in the offline portion at various rotor positions with a considerably reduced step size for better resolution. The calculated inductances are saved in 3-D lookup tables. These tables are then used in the online section, where the performance parameters such as speed, torque, fluxes, currents, and voltages are calculated. The division of the model into two sections can decrease the simulation time so that, once the inductances are calculated, most of the faults can be simulated in the online portion without the need for inductance matrices to be calculated again. The inclusion of actual winding functions, the air gap, and the stator and rotor slot openings make the results in good agreement with the results achieved using complex finite element-based models. The little simulation time compared with FEM models makes it suitable for advanced model-dependent diagnostic algorithms.

The compatibility of the proposed analytical and hybrid FEM-analytical models with the cluster computation makes the models suitable for exploiting distributed computational resources. It makes the model feasible for cloud computation, which is a crucial part of industry 4.0 standards. Moreover, the simulation time decreases drastically.

Towards the signal processing side, the motor current signature analysis (MCSA) is performed using various techniques combined with digital filters. The entire frequency spectrum of stator current was studied to segregate various frequency components according to their causes. This differentiation among various frequency components is essential for diagnostics algorithms when there is more than one system's fault. Moreover, the drive controller's impact is also investigated and concluded that in direct torque control (DTC) motor, the stator current possesses the slightest information regarding the rotor fault. The frequency spectrum is studied both in the steady-state and transient regimes. In the transient regime, it is proposed that, by selecting an appropriate value of power spectral density (confidence interval in case of wavelet), the fault representing regions can be made more legible.

The test rig was prepared with broken rotor bars, where several experiments were performed while running the motor under different loading and supply conditions. Finally, the simulation results taken from the proposed model and FEM are compared with the practical measurements for validation.

5.2 Future works

The proposed model can be used for the advanced fault diagnostic techniques, as the simulation time is considerably less, and it possesses the winding distribution and air-gap-related practicalities.

The model can be used in the inverse problem theory, where the motor's global signals (observables) can be used as input to estimate the design parameters. Unlike corresponding FEM models, the proposed model is less ill-posed, leading towards the more unique and stable solution of inverse maps. The comparison of the estimated design parameters with the rated parameters can lead to the cause of the fault.

The utilization of this model can open new prospects in the field of machine fault segregation. It can be done by comparing the practical faulty signals with simulated benchmark fault signals obtained from this proposed model.

The training of artificial intelligence-based fault diagnostic algorithms requires the collection of big data under various fault-case scenarios. The collection of this data is challenging to obtain from;

- Industry, as there is the least number of faulty motors working at a time due to preventive maintenance
- Laboratory, as only a limited number of destructive tests, can be performed

This proposed model can best serve this purpose, yielding various fault-case scenarios at various severity levels.

The proposed model can be used in various inverter-fed environments to study the inverter controller's impact on the fault representing frequencies.

Since the model includes the effect of spatial harmonics, it can be used for sensor-less speed estimation, at least in the steady-state regime, by detecting the principal slot components.

In developing this model, magnetic material permeability is considered infinite as the material saturation has less impact on the frequency components representing the faults. To further improve the accuracy of this model, it can be compensated using a non-linear function of flux and current in the online portion of the model by using the material's B-H curve as a lookup table or by modulating the air-gap with an appropriate sinusoidal function.

References

- [1] H. W. Penrose, "Test Methods for Determining the Impact of Motor Condition on Motor Efficiency and Reliability," *PhD Diss.*, vol. ALL-TEST P, no. LLC, Old Saybrook, CT, pp. 1–8.
- [2] P. Zhang, Y. Du, T. G. Habetler, and B. Lu, "A Survey of Condition Monitoring and Protection Methods for Medium-Voltage Induction Motors," *IEEE Trans. Ind. Appl.*, vol. 47, no. 1, pp. 34–46, Jan. 2011.
- [3] K. N. Gyftakis, P. A. Panagiotou, and D. Spyarakis, "Detection of simultaneous mechanical faults in 6-kV pumping induction motors using combined MCSA and stray flux methods," *IET Electr. Power Appl.*, p. elp2.12054, Mar. 2021.
- [4] K. N. Gyftakis and A. J. M. Cardoso, "Reliable Detection of Stator Interturn Faults of Very Low Severity Level in Induction Motors," *IEEE Trans. Ind. Electron.*, vol. 68, no. 4, pp. 3475–3484, Apr. 2021.
- [5] P. C. Krause and C. H. Thomas, "Simulation of Symmetrical Induction Machinery," *IEEE Trans. Power Appar. Syst.*, vol. 84, no. 11, pp. 1038–1053, 1965.
- [6] R. J. Lee, P. Pillay, and R. G. Harley, "D,Q reference frames for the simulation of induction motors," *Electr. Power Syst. Res.*, vol. 8, no. 1, pp. 15–26, Oct. 1984.
- [7] C. C. M. Cunha, V. B. S. Varejao, and B. J. C. Filho, "Simple model for squirrel cage induction machine with rotor asymmetries and its validation through experimental tests on a special motor," in *2008 34th Annual Conference of IEEE Industrial Electronics*, 2008, pp. 1385–1390.
- [8] C. C. M. Cunha, R. O. C. Lyra, and B. Filho, "Simulation and Analysis of Induction Machines With Rotor Asymmetries," *IEEE Trans. Ind. Appl.*, vol. 41, no. 1, pp. 18–24, Jan. 2005.
- [9] D. C. Patel and M. C. Chandorkar, "Transient modeling and analysis of induction motors with position effects in stator turn faults," in *2010 IEEE International Conference on Industrial Technology*, 2010, pp. 1251–1256.
- [10] G. M. Joksimovic and J. Penman, "The detection of inter-turn short circuits in the stator windings of operating motors," *IEEE Trans. Ind. Electron.*, vol. 47, no. 5, pp. 1078–1084, 2000.
- [11] J. Milimonfared, H. M. Kelk, S. Nandi, A. D. Minassians, and H. A. Toliyat, "A novel approach for broken-rotor-bar detection in cage induction motors," *IEEE Trans. Ind. Appl.*, vol. 35, no. 5, pp. 1000–1006, 1999.
- [12] H. A. Toliyat and T. A. Lipo, "Transient analysis of cage induction machines under stator, rotor bar and end ring faults," *IEEE Trans. Energy Convers.*, vol. 10, no. 2, pp. 241–247, Jun. 1995.
- [13] H. A. Toliyat, T. A. Lipo, and J. C. White, "Analysis of a concentrated winding induction machine for adjustable speed drive applications. I. Motor analysis," *IEEE Trans. Energy Convers.*, vol. 6, no. 4, pp. 679–683, 1991.
- [14] H. A. Toliyat, T. A. Lipo, and J. C. White, "Analysis of a concentrated winding induction machine for adjustable speed drive applications. II. Motor design and performance," *IEEE Trans. Energy Convers.*, vol. 6, no. 4, pp. 684–692, 1991.

- [15] A. M. El-Refaie, T. M. Jahns, and D. W. Novotny, "Analysis of Surface Permanent Magnet Machines With Fractional-Slot Concentrated Windings," *IEEE Trans. Energy Convers.*, vol. 21, no. 1, pp. 34–43, Mar. 2006.
- [16] J. Faiz and I. Tabatabaei, "Extension of winding function theory for nonuniform air gap in electric machinery," *IEEE Trans. Magn.*, vol. 38, no. 6, pp. 3654–3657, 2002.
- [17] S. Nandi, "Modeling of Induction Machines Including Stator and Rotor Slot Effects," *IEEE Trans. Ind. Appl.*, vol. 40, no. 4, pp. 1058–1065, Jul. 2004.
- [18] H. A. Toliyat, M. S. Arefeen, and A. G. Parlos, "A method for dynamic simulation of air-gap eccentricity in induction machines," *IEEE Trans. Ind. Appl.*, vol. 32, no. 4, pp. 910–918, 1996.
- [19] J. Faiz and M. Ojaghi, "Unified winding function approach for dynamic simulation of different kinds of eccentricity faults in cage induction machines," *IET Electr. Power Appl.*, vol. 3, no. 5, p. 461, 2009.
- [20] A. Marfoli, P. Bolognesi, L. Papini, and C. Gerada, "Mid-Complexity Circuital Model of Induction Motor with Rotor Cage: A Numerical Resolution," in *2018 XIII International Conference on Electrical Machines (ICEM)*, 2018, pp. 277–283.
- [21] J. Pippuri and A. Arkkio, "Time-Harmonic Induction-Machine Model Including Hysteresis and Eddy Currents in Steel Laminations," *IEEE Trans. Magn.*, vol. 45, no. 7, pp. 2981–2989, Jul. 2009.
- [22] A. Kumar, S. Marwaha, A. Marwaha, and N. S. Kalsi, "Magnetic field analysis of induction motor for optimal cooling duct design," *Simul. Model. Pract. Theory*, vol. 18, no. 2, pp. 157–164, Feb. 2010.
- [23] J. Martinez, A. Belahcen, and J. G. Detoni, "A 2D magnetic and 3D mechanical coupled finite element model for the study of the dynamic vibrations in the stator of induction motors," *Mech. Syst. Signal Process.*, vol. 66–67, pp. 640–656, Jan. 2016.
- [24] Ranran Lin and A. Arkkio, "3-D Finite Element Analysis of Magnetic Forces on Stator End-Windings of an Induction Machine," *IEEE Trans. Magn.*, vol. 44, no. 11, pp. 4045–4048, Nov. 2008.
- [25] P. C. Krause and C. H. Thomas, "Simulation of Symmetrical Induction Machinery," *IEEE Trans. Power Appar. Syst.*, vol. 84, no. 11, pp. 1038–1053, Nov. 1965.
- [26] A. R. Munoz and T. A. Lipo, "Complex vector model of the squirrel-cage induction machine including instantaneous rotor bar currents," *IEEE Trans. Ind. Appl.*, vol. 35, no. 6, pp. 1332–1340, 1999.
- [27] M. Jannati, N. R. N. Idris, and Z. Salam, "A new method for modeling and vector control of unbalanced induction motors," in *2012 IEEE Energy Conversion Congress and Exposition (ECCE)*, 2012, pp. 3625–3632.
- [28] G. Y. Sizov, Chia-Chou Yeh, and N. A. O. Demerdash, "Magnetic equivalent circuit modeling of induction machines under stator and rotor fault conditions," in *2009 IEEE International Electric Machines and Drives Conference*, 2009, pp. 119–124.
- [29] S. D. Sudhoff, B. T. Kuhn, K. A. Corzine, and B. T. Branecky, "Magnetic Equivalent Circuit Modeling of Induction Motors," *IEEE Trans. Energy Convers.*, vol. 22, no. 2, pp. 259–270, Jun. 2007.

- [30] A. Mahyob, M. Y. O. Elmoctar, P. Reghem, and G. Barakat, "Induction machine modelling using permeance network method for dynamic simulation of air-gap eccentricity," in *2007 European Conference on Power Electronics and Applications, EPE, 2007*.
- [31] J. Apsley and S. Williamson, "Analysis of multiphase induction machines with winding faults," *IEEE Trans. Ind. Appl.*, vol. 42, no. 2, pp. 465–472, Mar. 2006.
- [32] S. Williamson and E. R. Laithwaite, "Generalised harmonic analysis for the steady-state performance of sinusoidally-excited cage induction motors," *IEE Proc. B Electr. Power Appl.*, vol. 132, no. 3, p. 157, 1985.
- [33] S. Williamson and S. Smith, "Pulsating torque and losses in multiphase induction machines," in *Conference Record of the 2001 IEEE Industry Applications Conference. 36th IAS Annual Meeting (Cat. No.01CH37248)*, vol. 2, pp. 1155–1162.
- [34] S. Bachir, S. Tnani, J.-C. Trigeassou, and G. Champenois, "Diagnosis by parameter estimation of stator and rotor faults occurring in induction machines," *IEEE Trans. Ind. Electron.*, vol. 53, no. 3, pp. 963–973, Jun. 2006.
- [35] L. Wang, J. Jatskevich, and S. D. Pekarek, "Modeling of Induction Machines Using a Voltage-Behind-Reactance Formulation," *IEEE Trans. Energy Convers.*, vol. 23, no. 2, pp. 382–392, Jun. 2008.
- [36] A. Sapena-Bano, J. Martinez-Roman, R. Puche-Panadero, M. Pineda-Sanchez, J. Perez-Cruz, and M. Riera-Guasp, "Induction machine model with space harmonics for fault diagnosis based on the convolution theorem," *Int. J. Electr. Power Energy Syst.*, vol. 100, pp. 463–481, Sep. 2018.
- [37] A. Belahcen, A. Arkkio, and J. Martinez, "Broken bar indicators for cage induction motors and their relationship with the number of consecutive broken bars," *IET Electr. Power Appl.*, vol. 7, no. 8, pp. 633–642, Sep. 2013.
- [38] J. Faiz, B. M. Ebrahimi, H. A. Toliyat, and W. S. Abu-Elhaija, "Mixed-fault diagnosis in induction motors considering varying load and broken bars location," *Energy Convers. Manag.*, vol. 51, no. 7, pp. 1432–1441, Jul. 2010.
- [39] Z. Song, Y. Yu, F. Chai, and Y. Tang, "Radial Force and Vibration Calculation for Modular Permanent Magnet Synchronous Machine With Symmetrical and Asymmetrical Open-Circuit Faults," *IEEE Trans. Magn.*, vol. 54, no. 11, pp. 1–5, Nov. 2018.
- [40] V. Fireteanu, "Detection of the Short-Circuit Faults in the Stator Winding of Induction Motors based on Harmonics of the Neighboring Magnetic Field," *J. Phys. Conf. Ser.*, vol. 450, p. 012021, Jun. 2013.
- [41] J. Martinez, A. Belahcen, J. Detoni, and A. Arkkio, "A 2D FEM analysis of electromechanical signatures in induction motors under dynamic eccentricity," *Int. J. Numer. Model. Electron. Networks, Devices Fields*, vol. 27, no. 3, pp. 555–571, May 2014.
- [42] B. M. Ebrahimi, J. Faiz, and M. J. Roshtkhari, "Static-, Dynamic-, and Mixed-Eccentricity Fault Diagnoses in Permanent-Magnet Synchronous Motors," *IEEE Trans. Ind. Electron.*, vol. 56, no. 11, pp. 4727–4739, Nov. 2009.

- [43] A. Sapena-Bano *et al.*, "Harmonic Order Tracking Analysis: A Novel Method for Fault Diagnosis in Induction Machines," *IEEE Trans. Energy Convers.*, vol. 30, no. 3, pp. 833–841, Sep. 2015.
- [44] J. Cusido, L. Romeral, J. A. Ortega, J. A. Rosero, and A. Garcia Espinosa, "Fault detection in induction machines using power spectral density on the wavelet decomposition," *IEEE Trans. Ind. Electron.*, vol. 55, no. 2, pp. 633–643, 2008.
- [45] A. Sapena-Bano, J. Burriel-Valencia, M. Pineda-Sanchez, R. Puche-Panadero, and M. Riera-Guasp, "The Harmonic Order Tracking Analysis Method for the Fault Diagnosis in Induction Motors Under Time-Varying Conditions," *IEEE Trans. Energy Convers.*, vol. 32, no. 1, pp. 244–256, Mar. 2017.
- [46] T. J. Kang, C. Yang, Y. Park, D. Hyun, S. Bin Lee, and M. Teska, "Electrical Monitoring of Mechanical Defects in Induction Motor-Driven V-Belt-Pulley Speed Reduction Couplings," *IEEE Trans. Ind. Appl.*, vol. 54, no. 3, pp. 2255–2264, May 2018.
- [47] K. N. Gyftakis, P. A. Panagiotou, and S. Bin Lee, "Generation of Mechanical Frequency Related Harmonics in the Stray Flux Spectra of Induction Motors Suffering from Rotor Electrical Faults," *IEEE Trans. Ind. Appl.*, vol. 56, no. 5, pp. 4796–4803, Sep. 2020.
- [48] Y. Park, H. Choi, S. Bin Lee, and K. N. Gyftakis, "Search Coil-Based Detection of Nonadjacent Rotor Bar Damage in Squirrel Cage Induction Motors," *IEEE Trans. Ind. Appl.*, vol. 56, no. 5, pp. 4748–4757, Sep. 2020.
- [49] Y. Park *et al.*, "Stray flux monitoring for reliable detection of rotor faults under the influence of rotor axial air ducts," *IEEE Trans. Ind. Electron.*, vol. 66, no. 10, pp. 7561–7570, Oct. 2019.
- [50] P. A. Panagiotou, I. Arvanitakis, N. Lophitis, J. A. Antonino-Daviu, and K. N. Gyftakis, "On the broken rotor bar diagnosis using time–frequency analysis: 'Is one spectral representation enough for the characterisation of monitored signals?'," *IET Electr. Power Appl.*, vol. 13, no. 7, pp. 932–942, Jul. 2019.
- [51] T. Wang, H. Liu, L. Zhao, J. Huang, and Z. Hou, "Quantitative broken rotor bar fault detection for closed-loop controlled induction motors," *IET Electr. Power Appl.*, vol. 10, no. 5, pp. 403–410, May 2016.
- [52] Z. Hou, J. Huang, H. Liu, M. Ye, Z. Liu, and J. Yang, "Diagnosis of broken rotor bar fault in open- and closed-loop controlled wye-connected induction motors using zero-sequence voltage," *IET Electr. Power Appl.*, vol. 11, no. 7, pp. 1214–1223, Aug. 2017.
- [53] B. Asad, T. Vaimann, A. Belahcen, A. Kallaste, A. Rassõlkin, and M. N. Iqbal, "Broken rotor bar fault detection of the grid and inverter-fed induction motor by effective attenuation of the fundamental component," *IET Electr. Power Appl.*, Jul. 2019.
- [54] H. A. Toliyat, E. Levi, and M. Raina, "A review of RFO induction motor parameter estimation techniques," *IEEE Trans. Energy Convers.*, vol. 18, no. 2, pp. 271–283, Jun. 2003.
- [55] S. Bin Lee *et al.*, "Condition Monitoring of Industrial Electric Machines: State of the Art and Future Challenges," *IEEE Ind. Electron. Mag.*, vol. 14, no. 4, pp. 158–167, Dec. 2020.

- [56] B. K. Bose, *Modern power electronics and AC drives*. Prentice Hall, 2002.
- [57] M. Ranta, M. Hinkkanen, A. Belahcen, and J. Luomi, "Inclusion of hysteresis and eddy current losses in nonlinear time-domain inductance models," in *IECON 2011 - 37th Annual Conference of the IEEE Industrial Electronics Society*, 2011, pp. 1897–1902.
- [58] J. Pyrhonen, T. Jokinen, and V. Hrabovcov, *Design of Rotating Electrical*. 2008.
- [59] T. A. Lipo, *Analysis of synchronous machines: Second Edition*. 2017.
- [60] J. Davis and D. Novotny, "Equivalent Circuits for Single-Phase Squirrel-Cage Induction Machines with both Odd and Even Order MMF Harmonics," *IEEE Trans. Power Appar. Syst.*, vol. PAS-88, no. 7, pp. 1080–1086, Jul. 1969.
- [61] T. A. Lipa and T. A. Nondahl, "Pole-by-Pole d-q Model of a Linear Induction Machine," *IEEE Trans. Power Appar. Syst.*, vol. PAS-98, no. 2, pp. 629–642, Mar. 1979.
- [62] T. a H. A.Toliat, T. A. Lipo and J. C. White, "Analysis of a concentrated winding induction machine for adjustable speed drive applications. Part 1: Motor analysis," *Energy*, vol. 6, no. 4, pp. 1–5, 1991.
- [63] J. C. Moreira and T. A. Lipo, "Modeling of saturated AC machines including air gap flux harmonic components," *IEEE Trans. Ind. Appl.*, vol. 28, no. 2, pp. 343–349, 1992.
- [64] H. A. Toliat, M. M. Rahimian, and T. A. Lipo, "dq modeling of five phase synchronous reluctance machines including third harmonic of air-gap MMF," in *Conference Record of the 1991 IEEE Industry Applications Society Annual Meeting*, pp. 231–237.
- [65] S. Nandi, "Modeling of Induction Machines Including Stator and Rotor Slot Effects," *IEEE Trans. Ind. Appl.*, vol. 40, no. 4, pp. 1058–1065, Jul. 2004.
- [66] N. M. Elkasabgy, A. R. Eastham, and G. E. Dawson, "Detection of broken bars in the cage rotor on an induction machine," *IEEE Trans. Ind. Appl.*, vol. 28, no. 1, pp. 165–171, 1992.
- [67] A. Belahcen, J. Martinez, and T. Vaimann, "Comprehensive computations of the response of faulty cage induction machines," in *2014 International Conference on Electrical Machines (ICEM)*, 2014, pp. 1510–1515.
- [68] B. Asad, L. Eensalu, T. Vaimann, A. Kallaste, A. Rassolkin, and A. Belahcen, "The FEM Based Modeling and Corresponding Test Rig Preparation for Broken Rotor Bars Analysis," in *2019 IEEE 60th Annual International Scientific Conference on Power and Electrical Engineering of Riga Technical University, RTUCON 2019 - Proceedings*, 2019.
- [69] A. Villalonga, G. Beruvides, F. Castano, and R. E. Haber, "Cloud-Based Industrial Cyber-Physical System for Data-Driven Reasoning: A Review and Use Case on an Industry 4.0 Pilot Line," *IEEE Trans. Ind. Informatics*, vol. 16, no. 9, pp. 5975–5984, Sep. 2020.
- [70] Z. Chen *et al.*, "Deep Learning Research and Development Platform: Characterizing and Scheduling with QoS Guarantees on GPU Clusters," *IEEE Trans. Parallel Distrib. Syst.*, vol. 31, no. 1, pp. 34–50, Jan. 2020.

- [71] Y. Gao *et al.*, "Parallel End-to-End Autonomous Mining: An IoT-Oriented Approach," *IEEE Internet Things J.*, vol. 7, no. 2, pp. 1011–1023, Feb. 2020.
- [72] I. Bandyopadhyay, P. Purkait, and C. Koley, "A combined image processing and Nearest Neighbor Algorithm tool for classification of incipient faults in induction motor drives," *Comput. Electr. Eng.*, vol. 54, pp. 296–312, Aug. 2016.
- [73] H. Guesmi, S. Ben Salem, K. Bacha, and S. Zeadally, "Smart wireless sensor networks for online faults diagnosis in induction machine," *Comput. Electr. Eng.*, vol. 41, no. C, pp. 226–239, Jan. 2015.
- [74] J. Chen, K. Li, K. Bilal, X. Zhou, K. Li, and P. S. Yu, "A Bi-layered parallel training architecture for large-scale convolutional neural networks," *IEEE Trans. Parallel Distrib. Syst.*, vol. 30, no. 5, pp. 965–976, May 2019.
- [75] Y. You, Z. Zhang, C. J. Hsieh, J. Demmel, and K. Keutzer, "Fast Deep Neural Network Training on Distributed Systems and Cloud TPUs," *IEEE Trans. Parallel Distrib. Syst.*, vol. 30, no. 11, pp. 2449–2462, Nov. 2019.
- [76] S. R. Huang, K. H. Huang, K. H. Chao, and W. T. Chiang, "Fault analysis and diagnosis system for induction motors," *Comput. Electr. Eng.*, vol. 54, pp. 195–209, Aug. 2016.
- [77] V. Mukherjee, M. F. Far, F. Martin, and A. Belahcen, "Constrained Algorithm for the Selection of Uneven Snapshots in Model Order Reduction of a Bearingless Motor," *IEEE Trans. Magn.*, vol. 53, no. 6, Jun. 2017.
- [78] M. Farzam Far, F. Martin, A. Belahcen, P. Rasilo, and H. A. A. Awan, "Real-Time Control of an IPMSM Using Model Order Reduction," *IEEE Trans. Ind. Electron.*, pp. 1–1, Feb. 2020.
- [79] M. Farzam Far, F. Martin, A. Belahcen, L. Montier, and T. Henneron, "Orthogonal Interpolation Method for Order Reduction of a Synchronous Machine Model," *IEEE Trans. Magn.*, vol. 54, no. 2, Feb. 2018.
- [80] A. Silik, M. Noori, W. A. Altabey, R. Ghiasi, and Z. Wu, "Comparative analysis of wavelet transform for time-frequency analysis and transient localization in structural health monitoring," *SDHM Struct. Durab. Heal. Monit.*, vol. 15, no. 1, pp. 1–22, 2021.

Acknowledgements

I would like to express my sincere gratitude to my advisors for their continuous support and guidance through their immense knowledge, experience and motivation.

I am also thankful to my colleagues and fellow students for their help and support whenever I needed it.

I am also sincerely thankful to my family especially my beloved wife Dr. Amina Bilal. This course of studies would not have been possible without their encouragement, patience and support.

Abstract

Mathematical Modelling of Three Phase Squirrel Cage Induction Motor and Related Signal Processing for Fault Diagnostics

This thesis aims to study different analytical methods to model a squirrel cage induction motor, which should have minimal simulation time than the corresponding finite element method (FEM) based models. The purpose of doing so is to develop a model suitable to simulate all major faults and be used for advanced model-dependent fault diagnostic algorithms, such as parameters estimation and inverse problem theory. This thesis's second key objective is to study various signal-processing techniques for their pros and cons to detect fault at the embryonic stage and investigate the entire current harmonic spectrum of induction motors both in transient and steady-state regions. Thus, the motor under healthy and broken rotor bar (BRB) conditions are simulated, and experimental measurements are investigated for validation.

The dynamic d-q model with the inclusion of non-linear magnetization inductance was considered as a starting point. This model helps understand the machine's basic concepts because of its comprehensiveness and ability to produce compact equations, which can be used for drives as general and in observers and state estimators as particular. However, this model was found to be less suitable to simulate machine faults because of the considered approximations.

To address the d-q model limitations, the winding function analysis (WFA) based model was prepared. In this model, the analytical equations to calculate various inductances, resistances, currents, fluxes, torque, and speed are derived for the motor under investigation. These equations were simulated in MATLAB, giving results near to the practical measurements. The model is suitable for implementing some faults, such as BRB and broken end rings. Still, the consideration of constant air gap makes it less ideal for the implementation of eccentricity and saturation-related faults. Moreover, the spatial harmonics, which are very important for fault diagnostics and sensor-less speed estimation, cannot be simulated. Those approximations can be reduced with Fourier summation of higher-order harmonics (winding) and Taylor series to include inverse air gap functions but at the cost of the self-defined number and amplitude of harmonics.

To get more realistic results, the modified winding function analysis (MWFA) based model was prepared to ensure that all winding functions and air gap were defined as a function of stator and rotor individual and respective angles. The geometry of stator and rotor slots is considered to calculate the leakage inductances and various resistances. The self and mutual inductances between rotor and stator are computed with a stepping rotor. The results at each rotor position are saved in offline 3D lookup tables. During the online simulation, all pre-saved matrices are used as a rotor position function using their index value, and the performance parameters, such as currents, fluxes, torque, and speed, are calculated. The FEM and hybrid FEM-analytical models of the machine under investigation are prepared using commercial software to validate the results. The comparison of results shows an excellent agreement with a minimal simulation time and least ill-posedness for the proposed model compared to the corresponding FEM model.

Both analytical and hybrid FEM-analytical models are divided into online, offline portions and compatible for the solution on cluster computation. Their division in the

online and offline portions reduces the complexity and gives the model the freedom to simulate faults in the online portion without doing unnecessary offline calculations again. Moreover, the compatibility with cluster computation is excellent for exploiting distributed computational resources such as cloud computation, an integral part of industry 4.0 standards.

Towards the signal processing side, the fast Fourier transform (FFT) and wavelet transform (WT) are used extensively to study the steady-state and transient regime signals. The infinite impulse response (IIR) based digital filters are used to improve the motor's current spectrum's legibility. In this way, the total harmonics are segregated according to their cause of production. Moreover, the spectrum of current simulated from the proposed model is compared with that simulated using the FEM model and the test rig measurements. The comparison is made until a wide bandwidth of frequencies for further validation of the proposed model.

Moreover, the WFA based model is also investigated during the transient regime by doing the time-frequency analysis of the stator current. The recovered non-stationary signal's pattern is in good agreement with the one obtained from the practical measurements. The specific fault-related pattern during the transient interval can further enhance the model's effectiveness.

Kokkuvõte

Kolmefaasilise lühisrootoriga asünkroonmootori matemaatiline modelleerimine ning lähtuv rikke diagnostiline signaalitöötlus

Doktoritöö eesmärgiks on uurida analüütilisi meetodeid lühisrootoriga asünkroonmootori modelleerimiseks, mis vajavad oluliselt vähem simuleerimisaega kui samaväärsed lõplike elementide meetodil (FEM) baseeruvad mudelid. Seda tehakse omakorda eesmärgil, et välja töötada mudel, millega on võimalik simuleerida kõiki enim levinud elektrimasinate rikkeid, mida omakorda saab kasutada keerukates modelleerimisel baseeruvates diagnostilistes algoritmides, nagu parameetrite ennustamine ja pöördprobleemi teoorias. Teiseks oluliseks eesmärgiks antud doktoritöös on erinevate signaalitöötlusalgoritmide uurimine, hinnates nende eeliseid ja puuduseid, tuvastamaks rikkeid võimalikult varajases staadiumis ning võimaldades süvitsi analüüsida asünkroonmootorite terviklikku vooluspektrit nii siirete kui püsitalitluse olukordades. Selleks teostati väljatöötatud mudelil simulatsioonid nii korrasoleva kui purunenud rootorivarrastega mootoril ning mudel valideeriti eksperimentaalsete mõõtetulemustega.

Esialgseks mudeliks valiti mitte-lineaarse magneetimisinduktsiooniga dünaamiline d-q mudel. Antud mudel aitab mõista masina põhikontseptsioone, sest on piisavalt kõikehõlmav ning võimaldab genereerida kompaktsed valemeid, mida saab edasi kasutada elektriaramites näiteks olekujälgimis ja -hindamis funktsioonides. Samas kasutab mudel olulisi lihtsustusi, mistõttu ei ole see sobiv elektrimasinate rikete simuleerimiseks.

Et lahendada d-q mudelis esile kerkinud piiranguid, töötati välja masina mudel, mis baseerub mähise funktsiooni analüüsil. Antud mudeli baasil tuletatakse analüütilised valemid, mille abil leitakse mootori erinevad induktiivsused, takistused, voolud, magnetvood, moment ja kiirus. Neid valemid simuleeriti MATLAB keskkonnas, mis andis katselistele andmetele ligilähedasi tulemusi. Antud mudel sobib osaliselt rikete simuleerimiseks, nagu purunenud rootorivarrad ja lühisrõngad. Samas, kuna mudelis kasutatakse konstantset õhupilu, ei ole sellega ideaalselt võimalik simuleerida ekstsentrilisuse ja küllastusega seotud rikkeid. Lisaks, ei ole antud mudeliga võimalik ruumiliste harmooniliste simuleerimine, mis on vajalikud diagnostiliste indikaatoritena ning andurivabaks kiiruse ennustamiseks. Nimetatud lihtsustuste mõju saab vähendada Fourier' kõrgema järgu mähise harmoonikute summeerimisega ning Tayloriga rea kasutamisega, võttes arvesse pööratud õhupilu funktsiooni, kuid seda analüüsivate harmoonikute hulga ja amplituudide arvelt.

Realistlikumate tulemuste saamiseks valmistati parandatud mähise funktsiooni analüüsil baseeruv mudel, kus mähise funktsioonid ning õhupilu defineeritakse staatori ja rootori individuaalsete ning üksteisest sõltuvate nurkade funktsioonina. Staatori ja rootori uurete geomeetriat võetakse arvesse arvutamaks eri takistusi ja lekke induktiivsusi. Oma- ja vastastikinduktiivsuste arvutamiseks rootoris ja staatoris on kasutatud rootori sammulist nihutamist. Iga rootori positsiooni arvutustulemused salvestati kolmemõõtmelistesse teatmetabelitesse. Simuleerimise ajal kasutatakse varem salvestatud maatrikseid rootori positsiooni funktsioonina, arvestades nende indeks-väärtuseid, ning arvutatakse masina tööparameetrid nagu voolud, vood, moment ja kiirus. FEM ja hübriidsed FEM-analüütilised mudelid valmistati kasutades

kommertsiaalset tarkvara, et valideerida saadud tulemusi. Tulemuste võrdlus, võrreldes arendatud mudelit samaväärse FEM mudeliga, näitab suurepärase kokkulangevust, kasutades vähemat simuleerimisaega ning väiksemat arvu probleemi väärpüstistust.

Nii analüütilised kui hübriid FEM-analüütilised mudelid on jagatud aktiiv- ja passiivosadeks ning on ühildatavad klasterarvutuse lahendustesse. Selline jagamine tagab keerukuse vähendamise ja annab mudelile vabaduse rikete simuleerimiseks ilma vajaduseta korrata mittevajalikke passiivarvutusi. Lisaks on klasterarvutusega ühilduvus suurepärase võimalus jagatud arvutusvõimsuste kasutamiseks näiteks pilvearvutuse näol, toetades Tööstus 4.0 standardeid.

Signaalitöötluses kasutati laialdaselt kiire Fourier' teisenduse ja lainikeisenduse võimalusi masina püsitalitluse ja siirdeprotsesside signaalide põhjalikuks uurimiseks. Piiramatult siirdega filtril baseeruvaid digitaalfiltreid kasutati mootori vooluspektri loetavuse parendamiseks. See annab võimaluse harmoonikute eraldamiseks arvestades nende põhjustajaid. Arendatud mudeli simuleeritud vooluspektrit võrreldi FEM mudelil ja katseandmetest saadud vastavate spektritega, kasutades laia sagedusvahemikku, eesmärgiga valideerida arendatud mudeli korrektsust.

Lisaks on mähise funktsiooni analüüsil baseeruv mudelit uuritud siirete korral läbi staatorivoolu aeg-sageduse analüüsi. Saadud signaalikuju on tugevas vastavuses eksperimentaalsete mõõtetulemuste omaga. Mudelit saab edasi arendada arvestades spetsiifilisi rikkest põhjustatud signaalikuju muutusi siirdeprotsesside ajal.

Appendix

Publication I

Asad, B.; Vaimann, T.; Belahcen, A.; Kallaste, A.; Rassõlkin, A.; Ghafarokhi, P. S.; Kudelina, K. Transient Modeling and Recovery of non-Stationary Fault Signature for Condition Monitoring of Induction Motors. Appl. Sci., vol. 11 (6), 2806, Mar. 2021.

Article

Transient Modeling and Recovery of Non-Stationary Fault Signature for Condition Monitoring of Induction Motors

Bilal Asad ^{1,2,*} , Toomas Vaimann ¹ , Anouar Belahcen ^{1,2} , Ants Kallaste ¹ , Anton Rassõlkin ¹ , Payam Shams Ghafarokhi ³  and Karolina Kudelina ¹ 

- ¹ Department of Electrical Power Engineering and Mechatronics, Tallinn University of Technology, 19086 Tallinn, Estonia; toomas.vaimann@taltech.ee (T.V.); Anouar.Belahcen@aalto.fi (A.B.); ants.kallaste@taltech.ee (A.K.); anton.rassolkin@taltech.ee (A.R.); karolina.kudelina@taltech.ee (K.K.)
² Department of Electrical Engineering and Automation, Aalto University, FI-00076 Espoo, Finland
³ Department of Electrical Machine and Apparatus, Riga Technical University, LV-1658 Riga, Latvia; payam.shams-ghafarokhi@rtu.lv
 * Correspondence: bilal.asad@aalto.fi

Abstract: This paper presents the modeling and the broken rotor bar fault diagnostics by time–frequency analysis of the motor current under an extended startup transient time. The transient current-based nonstationary signal is retrieved and investigated for its time–frequency response to segregate the rotor faults and spatial harmonics. For studying the effect of reduced voltage on various parameters and the theoretical definition of the fault patterns, the winding function analysis (WFA)-based model is presented first. Moreover, an algorithm to improve the spectrum legibility is proposed. It is shown that by efficient utilization of the attenuation filter and consideration of the area containing the maximum power spectral density, the diagnostic algorithm gives promising results. The results are based on the machine’s analytical model and the measurements taken from the laboratory setup.

Keywords: condition monitoring; fault diagnosis; Fourier transform; induction motors; modeling; wavelet transform



Citation: Asad, B.; Vaimann, T.; Belahcen, A.; Kallaste, A.; Rassõlkin, A.; Ghafarokhi, P.S.; Kudelina, K. Transient Modeling and Recovery of Non-Stationary Fault Signature for Condition Monitoring of Induction Motors. *Appl. Sci.* **2021**, *11*, 2806. <https://doi.org/10.3390/app11062806>

Academic Editor:
Mohamed Benbouzid

Received: 17 February 2021
 Accepted: 18 March 2021
 Published: 21 March 2021

Publisher’s Note: MDPI stays neutral with regard to jurisdictional claims in published maps and institutional affiliations.



Copyright: © 2021 by the authors. Licensee MDPI, Basel, Switzerland. This article is an open access article distributed under the terms and conditions of the Creative Commons Attribution (CC BY) license (<https://creativecommons.org/licenses/by/4.0/>).

1. Introduction

Electrical machines have been showing their influential role in industrial and domestic applications since the second industrial revolution. This role is evident in electricity generation, such as wind power plants or electrical to mechanical energy converters, which are driving the industry. In various electrical machines, induction motors are ubiquitous because of their simple structure, good efficiency and easy maintenance. A variety of applications makes them consume more than fifty percent of the total energy generated worldwide.

The mechanically moving parts and harsh industrial environment make them vulnerable to faults. The electrical faults are mostly related to the stator, such as inter-turn short circuits, phase drop, voltage imbalance, earthing and inverter-related defects. However, the mechanical faults are mainly associated with the rotor, such as broken bars, bad bearings, eccentricity, broken end rings or inadequate foundations. All those faults are degenerative, making it crucial to detect them at the developing stage to avoid catastrophic situations. Various fault diagnostic techniques are available in the literature, such as vibration analysis, thermal analysis, acoustic analysis, electromagnetic field inference, leakage flux, infrared light detection and chemical analysis.

However, motor current signature analysis (MCSA)-based fault diagnostic techniques are gaining heightened popularity because of their noninvasive nature and lower complexity. Moreover, a vast field of data processing techniques improves their flexibility and makes them more reliable.

It is a well-studied fact that almost all rotor faults modulate the stator currents with specific frequency components. The detection of those frequency components can lead to the cause of the fault. The Fourier transform can be considered a foundation stone for all advanced signal processing techniques. The majority of MCSA-based methods depend on a fast Fourier transform (FFT) of the signal; for example, in [1], the authors used the FFT on the active and reactive currents of a motor to investigate the broken rotor bars and load oscillations. The authors of [2] used the FFT in conjunction with Park's vector to make an artificial ants clustering technique for the fault diagnostics of an induction motor. The Park's vector makes an entire domain of condition monitoring of electrical equipment [3–7], giving promising results if used in conjunction with FFT. In [8], the autoregressive method relied on a discrete-time Fourier transform (DTFT) and a notch filter. The researchers in [9] used the FFT to prove that slot harmonics could be used as potential indicators to detect broken rotor bars. In [10], the authors used an adaptive notch filter and FFT for broken rotor bar fault diagnostics of an induction motor. In [11], the FFT was used on simulations and practical results to investigate broken rotor bars and mechanical vibrations. In [12], Nandi used the FFT to study the stator current frequency spectrum for different fault conditions, and in [13], the FFT was used along with a band-stop filter for the detection of broken rotor bar frequencies.

However, there are certain limitations of the FFT, putting a question mark on its reliability for fault diagnostics. These limitations include spectral leakage, which is the power of the main components leaking into the subsequent frequency bins. If the acquired signal's length and sampling frequency are not good enough, the faults representing frequency components are highly likely to be buried under the corresponding primary frequency bins. This problem becomes worse when the motor is working under no-load or lesser-load conditions, as the faulty frequencies are the function of slip. The other issue of the FFT is that the signal should be in a steady state regime, be stationary and not have any discontinuities. These problems are becoming worse as the inverters are coming forward as an integral part of the drive system. The inverter-fed voltage is full of harmonics, which makes the frequency spectrum hazy to understand. Moreover, the drive control algorithms can also have an impact on the amplitude of the harmonics. For example, in the case of direct torque control (DTC) motors, the drive directly influences the current signal carrying all the information about the motor's health [14].

Researchers have tried several different techniques to cope with these problems. The use of Hilbert transforms to extract the signal's envelope, which possesses considerable information regarding the electrical machine's health, can be found in [15]. The authors in [16] used a fractional Fourier transform to recover the faulty frequencies from a non-stationary signal. In [17], the authors used a sliding discrete Fourier transform for the detection of broken rotor bars, while [18–21] used the wavelet technique to improve the accuracy. These techniques' capability to handle nonstationary signals opens a new paradigm in the field of fault diagnostics [22–24]. However, the poor time–frequency resolution is still a challenge.

This paper presents the following attractive features:

- For studying the impact of broken bars on different performance parameters, a WFA-based analytical model is developed. This model takes less simulation time to study the effect of low voltage and asymmetry on the machine's performance. It also helps to plot the faulty theoretical patterns used as a benchmark for differentiation among fault and spatial harmonics;
- Unlike most of the papers where a high inertia load or variable transformer is used, an industrial inverter-based low voltage test to extend the motor's transient interval is proposed. It is also described how an industrial inverter can reduce the voltage while maintaining a constant rated frequency. Increasing the transient length of the motor startup current improves the time–frequency resolution of the spectrum;

- An algorithm to improve the spectrum's legibility is proposed, which helps segregate various frequency patterns in the transient regime;
- The wavelet transform is preferred over the short-time Fourier transform (STFT) to avoid inherited FFT drawbacks. Moreover, a band-stop infinite impulse response (IIR) filter is used to attenuate the fundamental component, which improves the spectrum's legibility;
- It is proposed that the selection of time–frequency regions with a 95% confidence interval (CI) in the form of a contour plot gives a more unambiguous indication of faulty patterns. By adjusting the level of the CI, the spatial and switching frequency-based patterns can be avoided. To the best of the author's knowledge, this technique is not presented in the literature so far.

2. Theoretical Background

2.1. The Modeling of Induction Motor

Electrical machines' modeling is the first milestone in machine design, control, analysis and diagnostics. The famous modeling techniques are divided into two major categories: analytic and numerical. The commonly used analytic methods are two-axis theory [25], winding function method (WFM) [26–28], reluctance network [29] and convolution theorem-based models [30]. The finite element method (FEM)-based models are typical examples of numerical modeling of electrical machines. Although the numerical models have the least number of approximations, the complexity and computational time is the biggest drawback [31]. It becomes worst in the field of fault diagnostics, where the motor's symmetry cannot be exploited to reduce the simulation time. For the fault diagnostic in the transient regime, the V-shaped pattern made by the sideband frequencies is significant. This pattern generates because of the varying slip until the steady state region. This nonstationary signal moves in a bandwidth from 0 Hz to 50 Hz. Thus, the higher-order slotting harmonics become less significant for the analysis of the fault-based, nonstationary signal. The winding function-based model with much less complexity than the corresponding FEM-based models is essential to differentiate among several harmonics. Hence, the air gap is considered constant by neglecting the slot openings with the magnetic material's infinite permeability. The stator winding is approximated as a pure sinusoid, while the rotor turn function represents its actual cage structure. Various self and mutual inductances can be calculated using the winding function formula as in Equation (1). The analytical formulas for the calculation of different inductances given in Equations (2)–(6) are the solution of (1) for the winding functions, as described in [32]:

$$L_{ij}(\theta) = \mu_0 r l \int_0^{p\pi} g^{-1}(\varphi, \theta) N_i(\varphi, \theta) N_j(\varphi, \theta) d\theta \quad (1)$$

$$L_m = \frac{\mu_0 r l}{g} \left(\frac{p}{2} \right) \left(\frac{N_s}{p} \right)^2 \pi \quad (2)$$

$$L_{AB} = L_{BC} = L_{CA} = -\frac{L_m}{2} \quad (3)$$

$$L_{rkk} = \left(\frac{\mu_0 r l}{g} \right) \alpha_r \left[1 - \frac{\alpha_r}{p\pi} \right] \left(\frac{p}{2} \right) \quad (4)$$

$$L_{rki} = \left(\frac{\mu_0 r l}{g} \right) \left[-\frac{\alpha_r^2}{p\pi} \right] \left(\frac{p}{2} \right) \quad (5)$$

$$L_{sri}(\theta_r) = \left(\frac{\mu_0 r l N_s}{g} \right) \sin\left(\frac{\alpha_r}{2}\right) \cos(\theta_r + (i-1)\alpha_r + \frac{\alpha_r}{2}) \quad (6)$$

where μ_0 is the permeability of the free space; r is the machine's radius, which is taken as the center of the air gap; l is the machine's effective length; g is the air gap width; α_r is the angular displacement between two consecutive rotor bars; p is the number of the poles; N_s is the number of effective turns per phase in the stator; and θ and φ are the rotor and stator

angular positions from a reference point. In Equation (6), the inductance is multiplied with a cosine function of θr to emulate the rotating rotor, where integer i changes the angle of the respective rotor bar from the stator reference point. Lm is the magnetization inductance, L_{AB} , L_{BC} and L_{CA} are stator mutual inductances, L_{rkk} and L_{rki} are rotor self and mutual inductances and L_{sri} is the mutual inductance between the stator and rotor.

The performance parameters, such as torque, speed, currents and voltages, can be calculated using Equations (7)–(9):

$$\begin{bmatrix} V_s \\ 0 \end{bmatrix} = \begin{bmatrix} R_s & 0 \\ 0 & R_r \end{bmatrix} \begin{bmatrix} I_s \\ I_r \end{bmatrix} + \frac{d}{dt} \begin{bmatrix} L_{ss} & L_{sr} \\ L_{rs} & L_{rr} \end{bmatrix} \begin{bmatrix} I_s \\ I_r \end{bmatrix} \quad (7)$$

$$T_e = I_s^T \left(\frac{d}{d\theta} L_{rs} \right) I_r \quad (8)$$

$$J \frac{d}{dt} \omega_m = T_e - T_L - B_f \omega_m \quad (9)$$

where V_s is the stator input voltage vector and R_s and R_r are the stator and rotor resistance matrices of orders (3×3) and (40×40) , respectively. Similarly, L_{ss} , L_{sr} , L_{rs} and L_{rr} are the matrices containing stator–stator, stator–rotor, rotor–stator, and rotor–rotor self and mutual inductances at a specific rotor position. Moreover, T_e is the generated torque, I_s is the stator current, I_r is the rotor current, T_L is the loading torque, B_f is friction coefficient, ω_m is rotor angular velocity and J is the moment of inertia. The detailed model with slot openings and the actual winding functions can be found in [33].

2.2. The Fault Signature Equations and Modulation

Almost all rotor-related faults produce frequency components in the induction motor's current and the voltage spectrum as a slip function. The most common rotor faults can be diagnosed by detecting the frequencies represented by the equations shown in Table 1.

Table 1. Fault definition frequencies.

Fault	Modulating Frequencies
Broken Rotor Bars	$f_{BR} = f_s \pm 2ksf_s, \quad k = 1, 2, 3, \dots$ $f_{ecce} = \left[(kn_b \pm n_d) \left(\frac{1-s}{p} \right) \pm v \right] f_s$
PSH and Eccentricity	More precisely: $f_{ecce} = \left[1 \pm k \left(\frac{1-s}{p} \right) \right] f_s$ $f_{ecce} = f_s \pm kf_r, \quad k = 1, 2, 3, \dots$

where k is the harmonic order, v is the supply fed harmonics, f_s is the supply frequency, f_{br} are the broken bar frequencies, n_d is the dynamic eccentricity (0 for static and 1, 2, 3 . . . for dynamic), f_r is rotor frequency, s is the slip and p is the number of poles.

The phase current of an ideal and symmetrical machine can be defined as

$$i_a(t) = I_m \sin(\omega t + \alpha) \quad (10)$$

where I_m is the peak current, ω is the supply frequency in the angular domain and α is the phase angle. The unsymmetrical rotor with broken rotor bars, broken end rings or bad bearings starts modulating the current with a frequency dependent upon the rotor's speed and the modulation index, which depends upon the severity of the fault:

$$i_{af}(t) = [1 + m(t)]i_a(t) \quad (11)$$

where $m(t)$ is the modulating signal having a modulation index M , which depends on the number of broken bars (Nb) and the total number of rotor bars (Nt). If the rotor is rotating

and the winding distributions are considered as sinusoidal, the modulating signal is also a sinusoid, such that

$$m(t) = M \cos(\omega_o t + \varphi) \quad (12)$$

where $\omega_o = 2\pi f$ is the fault characteristic frequency and depends on its nature and the machine's slip. In the case of the broken rotor bars, the characteristic fault frequency is at $2sf_s$:

$$i_{af}(t) = [1 + M \cos(4\pi s f_s t + \varphi)] i_a(t) \quad (13)$$

$$f_o = 2s f_s \quad \text{and} \quad \omega_o = 2\pi(2s f_s) \quad (14)$$

$$m(t) = M \cos(4\pi s f_s t + \varphi) \quad (15)$$

$$i_{af}(t) = [1 + M \cos(4\pi s f_s t + \varphi)] I_m \sin(\omega t) \quad (16)$$

$$i_{af}(t) = I_m \sin(2\pi f_s t) + \left(\frac{M I_m}{2} \right) [\sin(2\pi f_s (1 + 2s)t + \varphi) + \sin(2\pi f_s (1 - 2s)t + \varphi)] \quad (17)$$

The modulation index M can be approximated as a ratio between the number of broken and total rotor bars [34]:

$$M \approx \frac{N_b}{N_t} \quad (18)$$

The sine terms with frequencies $f_s(1 + 2s)$ and $f_s(1 - 2s)$ in Equation (17) correspond to the right-hand side (RHS) and left-hand side (LHS) harmonics, which makes a pattern during the transient regime as the slip changes from the maximum value to some specific value, depending upon the load.

In the steady state current, each fault is represented with a particular frequency value, as described previously. In the transient region, the frequency changes continuously. The rapidly evolving slip in the transient regime gives rise to nonstationary signals making specific patterns. The most common causes are the rotor asymmetries, such as the inherent eccentricity, the principal slotting harmonics and the broken bars or end rings. Figure 1 presents the theoretical development of those patterns for a harmonic order of two.

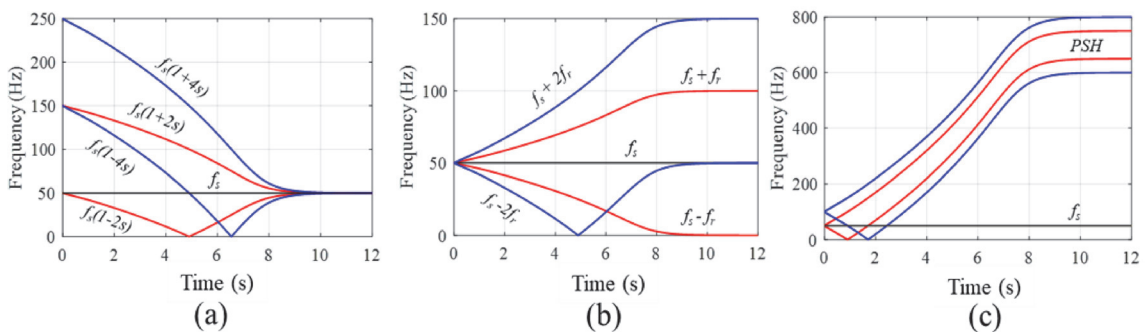


Figure 1. The development of frequency patterns in a transient regime due to (a) broken bars, (b) dynamic eccentricity and (c) principal slotting harmonics.

2.3. The Recovery of the Nonstationary Signal and Related Signal Processing

The frequency spectrum's legibility in either a steady state or transient regime depends on the signal's length and sampling frequency. The fault-representing frequencies are the function of motor slip, as described in Table 1. During the transient interval, the slip is not constant, but decreases with an increase in speed as the motor goes toward a steady state regime. This changing slip results in the creation of nonstationary signals in the transient domain. With a rated supply, this transient interval is so small that those patterns do not become visible. It becomes worse when the motor operates at a low load. The transient interval can be extended by decreasing the supply voltage with a high inertia load, while

the input voltage can be changed using a variable three-phase transformer or an industrial inverter. The increasing use of the frequency converter as a substantial part of the drive system increases the test's feasibility. By reducing the supply voltage while maintaining a constant frequency, the rotor's inertia can control the transient time of the motor. Moreover, with reduced voltage, the leakage inductance also takes more time to reach the steady state point, which also supports an extended transient interval. For any reliable signal processing-based diagnostic algorithm, the role of digital filters is undeniable.

Digital filters are the mathematical algorithms capable of reducing or enhancing specific parameters of a signal. They are used for either the separation of combined signals or the restoration of a distorted signal. Their diversified nature has many types, and they are being used extensively in almost every signal processing-based application.

They are the potential tool to remove the strong supply-based frequency components for improving the time–frequency spectrum's legibility. This is necessary because the fundamental component is powerful in amplitude compared with the fault-based harmonics, which are very weak, particularly at the fault's embryonic stage. Those low-amplitude frequency components become barely visible in the presence of the fundamental component.

To attenuate the fundamental component, the selection of an appropriate band-stop filter becomes very crucial. The infinite impulse response (IIR) band-stop filters, such as the Chebyshev II, can give promising results because of their steep transition band and low passband ripples among various digital filters. The excellent transition band and low passband ripples can reduce the filter's impact on the recovered signal.

In light of the mentioned theoretical aspects, the frequency spectrum resolution for transient and steady signals is improved in the following way, as presented in Figure 2:

- Measure the signal with the sampling frequency, meeting the Nyquist criterion. The sampling frequency can be improved later using data interpolation. This is necessary for the accurate detection of zero-crossing points. Moreover, any small constant offset due to data acquisition devices should be removed to avoid a high-amplitude 0 Hz component in the spectrum. This is achieved by subtracting the mean value of the signal from itself;
- Most signal processing techniques, such as DTFT, are sensitive to signal discontinuities and the fractional number of acquired cycles. This problem is solved by counting the integral number of cycles using zero-crossing detection. Saving the signal from the first until the last zero crossings will remove the starting and ending fractional portions of the signal;
- Each sinusoidal signal has three zero crossings, which can be exploited to get the integral number of cycles. If the number of zero crossings is odd, then the signal consists of an integral number of cycles; otherwise, the samples from the second-last zero-crossing until the end should be discarded;
- The band-stop IIR filter is then tuned to suppress the fundamental component;
- The recovered signal shows good spectral legibility both for frequency (steady state) and time–frequency (transient) analysis.

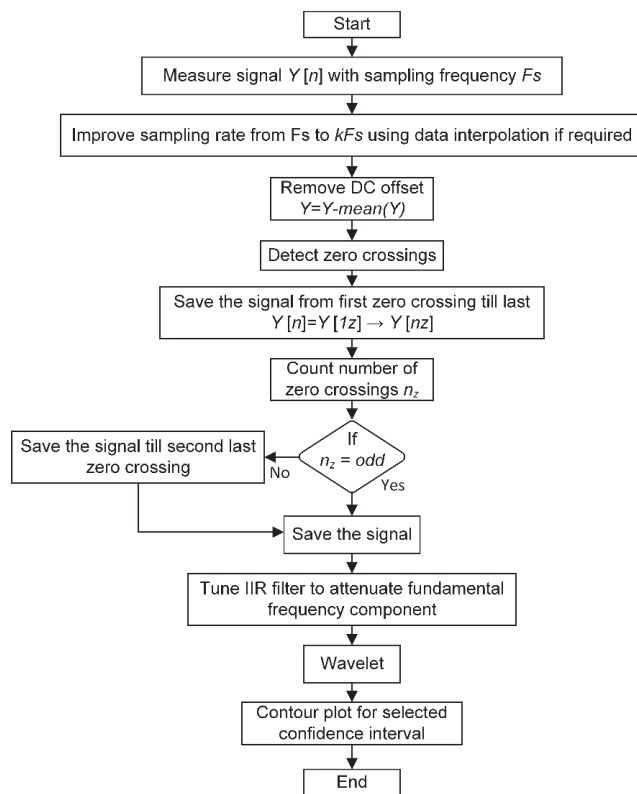


Figure 2. Flowchart for better frequency resolution and development of contour plot.

3. Simulation Results

The winding function model described in Section 2 was used for the transient and steady-state analysis of the motor's performance parameters under healthy and broken bar conditions. The broken bars were simulated by increasing the value of corresponding entries in the resistance matrix. Figure 3b shows the speed–torque dynamic response under healthy and faulty conditions. The zoomed window shows the shift of the operating point at the load application with a slight increase in the slip. The speed and torque ripples due to broken bars are visible in Figure 3a,b.

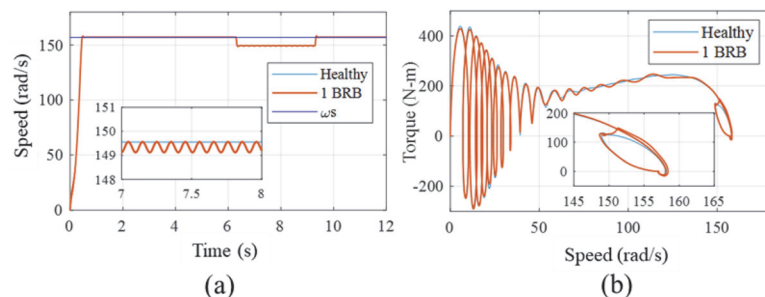


Figure 3. (a) The speed dynamic response under healthy and faulty cases. (b) The speed–torque dynamic response under the healthy and broken bar cases with shifting of the operating point upon the application of a load in the zoomed window.

These ripples were because of the fault-based induced voltage on the stator side. The frequency of those harmonics depended upon the slip, as discussed previously. During the transient interval, the slip changed dramatically from one to the nominal value, generating a nonstationary signal in the current. This transient interval was so narrow that any specific pattern was hardly visible with rated voltage conditions because of the low-frequency resolution. This phenomenon is described in Figure 4. The motor's simulated transient current at 10%, 15%, 25%, and the rated voltage is presented. The envelope is highlighted by plotting the absolute value of the analytical function given below in (19) and (20). In all subfigures, the x -axis represents the time in seconds while the y -axis represents the amplitude in amperes. Moreover, as the constant air-gap is considered in the simulation model, the non-stationary signal contains only broken bar based pattern.

$$i_A(t) = i(t) + j \hat{i}(t) \quad (19)$$

where $i(t)$ is the current, j is the imaginary unit representing the complex number and $\hat{i}(t)$ is its Hilbert-transformed signal. This can be achieved by the convolution of the signal with $1/\pi t$, as shown by the following equation:

$$H(t) = \frac{1}{\pi} \int_{-\infty}^{\infty} \left(\frac{f(x)}{t-x} \right) dx \quad (20)$$

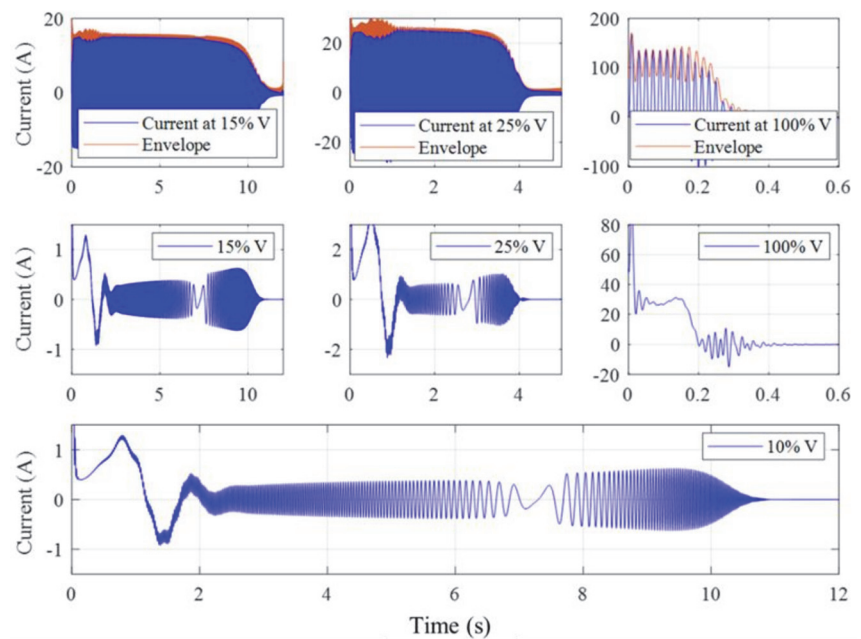


Figure 4. The motor's simulated startup currents at different voltage levels (**top row**), the recovered nonstationary signal (**middle row**) and the nonstationary signal at 10% of the rated voltage representing the changing frequency pattern (**bottom**).

All these steps can be achieved in Matlab by using the simple command `ab(hilbert(i[t]))`. The envelope contains all harmonics other than the fundamental component. For a steady state signal, the Hilbert filter is the right choice for attenuation of the fundamental component. However, in the transient regime, the phase shift of all frequency components poses a problem.

Hence, the nonstationary current signatures were recovered by attenuating the fundamental component using the IIR band-stop filter, as shown in Figure 4 (middle and last

row). With a decrease in the applied voltage, the fault-based nonstationary signal increased in length and became more legible. The time–frequency analysis of those non-stationary signals at rated voltage and 10% of the rated voltage is shown in Figure 5. With reduced voltage and the corresponding increase in the signal length, the V-shaped pattern became visible, being hardly present in the current at the rated voltage. Moreover, the supply frequency component (50 Hz) was attenuated using the proposed filter. The fault pattern became more legible by using filter and contour plots together. The contour plot shows the areas with a 95% confidence interval. With the rated voltage, the total power was confined in the region until 0.5 s without any pattern (Figure 5b), while with extended time, the pattern became visible as in Figure 5d. In the magnitude scalogram, the color bar represents the amplitude of the specific frequency component in amperes.

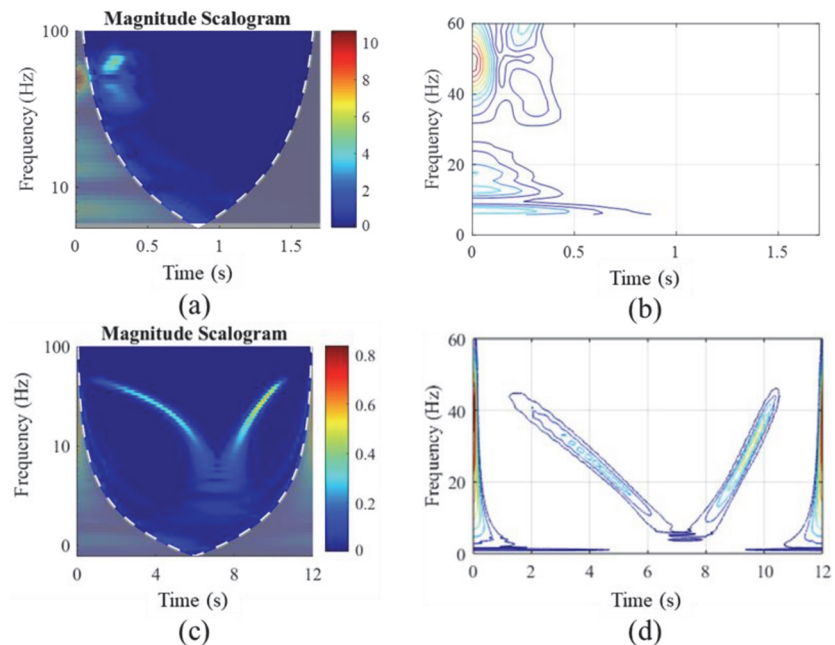


Figure 5. The time–frequency pattern of the simulated current with two broken bars at (a) the rated supply voltage, (b) the contour area of the maximum spectral density, (c) 10% of the nominal voltage and (d) the contour pattern for better legibility.

4. Practical Setup

The test rig consisted of a motor under investigation attached with a loading machine, industrial inverters and a data acquisition set-up. The motor, with specifications given in Table 2, was tested with healthy and broken bar-based rotors. The bars were broken by drilling radial holes having a depth equal to the total rotor slot height. The motor phase currents were measured under transient intervals using the Dewetron transient recorder. The measured signal’s sampling frequency was 10 kHz, which was good enough for better frequency resolution. The test set-up is shown in Figure 6. In the industrial inverter case, the variable voltage at a constant frequency could be achieved by changing the rated parameters. Since the voltage/Hz ratio in the scalar control remained constant, by changing the rated frequency with a constant rated voltage, the output voltage could be varied, as shown in Table 3. Moreover, the acceleration and deceleration time should be equal to zero to avoid the drive controller’s influence on the transient interval.

Table 2. The machine specifications.

Parameter	Symbol	Value
Number of poles	P	4
Number of phases	φ	3
Connection	-	Delta
Stator slots	Ns	36, non-skewed
Rotor bars	Nb	28, skewed
Rated voltage	V	400 V@50 Hz
Rated current	I	8.8 A
Rated power	Pr	7.5 kW @ 50 Hz

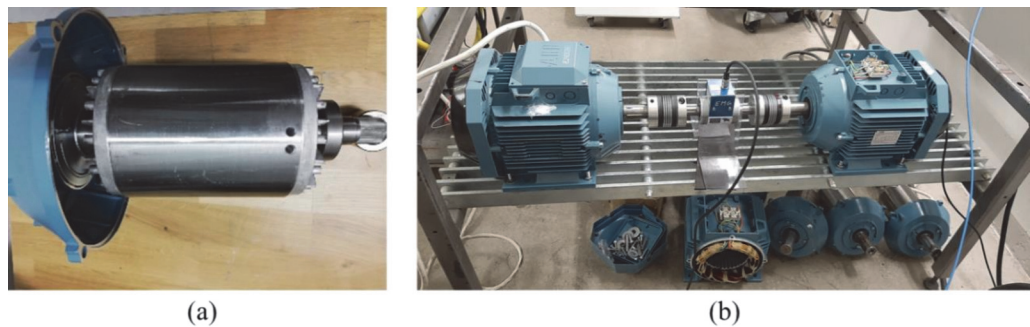


Figure 6. (a) The rotor with two broken bars. (b) The test bench with the loading motor on the right side and the test motor on the left side.

Table 3. The setting of the industrial inverter to achieve the desired voltage.

V_{rated} (V)	f_{rated} (Hz)	V/Hz	f_{set} (Hz)	V_{out} (V)
300	300	1	50	50
300	150	2	50	100
300	100	3	50	150
300	75	4	50	200
300	60	5	50	250
300	50	6	50	300

5. Results and Discussion

Figure 7 shows the motor’s transient current at 15%, 25% and 100% of the rated supply voltage with two broken bars. The recovered nonstationary signal was very legible at 10% of the supply voltage. Unlike the simulation-based results, these signals contained several higher-order harmonics. The most prominent causes of those harmonics were the non-sinusoidal stator and rotor winding distribution, the stator, the rotor slot openings and the magnetic material’s nonlinear behavior. However, those frequency components were of less significance, as the most prominent fault-based pattern remained in the bandwidth of 0–50 Hz.

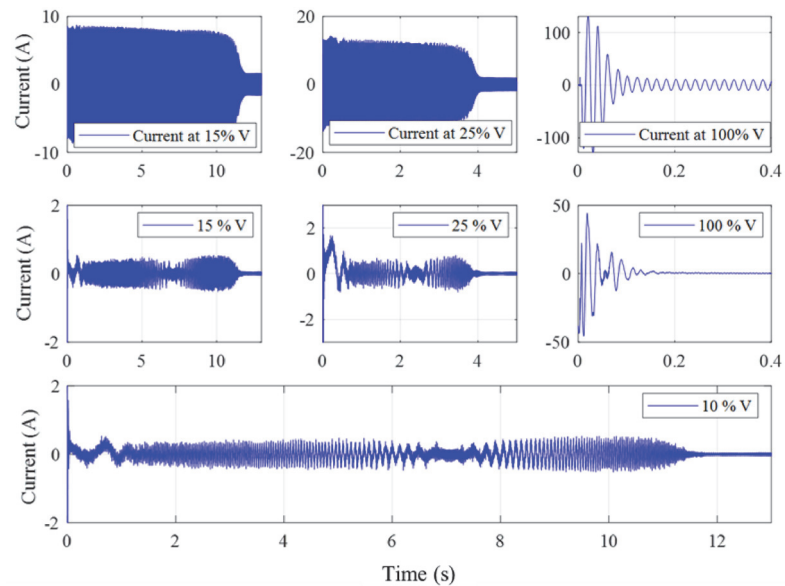


Figure 7. The motor's startup currents measured at different voltage levels (**top row**), the corresponding recovered nonstationary signals (**middle row**) and the nonstationary signal at 10% of the rated voltage representing the changing frequency pattern (**bottom**).

The frequency spectrum of the stator current during the steady state interval for healthy and broken rotor bars at no load and rated load conditions is shown in Figure 8. The spectrum in Figure 8b shows the evolution of the left-side band (LSB) and right-side band (RSB) harmonics. These harmonics are the function of slip, and the results are based on the measurements taken under rated load conditions.

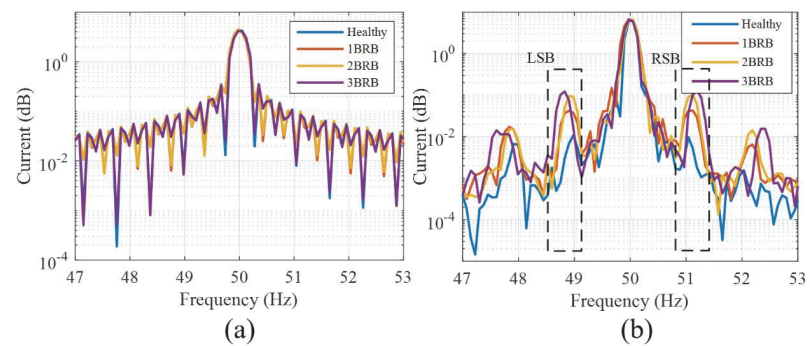


Figure 8. The frequency spectrum from 47 Hz to 53 Hz under healthy and broken rotor bar cases under steady state and (a) no-load and (b) rated-load conditions.

The sideband frequencies increased in amplitude with the increase in the number of broken bars. Besides that, the sideband fault frequencies tended to shift slightly away from the fundamental component with the rise in broken bars. With the increase in the number of broken bars, the average generated torque decreased with a slight rise in slip. The segregation of these components is very difficult from the rest of the harmonics if the entire spectrum is considered.

The severity of this problem increases with the decrease in load. As the load decreased, these harmonics started hiding under the fundamental component, with total disappear-

ance at the no load condition as in Figure 8a. Moreover, the skewness in the rotor and stator slots affected their amplitudes, making them less detectable at the developing stage. The skews tended to attenuate the rotor harmonics for smooth speed torque features. It is also important to mention that these harmonics remain venerable when the inverter feeds the motor. This effect can be in the form of a colossal number of harmonics fed by the inverter, making faulty frequencies even more difficult for segregation. Moreover, the impact of the drive controller cannot be ignored. This impact is worst in DTC-controlled motors, where the controller of the drive tries to eliminate the current harmonics to reduce torque ripples [14].

The leading causes of the speed and torque ripples were the current harmonics, due to non-sinusoidal winding distribution on the stator and rotor side, the supply-based odd multiples of the fundamental component even if the machine was grid-fed, the inherent dynamic eccentricity and the magnetic material's nonlinear behavior. Those harmonics are inevitable, even if the machine is in a healthy condition. Figure 9 shows those harmonics in the stator current spectrum of a grid-fed healthy motor working under 50% of the rated load. All the harmonics except the supply-fed one were the function of slip and tended to move away from the parent supply component with the increase in load. As discussed earlier, the legibility of those harmonics in the current spectrum not only depended upon slip but the fluctuating load, and the drive's controller also made the detection of desired components challenging.

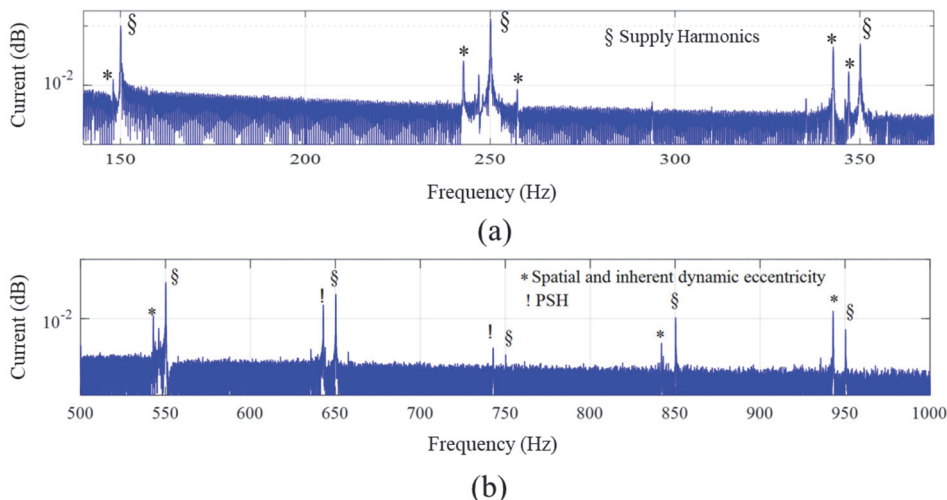


Figure 9. The generation of spatial harmonics in the stator current of the healthy machine (a) under a steady state regime with 50% of the rated load in the bandwidth of 100–400 Hz and (b) under a steady state regime with 50% of the rated load in the bandwidth of 500–1000 Hz.

To avoid all those problems, the inspection of the motor current under the transient regime showed promising results. For an increase in the transient time for better time–frequency resolution, the supply voltage could be reduced using a three-phase transformer or the industrial inverter, as discussed previously. With the increase in the applied voltage, the motor took less time to reach a steady state interval. Under the transient regime, the continuously decreasing slip moved the RHS and LHS frequency components toward the fundamental component. It made a V-shaped pattern whose width depended upon the transient time. An exceptional intention was needed here, as there were several slip-dependent frequency components, which could make similar patterns in the transient region. Those frequencies are the spatial and inherent dynamic eccentricity-based harmonics, which develop near all supply-fed higher-order harmonics.

Figure 10 shows the harmonics' development in the transient and steady state regime under the healthy condition with the attenuated fundamental component. It is evident that in the transient region, the rotor slotting and eccentricity-based harmonics made the V-shaped patterns, as in Figure 10a. Those patterns started from 50 Hz and vanished completely as they approached the parent supply component, as in Figure 10b. It is essential to differentiate them from the actual faulty patterns to avoid false alarms.

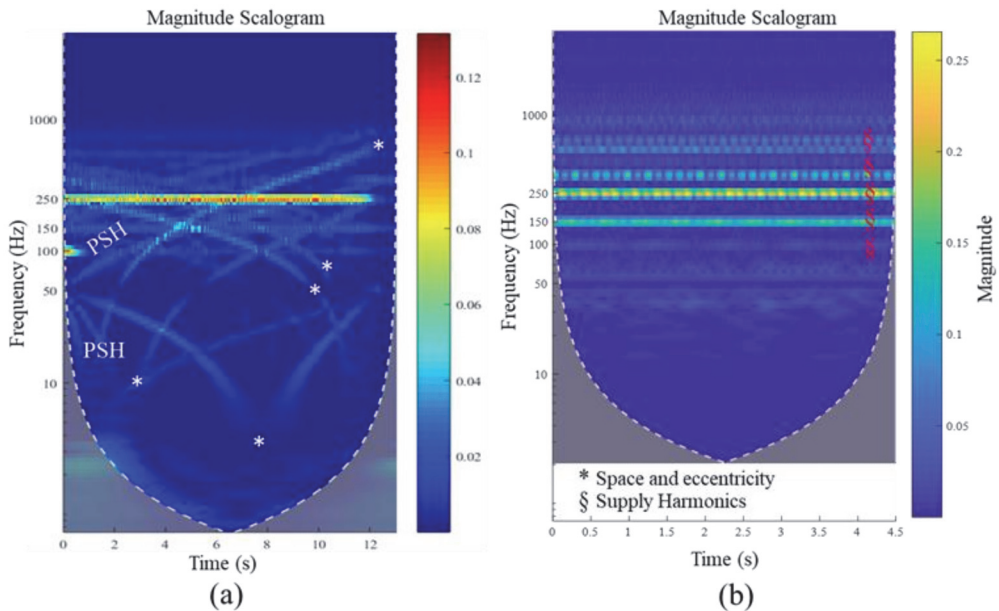


Figure 10. The generation of spatial harmonics in the stator current of the healthy machine. (a) The development of time–frequency patterns due to the space harmonics. (b) The time–frequency spectrum under a steady state regime under 50% of the rated load.

Figure 11 shows the time–frequency response, with the respective regions containing 85% of the total spectral energy in the contour plot for the healthy and broken bar cases. In the presence of the fundamental component, the faulty pattern is barely visible even in the extended current, as in Figure 11c. Moreover, the influence of the most potent supply component on the visibility of the fault pattern is evident in the contour plot. Although the faulty pattern is visible to some extent in the magnitude scalogram, it is absent in the contour plot, as the maximum spectral energy remained in the region near the fundamental component.

This pattern was not very legible because the sideband frequencies were lower in amplitude than the fundamental component. This pattern can be made very clear by attenuating the fundamental component, as shown in Figure 12. The IIR band-stop filter, having a filter order of two and a stopband attenuation of 40 showed promising results, while attenuating a narrow bandwidth of frequencies from 49.9 Hz to 50.1 Hz. Figure 12a shows the transient current envelope, while the evolution of spatial frequencies in the transient regime is presented in Figure 12b. The development of a faulty pattern with good legibility is shown in Figure 12c,d for one and two broken bars, respectively.

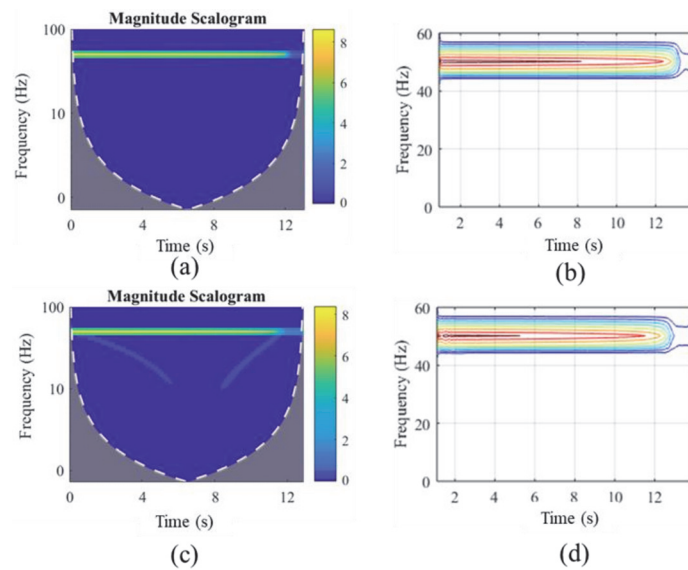


Figure 11. The results based on the measurements taken at 10% of the rated supply voltage. (a) The time–frequency response of the healthy motor’s phase current in the transient regime. (b) The respective contour plot. (c) The time–frequency response of the faulty motor’s phase current in the transient regime. (d) The respective contour plot with a 95% confidence interval.

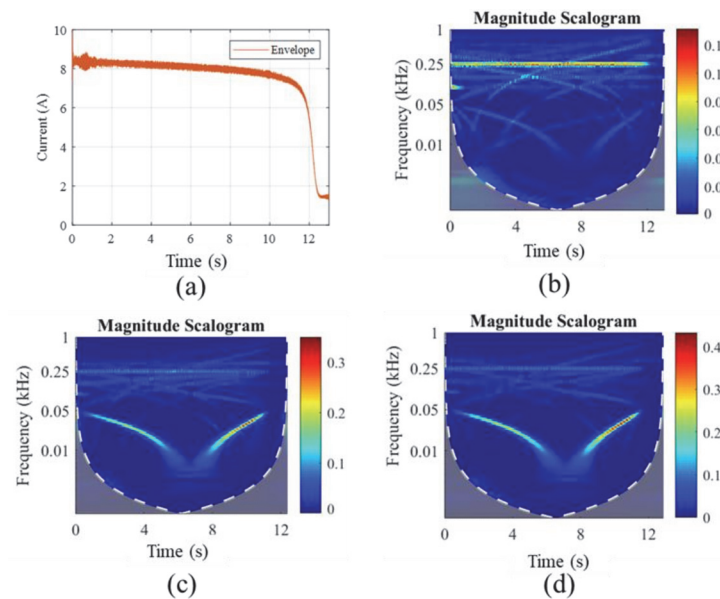


Figure 12. The results based on the measurements taken at 10% of the rated supply voltage. (a) The envelope of the motor’s phase current in the transient regime. (b) Time–frequency spectrum in the healthy case with an attenuated fundamental component. (c) Time–frequency spectrum in the case of one broken bar with the attenuated fundamental component. (d) Time–frequency spectrum in the case of two broken bar with an attenuated fundamental component.

The contour plot with a bump mother wavelet for the healthy and one broken rotor bar (BRB) cases is shown in Figure 13. Since the spatial harmonics were weaker than the fault frequencies, the contour plot shows the evolution of the sideband frequencies, which avoids confusion with the slotting-related patterns.

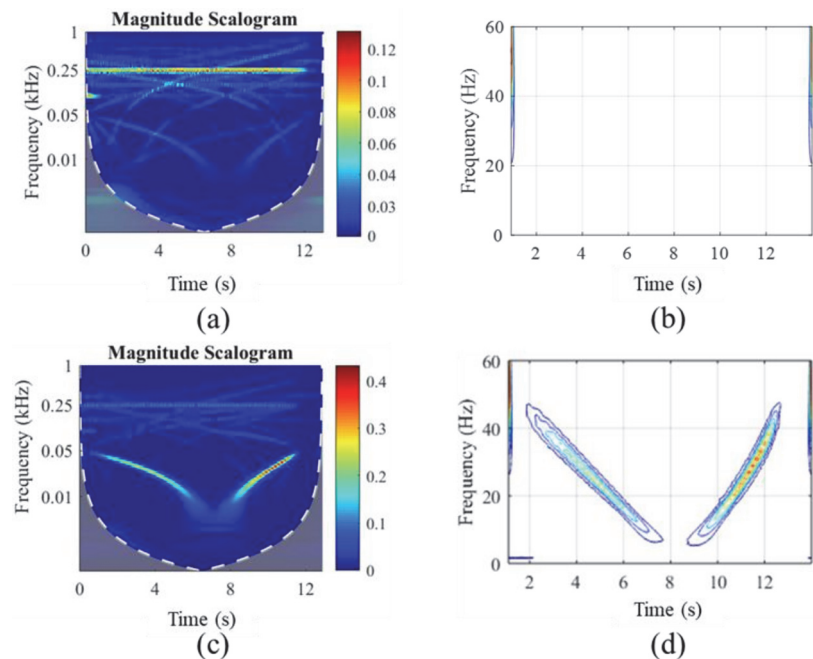


Figure 13. (a) The time–frequency plot of the healthy motor with 10% of the rated voltage. (b) The time–frequency contour plot. (c) The time–frequency plot for 1 BRB motor with 10% of the rated voltage. (d) The corresponding contour plot.

6. Conclusions

The broken rotor bars fault diagnostics by time–frequency analysis of the motor current under the transient period was investigated in this paper. The detection of fault frequencies in the steady state interval was prevalent in the literature but possessed several difficulties. Since the sideband frequencies were the function of slip, they became challenging to discover under low-load conditions. The spectral leakage of the prevailing supply components was hazardous for the visibility of faulty components, as they were fragile in amplitude. The spectral leakage was the function of the signal length, the sampling frequency and the type of window used to compute the FFT or wavelet.

Moreover, the inclusion of a vast bandwidth of inverter-fed frequencies made the detection of faulty frequencies hazier. The drive controller’s impact on reducing the current ripples was another fact, making fault diagnosis under a steady state regime difficult.

These drawbacks can be resolved by investigating the health in the transient regime. The transient interval’s biggest flaw is the little time, which reduces the resolution of the spectrum. This transient time can be increased by lowering the applied voltage without any external load. By doing so, the broken bars-based V-shaped pattern can be seen with great accuracy. Moreover, the FFT-based drawbacks are considerably reduced by using the wavelet approach. The transient spectrum’s legibility is further enhanced by attenuating the fundamental component with an IIR filter’s help. The IIR band-stop filter has a sharp transition interval and low passband ripples, having less influence on the remaining frequency components.

Several spatial and supply-related frequency patterns can cause a false alarm if they are not differentiated accurately from the actual faulty components. Those components are much weaker in amplitude compared with the fault-related frequencies. The use of the filter to attenuate those components is nearly impossible, as they are not stationary. Hence, the regions with the maximum spectral energy in the form of a contour plot are used, which can be easily adjusted as a threshold to show the pattern. The results are presented using the simulations and the measurements taken from a laboratory-based test rig.

The proposed approach can be used for the pattern-based training of advanced artificially intelligent (AI) diagnostic algorithms.

Author Contributions: Conceptualization, B.A., T.V. and A.B.; methodology, B.A., T.V. and A.B.; validation, A.K., A.R. and A.B.; data curation, B.A. and K.K.; writing—original draft preparation, B.A.; writing—review and editing, B.A., K.K. and A.R.; visualization, T.V. and P.S.G.; supervision, T.V., A.K. and A.B. All authors have read and agreed to the published version of the manuscript.

Funding: The research leading to these results received funding from the EEA/Norway Grants 2014–2021, Industrial Internet methods for electrical energy conversion systems monitoring and diagnostics.

Institutional Review Board Statement: Not applicable.

Informed Consent Statement: Not applicable.

Conflicts of Interest: The authors declare no conflict of interest.

References

- Bossio, G.R.; De Angelo, C.H.; Bossio, J.M.; Pezzani, C.M.; Garcia, G.O. Separating Broken Rotor Bars and Load Oscillations on IM Fault Diagnosis Through the Instantaneous Active and Reactive Currents. *IEEE Trans. Ind. Electron.* **2009**, *56*, 4571–4580. [\[CrossRef\]](#)
- Soualhi, A.; Clerc, G.; Razik, H. Detection and Diagnosis of Faults in Induction Motor Using an Improved Artificial Ant Clustering Technique. *IEEE Trans. Ind. Electron.* **2013**, *60*, 4053–4062. [\[CrossRef\]](#)
- Marques Cardoso, A.J.; Saraiva, E.S. On-line diagnostics of three-phase induction motors by Park's vector. In Proceedings of the ICEM, Pisa, Italy, 12–14 September 1988; pp. 231–234.
- Oliveira, L.M.R.; Cardoso, A.J.M. Extended Park's vector approach-based differential protection of three-phase power transformers. *IET Electr. Power Appl.* **2012**, *6*, 463. [\[CrossRef\]](#)
- Freire, N.M.A.; Estima, J.O.; Marques Cardoso, A.J. Open-Circuit Fault Diagnosis in PMSG Drives for Wind Turbine Applications. *IEEE Trans. Ind. Electron.* **2013**, *60*, 3957–3967. [\[CrossRef\]](#)
- Cruz, S.M.A.; Cardoso, A.J.M. Stator winding fault diagnosis in three-phase synchronous and asynchronous motors, by the extended Park's vector approach. *IEEE Trans. Ind. Appl.* **2001**, *37*, 1227–1233. [\[CrossRef\]](#)
- Cruz, M.A.; Marques Cardoso, S.A.J. Rotor Cage Fault Diagnosis in Three-Phase Induction Motors by Extended Park's Vector Approach. *Electr. Mach. Power Syst.* **2000**, *28*, 289–299.
- Ayhan, B.; Trussell, H.J.; Chow, M.Y.; Song, M.H. On the Use of a Lower Sampling Rate for Broken Rotor Bar Detection With DTFT and AR-Based Spectrum Methods. *IEEE Trans. Ind. Electron.* **2008**, *55*, 1421–1434. [\[CrossRef\]](#)
- Khezzar, A.; Kaikaa, M.Y.; El Kamel Oumaamar, M.; Boucherma, M.; Razik, H. On the Use of Slot Harmonics as a Potential Indicator of Rotor Bar Breakage in the Induction Machine. *IEEE Trans. Ind. Electron.* **2009**, *56*, 4592–4605. [\[CrossRef\]](#)
- Malekpour, M.; Phung, B.T.; Ambikairajah, E. Stator current envelope extraction for analysis of broken rotor bar in induction motors. In Proceedings of the 2017 IEEE 11th International Symposium on Diagnostics for Electrical Machines, Power Electronics and Drives (SDMPED), Tinos, Greece, 29 August–1 September 2017; pp. 240–246.
- Belahcen, A.; Martinez, J.; Vaimann, T. Comprehensive computations of the response of faulty cage induction machines. In Proceedings of the 2014 International Conference on Electrical Machines (ICEM), Berlin, Germany, 2–5 September 2014; IEEE: Piscataway, NJ, USA, 2014; pp. 1510–1515.
- Nandi, S.; Toliyat, H.A.; Li, X. Condition Monitoring and Fault Diagnosis of Electrical Motors—A Review. *IEEE Trans. Energy Convers.* **2005**, *20*, 719–729. [\[CrossRef\]](#)
- Asad, B.; Vaimann, T.; Kallaste, A.; Belahcen, A. Harmonic Spectrum Analysis of Induction Motor With Broken Rotor Bar Fault. In Proceedings of the 2018 IEEE 59th International Scientific Conference on Power and Electrical Engineering of Riga Technical University (RTUCon), Riga, Latvia, 12–13 November 2018; pp. 1–7.
- Asad, B.; Vaimann, T.; Belahcen, A.; Kallaste, A.; Rassõlkin, A.; Iqbal, M.N. Broken rotor bar fault detection of the grid and inverter-fed induction motor by effective attenuation of the fundamental component. *IET Electr. Power Appl.* **2019**, *13*, 2005–2014. [\[CrossRef\]](#)

15. Puche-Panadero, R.; Pineda-Sanchez, M.; Riera-Guasp, M.; Roger-Folch, J.; Hurtado-Perez, E.; Perez-Cruz, J. Improved Resolution of the MCSA Method Via Hilbert Transform, Enabling the Diagnosis of Rotor Asymmetries at Very Low Slip. *IEEE Trans. Energy Convers.* **2009**, *24*, 52–59. [\[CrossRef\]](#)
16. Pineda-Sanchez, M.; Riera-Guasp, M.; Antonino-Daviu, J.A.; Roger-Folch, J.; Perez-Cruz, J.; Puche-Panadero, R. Diagnosis of Induction Motor Faults in the Fractional Fourier Domain. *IEEE Trans. Instrum. Meas.* **2010**, *59*, 2065–2075. [\[CrossRef\]](#)
17. Moussa, M.A.; Boucherma, M.; Khezzer, A. A Detection Method for Induction Motor Bar Fault Using Sidelobes Leakage Phenomenon of the Sliding Discrete Fourier Transform. *IEEE Trans. Power Electron.* **2017**, *32*, 5560–5572. [\[CrossRef\]](#)
18. Kia, S.H.; Henao, H.; Capolino, G.-A. Diagnosis of Broken-Bar Fault in Induction Machines Using Discrete Wavelet Transform Without Slip Estimation. *IEEE Trans. Ind. Appl.* **2009**, *45*, 1395–1404. [\[CrossRef\]](#)
19. Singh, S.; Kumar, N. Detection of Bearing Faults in Mechanical Systems Using Stator Current Monitoring. *IEEE Trans. Ind. Inform.* **2017**, *13*, 1341–1349. [\[CrossRef\]](#)
20. Kang, M.; Kim, J.-M. Reliable Fault Diagnosis of Multiple Induction Motor Defects Using a 2-D Representation of Shannon Wavelets. *IEEE Trans. Magn.* **2014**, *50*, 1–13. [\[CrossRef\]](#)
21. Sapena-Bano, A.; Pineda-Sanchez, M.; Puche-Panadero, R.; Martinez-Roman, J.; Matic, D. Fault Diagnosis of Rotating Electrical Machines in Transient Regime Using a Single Stator Current's FFT. *IEEE Trans. Instrum. Meas.* **2015**, *64*, 3137–3146. [\[CrossRef\]](#)
22. Antonino-Daviu, J. Electrical monitoring under transient conditions: A new paradigm in electric motors predictive maintenance. *Appl. Sci.* **2020**, *10*, 6137. [\[CrossRef\]](#)
23. Gyftakis, K.N.; Spyropoulos, D.V.; Mitronikas, E. Advanced Detection of Rotor Electrical Faults in Induction Motors at Start-up. *IEEE Trans. Energy Convers.* **2020**. [\[CrossRef\]](#)
24. Gyftakis, K.N.; Panagiotou, P.A.; Lee, S. Bin Generation of Mechanical Frequency Related Harmonics in the Stray Flux Spectra of Induction Motors Suffering from Rotor Electrical Faults. *IEEE Trans. Ind. Appl.* **2020**, *56*, 4796–4803. [\[CrossRef\]](#)
25. Cunha, C.C.M.; Lyra, R.O.C.; Filho, B. Simulation and Analysis of Induction Machines With Rotor Asymmetries. *IEEE Trans. Ind. Appl.* **2005**, *41*, 18–24. [\[CrossRef\]](#)
26. Faiz, J.; Ojaghi, M. Unified winding function approach for dynamic simulation of different kinds of eccentricity faults in cage induction machines. *IET Electr. Power Appl.* **2009**, *3*, 461. [\[CrossRef\]](#)
27. Nandi, S. Modeling of Induction Machines Including Stator and Rotor Slot Effects. *IEEE Trans. Ind. Appl.* **2004**, *40*, 1058–1065. [\[CrossRef\]](#)
28. Marfoli, A.; Bolognesi, P.; Papini, L.; Gerada, C. Mid-Complexity Circuitual Model of Induction Motor with Rotor Cage: A Numerical Resolution. In Proceedings of the 2018 XIII International Conference on Electrical Machines (ICEM), Alexandroupoli, Greece, 3–6 September 2018; pp. 277–283.
29. Sudhoff, S.D.; Kuhn, B.T.; Corzine, K.A.; Branecky, B.T. Magnetic Equivalent Circuit Modeling of Induction Motors. *IEEE Trans. Energy Convers.* **2007**, *22*, 259–270. [\[CrossRef\]](#)
30. Sapena-Bano, A.; Martinez-Roman, J.; Puche-Panadero, R.; Pineda-Sanchez, M.; Perez-Cruz, J.; Riera-Guasp, M. Induction machine model with space harmonics for fault diagnosis based on the convolution theorem. *Int. J. Electr. Power Energy Syst.* **2018**, *100*, 463–481. [\[CrossRef\]](#)
31. Sapena-Bano, A.; Chinesta, F.; Pineda-Sanchez, M.; Aguado, J.V.; Borzacchiello, D.; Puche-Panadero, R. Induction machine model with finite element accuracy for condition monitoring running in real time using hardware in the loop system. *Int. J. Electr. Power Energy Syst.* **2019**, *111*, 315–324. [\[CrossRef\]](#)
32. Asad, B.; Vaimann, T.; Kallaste, A.; Rassolkin, A.; Belahcen, A. Winding Function Based Analytical Model of Squirrel Cage Induction Motor for Fault Diagnostics. In Proceedings of the 2019 26th International Workshop on Electric Drives: Improvement in Efficiency of Electric Drives (IWED), Moscow, Russia, 30 January–2 February 2019; pp. 1–6.
33. Asad, B.; Vaimann, T.; Belahcen, A.; Kallaste, A.; Rassolkin, A.; Iqbal, M.N. Modified Winding Function-based Model of Squirrel Cage Induction Motor for Fault Diagnostics. *IET Electr. Power Appl.* **2020**, *14*, 1722–1734. [\[CrossRef\]](#)
34. Bellini, A.; Filippetti, F.; Franceschini, G.; Tassoni, C.; Kliman, G.B. Quantitative evaluation of induction motor broken bars by means of electrical signature analysis. *IEEE Trans. Ind. Appl.* **2001**, *37*, 1248–1255. [\[CrossRef\]](#)

Publication II

Asad, B.; Vaimann, T.; Belahcen, A.; Kallaste, A.; Rassõlkin, A.; Iqbal, M. N. The Cluster Computation-Based Hybrid FEM–Analytical Model of Induction Motor for Fault Diagnostics. Appl. Sci., vol. 10 (21), 7572, Oct. 2020.

Article

The Cluster Computation-Based Hybrid FEM–Analytical Model of Induction Motor for Fault Diagnostics

Bilal Asad ^{1,2,*}, Toomas Vaimann ¹, Anouar Belahcen ^{1,2}, Ants Kallaste ¹,
Anton Rassõlkin ¹ and M. Naveed Iqbal ¹

¹ Department of Electrical Power Engineering and Mechatronics, Tallinn University of Technology, 19086 Tallinn, Estonia; toomas.vaimann@taltech.ee (T.V.); Anouar.Belahcen@aalto.fi (A.B.); ants.kallaste@taltech.ee (A.K.); anton.rassolkin@taltech.ee (A.R.); miqbal@taltech.ee (M.N.I.)

² Department of Electrical Engineering and Automation, Aalto University, FI-00076 Espoo, Finland

* Correspondence: bilal.asad@taltech.ee

Received: 8 October 2020; Accepted: 26 October 2020; Published: 27 October 2020



Abstract: This paper presents a hybrid finite element method (FEM)–analytical model of a three-phase squirrel cage induction motor solved using parallel processing for reducing the simulation time. The growing development in artificial intelligence (AI) techniques can lead towards more reliable diagnostic algorithms. The biggest challenge for AI techniques is that they need a big amount of data under various conditions to train them. These data are difficult to obtain from the industries because they contain low numbers of possible faulty cases, as well as from laboratories because a limited number of motors can be broken for testing purposes. The only feasible solution is mathematical models, which in the long run can become part of advanced diagnostic techniques. The benefits of analytical and FEM models for their speed and accuracy respectively can be exploited by making a hybrid model. Moreover, the concept of cloud computing can be utilized to reduce the simulation time of the FEM model. In this paper, a hybrid model being solved on multiple processors in a parallel fashion is presented. The results depict that by dividing the rotor steps among several processors working in parallel, the simulation time reduces considerably. The simulation results under healthy and broken rotor bar cases are compared with those taken from a laboratory setup for validation.

Keywords: induction motors; fault diagnosis; modeling; finite element analysis; parallel processing

1. Introduction

Electrical machines, particularly induction motors, are indispensable in almost all sectors of our modern-day society. In the form of conveyor belt movers, compressors, electric vehicles, fans, and pumps, etc., they consume more than 50% of the total generated energy worldwide [1]. This fact makes their predictive maintenance very important, to avoid any catastrophic situation. As the world is moving towards industry 4.0, predictive maintenance is becoming more important—as contrasted to preventive or reactive maintenance. Unlike preventive or reactive maintenance, in predictive maintenance we monitor the behavior of an electrical machine and anticipate failures before they occur.

Predictive maintenance allows the servicing of the machine when it needs. By doing so, the system's downtime can exponentially decrease with a resultant decrease in the maintenance cost. A variety of conventional condition-monitoring techniques have been discussed in literature over the past few decades, such as motor current signature analysis (MCSA) [2–5], thermal analysis [6–8], vibration [9], acoustics [10,11], stray flux monitoring [12,13], partial discharges [14], air-gap flux monitoring [15], etc.

Although these techniques are well-established, compatible with a variety of signal-processing techniques, and require fewer computational resources, they possess several drawbacks. The most

prominent drawbacks are relevant to expensive sensors—such as in the case of thermal analysis and the poor legibility of fault-based frequency components at the incipient stage, as in motor current signature analysis (MCSA)-based techniques. Moreover, these techniques depend upon various constraints such as machine structure, the industrial environment, external noise, bad load-coupling, poor foundation, and the impact of the drive controller, etc. The segregation of frequency components when there is more than one fault is another challenging task in MCSA-based diagnostic techniques. It becomes worse when the industrial inverters inject several frequency components as well.

The industrial inverters with complex control algorithms are becoming a crucial part of a drive system. In this case, the definition of faults goes beyond the domain of simple machine equations. The use of conventional diagnostic techniques, while neglecting all subsystems of the drive, can increase the false or missed alarm rate.

To avoid all those problems and to make diagnostic algorithms more reliable, advanced model-dependent and artificial intelligence (AI) based techniques can give promising results. The majority of rotating machine faults are degenerative, which makes fault diagnosis a pattern recognition problem. Due to a variety of global signals and different faults, pattern recognition is not a straightforward problem. Therefore, a reliable diagnostic algorithm can be a combination of data processing for feature extraction and recognition through AI techniques. Various AI techniques such as probability-based, classification, statistical learning, mathematical optimization, and convex optimization can be found in the literature [16]. The statistical and classification-based methods are gaining increasing popularity in uses such as support vector machines (SVM) [17–19], artificial neural networks (ANN) [20–22], Bayesian classifiers, Naïve Bayes classifiers [23–25], machine learning [26,27], k-nearest neighbor algorithm [28–30], etc.

Almost all AI-based diagnostic techniques need a large number of data samples under various conditions. Those conditions may include signals under healthy, faulty, loaded, and no-load conditions. Moreover, various kinds of faults with different severity levels under a variety of loading conditions can better train advanced AI-based techniques. The collection of large amounts of data with different constraints is practically impossible both from industry and laboratory environments. Because, first, in industries there are few faulty machines and, secondly, the type and level of faults in industry machines are unknown at first—which is necessary information for training the diagnostic algorithms. In the laboratory, conducting a large number of destructive tests is not economically feasible. The only optimal way is to rely on the accurate mathematical models of the machine. Using mathematical models, almost any kind of fault in any type of machine with different natures of load can be simulated to train the diagnostic algorithm.

A variety of machine modeling techniques are available in the literature, which can be broadly classified into two categories; analytical and numerical. The two-axis theory-based models [31–33] are being effectively utilized for control and analysis. Although those models are simple to understand, comprehensive, and fast, they are not suitable for fault simulations because of various approximations such as sinusoidal stator and rotor windings distribution, uniform air gap, no inter-bar currents, and no material saturation, etc. The multiple coupled circuit theory-based models such as winding function analysis (WFA) [34,35], modified winding function analysis (MWFA) [36,37], and extended MWFA [37] allow the inclusion of practical stator and rotor winding functions, the stator and rotor slots openings, and non-linear functions for material saturation. Those models can be used to simulate the majority of faults with very much less simulation time and computational complexity, but they do not remain straightforward while dealing with different types of machines with complex geometrical features. Similarly, other analytical models such as magnetic equivalent circuit [38], generalized harmonic analysis [39], voltage behind reactance [40], and convolution theorem [41] can be used for the simulation of various faults in induction machines but at the cost of material and geometry-related approximations.

Having the ability to deal with almost all kind of geometries and material properties, and the compatibility to solve various kinds of problems, the finite element method (FEM)-based modeling techniques are gaining heightened popularity. Using FEM, a vast variety of electromagnetic [42,43],

thermal [44], fluid dynamics [45], structural [46], and related problems can be solved with incredible accuracy. In FEM, the geometry of the system is divided into a considerable number of mesh elements represented by nodes and the solution of each node leads toward the final solution. Indeed, it requires significantly powerful computational resources and a large memory to save intermediate results. Although modern computers with advanced processors are very strong, they need a long time, from several minutes to days, for the solution of highly unsymmetrical machines. The saving of simulation time for fault diagnostics is very important for the collection of vast amounts of data, which can be used as a benchmark for advanced fault diagnostic techniques.

Many methods to diminish these problems have been presented in the literature such as; the hybrid analytical–FEM model [47,48], the model order reduction [49–51], and sparse subspace learning (SSL) [52], etc. These methods have their own limitations as they rely on statistical and interpolation techniques, which are different for different kinds of machines. Problems such as the reducibility of the model and the precision of the input grid can lead to the increased complexity of the model.

As the world is moving towards industry 4.0 standards and cloud computation, the computational resources are becoming unlimited. These resources can be in the form of software applications, processing power, and data storage. All these resources are very important for big data-based advanced diagnostic techniques such as machine learning [53], deep learning [54], parallel autonomous mining [55], image processing [56], online wireless monitoring through smart sensors [57], and neural networks [58–60], etc. The basic building blocks of the cloud computation are infrastructure as a service (IaaS), platform as a service (PaaS), and software as a service (SaaS). Those building blocks can be utilized for big data storage, custom software development, and computer application utilization respectively.

In order to curtail the complexity related problems of FEM models, the concept of parallel processing by utilizing the cluster of computers is presented in this paper. Unlike most of the papers where the simulation speed of FEM models is increased either by exploiting the symmetry (which is not true in the case of faulty machines) or by data interpolation, in this paper the complete two-dimensional (2D) geometry of a three-phase squirrel cage induction motor is solved on multiple processor cores working in parallel with each other. All inductances are calculated by doing a magneto-static solution of the machine at several rotor positions. The calculated inductances are saved in the three-dimensional (3D) lookup table as a function of the rotor position. The dynamic behavior is then studied in MATLAB/Simulink, and the results are validated by comparing them with the measurements taken from the laboratory test rig.

2. The Motor's Model

The voltage equations of a squirrel-cage induction motor with a stationary stator and short-circuited rotor cage can be described using magnetic coupled circuits theory as follows:

$$\mathbf{V}_s = \mathbf{I}_s \mathbf{R}_s + \frac{d}{dt}(\mathbf{L}_{ss} \mathbf{I}_s + \mathbf{L}_{sr} \mathbf{I}_r) \quad (1)$$

$$\mathbf{0} = \mathbf{I}_r \mathbf{R}_r + \frac{d}{dt}(\mathbf{L}_{rs} \mathbf{I}_s + \mathbf{L}_{rr} \mathbf{I}_r) \quad (2)$$

where \mathbf{V}_s , \mathbf{I}_s , \mathbf{I}_r , \mathbf{R}_s , \mathbf{R}_r , \mathbf{L}_{ss} , \mathbf{L}_{sr} , and \mathbf{L}_{rr} are the vectors containing the machine's voltage, currents, resistances, and inductances respectively. The stator–stator, stator–rotor, rotor–stator, and rotor–rotor self and mutual inductance matrices (\mathbf{L}_{ss} , \mathbf{L}_{sr} , \mathbf{L}_{rs} , and \mathbf{L}_{rr}) can be defined as follows;

$$\mathbf{L}_{ss} = \begin{bmatrix} L_{aas} & L_{abs} & L_{acs} \\ L_{bas} & L_{bbs} & L_{bcs} \\ L_{cas} & L_{cbs} & L_{ccs} \end{bmatrix}, \quad (3)$$

$$\mathbf{L}_{sr} = \begin{bmatrix} L_{ar1} & L_{ar2} & \cdots & L_{ari} & \cdots & L_{arn} & L_{are} \\ L_{br1} & L_{br2} & \cdots & L_{bri} & \cdots & L_{brn} & L_{bre} \\ L_{cr1} & L_{cr2} & \cdots & L_{cri} & \cdots & L_{crn} & L_{cre} \end{bmatrix}, \quad (4)$$

$$\mathbf{L}_{rr} = \begin{bmatrix} L_{r1r1} & L_{r1r2} & \cdots & L_{r1ri} & \cdots & L_{r1rn} & L_{r1re} \\ L_{r2r1} & L_{r2r2} & \cdots & L_{r2ri} & \cdots & L_{r2rn} & L_{r2re} \\ \vdots & \vdots & \vdots & \vdots & \vdots & \vdots & \vdots \\ L_{rir1} & L_{rir2} & \cdots & L_{riri} & \cdots & L_{rirn} & L_{rire} \\ \vdots & \vdots & \vdots & \vdots & \vdots & \vdots & \vdots \\ L_{rnr1} & L_{rnr2} & \cdots & L_{rnri} & \cdots & L_{rnrn} & L_{rnre} \\ L_{rer1} & L_{rer2} & \cdots & L_{reri} & \cdots & L_{rern} & L_{rere} \end{bmatrix} \quad (5)$$

$$\mathbf{R}_{rr} = \begin{bmatrix} 2(R_b + r_e) & -R_b & 0 & 0 & \cdots & 0 & -R_b & -r_e \\ -R_b & 2(R_b + r_e) & -R_b & 0 & \cdots & 0 & 0 & -r_e \\ 0 & -R_b & 2(R_b + r_e) & -R_b & \cdots & 0 & 0 & -r_e \\ \vdots & \vdots & \vdots & \vdots & \vdots & \vdots & \vdots & \vdots \\ 0 & 0 & 0 & 0 & \cdots & 2(R_b + r_e) & -R_b & -r_e \\ -R_b & 0 & 0 & 0 & \cdots & -R_b & 2(R_b + r_e) & -r_e \\ -r_e & -r_e & -r_e & -r_e & \cdots & -r_e & -r_e & n_b r_e \end{bmatrix} \quad (6)$$

The last rows and columns in \mathbf{L}_{sr} , \mathbf{L}_{rr} , and \mathbf{R}_{rr} correspond to the end ring values, which can be neglected in case of a perfect symmetrical machine, as the net end ring current is always zero. In unsymmetrical machines, these entries are important to simulate the end ring faults and to avoid the singularity problems while taking the inverse of inductance matrices.

For the ease of implementation, all these matrices can be grouped.

$$\mathbf{V}_s = \begin{bmatrix} v_{as} & v_{bs} & v_{cs} \end{bmatrix}^T \quad (7)$$

$$\mathbf{I}_s = \begin{bmatrix} i_{as} & i_{bs} & i_{cs} \end{bmatrix}^T \quad (8)$$

$$\mathbf{I}_r = \begin{bmatrix} i_{r1} & i_{r2} & \cdots & i_{rn} & i_{re} \end{bmatrix}^T \quad (9)$$

$$\mathbf{L} = \begin{bmatrix} L_{ss} & L_{sr} \\ L_{rs} & L_{rr} \end{bmatrix} \quad (10)$$

The currents, torque, and speed can be calculated as:

$$\begin{bmatrix} \mathbf{I}_s \\ \mathbf{I}_r \end{bmatrix} = \begin{bmatrix} L_{ss} & L_{sr} \\ L_{rs} & L_{rr} \end{bmatrix}^{-1} \int \left[\begin{bmatrix} \mathbf{V}_s \\ 0 \end{bmatrix} - \begin{bmatrix} \mathbf{R}_s & 0 \\ 0 & \mathbf{R}_r \end{bmatrix} \begin{bmatrix} \mathbf{I}_s \\ \mathbf{I}_r \end{bmatrix} \right] dt \quad (11)$$

$$T_e = \mathbf{I}_s^T \left(\frac{d}{d\theta} \mathbf{L}_{rs} \right) \mathbf{I}_r \quad (12)$$

In the matrices form:

$$T_e = \frac{1}{2} \left(\frac{p}{2} \right) \begin{bmatrix} \mathbf{I}_s \\ \mathbf{I}_r \end{bmatrix}^T \frac{d}{d\theta} \begin{bmatrix} L_{ss} & L_{sr} \\ L_{rs} & L_{rr} \end{bmatrix} \begin{bmatrix} \mathbf{I}_s \\ \mathbf{I}_r \end{bmatrix} \quad (13)$$

$$J \frac{d}{dt} \omega_m = T_e - T_L - B \omega_m \quad (14)$$

All inductances and resistances need to be calculated with stepping rotor and save them in 3D lookup tables where the third dimension corresponds to the rotor position as shown in Figure 1. All calculations can be done in offline environment using a magneto-static FEM solution and in the

online environment the rotor position can be used as an index value to call a corresponding matrix from the lookup table to calculate the performance parameters like speed and torque, etc.

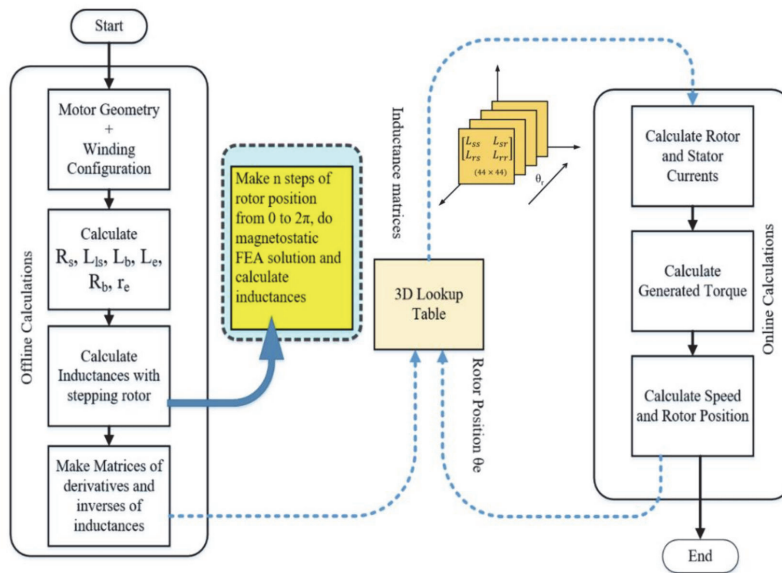


Figure 1. The schematic diagram of inductances calculations and their implementations for dynamic simulation.

3. LAN Network for Cluster Formation

Parallel computing is a form of concurrent computing where several workouts can be performed in the overlapping periods. Generally, any large problem can be divided into n -small problems, which can be solved simultaneously. Unlike traditional serial programs, the divided problem segments should be independent of each other so that they can run on different processors and the solutions can be combined on the client machine at the end. The general schematic diagram of distributed parallel computation is shown in Figure 2. The client machines, job scheduler, WIFI or LAN network, and the worker processors, are the main parts of the distributed cloud computation. The function of the job scheduler is to divide and distribute the segments of the bigger problem into cluster computers. The cluster computers can further divide their portion among their cores in the same manner.

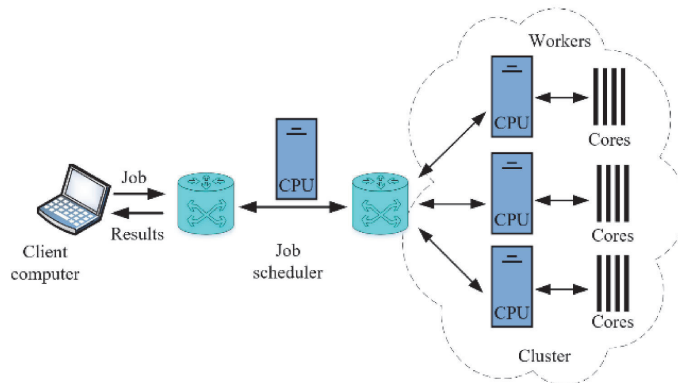


Figure 2. The cluster formation and utilization for parallel processing.

4. Inductances Calculations

In the case of electrical machines, most of the faults such as eccentricity, broken bars, and stator inter-turn short circuits make the machines unsymmetrical. Due to this fact, the complexity reduction techniques such as exploitation of symmetry by considering symmetric and non-symmetric boundary conditions and model order reduction becomes more tedious. The only best optimal and reliable way for fault diagnostics is to simulate the entire machine at various rotor positions. Since the solution at a distinct rotor position is independent of the solution at subsequent rotor positions, the total “n” rotor steps can be divided into various segments. The magneto-static problems of different rotor position sectors such as, $(0 \rightarrow \theta_1)$, $(\theta_2 \rightarrow \theta_3)$, \dots , $(\theta_{n-1} \rightarrow \theta_n)$, $(\theta_{n+1} \rightarrow 2\pi)$ can be divided among the workers for parallel processing.

Figure 3 shows the required steps to calculate the inductances at different rotor positions. The computer cluster consists of four computers making a local area network (LAN). Each computer is Intel(R) Core(TM) i7-7500 CPU @ 3.41 GHz with 8 GB RAM and four cores. The finite element method (FEM) based model is constructed using open-access software FEMM 4.0. For making the model and collecting the results, FEMM is interfaced with MATLAB. After making the machine geometry and winding configuration on FEMM, MATLAB works as a job scheduler. It divides the total number of rotor steps among worker computers and their cores and receives the end results.

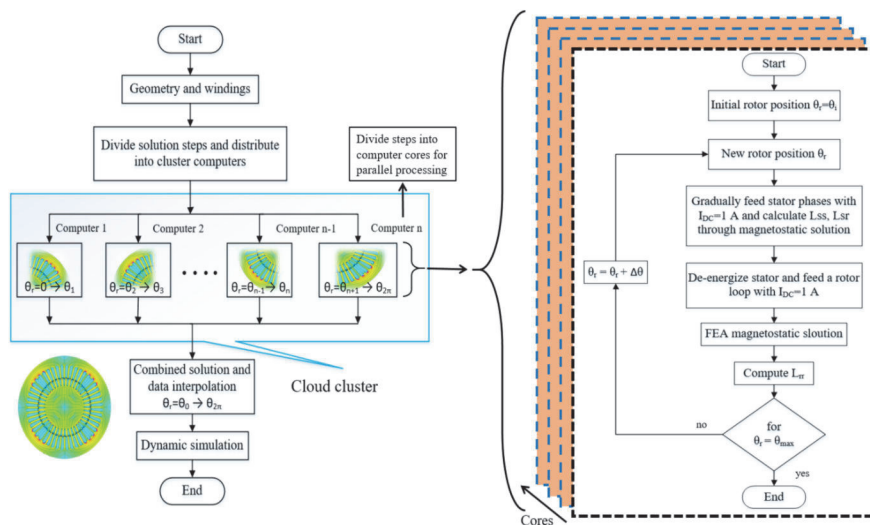


Figure 3. The division of rotor steps among various computers and their cores for parallel computation and the procedure of inductances calculation.

For better accuracy, a considerable number of mesh elements (250,160) with (125,177) nodes are solved having a precision of 1×10^{-8} at each rotor step. The FEMM 4.0 achieves this precision through a conjugate gradient solver with the help of multiple successive approximation iterations. Since the inductance profiles change with the change in the air gap, the selection of an appropriate rotor step size is very important. The changing air gap is the function of stator and rotor slot openings [37], which becomes very prominent when the openings on both sides align with each other and lead to the abruptly changing inductance derivatives. As the rotor and stator, slots are different in number, their least count multiple (LCM) can be a minimum choice regarding the number of rotor steps. By doing so, some phase inductances can be considered as shifted copies of the other phase inductances. In this case, the number of total rotor steps or solution samples will be divisible by the total number of rotor bars and the number of samples corresponding to 120 and 240 degrees for stator phases. For example,

if the number of rotor steps is ($40 \times 48 = 1920$), the L_{bb} will be equal to $(120 \times 1920/360)$ samples shifted copy of L_{aa} . The same is true in the case of rotor bar inductances, only self and mutual inductances of a single loop need to be calculated, the rest of them are shifted copies. However, special attention is needed if the fault changes all the inductances symmetrically or not.

5. The Simulation Results

At each rotor position, every individual stator phase is energized with a unity DC current, and relevant inductances are calculated by integrating the magnetic vector potential over the coil area as shown by the following equations.

$$L_{self} = \frac{\int_{si} A \cdot J \, da}{i^2} \quad (15)$$

$$L_{mutual} = \frac{n_2}{i_1 a_2} \left(\int_{+si} A_1 da_1 - \int_{-si} A_1 da_2 \right) \quad (16)$$

where A is the vector potential, J is the current density, n is the number of turns per phase, i is the phase current, the subscript “ si ” is for surface integral. The first bracket term in Equation (16) is the integration of the vector potential of coils with positive current or the coils pointing out of the page. The second term corresponds to the coils with negative current or pointing into the page, a_2 is the cross-sectional area of the coil, which is approximately equal to the slot area multiplied with the filling factor. The motor’s magnetic flux distribution after the energizing phase “ a ” with 1 A DC current is shown in Figure 4. The highlighted slots contain phase “ a ” winding whose surface integral of magnetic potential is equal to self-inductance L_{aa} at the specific rotor position as in Equation (15).

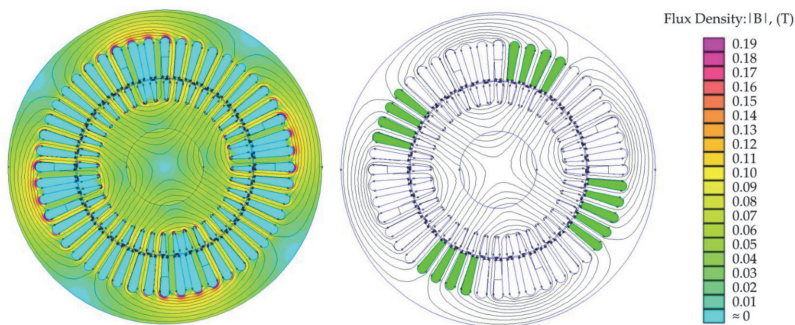


Figure 4. The flux distribution with energized phase “ a ” with $I_{DC} = 1$ A, and the selection of slots for vector potential integral for calculation of self-inductance L_{aa} .

Similarly, all stator–stator self and mutual and stator–rotor mutual inductances can be calculated. The rotor–rotor self and mutual inductances are calculated by energizing a single rotor loop with unity DC current as shown in Figure 5. Only one rotor loop needs to be energized and solved for its inductances, and the rest of them possess the same solution with a phase shift equal to the angle difference between them.

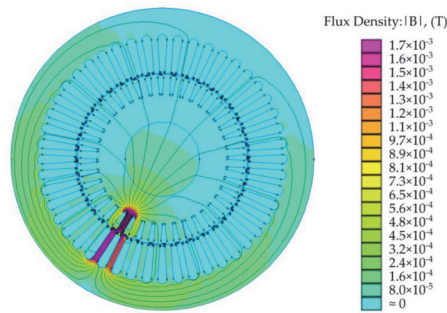


Figure 5. Flux distribution due to energized rotor loop with $I_{DC} = 1$ A for the calculation of rotor inductances.

Since the solution is for the 2D model, the effect of end windings is compensated by using additional end winding leakage inductance and resistance using the following analytical formulas.

$$L_{ew} = \frac{Q_s}{m} q \left(\frac{Z_q}{a} \right)^2 \mu_0 l_w \lambda_w \quad (17)$$

where Q_s is the number of stator slots, Z_q is the number of conductors per slot, a is the number of winding parallel paths per phase, m is the total number of stator phases, and q is the number of slots in a pole captured by an individual phase. l_w is the average length of the end winding, λ_w is the permeance factor which is 0.20 for the motor under investigation. The same formula can be used to calculate the leakage inductance of the rotor end rings. For building the resistance matrix, various stator- and rotor-related resistances are calculated using resistivity formula where the skinning and proximity effects are neglected because of the DC supply current;

$$R = \frac{\rho l}{A} \quad (18)$$

where ρ is the resistivity, A is the cross-sectional area, and l is the length of the conductor. The effective slot area (ESA) is equal to the total area of slot multiplied with the filling factor, which is 0.60 for the machine under investigation. The conductor cross-sectional area can be calculated by dividing the ESA with the total number of conductors in the slot, which are 17 in this case. The resistance of the end windings is included by increasing the length of the per phase conductor corresponding to the length of the end winding. Since the stator and rotor windings are energized with unity DC current, the effects such as proximity, skinning, material saturation, and eddy currents are neglected as the focus is towards the simulation time reduction. However, they can be included in the online section analytically.

Figure 6 shows various inductances as a function of the rotor position. All self and mutual inductances are the functions of the air gap, which changes with the stepping rotor. This phenomenon is evident in the inductance profiles, which are calculated with a rotor step size of 0.1875 degrees. The self- and mutual inductances of stator have five cycles until an angle of 45 degrees, which corresponds to 40 cycles until 360 degrees. This is because the rotor has 40 bars having 40 slot openings. The stator inductances consider the stator air gap as static while rotor associated air gap moves with the moving rotor. The same is true for rotor self- and mutual inductances, which have six cycles per 45 degrees corresponding to 48 cycles till 360 degrees. Where 48 is the number of stator slots and for rotor inductances, the rotor-associated air gap remains static while the stator gap has a relative motion.

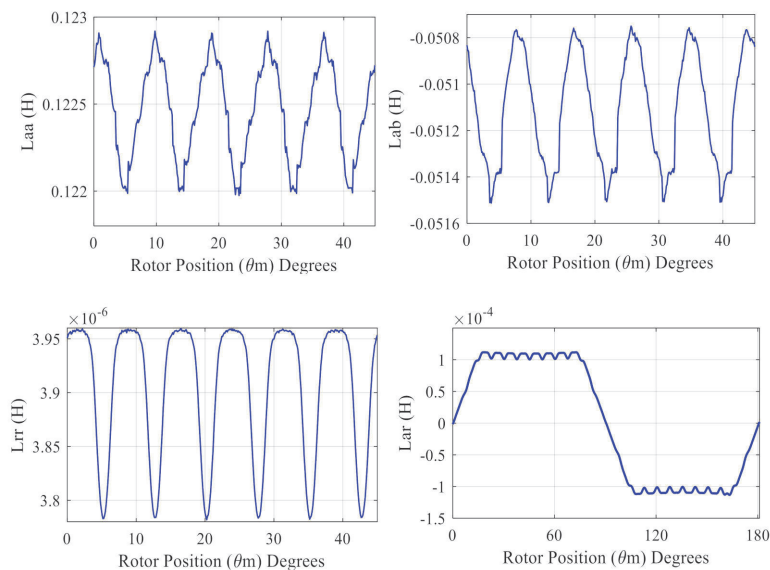


Figure 6. The calculated inductances as a function of the rotor position.

6. Test Setup

The test rig consists of two identical motors with specifications given in Table 1. Both machines are attached back to back on the same mechanical foundation as shown in Figure 7. The first motor is the test motor while the second acts as a loading machine. The grid supplies the test machine while the loading machine is controlled using ABB ACS-880 industrial inverter for better controllability of slip. The measurement time of the stator current of the test machine under healthy and broken bar cases is 100 sec with a sampling frequency of 10 kHz.

Table 1. Motor specifications.

Sr. No.	Parameter	Symbol	Value
1	Rated speed	N_r	1400 rpm@50 Hz
2	Rated power	P_r	18 kW@50 Hz
3	Connection	Y, Δ	Star (Y)
4	Power factor	$\cos\phi$	0.860
5	Number of poles	P	4
6	Number of rotor bars	N_{rb}	40
7	Number of stator slots	N_s	48

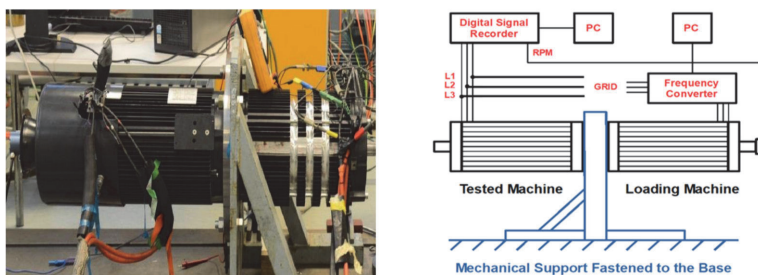


Figure 7. The test rig and its block diagram.

7. Results and Discussion

7.1. Stator Current Spectrum under Healthy and Broken Rotor Bar Cases

The varying inductances give rise to the harmonics in the stator voltage and currents. The most prominent of them are supply based and spatial harmonics. A comparison of the frequency spectrum of stator current obtained from the proposed model and the measurements taken from the laboratory test rig is shown in Figure 8. The only additional harmonics in the practical signal are the third harmonics coming from the supply side. Another major source of harmonics in the signal spectrum is the fault, which can act as a definition component for condition monitoring. Figure 9 shows the development of the left side harmonics (LSH) due to the broken bars at the rated load.

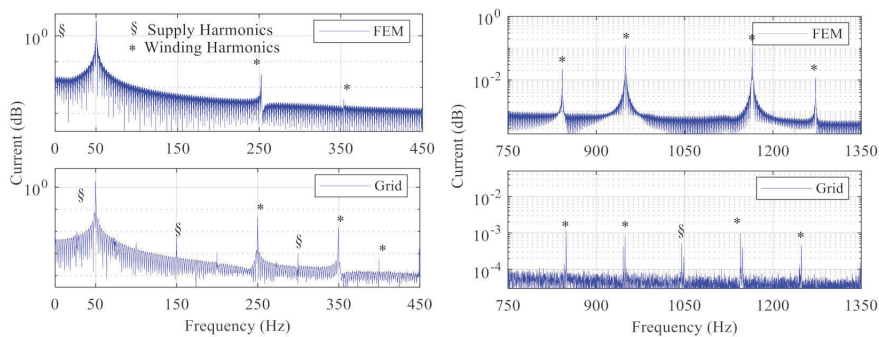


Figure 8. The frequency spectrum of stator current obtained from the proposed model and laboratory-based measurements.

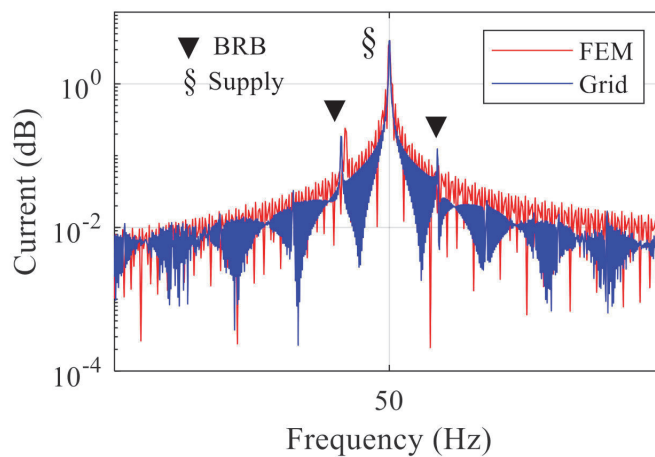


Figure 9. The broken rotor bars-based side-band frequencies.

7.2. Time Comparison

The overall computational speed of each worker (computer) can be increased by using all cores in a parallel fashion. This increase in speed is because of increased cache, which reduces memory latency; the parallel handling of the independent instructions; and the improved performance of the processor power wall. The per-step computational time for the calculation of inductances relevant to a single phase (L_{aa} , L_{ab} , L_{ac} , and L_{ar}) at different rotor positions by using the different number of

cores is shown in Figure 10a. Since, with the increase in the number of cores, more processing power is being utilized, the per-step calculation time increases. Moreover, the variation in the calculation time with the increase in the number of cores also increases, which depends upon the processor being utilized by auxiliary programs like Windows, etc. Figure 10b shows the mean per-step simulation time, which increases from 100 to 200 s per step with the increase in the utilization of processing power from about 25% (one core) to 94% (four cores). The mean simulation time is calculated because each step takes a slightly different time for calculation because of the change in the number of mesh elements and the other programs running in parallel. The overall calculation time for all inductances for 1920 rotor positions is shown in Figure 10c. It is obvious that even the per step simulation time with an increase in the parallel processing increases, but the total calculation time decreases dramatically. Meanwhile, Figure 10d shows the time taken by the cluster of four computers working as a LAN. The simulation time decreases considerably and the non-linear decrease in time is due to the latency of the network. It is worth mentioning that the job scheduler prefers cores of different computers to work in parallel. This is the reason why the computational time in Figure 10d with four cores of different computers working in parallel is considerably less than the time taken by one computer with all four cores engaged in parallel as shown in Figure 10c.

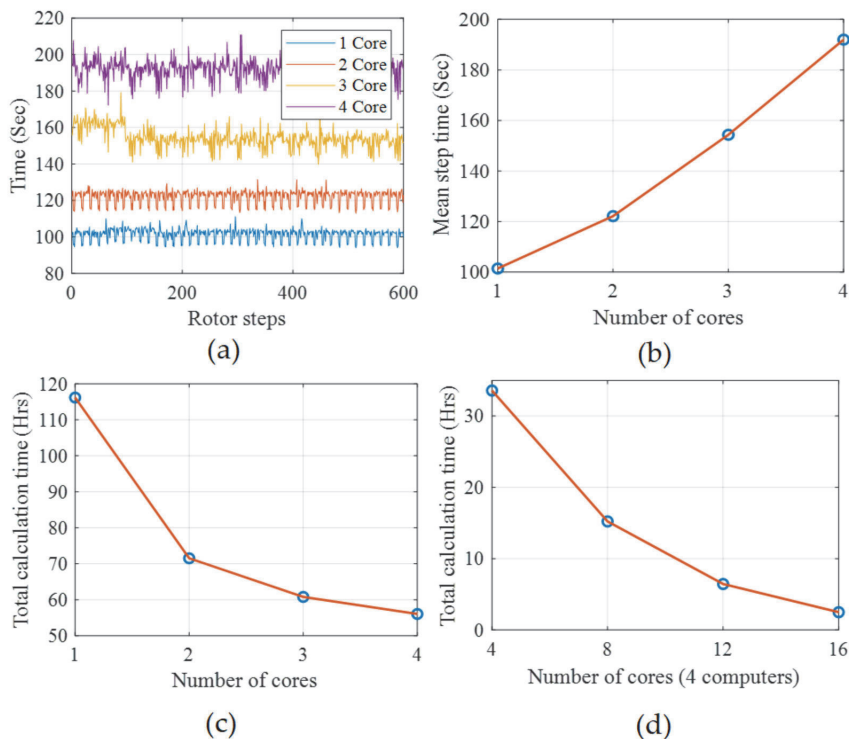


Figure 10. The simulation time, (a) per step with different number of single computer workers (cores) in parallel, (b) the mean per-step time with different number of cores of a single computer working in parallel, (c) overall time on one computer with different cores engaged in parallel, (d) overall time with different number of computers making a cluster with distributed cores in parallel.

8. Conclusions

This paper presents a hybrid FEM–analytical model solved in a parallel fashion on a cluster of computers for the reduction of computational time. The artificial intelligence (AI) based

condition-monitoring techniques for predictive maintenance of electrical machines is gaining heightened popularity. This is not only because of their ability to detect faults at the incipient stage but also because of their aptitude for faults segregation. The accurate model of the electrical machines is the key element of these techniques, which is crucial for the collection of big data under various healthy and faulty conditions. This data is essential for the training of the diagnostic systems and for making the safety rules. Among several modeling techniques, the FEM-based models have proved their accuracy in the field of electrical machine design for the past few decades. The FEM models have very few approximations and can deal with almost any kind of geometrical complexities of the system as compared to their analytical counterparts. The analytical models have their own attractions, such as the reduced simulation time and the development of analytical equations, which are integral parts of drives and inverse problem theory, etc. The biggest challenge for FEM-based models is their complexity in the forms of computational time and required memory. While on the analytical side, the approximations are fatal for any reliable diagnostic algorithm. The world is witnessing the exponentially increasing trend in the power of processors and sophisticated IT networks, which leads toward cloud computation and industry 4.0 standards.

By exploiting the benefits of analytical, FEM models, and cloud computation, this paper proposes a hybrid analytical–FEM model for the simulation of the machine under healthy and faulty conditions with reduced calculation time. Most of the techniques dealing with the reduction in the simulation time of FEM models fail when the machine is in a faulty condition, which makes it purely unsymmetrical. Moreover, any approximation for the sake of reduced complexity can decrease the reliability of the model-dependent diagnostic algorithm. With the development of more sophisticated processors and industry 4.0 standards, the complete models of the system can be solved in very much less time as compared to the conventional techniques. In this paper, the model is first divided into offline and online portions. All the inductances and other necessary parameters are calculated in the offline section, and the results are saved in 3D matrices as a function of rotor position. Once the inductances are calculated, they can be used in an online dynamic model where the performance parameters such as speed, torque, flux, and currents can be investigated under different conditions. In the case of some faults such as broken bars or broken end rings, the inductance matrices need not be calculated again but the fault can be manipulated in the online portion. This can be achieved by changing the values of the corresponding elements in the resistance matrix. For reducing the calculation time, the FEM model is divided into several computers before dividing the specific portion into the cores of any particular processor. For making a computer cluster resembling a cloud, four computers having the same specifications were used as a local area network. The total rotor steps were then divided into several cores working in parallel and the results were collected on the main computer. This technique reduces the simulation time drastically without any need for model approximation. For the validation of results, the frequency spectrum of simulated stator current is compared with the one measured in the laboratory setup under healthy and broken rotor bar cases.

Author Contributions: Conceptualization, B.A., T.V., and A.B.; methodology, B.A., T.V., and A.B.; validation, A.K., A.R., and A.B.; data curation, B.A.; writing—original draft preparation, B.A.; writing—review and editing, A.R., and M.N.I.; visualization, T.V.; supervision, T.V., and A.B. All authors have read and agreed to the published version of the manuscript.

Funding: This research received no external funding.

Conflicts of Interest: The authors declare no conflict of interest.

References

1. Saidur, R. A review on electrical motors energy use and energy savings. *Renew. Sustain. Energy Rev.* **2010**, *14*, 877–898. [\[CrossRef\]](#)
2. Sahraoui, M.; Cardoso, A.J.M.; Ghoggal, A. The use of a modified prony method to track the broken rotor bar characteristic frequencies and amplitudes in three-phase induction motors. *IEEE Trans. Ind. Appl.* **2015**, *51*, 2136–2147. [\[CrossRef\]](#)

3. Naha, A.; Samanta, A.K.; Routray, A.; Deb, A.K. Low Complexity Motor Current Signature Analysis Using Sub-Nyquist Strategy with Reduced Data Length. *IEEE Trans. Instrum. Meas.* **2017**, *66*, 3249–3259. [\[CrossRef\]](#)
4. Asad, B.; Vaimann, T.; Belahcen, A.; Kallaste, A.; Rassölkin, A.; Iqbal, M.N. Broken rotor bar fault detection of the grid and inverter-fed induction motor by effective attenuation of the fundamental component. *IET Electr. Power Appl.* **2019**, *13*, 2005–2014. [\[CrossRef\]](#)
5. Zhen, D.; Wang, T.; Gu, F.; Ball, A. Fault diagnosis of motor drives using stator current signal analysis based on dynamic time warping. *Mech. Syst. Signal Process.* **2013**, *34*, 191–202. [\[CrossRef\]](#)
6. Garcia-Ramirez, A.G.; Morales-Hernandez, L.A.; Osornio-Rios, R.A.; García-Pérez, A.; Romero-Troncoso, R.D.J. Thermographic Technique as a Complement for MCSA in Induction Motor Fault Detection. In Proceedings of the 2014 International Conference on Electrical Machines (ICEM), ICEM 2014, Berlin, Germany, 2–5 September 2014; pp. 1940–1945.
7. Taheri-Garavand, A.; Ahmadi, H.; Omid, M.; Mohtasebi, S.S.; Mollazade, K.; Smith, A.J.R.; Carlomagno, G.M. An intelligent approach for cooling radiator fault diagnosis based on infrared thermal image processing technique. *Appl. Therm. Eng.* **2015**, *87*, 434–443. [\[CrossRef\]](#)
8. Glowacz, A.; Glowacz, Z. Diagnostics of stator faults of the single-phase induction motor using thermal images, MoASoS and selected classifiers. *Measurement* **2016**, *93*, 86–93. [\[CrossRef\]](#)
9. Luong, P.; Wang, W. Smart Sensor-Based Synergistic Analysis for Rotor Bar Fault Detection of Induction Motors. *IEEE/ASME Trans. Mechatronics* **2020**, *25*, 1067–1075. [\[CrossRef\]](#)
10. Caesarendra, W.; Kosasih, B.; Tieu, A.K.; Zhu, H.; Moodie, C.A.; Zhu, Q. Acoustic emission-based condition monitoring methods: Review and application for low speed slew bearing. *Mech. Syst. Signal Process.* **2016**, *72–73*, 134–159. [\[CrossRef\]](#)
11. Vaimann, T.; Sobra, J.; Belahcen, A.; Rassölkin, A.; Rolak, M.; Kallaste, A. Induction machine fault detection using smartphone recorded audible noise. *IET Sci. Meas. Technol.* **2018**, *12*, 554–560. [\[CrossRef\]](#)
12. Henao, H.; Demian, C.; Capolino, G.-A. A frequency-domain detection of stator winding faults in induction machines using an external flux sensor. *IEEE Trans. Ind. Appl.* **2003**, *39*, 1272–1279. [\[CrossRef\]](#)
13. Frosini, L.; Harlisca, C.; Szabo, L. Induction Machine Bearing Fault Detection by Means of Statistical Processing of the Stray Flux Measurement. *IEEE Trans. Ind. Electron.* **2015**, *62*, 1846–1854. [\[CrossRef\]](#)
14. Stone, G.C.; Sedding, H.G.; Chan, C. Experience With Online Partial-Discharge Measurement in High-Voltage Inverter-Fed Motors. *IEEE Trans. Ind. Appl.* **2018**, *54*, 866–872. [\[CrossRef\]](#)
15. Mirzaeva, G.; Saad, K.I.; Jahromi, M.G. Comprehensive Diagnostics of Induction Motor Faults Based on Measurement of Space and Time Dependencies of Air Gap Flux. *IEEE Trans. Ind. Appl.* **2017**, *53*, 2657–2666. [\[CrossRef\]](#)
16. Liu, R.; Yang, B.; Zio, E.; Chen, X. Artificial intelligence for fault diagnosis of rotating machinery: A review. *Mech. Syst. Signal Process.* **2018**, *108*, 33–47. [\[CrossRef\]](#)
17. Konar, P.; Chattopadhyay, P. Bearing fault detection of induction motor using wavelet and Support Vector Machines (SVMs). *Appl. Soft Comput.* **2011**, *11*, 4203–4211. [\[CrossRef\]](#)
18. Li, X.; Wang, K.; Jiang, L. The Application of AE Signal in Early Cracked Rotor Fault Diagnosis with PWVD and SVM. *J. Softw.* **2011**, *6*, 1969–1976. [\[CrossRef\]](#)
19. Soualhi, A.; Medjaher, K.; Zerhouni, N. Bearing Health Monitoring Based on Hilbert–Huang Transform, Support Vector Machine, and Regression. *IEEE Trans. Instrum. Meas.* **2015**, *64*, 52–62. [\[CrossRef\]](#)
20. Sadeghian, A.; Ye, Z.; Wu, B. Online Detection of Broken Rotor Bars in Induction Motors by Wavelet Packet Decomposition and Artificial Neural Networks. *IEEE Trans. Instrum. Meas.* **2009**, *58*, 2253–2263. [\[CrossRef\]](#)
21. Bin, G.F.; Gao, J.J.; Li, X.J.; Dhillon, B.S. Early fault diagnosis of rotating machinery based on wavelet packets—Empirical mode decomposition feature extraction and neural network. *Mech. Syst. Signal Process.* **2012**, *27*, 696–711. [\[CrossRef\]](#)
22. Prieto, M.D.; Cirrincione, G.; Espinosa, A.G.; Ortega, J.A.; Henao, H. Bearing Fault Detection by a Novel Condition-Monitoring Scheme Based on Statistical-Time Features and Neural Networks. *IEEE Trans. Ind. Electron.* **2013**, *60*, 3398–3407. [\[CrossRef\]](#)
23. Wang, J.; Liu, S.; Gao, R.X.; Yan, R. Current envelope analysis for defect identification and diagnosis in induction motors. *J. Manuf. Syst.* **2012**, *31*, 380–387. [\[CrossRef\]](#)
24. Palácios, R.H.C.; Da Silva, I.N.; Goedtel, A.; Godoy, W.F. A comprehensive evaluation of intelligent classifiers for fault identification in three-phase induction motors. *Electr. Power Syst. Res.* **2015**, *127*, 249–258. [\[CrossRef\]](#)

25. Wan, X.; Wang, D.; Tse, P.W.; Xu, G.; Zhang, Q. A critical study of different dimensionality reduction methods for gear crack degradation assessment under different operating conditions. *Measurement* **2016**, *78*, 138–150. [\[CrossRef\]](#)
26. Ali, M.Z.; Shabbir, N.S.K.; Zaman, S.M.K.; Liang, X. Single- and Multi-Fault Diagnosis Using Machine Learning for Variable Frequency Drive-Fed Induction Motors. *IEEE Trans. Ind. Appl.* **2020**, *56*, 2324–2337. [\[CrossRef\]](#)
27. Shao, S.; Yan, R.; Lu, Y.; Wang, P.; Gao, R.X. DCNN-Based Multi-Signal Induction Motor Fault Diagnosis. *IEEE Trans. Instrum. Meas.* **2020**, *69*, 2658–2669. [\[CrossRef\]](#)
28. Jung, U.; Koh, B.-H. Wavelet energy-based visualization and classification of high-dimensional signal for bearing fault detection. *Knowl. Inf. Syst.* **2015**, *44*, 197–215. [\[CrossRef\]](#)
29. Pandya, D.H.; Upadhyay, S.H.; Harsha, S.P. Fault diagnosis of rolling element bearing with intrinsic mode function of acoustic emission data using APF-KNN. *Expert Syst. Appl.* **2013**, *40*, 4137–4145. [\[CrossRef\]](#)
30. He, D.; Li, R.; Zhu, J. Plastic Bearing Fault Diagnosis Based on a Two-Step Data Mining Approach. *IEEE Trans. Ind. Electron.* **2013**, *60*, 3429–3440. [\[CrossRef\]](#)
31. Baccarini, L.M.R.; De Menezes, B.R.; Caminhas, W.M. Fault induction dynamic model, suitable for computer simulation: Simulation results and experimental validation. *Mech. Syst. Signal Process.* **2010**, *24*, 300–311. [\[CrossRef\]](#)
32. Cunha, C.C.M.; Oliveira, P.; Lyra, R.; Filho, B.C. Simulation and analysis of induction machines with rotor asymmetries. *IEEE Trans. Ind. Appl.* **2005**, *41*, 18–24.
33. Liang, J.; Qiu, Y.; Zhao, M.; Kang, S.; Lu, H. The modeling and numerical simulations of wind turbine generation system with free vortex method and simulink. *Energy Convers. Manag.* **2015**, *103*, 762–777.
34. Lubin, T.; Hamiti, T.; Razik, H.; Rezzoug, A. Comparison Between Finite-Element Analysis and Winding Function Theory for Inductances and Torque Calculation of a Synchronous Reluctance Machine. *IEEE Trans. Magn.* **2007**, *43*, 3406–3410.
35. Raziee, S.M.; Misir, O.; Ponick, B. Winding Function Approach for Winding Analysis. *IEEE Trans. Magn.* **2017**, *53*, 1–9.
36. Nandi, S. A Detailed Model of Induction Machines With Saturation Extendable for Fault Analysis. *IEEE Trans. Ind. Appl.* **2004**, *40*, 1302–1309.
37. Asad, B.; Vaimann, T.; Belahcen, A.; Kallaste, A.; Rassõlkin, A.; Iqbal, M.N. Modified winding function-based model of squirrel cage induction motor for fault diagnostics. *IET Electr. Power Appl.* **2020**, *14*, 1722–1734.
38. Sudhoff, S.D.; Kuhn, B.T.; Corzine, K.A.; Branecky, B.T. Magnetic Equivalent Circuit Modeling of Induction Motors. *IEEE Trans. Energy Convers.* **2007**, *22*, 259–270.
39. Apsley, J.M.; Williamson, S. Analysis of Multi-Phase Induction Machines with Winding Faults. In Proceedings of the IEEE International Conference on Electric Machines and Drives, San Antonio, TX, USA, 15 May 2005; pp. 249–255.
40. Wang, L.; Jatskevich, J.; Pekarek, S.D. Modeling of induction machines using a voltage-behind-reactance formulation. *IEEE Trans. Energy Convers.* **2008**, *23*, 382–392.
41. Sapena-Bano, A.; Martinez-Roman, J.; Puche-Panadero, R.; Pineda-Sanchez, M.; Perez-Cruz, J.; Riera-Guasp, M. Induction machine model with space harmonics for fault diagnosis based on the convolution theorem. *Int. J. Electr. Power Energy Syst.* **2018**, *100*, 463–481.
42. Ding, Q.; Yang, Z.; Sun, X.; Zhao, Q.; Zhu, H. Analysis of rotor slot width influence on a bearingless induction motor. *Comput. Electr. Eng.* **2020**, *81*, 106534.
43. Belahcen, A.; Rasilo, P.; Arkkio, A. Segregation of Iron Losses From Rotational Field Measurements and Application to Electrical Machine. *IEEE Trans. Magn.* **2014**, *50*, 893–896. [\[CrossRef\]](#)
44. Zhang, H. Online Thermal Monitoring Models for Induction Machines. *IEEE Trans. Energy Convers.* **2015**, *30*, 1–9. [\[CrossRef\]](#)
45. Zhang, Y.; Ruan, J.; Huang, T.; Yang, X.; Zhu, H.; Yang, G. Calculation of Temperature Rise in Air-cooled Induction Motors Through 3-D Coupled Electromagnetic Fluid-Dynamical and Thermal Finite-Element Analysis. *IEEE Trans. Magn.* **2012**, *48*, 1047–1050. [\[CrossRef\]](#)
46. Bourchas, K.; Stening, A.; Soulard, J.; Broddelfalk, A.; Lindenmo, M.; Dahlen, M.; Gyllensten, F. Quantifying Effects of Cutting and Welding on Magnetic Properties of Electrical Steels. *IEEE Trans. Ind. Appl.* **2017**, *53*, 4269–4278. [\[CrossRef\]](#)

47. Sapena-Bano, A.; Chinesta, F.; Pineda-Sanchez, M.; Aguado, J.; Borzacchiello, D.; Puche-Panadero, R. Induction machine model with finite element accuracy for condition monitoring running in real time using hardware in the loop system. *Int. J. Electr. Power Energy Syst.* **2019**, *111*, 315–324. [[CrossRef](#)]
48. Ghahfarokhi, P.S.; Belahcen, A.; Kallaste, A.; Vaimann, T.; Gerokov, L.; Rassolkin, A. Thermal Analysis of a SynRM Using a Thermal Network and a Hybrid Model. In Proceedings of the 2018 23rd International Conference on Electrical Machines, ICEM 2018, Alexandroupoli, Greece, 3–6 September 2018; pp. 2682–2688.
49. Mukhrejee, V.; Far, M.F.; Martin, F.; Belahcen, A. Constrained Algorithm for the Selection of Uneven Snapshots in Model Order Reduction of a Bearingless Motor. *IEEE Trans. Magn.* **2017**, *53*, 1–4. [[CrossRef](#)]
50. Far, M.F.; Martin, F.; Belahcen, A.; Rasilo, P.; Awan, H.A.A. Real-Time Control of an IPMSM Using Model Order Reduction. *IEEE Trans. Ind. Electron.* **2020**, *1*. [[CrossRef](#)]
51. Far, M.F.; Martin, F.; Belahcen, A.; Montier, L.; Henneron, T. Orthogonal Interpolation Method for Order Reduction of a Synchronous Machine Model. *IEEE Trans. Magn.* **2018**, *54*, 1–6.
52. Borzacchiello, D.; Aguado, J.V.; Chinesta, F. Non-intrusive Sparse Subspace Learning for Parametrized Problems. *Arch. Comput. Methods Eng.* **2019**, *26*, 303–326. [[CrossRef](#)]
53. Villalonga, A.; Beruvides, G.; Castano, F.; Haber, R.E. Cloud-Based Industrial Cyber–Physical System for Data-Driven Reasoning: A Review and Use Case on an Industry 4.0 Pilot Line. *IEEE Trans. Ind. Informatics* **2020**, *16*, 5975–5984. [[CrossRef](#)]
54. Chen, Z.; Quan, W.; Wen, M.; Fang, J.; Yu, J.; Zhang, C.; Luo, L. Deep Learning Research and Development Platform: Characterizing and Scheduling with QoS Guarantees on GPU Clusters. *IEEE Trans. Parallel Distrib. Syst.* **2020**, *31*, 34–50. [[CrossRef](#)]
55. Gao, Y.; Ai, Y.; Tian, B.; Chen, L.; Wang, J.; Cao, D.; Wang, F.-Y. Parallel End-to-End Autonomous Mining: An IoT-Oriented Approach. *IEEE Internet Things J.* **2020**, *7*, 1011–1023. [[CrossRef](#)]
56. Bandyopadhyay, I.; Purkait, P.; Koley, C. A combined image processing and Nearest Neighbor Algorithm tool for classification of incipient faults in induction motor drives. *Comput. Electr. Eng.* **2016**, *54*, 296–312. [[CrossRef](#)]
57. Guesmi, H.; Ben Salem, S.; Bacha, K. Smart wireless sensor networks for online faults diagnosis in induction machine. *Comput. Electr. Eng.* **2015**, *41*, 226–239. [[CrossRef](#)]
58. Chen, J.; Li, K.; Bilal, K.; Zhou, X.; Li, K.; Yu, P.S. A Bi-layered Parallel Training Architecture for Large-Scale Convolutional Neural Networks. *IEEE Trans. Parallel Distrib. Syst.* **2019**, *30*, 965–976. [[CrossRef](#)]
59. You, Y.; Zhang, Z.; Hsieh, C.-J.; Demmel, J.; Keutzer, K. Fast Deep Neural Network Training on Distributed Systems and Cloud TPUs. *IEEE Trans. Parallel Distrib. Syst.* **2019**, *30*, 2449–2462. [[CrossRef](#)]
60. Huang, S.-R.; Huang, K.-H.; Chao, K.-H.; Chiang, W.-T. Fault analysis and diagnosis system for induction motors. *Comput. Electr. Eng.* **2016**, *54*, 195–209. [[CrossRef](#)]

Publisher's Note: MDPI stays neutral with regard to jurisdictional claims in published maps and institutional affiliations.



© 2020 by the authors. Licensee MDPI, Basel, Switzerland. This article is an open access article distributed under the terms and conditions of the Creative Commons Attribution (CC BY) license (<http://creativecommons.org/licenses/by/4.0/>).

Publication III

Asad, B.; Vaimann, T.; Belahcen, A.; Kallaste, A.; Rassõlkin, A.; Heidari, H. (2020). The Low Voltage Start-up Test of Induction Motor for the Detection of Broken Bars. International conference on electrical machines (ICEM 2020), Gothenburg, Sweden, August 23-26. IEEE, 1481–1487.

The Low Voltage Start-up Test of Induction Motor for the Detection of Broken Bars

B. Asad, T. Vaimann, A. Belahcen, *Senior Member, IEEE*, A. Kallaste, A. Rassõlkin, H. Heidari

Abstract—This paper presents the broken rotor bar fault diagnostics by time-frequency analysis of motor current under extended startup transient time achieved by reducing the applied voltage. The fault diagnostics under a steady stage regime has been a topic of interest since the past few decades. The main aim has been focused on the detection of fault-based frequencies which are the function of slip. Those frequencies become very less legible under low load conditions and totally disappear under no-load conditions. Moreover, the stator and rotor slot skews have a potential attenuation impact on them. To avoid these problems, the time-frequency analysis of motor startup current is investigated in this paper using a wavelet approach. To improve the legibility of the spectrum, the transient time is extended by reducing the supply voltage of the machine under no external load. By reducing the supply voltage, the inertia of the rotor acts as a load to increase the transient time which is essential for better resolution. The results are based on the practical measurements taken from the laboratory setup under healthy and faulty conditions.

Index Terms—Condition monitoring, Fault diagnosis, Fourier transforms, Induction motors, wavelet transforms.

I. INTRODUCTION

Electrical machines have been showing their influential role in industrial and domestic applications since the second industrial revolution. This role is evident in the form of electricity generation such as wind power plants or electrical to mechanical energy converters, driving the cycles of the industry. Out of a variety of electrical machines, induction motors are being used extensively because of their simple structure, good efficiency, and easy maintenance. As a consumer, electrical machines are consuming more than fifty percent of the total energy generated worldwide.

The mechanically moving parts and rough industrial environment make ten vulnerable to the faults. The electrical faults are mainly related to the stator such as inter-turn short circuits, phase drop, voltage imbalance, earthing and inverter related faults. However, the mechanical faults are mainly associated with the rotor such as broken bars, bad bearings, eccentricity, broken end rings or bad foundations etc. All those faults are degenerative in nature which makes it very crucial to detect them at the incipient stage to avoid any catastrophic situation. A variety of fault diagnostic techniques

can be found in literature, such as vibration analysis, thermal analysis, acoustic analysis, electromagnetic field inference, leakage flux, infrared light detection, and chemical analysis, etc.

However, the motor current signature analysis (MCSA) based fault diagnostic techniques are being extensively used in research, because of their noninvasive nature and least complexity. Moreover, a huge domain of data processing techniques improves their flexibility and makes them more reliable.

It is a well-studied fact that every fault modulates the stator current with a certain bandwidth of frequencies. The detection of those frequency components can lead to the cause of the fault. The Fourier transform can be considered as a foundation stone for all advanced signal processing techniques. The majority of MCSA based techniques depend on fast Fourier transform (FFT) of the signal, e.g. in [1], the authors used the FFT on active and reactive currents of a motor to investigate the broken rotor bars and load oscillations. Authors of [2] used the FFT in conjunction with Park's vector to make artificial ants clustering technique for the fault diagnostics of induction motor. In [3], the autoregressive method is relying on discrete-time Fourier transform (DTFT) and notch filter. Researchers in [4] used the FFT to prove that the slot harmonics can be used as potential indicators to detect the broken rotor bars. In [5], the authors used an adoptive notch filter and FFT for broken rotor bar fault diagnostics of induction motor. Authors of [6] used the FFT on simulations and practical results to investigate the broken rotor bars and mechanical vibrations. In [7], Nandi used the FFT extensively to study the frequency spectrum of the stator current for different fault conditions. [8] Used FFT along with a bandstop filter for the detection of broken rotor bar frequencies.

There are various limitations of FFT putting a question mark on its reliability. These limitations include the spectral leakage, which is the power of the fundamental component leaking into the subsequent frequency bins. If the length and sampling frequency of the acquired signal is not good enough, the fault representing frequency components are highly likely to be buried under the main frequency bin. This problem becomes worse when the motor is working under no-load or fewer load conditions, as the faulty frequencies are the function of the slip. The other problem of FFT is that the signal should be in a steady-state regime, stationary and should not have any discontinuities. These problems are becoming worse as the inverters are coming forward as an integral part of the drive system. The inverter fed voltage is

B. Asad, T. Vaimann, A. Kallaste, A. Rassõlkin and H. Heidari are with the Department of Electrical Power Engineering and Mechatronics, Tallinn University of Technology, Estonia (e-mail: biasad@ttu.ee)

A. Belahcen is with Department of Electrical Engineering and Automation, Aalto University, Espoo, Finland and with the Department of Electrical Power Engineering and Mechatronics, Tallinn University of Technology, Estonia (e-mail: anouar.belahcen@aalto.fi)

full of harmonics which makes the entire frequency spectrum hazy. Moreover, the control algorithms being used in drives can also have an impact on the amplitude of harmonics. For example, in the case of direct torque control (DTC) motors, the drive has its direct influence on the current signal carrying all the information about the health of the motor [9].

Researchers have tried several different techniques to cope with those problems. The use of Hilbert transforms to extract the envelope of the signal, which, possess considerable information regarding the health of electrical machines can be found in [10]. The authors in [11] used fractional Fourier transform to recover the faulty frequencies from a non-stationary signal. In [12] authors used sliding discrete Fourier transform for the detection of broken rotor bars, while [13] [14] [15] used the wavelet technique to improve the accuracy. In this paper, a low voltage test to extend the transient interval of the motor is proposed. By increasing the transient time of the motor startup current, the time-frequency resolution of the frequency spectrum can be improved. The use of the transient interval reduces the FFT based conventional problems. All the measurements are taken without any external load to prove the effectiveness of the method. The wavelet transform is preferred over short-time Fourier transform (STFT) to avoid inherited FFT drawbacks. Moreover, a band stop infinite impulse response (IIR) filter is used to attenuate the fundamental component which improves the legibility of the spectrum.

II. THEORETICAL BACKGROUND

A. Modulation of Fault

The phase current of an ideal and symmetrical machine can be described as:

$$i_a(t) = I_m \sin(\omega t + \alpha) \quad (1)$$

where I_m is the peak current, ω is supply frequency and α is the phase angle. The unsymmetrical rotor with broken rotor bars, broken end rings or bad bearings starts modulating the current with a frequency-dependent upon the speed of the rotor and the modulation index depending upon the severity of the fault.

$$i_{af}(t) = [1 + m(t)]i_a(t) \quad (2)$$

where $m(t)$ is the modulating signal, having a modulation index M , which depends on the number of broken bars (N_b) and the total number of rotor bars (N_t). If the rotor is rotating and the winding distributions are considered as sinusoidal, the modulating signal is also a sinusoid, i.e.:

$$m(t) = M \cos(\omega_o t + \phi) \quad (3)$$

where $\omega_o = 2\pi f_o$, is the fault characteristic frequency and depends upon the nature of the fault and the slip of the machine. In case of broken rotor bars, the characteristic fault frequency is at $2sf_s$:

$$f_o = 2sf_s \quad \text{and} \quad \omega_o = 2\pi(2sf_s) \quad (4)$$

$$m(t) = M \cos(4\pi sf_s t + \phi) \quad (5)$$

$$i_{af}(t) = [1 + M \cos(4\pi sf_s t + \phi)]i_a(t) \quad (6)$$

$$i_{af}(t) = [1 + M \cos(4\pi sf_s t + \phi)]I_m \sin(\omega t + \alpha) \quad (7)$$

$$i_{af}(t) = I_m \sin(2\pi sf_s t) \left(\frac{MI_m}{2} \right) [\sin(2\pi f_s(1 + 2s)t + \phi + \alpha) + \sin(2\pi f_s(1 - 2s)t + \phi + \alpha)] \quad (8)$$

where the modulation index M can be approximated as a ratio of the number of broken rotor bars and the total number of bars as in [16]

$$m \approx \frac{N_b}{N_t} \quad (9)$$

B. The Fast Fourier Transform

Being able to segregate any stationary signal into its frequency components, Fourier transform can be considered as a foundation stone of conventional and advanced signal processing based fault diagnostic techniques. A very good overview and history of Fourier transform can be found in [17]. The discrete Fourier transform (DFT) shown by (10) can convert a signal of finite length represented by a finite number of equally spaced samples to a signal of the same length represented by equally spaced frequency bins. The DFT can be solved with less computational complexity using an algorithm called Fast Fourier transform (FFT).

$$X_n = \sum_{n=0}^{N-1} x_n e^{-i2\pi kn/N}, \quad k = 0, 1, 2, \dots, (N-1) \quad (10)$$

where x_n , is the discrete sampled signal and N is the number of samples, which should be a number in power of 2, i.e. $N = 2^x$ to reduce the computational time and spectral leakage. The frequency resolution is very important in various signal processing techniques in order to detect weak faulty harmonics. It can be defined as the separation between two consecutive frequency bins. The least the difference is, the better the resolution could be. It depends upon the sampling frequency and measurement length of the signal as shown by the following equations.

$$t_{sig} = t_s \times N = N/f_s \quad (11)$$

$$df = 1/t_{sig} = f_s/N = BW/SL \quad (12)$$

$$SL = N/2 \quad (13)$$

where df is the frequency resolution, f_s is the sampling frequency, BW is the bandwidth, SL is the number of spectral lines, t_{sig} is the measurement or acquisition time of the signal and N is the number of data points used in FFT or the total number of samples. It is evident that frequency resolution can only be increased by increasing the measurement time, also called the acquisition or frame time, of the signal. Frequency resolution can also be increased by zero paddings of the signal called the spectral interpolation.

The prominent drawbacks of DFT for fault diagnostics can be described as. It is unable to deal with non-stationary signals. The high sampling rate and increased length of the

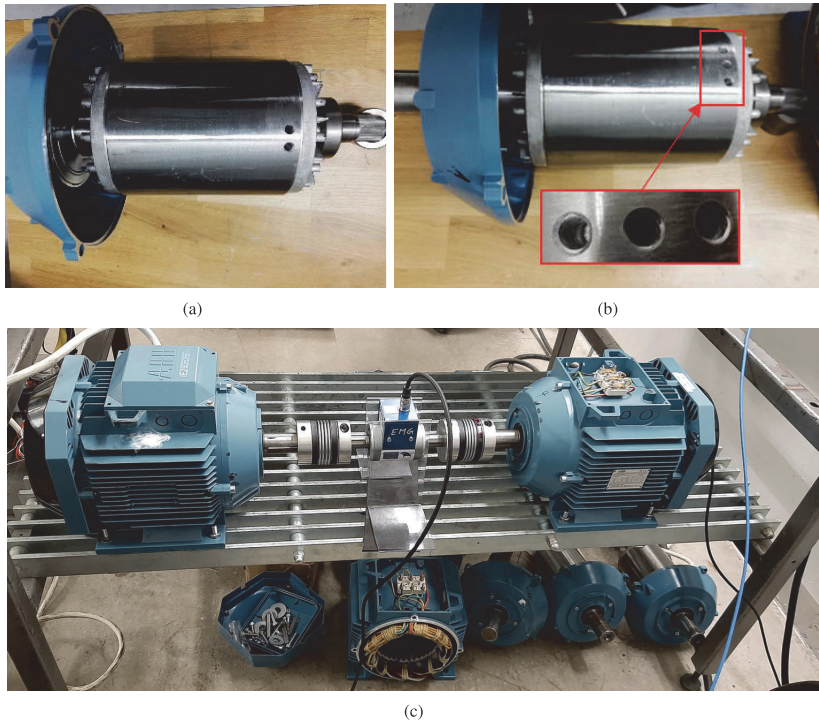


Fig. 1. The test rig preparation (a) The rotor with two broken bars, (b) The rotor with three broken bars, (c) The test bench with loading motor on right side and test motor on left side.

signal increase the complexity of the diagnostic algorithm. The discontinuities in the signal can lead to wrong results. The small faulty frequencies always remain vulnerable to be buried under some strong frequency components due to their spectral leakage. Moreover, it cannot give any time-frequency spectrum of the signal, which is very essential while handling non-stationary signals such as in the transient regime. The motor's slip changes rapidly during startup or shut down transient intervals of the motor operation. This fact can be exploited to detect faults under a transient regime with improved legibility. It can be done by using the short-time Fourier transform (STFT), where the complete signal is divided into n small segments. Each segment is considered as stationary and its DFT is calculated using the FFT algorithm. This approach gives the time-frequency representation of the signal but at the cost of increased complexity and inherited drawbacks of the FFT algorithm. Moreover, the selection of different types of windows is very important for different types of signals.

C. Wavelet Transform

The above-mentioned problems of DFT and STFT can be minimized using the wavelet approach. In this approach, a window of some predefined frequency and amplitude is swiped across the entire signal to see where it closely

matches the signal. This window is called mother wavelet while its frequency is saved as scale a and position by b . The resultant cwt coefficients $X_w(a, b)$, contains the time-frequency information of the signal as shown by (14). The signal can be reconstructed using these coefficients by taking the inverse wavelet transform. The process is repeated several time to detect different frequency components at different times.

$$X_w(a, b) = \frac{1}{|a|^{1/2}} \int_{-\infty}^{\infty} x(t) \bar{\psi} \left(\frac{t-b}{a} \right) dt \quad (14)$$

The legibility of the frequency spectrum in either steady-state or transient regime depends upon the length of the signal. The slip of the motor defines the position of the faulty frequency components as described in the previous equations. During the transient interval, the slip is not constant but decreases with an increase in speed as the motor goes towards a steady-state regime. This change in the slip can develop some specific patterns in the time-frequency spectrum. Most of the time, this transient interval is so small that those patterns do not become visible. This fact becomes even worse when the motor operates at low load conditions. In this paper, this transient interval is extended by decreasing the supply voltage. By doing so, the inertia of the rotor can be used to control the transient time of the motor.

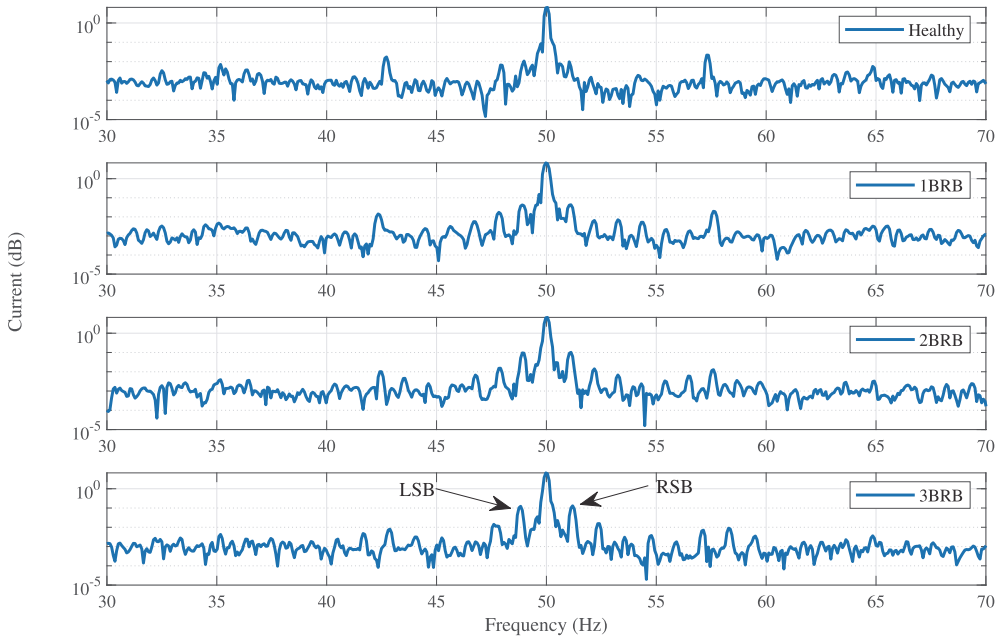


Fig. 2. The frequency spectrum from 30 Hz to 70 Hz showing the development of faulty frequency components.

III. PRACTICAL SETUP

The test rig consists of a motor under investigation attached with a loading machine, the three-phase variable transformer and data acquisition setup. The motor with specifications given in Table I, is tested with healthy and broken bar-based rotors. The bars are broken by drilling radial holes having a depth equal to the total rotor slot height. The motor phase currents are measured under transient intervals using the Dewetron transient recorder. The sampling frequency of the measured signal is 10000 Hz, which is enough for better resolution as the machine is grid fed. The test setup is shown

TABLE I
THE MACHINE SPECIFICATIONS.

Parameter	Symbol	Value
Number of poles	P	4
Number of phases	ϕ	3
Connection	-	Delta
Stator slots	N_s	36; Non-skewed
Rotor slots	N_r	28; skewed
Rated voltage	V	400V@50 Hz
Rated current	I	8.8A
Rated power	P_r	7.5 kW@50 Hz

in Fig. 1.

IV. RESULTS AND DISCUSSION

The frequency spectrum of stator current under healthy and broken rotor bars at rated load condition is shown in Figs. 2 and 3. The spectrum in Fig. 2 shows the evolution of left side band (LSB) and right-side band (RSB) harmonics. These harmonics are the function of slip and the results are based

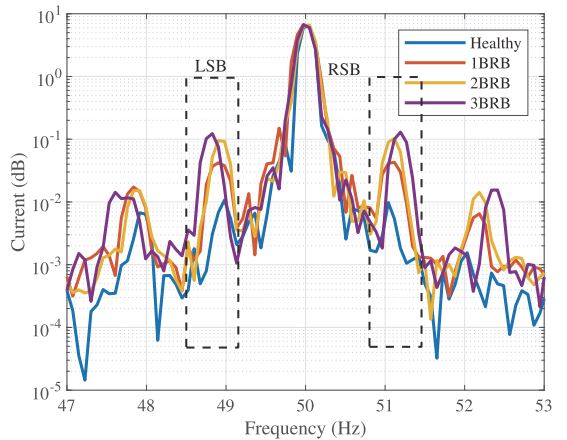


Fig. 3. The development of left side band (LSB) and right side band (RSB) frequencies with the increase in the number of broken bars.

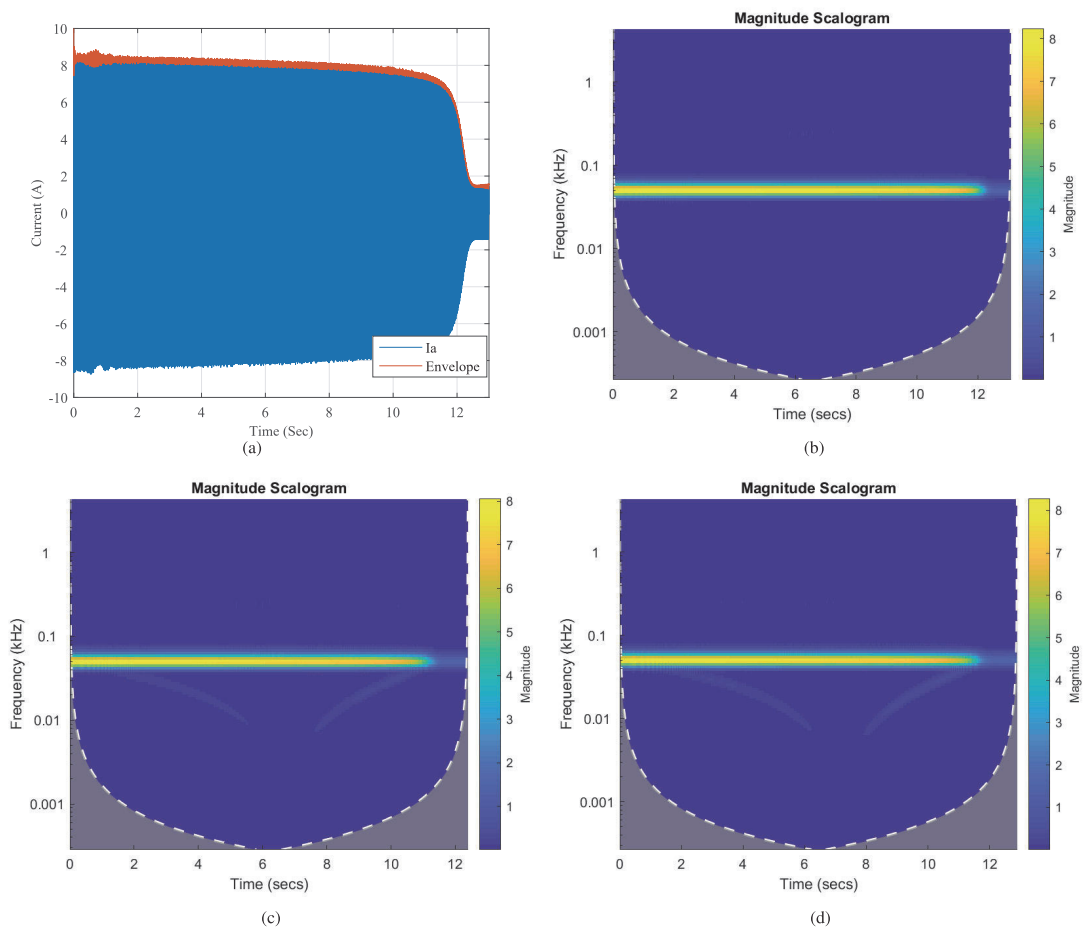


Fig. 4. (a) Motor's phase current and corresponding envelope under transient regime, (b) Time-frequency spectrum in healthy case, (c) Time-frequency spectrum in 1 broken bar case, (d) Time-frequency spectrum in 2 broken bars case.

on the measurements taken under rated load condition. It is evident that the side-band frequencies increase in amplitude with the increase in the number of broken bars. In addition, the side-band fault frequencies tend to shift slightly away from the fundamental component with the increase in the number of bars as shown in Fig.3. This is because with the increase in the number of broken bars the average generated torque decreased with a slight increase in slip. The legibility of these harmonics is very poor, and it is very difficult to segregate them from the rest of the harmonics as shown in Fig. 2. The severity of this problem increases with the decrease in load. As the load decreases, these harmonics start hiding under a strong fundamental component with a total disappearance at no-load condition. Moreover, the skewness in the rotor and stator slots affects their amplitude making them less detectable at the incipient stage. It is also important to mention that these harmonics also remain venerable when

the inverter feeds the motor. This effect can be in the form of a huge number of harmonics being fed by the inverter, which makes faulty frequencies even more difficult to be segregated. Moreover, the impact of the drive controller cannot be ignored. This impact is severed in the case of DTC controlled motors, where the controller of drive tries to eliminate the current harmonics to reduce torque ripples [9].

To avoid all those problems, the inspection of motor current under the transient regime shows promising results. In order to increase the transient time for better time-frequency resolution, the supply voltage can be reduced. Several experiments are performed at 15%, 25%, 50%, 75%, and 100% of nominal voltage without external load. By reducing the voltage the inertia of the motor's rotor acts as a load and increases the transient time. With the increase in the applied voltage, the motor takes less time to reach a steady-state inter-

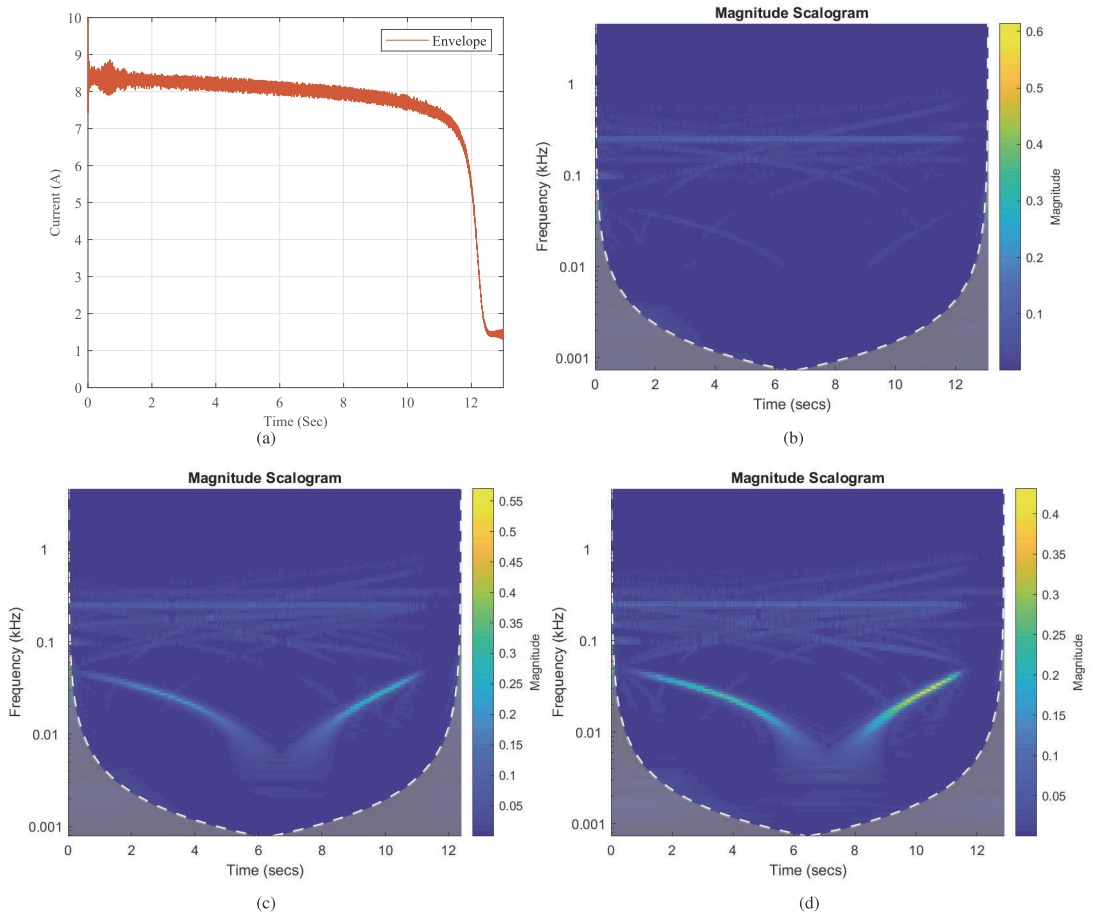


Fig. 5. (a) The envelope of motor's phase current in transient regime, (b) Time-frequency spectrum in healthy case with attenuated fundamental component, (c) Time-frequency spectrum in 1 broken bar case with attenuated fundamental component, (d) Time-frequency spectrum in 2 broken bars case with attenuated fundamental component.

val. Under the transient regime, the continuously decreasing slip moves the RHS and LHS frequency components towards fundamental components. This makes a V-shaped pattern whose width depends upon the transient time as shown in Fig. 4 where the supply voltage is 15% of the nominal voltage. This pattern is not well legible because the sideband frequencies are very small in amplitude as compared to the fundamental component. This pattern can be made very clear by attenuating the fundamental component as shown in Fig. 5. The infinite impulse response (IIR) bandstop filter is used to remove the fundamental component.

V. CONCLUSIONS

The broken rotor bars fault diagnostics by time-frequency analysis of motor current under transient period is investigated in this paper. The detection of fault frequencies in

the steady-state interval is very common in literature but possesses several difficulties. Since the sideband frequencies are the function of slip, they become very difficult to discover under low load conditions. The spectral leakage of the powerful supply components is very dangerous for the visibility of faulty components as they are very weak in amplitude. This spectral leakage is also the function of signal length, the sampling frequency and the type of the window used to compute FFT.

Moreover, the inclusion of a huge bandwidth of inverter fed frequencies makes the detection of faulty frequencies hazier. The impact of the drive controller to reduce the current ripples is another fact, which makes the fault diagnostic under a steady-state regime difficult.

These drawbacks can be resolved by investigating the health in the transient regime. The biggest drawback of the

transient interval is a minor time, which reduces the resolution of the spectrum. This transient time can be increased by reducing the applied voltage without any external load. By doing so the broken bars based v-shaped pattern can be seen with great accuracy. Moreover, the FFT based drawbacks are considerably reduced by using the wavelet approach. The legibility of the transient spectrum is further enhanced by attenuating the fundamental component with the help of an IIR filter.

The IIR bandstop filter has a sharp transition interval and low passband ripples having less impact on the remaining frequency components. The results are validated using the measurements taken from a laboratory-based test rig.

REFERENCES

- [1] G. Bossio, C. De Angelo, J. Bossio, C. Pezzani, and G. Garcia, "Separating Broken Rotor Bars and Load Oscillations on IM Fault Diagnosis Through the Instantaneous Active and Reactive Currents," *IEEE Transactions on Industrial Electronics*, vol. 56, no. 11, pp. 4571–4580, Nov. 2009.
- [2] A. Soualhi, G. Clerc, and H. Razik, "Detection and Diagnosis of Faults in Induction Motor Using an Improved Artificial Ant Clustering Technique," *IEEE Transactions on Industrial Electronics*, vol. 60, no. 9, pp. 4053–4062, Sep 2013.
- [3] B. Ayhan, H. Trussell, Mo-Yuen Chow, and Myung-Hyun Song, "On the Use of a Lower Sampling Rate for Broken Rotor Bar Detection With DTFT and AR-Based Spectrum Methods," *IEEE Transactions on Industrial Electronics*, vol. 55, no. 3, pp. 1421–1434, Mar 2008.
- [4] A. Khezzar, M. Kaikaa, M. El Kamel Oumaamar, M. Boucherma, and H. Razik, "On the Use of Slot Harmonics as a Potential Indicator of Rotor Bar Breakage in the Induction Machine," *IEEE Transactions on Industrial Electronics*, vol. 56, no. 11, pp. 4592–4605, Nov. 2009.
- [5] M. Malekpour, B. T. Phung, and E. Ambikairajah, "Stator current envelope extraction for analysis of broken rotor bar in induction motors," in *2017 IEEE 11th International Symposium on Diagnostics for Electrical Machines, Power Electronics and Drives (SDEMPED)*. IEEE, Aug 2017, pp. 240–246.
- [6] A. Belahcen, J. Martinez, and T. Vaimann, "Comprehensive computations of the response of faulty cage induction machines," in *2014 International Conference on Electrical Machines (ICEM)*. IEEE, Sep 2014, pp. 1510–1515.
- [7] S. Nandi, H. Toliyat, and X. Li, "Condition Monitoring and Fault Diagnosis of Electrical Motors—A Review," *IEEE Transactions on Energy Conversion*, vol. 20, no. 4, pp. 719–729, Dec. 2005.
- [8] B. Asad, T. Vaimann, A. Kallaste, and A. Belahcen, "Harmonic Spectrum Analysis of Induction Motor With Broken Rotor Bar Fault," in *2018 IEEE 59th International Scientific Conference on Power and Electrical Engineering of Riga Technical University (RTUCON)*. IEEE, Nov. 2018, pp. 1–7.
- [9] B. Asad, T. Vaimann, A. Belahcen, A. Kallaste, A. Rassõlkin, and M. N. Iqbal, "Broken rotor bar fault detection of the grid and inverter-fed induction motor by effective attenuation of the fundamental component," *IET Electric Power Applications*, Jul. 2019.
- [10] R. Puche-Panadero, M. Pineda-Sanchez, M. Riera-Guasp, J. Roger-Folch, E. Hurtado-Perez, and J. Perez-Cruz, "Improved Resolution of the MCSA Method Via Hilbert Transform, Enabling the Diagnosis of Rotor Asymmetries at Very Low Slip," *IEEE Transactions on Energy Conversion*, vol. 24, no. 1, pp. 52–59, Mar. 2009.
- [11] M. Pineda-Sanchez, M. Riera-Guasp, J. A. Antonino-Daviu, J. Roger-Folch, J. Perez-Cruz, and R. Puche-Panadero, "Diagnosis of Induction Motor Faults in the Fractional Fourier Domain," *IEEE Transactions on Instrumentation and Measurement*, vol. 59, no. 8, pp. 2065–2075, Aug. 2010.
- [12] M. A. Moussa, M. Boucherma, and A. Khezzar, "A Detection Method for Induction Motor Bar Fault Using Sidelobes Leakage Phenomenon of the Sliding Discrete Fourier Transform," *IEEE Transactions on Power Electronics*, vol. 32, no. 7, pp. 5560–5572, Jul. 2017.
- [13] S. Kia, H. Henao, and G.-A. Capolino, "Diagnosis of Broken-Bar Fault in Induction Machines Using Discrete Wavelet Transform Without Slip Estimation," *IEEE Transactions on Industry Applications*, vol. 45, no. 4, pp. 1395–1404, Jul. 2009.
- [14] S. Singh and N. Kumar, "Detection of Bearing Faults in Mechanical Systems Using Stator Current Monitoring," *IEEE Transactions on Industrial Informatics*, vol. 13, no. 3, pp. 1341–1349, Jun. 2017.
- [15] M. Kang and J.-M. Kim, "Reliable Fault Diagnosis of Multiple Induction Motor Defects Using a 2-D Representation of Shannon Wavelets," *IEEE Transactions on Magnetics*, vol. 50, no. 10, pp. 1–13, Oct. 2014.
- [16] A. Bellini, F. Filippetti, G. Franceschini, C. Tassoni, and G. Kliman, "Quantitative evaluation of induction motor broken bars by means of electrical signature analysis," *IEEE Transactions on Industry Applications*, vol. 37, no. 5, pp. 1248–1255, 2001.
- [17] M. T. Heideman, D. H. Johnson, and C. S. Burrus, "Gauss and the history of the Fast Fourier Transform," *IEEE Acoustics, Speech, and Signal Processing Magazine*, vol. 1, no. October, pp. 14–21, 1984.

VI. BIOGRAPHIES

Bilal Asad was born in 1986 in Pakistan. He received his BSc in Electronics Engineering from The Islamia University of Bahawalpur and MSc in Electrical Engineering from University of Engineering and Technology (UET) Lahore, Pakistan in 2007 and 2011 respectively. Currently he is a PhD student in the Department of Electrical Power Engineering and Mechatronics, Tallinn University of Technology, Estonia. His area of interest includes design, modeling and fault diagnostics of electrical machines.

Toomas Vaimann (S'11-M'14) was born in Pärnu, Estonia, in 1984. He received his BSc, MSc and PhD degrees in Electrical Engineering from Tallinn University of Technology, Estonia in 2007, 2009 and 2014 respectively. He is currently a senior researcher in Tallinn University of Technology, Department of Electrical Power Engineering and Mechatronics. He has been working in several companies as electrical engineer. He is member of IEEE, Estonian society of Moritz Hermann Jacobi and Estonian Society of Electrical Power Engineering.

Anouar Belahcen (M'13-SM'15) was born in Essaouira, Morocco, in 1963. He received the BSc degree in physics from the University Sidi Mohamed Ben Abdellah Fes, Morocco, in 1988 and the MSc (Tech.) and Doctor (Tech.) degrees from Helsinki University of Technology, Finland, in 1998 and 2004 respectively. From 2008 to 2013, he has been working as Adjunct Professor in the field of coupled problems and material modeling at Aalto University, Finland. Since 2011 he is Professor of electrical machines at Tallinn University of Technology, Estonia and in 2013 he became Professor of Energy and Power at Aalto University. His research interests are numerical modeling of electrical machines, especially magnetic material modeling, coupled magnetic and mechanical problems, magnetic forces and magnetostriction.

Ants Kallaste (M'13) was born in Pärnu, Estonia, in 1980. He received his BSc, MSc and PhD degrees in Electrical Engineering from Tallinn University of Technology, Estonia in 2004, 2006 and 2013 respectively. He is currently a senior researcher in Tallinn University of Technology, Department of Electrical Power Engineering and Mechatronics. He has been working in several companies as electrical engineer. His main research interests include permanent magnet machine design and wind turbines.

Anton Rassõlkin received Ph. D. degree in electric drives and power electronics from Tallinn University of Technology in 2014. His main research interests are in the field of electric drives and their control systems as well as in the fields of electrical machines and electric transportation. He works as a Research Scientist at the Department of Electrical Power Engineering and Mechatronics at Tallinn University of Technology, Department of Electrical Power Engineering and Mechatronics, Tallinn University of Technology, Ehitajate tee 5, 19086 Tallinn, Estonia.

Hamidreza Heidari was born in Zanjan, Iran, in 1989. He received his B.Sc. and M.Sc. degrees in electronics engineering from the university of Zanjan, Iran. He is currently working towards Ph.D. degree in electrical engineering from Tallinn university of technology. His research interests include analysis and control of electrical machines.

Publication IV

B. Asad, T. Vaimann, A. Belahcen, A. Kallaste, A. Rassõlkin, M. Naveed Iqbal. Modified Winding Function-based Model of Squirrel Cage Induction Motor for Fault Diagnostics. IET Electric Power Applications, vol. 14 (9), pp. 1722–1734, May 2020.

Modified winding function-based model of squirrel cage induction motor for fault diagnostics

ISSN 1751-8660

Received on 12th December 2019

Revised 9th April 2020

Accepted on 4th May 2020

E-First on 1st July 2020

doi: 10.1049/iet-epa.2019.1002

www.ietdl.org

Bilal Asad¹ ✉, Toomas Vaimann¹, Anouar Belahcen², Ants Kallaste¹, Anton Rassõlkin¹, Muhammad Naveed Iqbal¹

¹Department of Electrical Power Engineering and Mechatronics, Tallinn University of Technology, Ehitajate tee 5, Tallinn, Estonia

²Department of Electrical Engineering and Automation, Aalto University, 02150 Espoo, Finland

✉ E-mail: biasad@taltech.ee

Abstract: This study presents the modelling and simulation of a squirrel cage induction motor using a modified winding function-based method. The aim of the model is to compute the motor's performance parameters, which are similar to the results obtained using the finite element method (FEM) with a considerably reduced simulation time. This fact can make this model good for iterations based optimisation and fault diagnostic algorithms. For this purpose, the actual stator and rotor winding functions and the air gap, with the inclusion of rotor and stator slots, are defined as conditional expressions. The resistances and various inductances are calculated with stepping rotor, saved in lookup tables and are used to calculate speed, torque, and currents of the motor. For the validation of the model, the frequency spectrum of stator current is compared with the one calculated using FEM and measurements taken in the laboratory setup under healthy and broken rotor bar conditions.

1 Introduction

The fault diagnostics of electrical machines at the incipient stage is very important, in order to avoid any catastrophic situation, resulting in complete process failure and huge economic loss. Among various fault diagnostic techniques, such as infrared detection, electromagnetic field inference, acoustics and vibration analysis, motor current signature analysis (MCSA) is very popular because of its simplicity and versatility. It can be used for the estimation of design parameters by considering it in model-dependent techniques such as inverse problem theory. Since electrical machines are complex systems where several parameters are associated with each other, the detection of exact cause of the fault is a challenging task. A lot of work has already been done in the field of fault diagnostics, such as MCSA, which is the most cited in the literature. However, due to the inevitable inclusion of complex control algorithms and inverters, these techniques become hazy [1–3]. The conventional techniques become worst when there are multiple faults in the machine. This makes the segregation of faults a challenging task, e.g. the cooling ducts in the rotor can imitate as broken rotor bars [4]. The effective utilisation of the model for parameters estimation for control and fault diagnostic can be a promising technique that can avoid the above-mentioned problems. The drawbacks of the model's complexity and required computational power is not a big issue, as the world is moving towards Industry 4.0 and cloud computation, which provides unlimited resources. In the field of inverse problem theory, hardware-in-the-loop or parameters estimation, the motor's global parameters, such as speed, torque or currents, can be used in an inverse manner to estimate the design parameters, such as inductances and resistances, etc. [5]. The comparison of those estimated parameters with the design parameters can lead to the health estimation of the machine. Hence, the model of the motor should be a good replica of the actual system that is able to simulate various faults in the motor with minimal simulation time. The more accurate the model of the motor is, the better the estimation of the parameters would be. Since most of the faults are degenerative in nature, the model should be fast and sensitive enough to detect the faults at a very early stage. In other words, it should have as few approximations as possible. The motor modelling techniques available in the literature can be divided into

two main streams: analytical and numerical. The most common techniques along with their attributes are summarised in Table 1.

The two-axis theory (d - q)-based models are very common in literature. The detailed dynamic analysis of wound rotor induction motor under balanced and unbalanced conditions in various reference frames can be found in [6], while a similar kind of analysis without the unbalances is available in [7]. The authors in [8] used the d - q model in conjunction with coupled magnetic circuit theory in order to consider the actual non-sinusoidal distribution of the rotor winding. The d - q modelling-based analysis of broken rotor bars is presented in [9, 10], where the authors transformed the rotor d - q currents into n -loop currents in each iteration.

The authors in [11] used d - q modelling to represent an unbalanced three-phase motor having a stator open circuit, with an equivalent unbalanced two-phase motor to present a new fault-tolerant vector control method. The transient model for the analysis of stator turn faults is presented in [12]. These models are simple to understand, comprehensive, good for dynamic analysis and better for drive systems but they have various simplifications, which make them less attractive in the field of fault diagnostics. These simplifications include the sinusoidal distribution of stator and rotor windings. They can be converted to the actual windings but at the cost of increased complexity. The constant air gap by referring stator and rotor parameters on either side eliminates spatial harmonics, which are very important for fault diagnostics. This leads to constant inductances, eliminating their dependency on the rotor position and the non-linear nature of magnetic material. Most of the above-mentioned problems can be resolved by considering the multiple coupled circuit (MCC) theory, which allows the modelling of the unbalanced machine. The authors of [15] used winding function analysis (WFA) for modelling a three-phase squirrel cage induction motor (SQIM) with stator inter-turn short circuit fault. In [13], the authors used it to simulate SQIM with broken rotor bars. The analysis of various faults, such as stator phase disconnection, broken bars and broken end rings, is presented in [14], while the approach was used for the analysis of adjustable speed drive applications in [33, 34]. The authors of [35] used this technique to model a permanent magnet machine with a fractional slot concentrated winding. The air gap is considered as constant in the majority of WFA-based papers, which do not allow

to simulate eccentricity faults and the rotor slot harmonics are potentially ignored. Moreover, the uniform air gap makes it difficult to deal with material non-linearities. These problems can be solved by using the modified WFA (MWFA) method, where the slot openings of the stator and rotor can be considered by making the air gap as a function of the stator and rotor position. The authors in [36] extended the WFA-based method to simulate electrical machines with a non-uniform air gap. The use of the MWFA to model the stator and rotor slot effects for speed sensorless drive systems is presented in [37]. The static and dynamic eccentricities are presented in [16, 17] respectively. Unlike [37], where the air gap permeance is approximated by cosine series functions, [38] used the actual stator and rotor slot opening functions and a medium magnetic equipotential surface to simulate the machine. By doing so, the authors obtained results very close to the ones obtained from finite element method (FEM). The simulation time was further reduced by exploiting the symmetry of the rotor cage, which is not true in case of faulty machines. The analytical models show their limitations, while dealing with complex geometries, material properties and non-linearities, etc. These problems can leave them unsuitable for fault diagnostics, making some advanced techniques inevitable. The FEM has been extensively used in literature to tackle the mentioned problems. The authors in [39] used FEM to model an induction machine with the inclusion of eddy current and hysteresis in steel laminations. The magnetic field analysis of induction motors with cooling ducts is presented in [40]. The authors of [41] used this technique to study the vibrations in an induction motor with a 2D magnetic solution and coupled with a 3D mechanical model of the stator, to reduce the complexity. For the same purpose, the authors of [42]

used a quasi 3D FEM to compute the magnetic forces on stator end windings of an induction machine. Although the FEM-based models are very close approximations of the actual systems they present a high level of complexity and thus unaffordable computation time, especially in real-time applications. Since under faulty condition the motor becomes unsymmetrical, the solution of the complete geometry is necessary, causing an extensive increase in the number of mesh elements. Although modern-day computers are powerful, still the FEM-based models require considerable time for simulation, which makes them unsuitable for the use in model-dependent diagnostic algorithms.

In this study, a detailed analytical model of a SQIM using MWFA is presented with the following attractive features:

- Unlike most of the authors who have defined first strong harmonics in the form of Fourier sum, which makes the spectrum bandwidth limited. In the proposed model, all winding and air gap functions are defined as notational or conditional expressions. This approach makes the model independent of the selective number of frequency components in the flux density and ensures the contribution of complete spectrum.
- The air gap is made as a function of rotor and stator slot openings, which includes the spatial harmonics.
- The inclusion of rotor slot harmonics makes the model suitable for sensor-less speed drive systems.
- The model is so generic that almost all kinds of faults such as broken rotor bars, static and dynamic eccentricity and stator short circuits can be simulated. However, in this study, the broken bars are discussed.

Table 1 Common modelling techniques with corresponding attributes

Technique	Variants	Faults and applications	Attributes
<i>D</i> – <i>Q</i> modelling	<ul style="list-style-type: none"> • <i>d</i>–<i>q</i> • modified <i>d</i>–<i>q</i> 	<ul style="list-style-type: none"> • drives • dynamic analysis [6–8] • broken rotor bars [9, 10] • broken end rings [9, 10] • stator open circuit [11] • stator short circuit [12] 	<p>pros:</p> <ul style="list-style-type: none"> • simple • comprehensive • provides good equations for parameters estimation • good for control and drives <p>cons:</p> <ul style="list-style-type: none"> • negligible saturation • uniform air gap • sinusoidal stator winding • no inter-bar currents • no spatial harmonics • no eccentricity faults • no skin effects • difficult to deal with asymmetries, which are inevitable with the fault
MCC	<ul style="list-style-type: none"> • WFA • MWFA • extended MWFA 	<ul style="list-style-type: none"> • broken rotor bars [13] • broken end rings • stator open circuit [14] • stator short circuit [15] • dynamic eccentricity [16] • static eccentricity [17] • corroded rotor bars • bearing faults 	<p>pros:</p> <ul style="list-style-type: none"> • non-uniform air gap • practical winding functions • saturation can be defined analytically • various kind of faults can be simulated • low computation time as compared to FEM • a very good tradeoff between complexity and accuracy <p>cons:</p> <ul style="list-style-type: none"> • some geometrical constraints are difficult to handle, such as cooling ducts in stator or rotor
magnetic coupling	• magnetic reluctance method	<ul style="list-style-type: none"> • broken rotor bars [18] • broken end rings [19] • stator open circuit • stator short circuit [18] • dynamic eccentricity [20] • static eccentricity [20] 	<p>pros:</p> <ul style="list-style-type: none"> • can include spatial dependencies • computationally less intense than FEM but more than MCC • it can include geometry, material parameters, and winding distribution <p>cons:</p> <ul style="list-style-type: none"> • since all slots need to be modelled and the faulty machine is no longer symmetrical, the model becomes very complex

Technique	Variants	Faults and applications	Attributes
others analytical	<ul style="list-style-type: none"> • generalised harmonic analysis [21–23] • concordia transformation [24] • voltage behind reactance [25] • convolution based [26] 	<ul style="list-style-type: none"> • winding faults [16, 17] • losses and torque pulsation [23] • stator short circuit and broken rotor bars [24, 25] • broken rotor bars [26] 	<p>pros:</p> <ul style="list-style-type: none"> • concordia transformation reduces the number of state variables. • the convolution-based method is fast and allows to handle various non-ideal parameters <p>cons:</p> <ul style="list-style-type: none"> • the generalised harmonic analysis limits the number of harmonics taken into consideration • inclusion of non-uniform air gap is not straightforward in two-axis theory-based models • non-linearities will increase the complexity of analytical equations in two-axis theory-based models • concordia transform inherits the problems of d-q modelling • convolution theorem inherits the drawbacks of FFT whilst the air gap is taken as constant <p>pros:</p> <ul style="list-style-type: none"> • complex geometries can be considered • non-linearities, such as saturation, skinning effect, and non-idealities can be considered • all kind of faults can be simulated the combination of FEM and analytical modelling can be a good choice <p>cons:</p> <ul style="list-style-type: none"> • the computational complexity is the biggest problem and becomes worst in case fault diagnostics where symmetry is no longer present. The problem becomes worst for 3D analysis. Unsuitable for hardware-in-the-loop environment and inverse problem theory
Finite element analysis	<ul style="list-style-type: none"> • static • time-stepping • quasi-static • 2D • 3D 	<ul style="list-style-type: none"> • broken rotor bars [27, 28] • broken end rings [28] • stator open circuit [29] • stator short circuit [30] • dynamic eccentricity [31] • static eccentricity [32] 	

- The very short simulation time as compared to that taken by FEM makes the model suitable for advanced model dependent diagnostic algorithms.
- The achieved results are compared with the ones from the FEM model and measurements taken from the practical setup.
- The model allows for the inclusion of magnetic saturation effects, which can be considered as a potential improvement.
- The division of the model into offline and online parts can further reduce the complexity by avoiding the unnecessary computations for various fault simulations.

This study is organised in the way that Section 2 presents the generalised mathematical model of the machine. The block diagram showing the implementation strategy is presented in Section 3. The impact of stator and rotor slots on the air gap permeance function is presented in Section 4, while the winding functions and calculation of various inductances are discussed in Section 5. Section 6 presents the simulation results, while the practical measurement setup and the validation of the results are presented in Sections 7 and 8, respectively. The conclusions are discussed in Section 9.

2 Mathematical model

According to magnetically coupled circuit model, the voltage equations of the stationary three-phase stator and rotating n -phase rotor can be described as:

$$V_s = I_s R_s + \frac{d}{dt} \phi_s \quad (1)$$

$$0 = I_r R_r + \frac{d}{dt} \phi_r \quad (2)$$

where V_s , I_s , I_r , R_s , R_r , ϕ_s and ϕ_r are vectors expressing voltage, current, resistance and flux of each stator phase and rotor bar. The stator and rotor fluxes can be represented as:

$$\phi_s = L_{ss} I_s + L_{sr} I_r \quad (3)$$

$$\phi_r = L_{rs} I_s + L_{rr} I_r = L_{sr}^T I_s + L_{rr} I_r \quad (4)$$

where L_{ss} , L_{sr} , L_{rs} and L_{rr} are the stator–stator, stator–rotor, rotor–stator, and rotor–rotor self and mutual inductance matrices described as follows:

$$L_{ss} = \begin{bmatrix} L_{aas} & L_{abs} & L_{acs} \\ L_{bas} & L_{bbs} & L_{bcs} \\ L_{cas} & L_{cbs} & L_{ccs} \end{bmatrix} \quad (5)$$

$$L_{sr} = \begin{bmatrix} L_{ar1} & L_{ar2} & \cdots & L_{ar_i} & \cdots & L_{ar_n} & L_{ar_e} \\ L_{br1} & L_{br2} & \cdots & L_{br_i} & \cdots & L_{br_n} & L_{br_e} \\ L_{cr1} & L_{cr2} & \cdots & L_{cr_i} & \cdots & L_{cr_n} & L_{cr_e} \end{bmatrix} \quad (6)$$

$$L_{rr} = \begin{bmatrix} L_{r1r1} & L_{r1r2} & \cdots & L_{r1r_i} & \cdots & L_{r1r_n} & L_{r1r_e} \\ L_{r2r1} & L_{r2r2} & \cdots & L_{r2r_i} & \cdots & L_{r2r_n} & L_{r2r_e} \\ \vdots & \vdots & \vdots & \vdots & \vdots & \vdots & \vdots \\ L_{r_i r1} & L_{r_i r2} & \cdots & L_{r_i r_i} & \cdots & L_{r_i r_n} & L_{r_i r_e} \\ \vdots & \vdots & \vdots & \vdots & \vdots & \vdots & \vdots \\ L_{rn r1} & L_{rn r2} & \cdots & L_{rn r_i} & \cdots & L_{rn r_n} & L_{rn r_e} \\ L_{re r1} & L_{re r2} & \cdots & L_{re r_i} & \cdots & L_{re r_n} & L_{re r_e} \end{bmatrix} \quad (7)$$

In the matrices, the elements with subscripts a , b , c , r and r_e represent stator's three phases, rotor bars and rotor end ring related entries, respectively (see (8)). Under the symmetrical condition,

$$R_{rr} = \begin{bmatrix} 2(R_b + r_c) & -R_b & 0 & 0 & \cdots & 0 & \cdots & 0 & -R_b & -r_c \\ -R_b & 2(R_b + r_c) & -R_b & 0 & \cdots & 0 & \cdots & 0 & 0 & -r_c \\ 0 & -R_b & 2(R_b + r_c) & -R_b & \cdots & 0 & \cdots & 0 & 0 & -r_c \\ \vdots & \vdots & \vdots & \vdots & \vdots & \vdots & \vdots & \vdots & \vdots & \vdots \\ 0 & 0 & 0 & 0 & \cdots & 0 & \cdots & 2(R_b + r_c) & -R_b & -r_c \\ -R_b & 0 & 0 & 0 & \cdots & 0 & \cdots & -R_b & 2(R_b + r_c) & -r_c \\ -r_c & -r_c & -r_c & -r_c & \cdots & -r_c & \cdots & -r_c & -r_c & n_b r_c \end{bmatrix} \quad (8)$$

the last rows and columns containing only end ring resistance and mutual inductances can be neglected, because the net current in the end ring is zero, but it can lead to a problem of singularities in the simulation, while taking the inverse of the matrices. Moreover, they can be used to simulate end ring related asymmetries and faults.

For the ease of implementation, all these matrices can be grouped together:

$$V_s = [v_{as} \quad v_{bs} \quad v_{cs}]^T \quad (9)$$

$$I_s = [i_{as} \quad i_{bs} \quad i_{cs}]^T \quad (10)$$

$$I_r = [i_{r1} \quad i_{r2} \quad \cdots \quad i_{rn} \quad i_{re}]^T \quad (11)$$

$$L = \begin{bmatrix} L_{ss} & L_{sr} \\ L_{rs} & L_{rr} \end{bmatrix} \quad (12)$$

Leading to the matrix equation:

$$\begin{bmatrix} V_s \\ 0 \end{bmatrix} = \begin{bmatrix} R_s & 0 \\ 0 & R_r \end{bmatrix} \begin{bmatrix} I_s \\ I_r \end{bmatrix} + \frac{d}{dt} \begin{bmatrix} L_{ss} & L_{sr} \\ L_{rs} & L_{rr} \end{bmatrix} \begin{bmatrix} I_s \\ I_r \end{bmatrix} \quad (13)$$

From where currents and torque are calculated as:

$$\begin{bmatrix} I_s \\ I_r \end{bmatrix} = \begin{bmatrix} L_{ss} & L_{sr} \\ L_{rs} & L_{rr} \end{bmatrix}^{-1} \int \left[\begin{bmatrix} V_s \\ 0 \end{bmatrix} - \begin{bmatrix} R_s & 0 \\ 0 & R_r \end{bmatrix} \begin{bmatrix} I_s \\ I_r \end{bmatrix} \right] dt \quad (14)$$

$$T_e = I_s^T \left(\frac{d}{d\theta} L_{sr} \right) I_r \quad (15)$$

In the matrices form:

$$T_e = \frac{1}{2} \left(\frac{p}{2} \right) \begin{bmatrix} I_s \\ I_r \end{bmatrix}^T \frac{d}{d\theta} \begin{bmatrix} L_{ss} & L_{sr} \\ L_{rs} & L_{rr} \end{bmatrix} \begin{bmatrix} I_s \\ I_r \end{bmatrix} \quad (16)$$

It is worth mentioning here that the derivatives of L_{ss} and L_{rr} are no longer zero as they are the functions of air gap which is changing with rotor position.

The rotor bar and stator phase resistances are calculated by using the formula:

$$R = \left(\frac{\rho l}{A} \right) \quad (17)$$

where ρ is the resistivity, A is the effective slot area and l is the slot length.

The per turn length (l_p) of stator coil is calculated by adding the length of the end winding (l_{ew}) with the effective length (l) of the machine.

$$l_{pt} = l + l_{ew} \quad (18)$$

The dynamic equation of the rotor is given by:

$$J \frac{d}{dt} \omega_m = T_e - T_L - B \omega_m \quad (19)$$

where B is the friction coefficient, ω_m is the rotor angular speed, J is the rotor's moment of inertia, T_e and T_L are the generated and load torques, respectively.

3 Block diagram and description

The implementation strategy can be divided into two steps: offline calculations (Matlab script) saved as 3D lookup tables and online calculations (Simulink), as presented in the block diagram shown in Fig. 1. In the offline calculations, the geometry and corresponding stator and rotor winding functions are considered as input parameters. The slots geometry is used to calculate the resistances matrices by considering the number of conductors, area of slot and filling factor, which is 0.60 in this case. The rotor and stator leakage inductances are calculated using analytical equations discussed in [43]. The stator end windings are compensated by increasing the per turn length as given in (18) and by including the end winding leakage inductance L_{ew} (0.34 mH) which is calculated using (37) in Appendix.

Since the inductances are the functions of the air gap, which changes with the change in the rotor position, the rotor's mechanical angle (2π) is divided into ($n \times Q_s \times n_b$) steps, where n is an integer while Q_s and n_b are the number of stator and rotor slots, respectively. All the parameters are calculated at each position of stepping rotor.

The calculated data at each rotor position corresponds to a 2D matrix as shown by (5)–(8). All those 2D matrices are stacked in a 3D lookup table, which are called as a function of rotor position and performance parameters, such as currents, fluxes, torque and speed, are calculated. The integration of the rotor speed gives the new rotor position, which is used to change the index of the lookup table to for the corresponding 2D matrix.

4 Air gap permeance function

The air gap permeance function $P(\theta, \alpha)$ can be defined as:

$$P(\theta, \alpha) = \frac{1}{g_s(\theta) + g_r(\theta, \alpha)} \quad (20)$$

where $g_s(\theta)$, $g_r(\theta, \alpha)$, $g_s(\theta) + g_r(\theta, \alpha)$ and $P(\theta, \alpha)$ are air gaps associated with the stator, rotor, equivalent and the inverse air gap function in stator frame of reference, respectively. Moreover, θ is the angle of stator from any fixed reference point and α is the rotor angle in stator reference frame.

The stator and rotor linked air gaps are calculated in the way that the centre of the machine's air gap is taken as a reference line. In this way, the total air gap can be divided into stator and rotor associated air gaps. The slot opening without any conductor of winding on the stator side is used to change the air gap as a function of the stator's mechanical angle. This change is in the form of increase in the air gap, equivalent to the height of the slot opening without winding. Similarly, rotor bar depth is used to change the rotor's associated air gap. Both air gaps are added together to get the equivalent air gap at each rotor position. These air gap functions for one stator and rotor slot can be defined as follows:

$$g_s(\theta) = \begin{cases} r_g + h_{11} & 0 \leq \theta \leq B_{11} \\ r_g & B_{11} < \theta \leq (B_{11} + B_{12}) \end{cases} \quad (21)$$

$$g_r(\theta, \alpha) = \begin{cases} r_g + h_{21} & 0 \leq \theta \leq B_{21} \\ r_g & B_{21} < \theta \leq (B_{11} + B_{r1}) \end{cases} \quad (22)$$

where B_{11} , B_{1t} , B_{21} , B_{rt} , h_{11} and h_{21} are the width of the stator slot opening, stator tooth tip, rotor slot opening, rotor tooth tip, stator slot depth without winding, and the rotor bar depth, respectively as given in Fig. 2. Fig. 3 shows the stator and rotor associated air gaps until (2π) electrical angle, which is equivalent to half of the mechanical geometry, since the machine is four-pole. The net air gap with its inverse function at a particular position is also shown in the figure, where the distinguished (extended) lines are representing the points where rotor and stator slots overlap with each other. r_g is the average air gap radius and can be calculated as

$$r = \frac{(D_s - D_r)}{2} \quad (23)$$

For a more accurate representation of radius, (23) can be modified as follows:

$$r_g(\theta, \alpha) = r + \frac{g_s(\theta) + g_r(\theta, \alpha)}{2} \quad (24)$$

5 Winding function and inductances calculation

The inductances are dependent on the air gap permeance $P(\theta, \alpha)$, which is not a constant but a function of stator and rotor slot openings as described in (20)–(22). The winding function can be described as [37]:

$$N_i(\theta) = \left(n_i(\theta) - \frac{\langle P n_i \rangle}{\langle P \rangle} \right) \quad (25)$$

where n_i , N_i and P are the turn function, winding function and the air gap permeance function, respectively. For a p pole machine, the

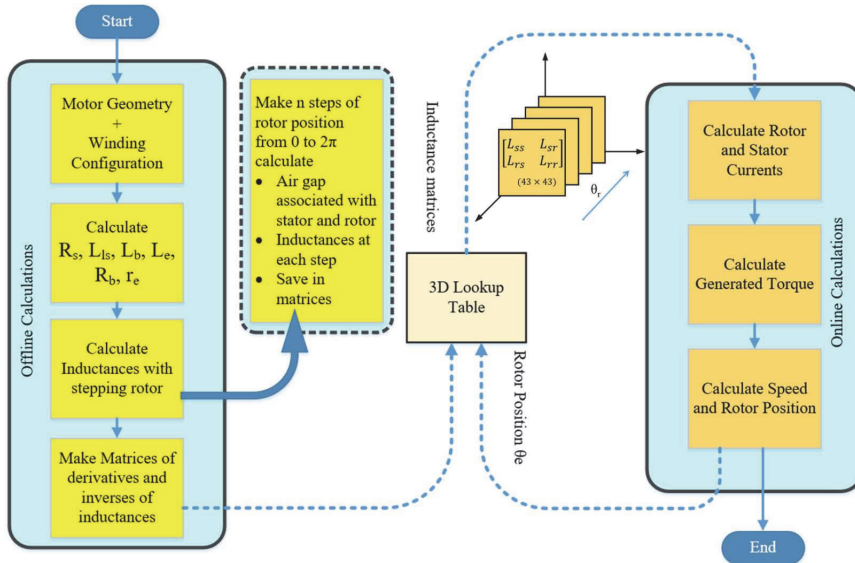


Fig. 1 Flowchart diagram of modelling and simulation

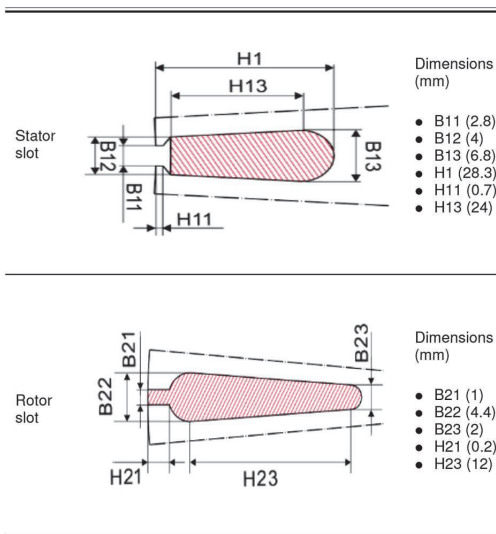


Fig. 2 Slots dimensions of the machine under investigation

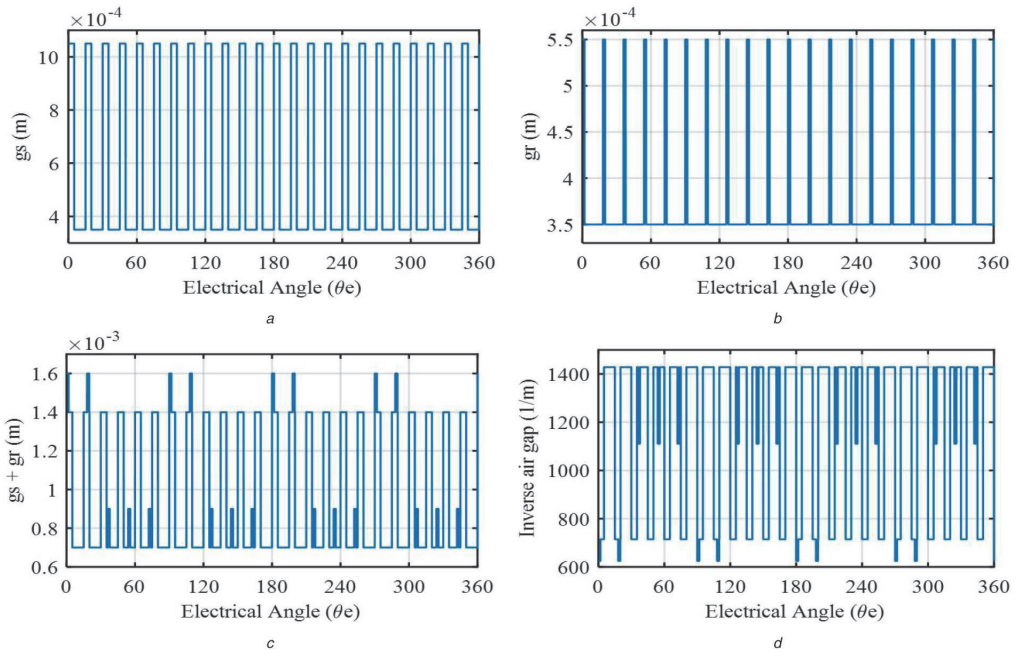


Fig. 3 Air gap function of

- (a) Stator (g_s),
- (b) Rotor (g_r),
- (c) Net equivalent ($g_s + g_r$),
- (d) Inverse air gap function at some specific rotor position

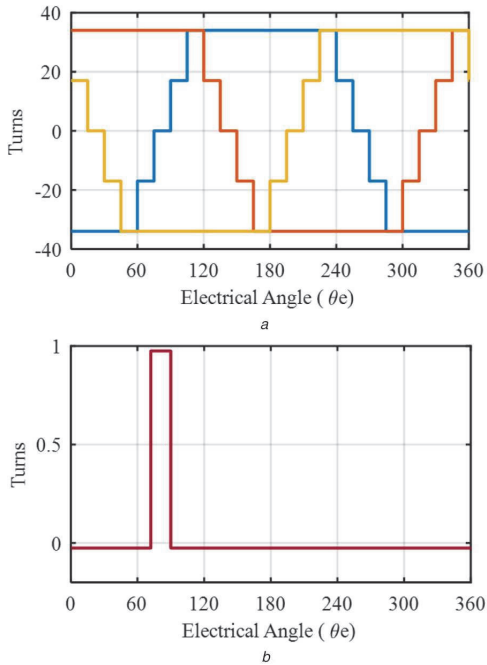


Fig. 4 Winding functions

- (a) Three phase stator,
- (b) One loop of rotor

average or mean value of any function $f(\theta_e)$ can be calculated as shown below:

$$\langle f \rangle = \frac{1}{p\pi} \int_0^{p\pi} f(\theta_e) d\theta_e \quad (26)$$

The stator and rotor winding functions are shown in Fig. 4, which are calculated using conditional analytic expressions (38). Each stator slot contains 17 conductors with a coil pitch equivalent to 12 slots. The rotor winding function is calculated by considering one conductor per slot. The winding function based inductances, while considering constant radius, can be calculated using the following equation:

$$L_{ij}(\theta) = \mu_o r l \int_0^{2\pi} P(\theta, \alpha) N_i(\theta, \alpha) n_j(\theta, \alpha) d\theta \quad (27)$$

This equation can be written as a mean value function as in (26):

$$L_{ij}(\theta) = 2\pi\mu_o r l \langle P(\theta, \alpha) N_i(\theta, \alpha) n_j(\theta, \alpha) \rangle \quad (28)$$

or in the form of turn functions:

$$L_{ij}(\theta) = 2\pi\mu_o r l \left[\langle P(\theta, \alpha) n_i(\theta, \alpha) n_j(\theta, \alpha) \rangle - \frac{\langle P(\theta, \alpha) n_i(\theta, \alpha) \rangle \langle P(\theta, \alpha) n_j(\theta, \alpha) \rangle}{\langle P(\theta, \alpha) \rangle} \right] \quad (29)$$

If the average radius of air gap is considered as (24) then:

$$L_{ij}(\theta) = 2\pi\mu_o l \langle r_g(\theta, \alpha) P(\theta, \alpha) N_i(\theta, \alpha) n_j(\theta, \alpha) \rangle \quad (30)$$

Equation (30) describes that the inductances are the function of average air gap radius, air gap permeance function and winding functions and all of them depend upon the relative position of stator and rotor. Unlike most of the inductance equations in literature, the elimination of integrators with mean value function as in (30) (32–35) further reduces the complexity and increases the ease of its implementation. Various inductances, such as stator–

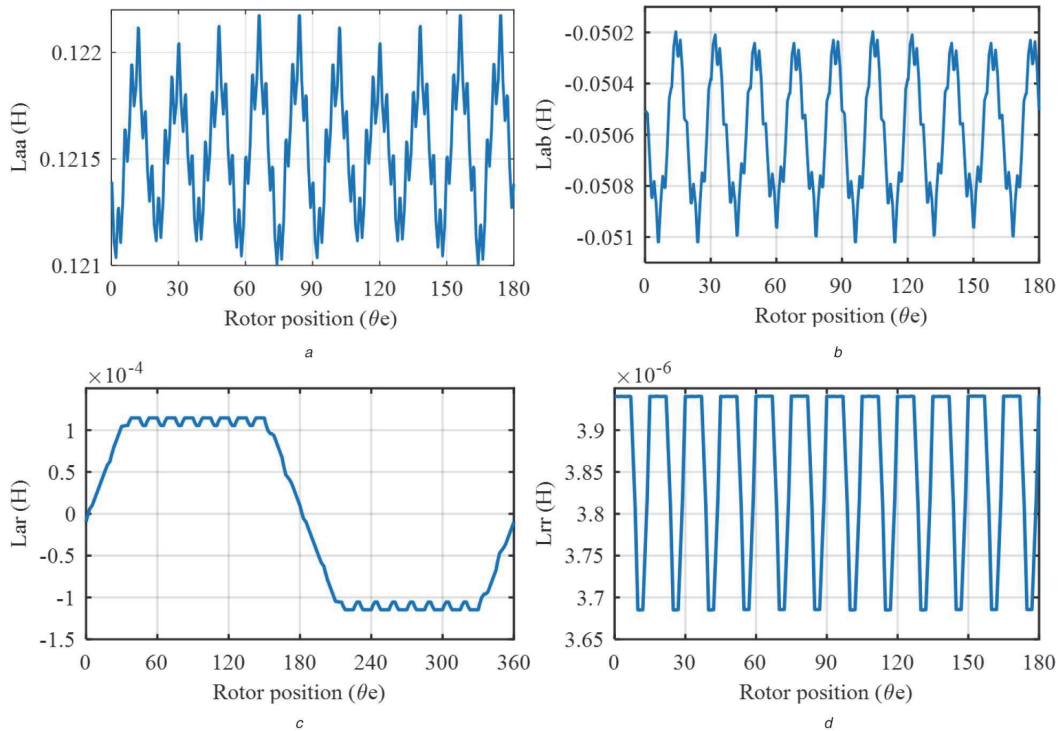


Fig. 5 Calculated inductances

- (a) Stator to stator self (L_{aa}),
 (b) Stator to stator mutual (L_{ab}),
 (c) Stator to rotor (L_{ar}),
 (d) Rotor to rotor (L_{rr}) with respect to the rotor position

stator self, stator–stator mutual, stator–rotor mutual and rotor–rotor self, are shown in Fig. 5.

All these inductances are calculated with a considerable number of rotor steps ($10 \times n_b \times Q_s$) to improve the resolution, where n_b and Q_s are 40 and 48, respectively, taken from machine under investigation. The corresponding derivatives of the inductances shown in Fig. 5 are presented in Fig. 6. The rate of change of inductances with respect to rotor position (derivative) is no longer zero. It oscillates across the zero lines and increases with the increase in the air gap variations. The calculated results for inductances, their derivatives and inverses are saved in matrices generating three 3D lookup tables each having a dimension of ($44 \times 44 \times 19200$). The resistances and leakage inductances are calculated based on geometry and number of turns on stator and rotor side as given in Fig. 2.

6 Simulation results

For the online simulation, the pre-calculated inductances and resistances are used to calculate various performance parameters of the motor. The 2D matrices are called as a function of rotor position from 3D lookup tables using their index value.

The broken bars are simulated by adding a series resistance of 1 M Ω in-circuit editor of FEM in a commercial software called Infolytica with a considerable number of mesh elements with the inclusion of additional resistance and reactance to compensate the end windings. The same is done by increasing the resistance of the bar related entries (31) in the resistance matrix of the proposed model, which is made using the equivalent rotor circuit model, as shown in Fig. 7. Since the inductances do not depend upon the resistance of the rotor bar, they do not need to be calculated again. The only change in the respective elements of the resistance matrix can simulate the broken bar case, which reduces the simulation

time. The rotor speed under healthy and broken rotor bar conditions is shown in Fig. 8.

Both FEM and analytical simulations are performed at rated load conditions with motor specifications given in Table 2 and the results are shown in the steady-state regime.

Both speed and torque waveforms, calculated using FEM and proposed analytical model, are in good agreement with each other. The visible oscillations under healthy conditions are because of the winding and the rotor slot harmonics. Under the broken rotor bar cases, the increase in the amplitude of speed ripples with the increase in the number of broken rotor bars is evident in both cases. This oscillation is responsible for generating the right side harmonic (RSH) in the current spectrum. The 2D FEM model is solved for 2 s, equivalent to 100 periods, with a time-stepping of 0.033 ms, corresponding to a sampling frequency of about 30 kHz. It takes about 0.7 s to calculate each step and about 12 h for a total of 60,000 time steps with the computer specifications given in Table 3. The proposed analytical model calculates all parameters in just 3 min including both offline and online calculations with the same sampling frequency. The FEM model needs to be simulated again each time for each broken rotor bar case. However, in the proposed model only the change in the resistance matrix is enough, which reduces the complexity considerably. Moreover, most of the faults can be simulated in the online portion without going through the offline calculations again. By exploiting these facts, the model speed can be increased considerably which is very crucial for diagnostic algorithms.

7 Practical measurement setup

For practical measurements, two similar machines are connected back to back on a common mechanical foundation as shown in Fig. 9. One motor acts as a loading machine, which is being fed with an industrial inverter for better accuracy and slip

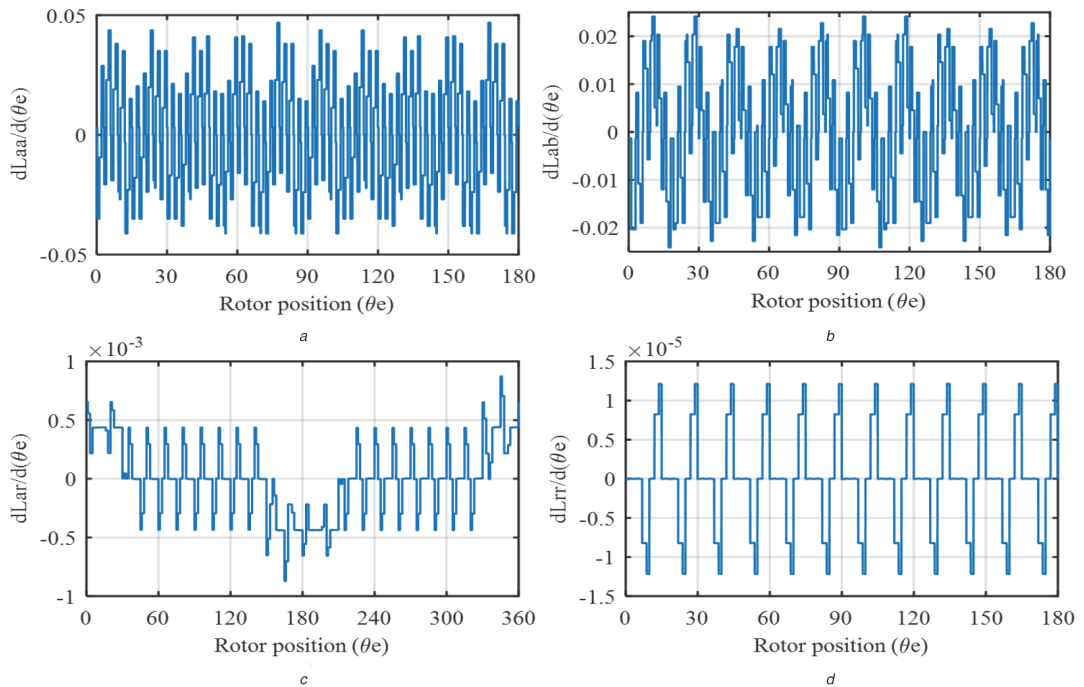


Fig. 6 Derivative of the
(a) Stator to stator self (L_{aa}),
(b) Stator to stator mutual (L_{ab}),
(c) Stator to rotor (L_{ar}),
(d) Rotor to rotor (L_{rr}) with respect to the rotor position

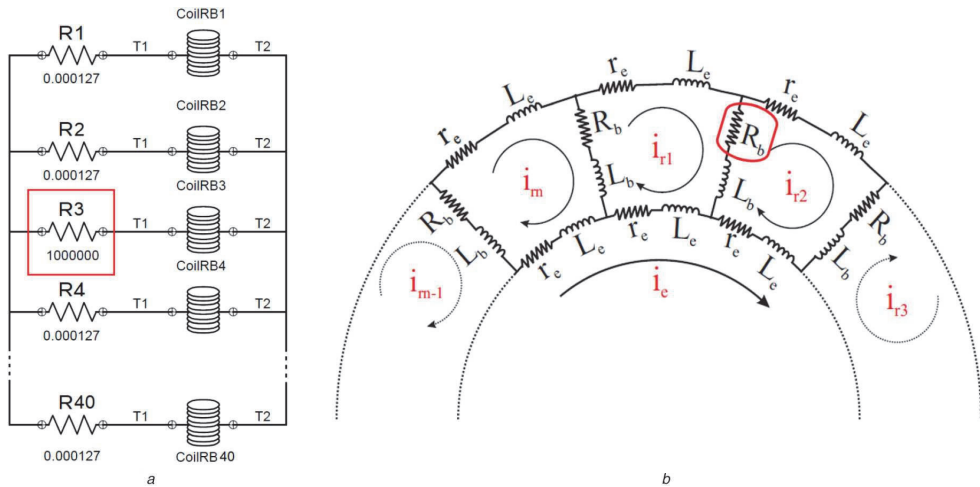


Fig. 7 Rotor schematic diagram with broken bar
(a) Infolytica circuit editor,
(b) Proposed model

controllability. The load side inverter is working under scalar mode to have less impact as in the case of direct torque control (DTC) mode. The motor under investigation is fed from the grid, while using the star connection scheme. The rotors with broken bars are prepared by drilling radial holes of equivalent length and width in them. The stator phase currents are measured with a sampling frequency of 10 kHz until 60 s for better frequency resolution. The measurements are taken under healthy, one, two and three broken bar cases.

8 Validation of results using the frequency spectrum

For validation, the frequency spectrum of the stator current simulated using the proposed model, FEM and measured from test rig, is compared. The harmonics visible in the motor current spectrum are caused by various reasons but the most prominent causes are: the winding distribution, the stator and rotor slot openings, asymmetry due to any fault, non-linear material characteristics and the supply. These harmonics give rise to the

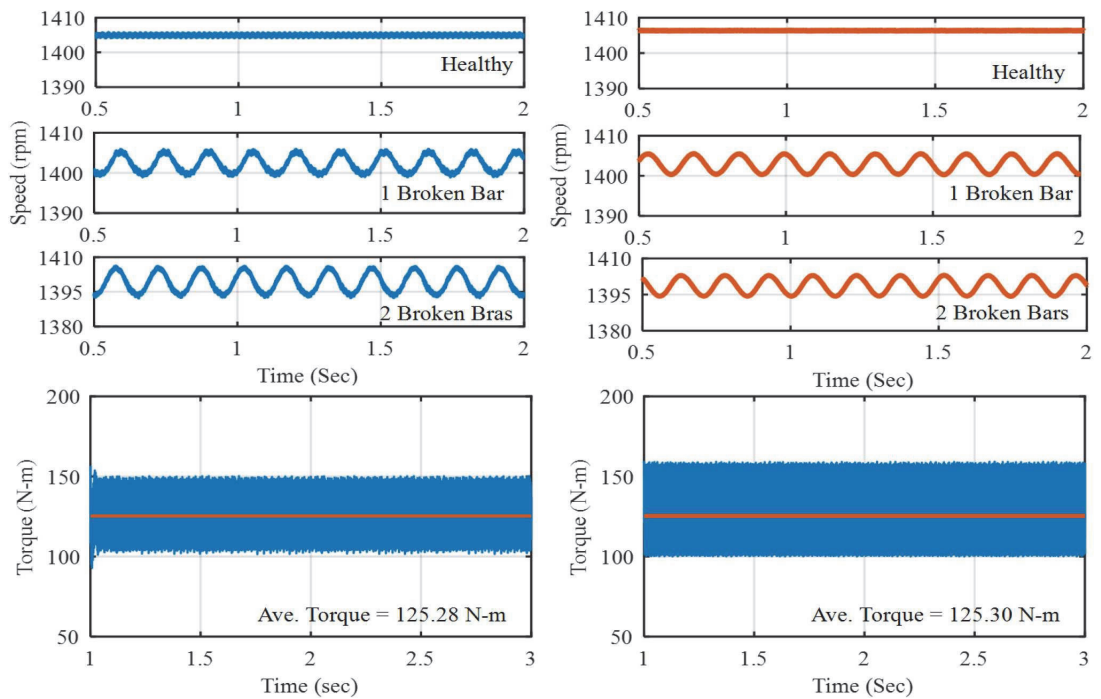


Fig. 8 Simulated speed and torque under healthy and broken rotor bar cases using FEM (left) and the proposed model (right)

Table 2 Motor specifications

Parameters	Symbol	Value
rated speed	Nr	1400 rpm @ 50 Hz
rated power	Pr	18 kW @ 50 Hz
connection	—	Star (Y)
power factor	$\cos\phi$	0.860
number of poles	P	4
number of rotor bars	Nb	40
number of stator slots	Qs	48

Table 3 Comparison of the simulation time

Model	Computer specs	Simulation time
MWFA	Intel(R) Core(TM) i7-7500 CPU	3 min
FEM		12 h (1-time step/0.72 s)

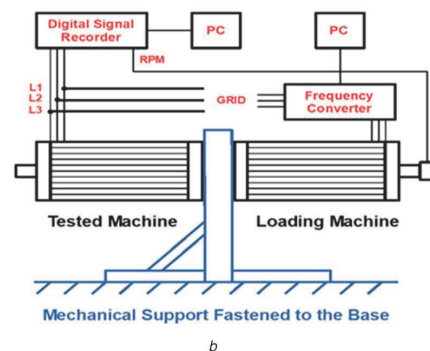
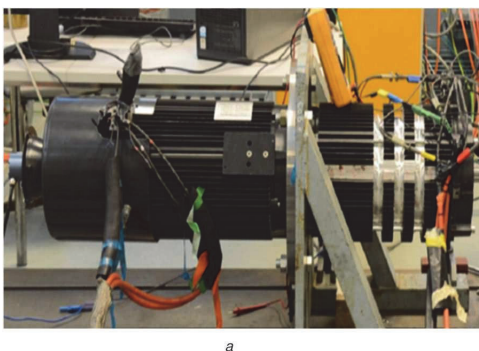


Fig. 9 The test-bench and data acquisition setup

(a) Laboratory setup for measurement,
(b) Block diagram of the test rig

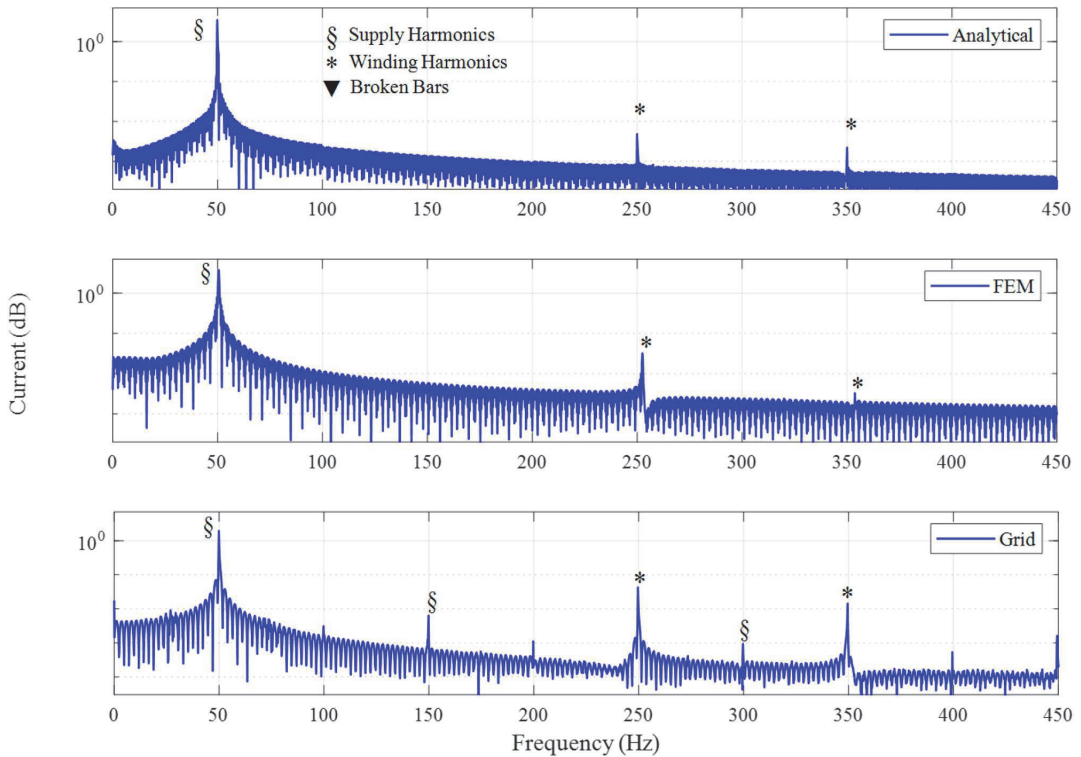


Fig. 10 Frequency spectrum (0–450 Hz) of the stator current using the proposed model, FEM and practical measurements from top to bottom in healthy and no-load cases

speed and torque ripples, increase eddy current and hysteresis losses and decrease efficiency. Since majority of the higher-order harmonics are slip dependent, they can be used constructively for sensor-less speed estimation at least under steady state regime. The harmonics until 450 Hz are presented in Fig. 10.

Since the winding configuration is stepped distributed, the odd multiples of fundamental components are clearly visible and are in good agreement with FEM and measurement-based results. In the case of experimental measurement based spectrum, some additional components are apparent because of the grid fed harmonics [3]. Similarly, the frequencies from 750 to 1500 Hz are presented in Fig. 11, where the winding harmonics at 850, 950, 1150 and 1250 Hz are evident in case of all analytical, FEM and practical measurements. These frequencies are present mainly because of the rotor slot harmonics, also called principal slot harmonics (PSHs).

Since these results are at no load under healthy conditions, all components are at odd multiples of fundamental frequency and tend to move with the change in load. The development of the left side harmonic (LSH) at 43.4 Hz and the RSH at 53.5 Hz is due to broken rotor bars at rated load conditions, as presented in Fig. 12. The fault-based frequency components can be defined using the (36) in Appendix.

In case of FEM, the RSH is absent since the measurements are based on a 2D model, where the effect of speed ripples is neglected. Similarly, the frequency spectrum related with principle slot harmonics at rated load and broken rotor bar conditions is shown in Figs. 13 and 14. The comparison of frequency spectra from the perspective of fault diagnostic reveals that the utilisation of higher-order harmonics can be a better choice for the condition monitoring of the machine.

This is because of the fact that the fundamental component, being the strongest, has the largest spectral leakage as compared to the higher-order slotting harmonics. This means that under low-speed conditions the RSH and LSH are more likely to be buried under the fundamental component. This impact is small in case of

PSH, which makes the model more suitable for fault diagnostic algorithms. The frequency spectra are studied using simple discrete time Fourier transform with a sampling frequency of 30 kHz. The spectral leakage is reduced by exploiting the benefits of Hamming window.

9 Conclusions

In this study, a detailed time-stepping analytical model of a SQIM using MWFA is presented, with following attractive features:

Unlike most of the papers cited previously, where only low order harmonics are taken into account in the form of Fourier summation of certain sinusoids having specific frequency and amplitude, the actual stator and rotor winding functions are defined in the form of conditional analytical expressions. This approach makes the model independent of the selective number of frequency components and do not limit the spectrum bandwidth.

The air gap is made as a function of rotor and stator slot openings, which includes the spatial harmonics. Moreover, the inclusion of the air gap as a function of stator and rotor angles, makes the model suitable for the implementation of air gap related faults, such as eccentricity.

The inclusion of rotor slot harmonics makes the model suitable for sensor-less speed drive systems. The fact that these harmonics have less spectral leakage as compared to the fundamental component, makes them a potential candidate for fault detection, even under fewer load conditions.

The model is so generic that most of the fault types, such as broken rotor bars, static and dynamic eccentricity, and stator short circuits, can be simulated.

The very small simulation time, as compared to that used by FEM, makes the model suitable for advanced diagnostic algorithms, such as iterations based estimation of design parameters, hardware-in-the-loop, inverse problem theory and other model-based diagnostic procedures.

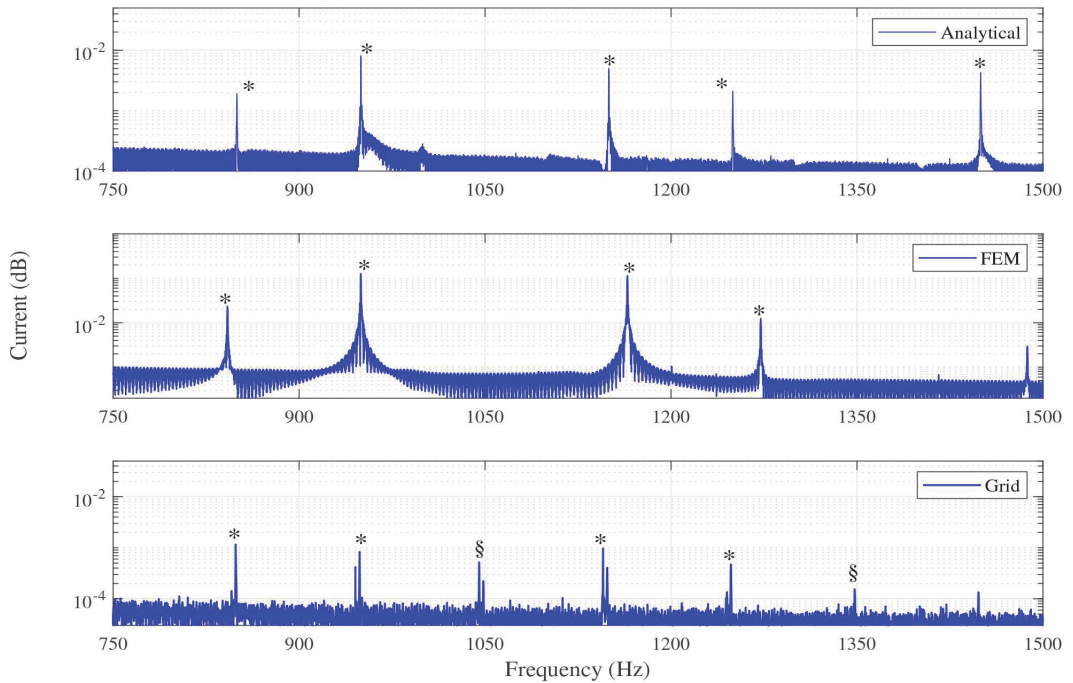


Fig. 11 Frequency spectrum (750–1500 Hz) of the stator current using the proposed model, FEM and practical measurements from top to bottom in healthy and no-load cases

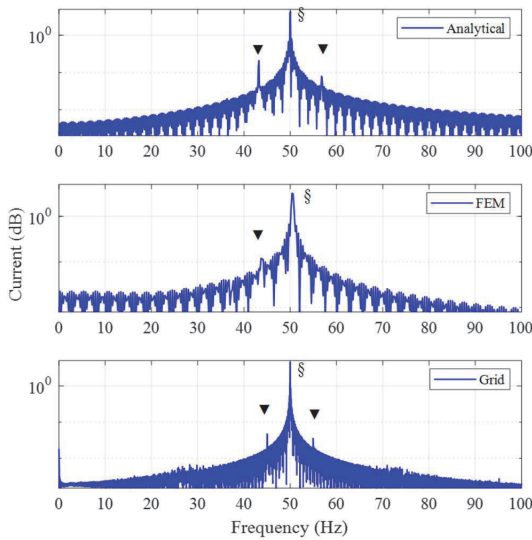


Fig. 12 Frequency spectrum (0–100 Hz) representing LSH and RSH under broken rotor bar at rated load condition

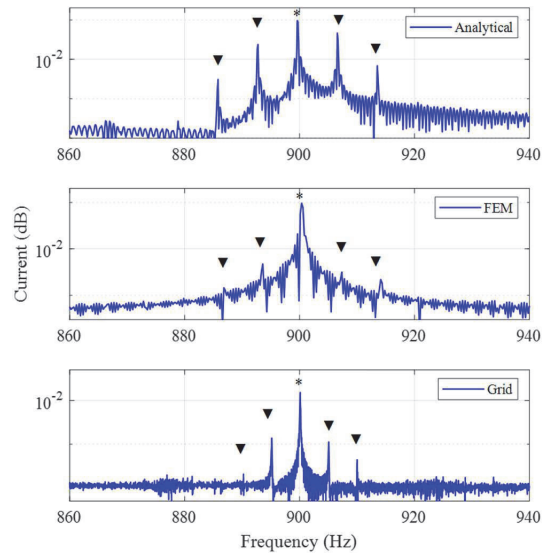


Fig. 13 PSH with subsequent broken bar frequencies showing less spectral leakage as compared to the fundamental component

The model is also suitable for the iterative optimisation of various design parameters, such as winding functions, slot openings, and air gap, etc. The achieved results are in good agreement with the ones taken from the FEM model and laboratory measurements.

The separate modelling and simulation parts can further reduce the complexity and calculation time in the way that once the inductances are calculated, almost all kind of faults can be simulated by making corresponding changes in them.

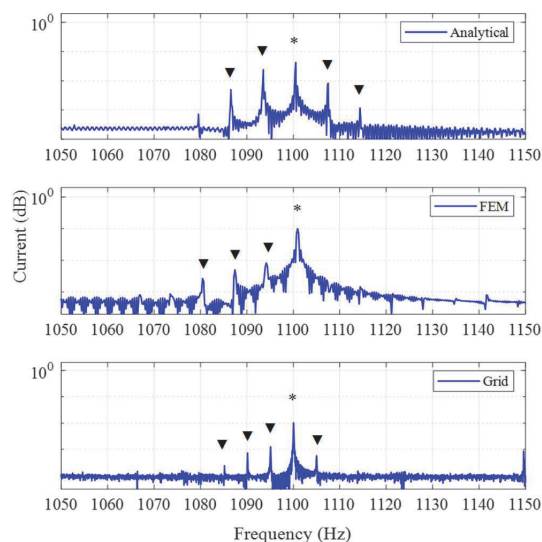


Fig. 14 Higher order spatial harmonics with broken rotor bar-based frequencies

10 References

- [1] Wang, T., Liu, H., Zhao, L., *et al.*: 'Quantitative broken rotor bar fault detection for closed-loop controlled induction motors', *IET Electr. Power Appl.*, 2016, **10**, (5), pp. 403–410
- [2] Hou, Z., Huang, J., Liu, H., *et al.*: 'Diagnosis of broken rotor bar fault in open- and closed-loop controlled wye-connected induction motors using zero-sequence voltage', *IET Electr. Power Appl.*, 2017, **11**, (7), pp. 1214–1223
- [3] Asad, B., Vaimann, T., Belahcen, A., *et al.*: 'Broken rotor bar fault detection of the grid and inverter-fed induction motor by effective attenuation of the fundamental component', *IET Electr. Power Appl.*, 2019, **13**, pp. 2005–2014
- [4] Park, Y., Yang, C., Kim, J., *et al.*: 'Stray flux monitoring for reliable detection of rotor faults under the influence of rotor axial air ducts', *IEEE Trans. Ind. Electron.*, 2019, **66**, (10), pp. 7561–7570
- [5] Toliyat, H.A., Levi, E., Raina, M.: 'A review of RFO induction motor parameter estimation techniques', *IEEE Trans. Energy Convers.*, 2003, **18**, (2), pp. 271–283
- [6] Krause, P.C., Thomas, C.H.: 'Simulation of symmetrical induction machinery', *IEEE Trans. Power Appar. Syst.*, 1965, **84**, (11), pp. 1038–1053
- [7] Lee, R.J., Pillay, P., Harley, R.G.: 'D-Q reference frames for the simulation of induction motors', *Electr. Power Syst. Res.*, 1984, **8**, (1), pp. 15–26
- [8] Munoz, A.R., Lipo, T.A.: 'Complex vector model of the squirrel-cage induction machine including instantaneous rotor bar currents', *IEEE Trans. Ind. Appl.*, 1999, **35**, (6), pp. 1332–1340
- [9] Cunha, C.C.M., Varejaio, V.B.S., Filho, B.J.C.: 'Simple model for squirrel cage induction machine with rotor asymmetries and its validation through experimental tests on a special motor'. 2008 34th Annual Conf. of IEEE Industrial Electronics, Orlando, FL, USA, 2008, pp. 1385–1390
- [10] Cunha, C.C.M., Lyra, R.O.C., Filho, B.: 'Simulation and analysis of induction machines with rotor asymmetries', *IEEE Trans. Ind. Appl.*, 2005, **41**, (1), pp. 18–24
- [11] Jannati, M., Idris, N.R.N., Salam, Z.: 'A new method for modeling and vector control of unbalanced induction motors'. 2012 IEEE Energy Conversion Congress and Exposition (ECCE), Raleigh, NC, USA, 2012, pp. 3625–3632
- [12] Patel, D.C., Chandorkar, M.C.: 'Transient modeling and analysis of induction motors with position effects in stator turn faults'. 2010 IEEE Int. Conf. on Industrial Technology, Vina del Mar, Chile, 2010, pp. 1251–1256
- [13] Milimonfared, J., Kelk, H.M., Nandi, S., *et al.*: 'A novel approach for broken-rotor-bar detection in cage induction motors', *IEEE Trans. Ind. Appl.*, 1999, **35**, (5), pp. 1000–1006
- [14] Toliyat, H.A., Lipo, T.A.: 'Transient analysis of cage induction machines under stator, rotor bar and end ring faults', *IEEE Trans. Energy Convers.*, 1995, **10**, (27), pp. 241–247
- [15] Joksimovic, G.M., Penman, J.: 'The detection of inter-turn short circuits in the stator windings of operating motors', *IEEE Trans. Ind. Electron.*, 2000, **47**, (5), pp. 1078–1084
- [16] Faiz, J., Ojaghi, M.: 'Unified winding function approach for dynamic simulation of different kinds of eccentricity faults in cage induction machines', *IET Electr. Power Appl.*, 2009, **3**, (5), pp. 461–470
- [17] Toliyat, H.A., Arefeen, M.S., Parlos, A.G.: 'A method for dynamic simulation of air-gap eccentricity in induction machines', *IEEE Trans. Ind. Appl.*, 1996, **32**, (4), pp. 910–918
- [18] Sizov, G.Y., Yeh, C.-C., Demerdash, N.A.O.: 'Magnetic equivalent circuit modeling of induction machines under stator and rotor fault conditions'. 2009 IEEE Int. Electric Machines and Drives Conf., Miami, FL, USA, 2009, pp. 119–124

- [19] Sudhoff, S.D., Kuhn, B.T., Corzine, K.A., *et al.*: 'Magnetic equivalent circuit modeling of induction motors', *IEEE Trans. Energy Convers.*, 2007, **22**, (2), pp. 259–270
- [20] Mahyob, A., Elmactar, M.Y.O., Reghem, P., *et al.*: 'Induction machine modeling using permeance network method for dynamic simulation of air-gap eccentricity'. 2007 European Conf. on Power Electronics and Applications, Aalborg, Denmark, 2007, pp. 1–9
- [21] Apsley, J., Williamson, S.: 'Analysis of multiphase induction machines with winding faults', *IEEE Trans. Ind. Appl.*, 2006, **42**, (2), pp. 465–472
- [22] Williamson, S., Laithwaite, E.R.: 'Generalised harmonic analysis for the steady-state performance of sinusoidally-excited cage induction motors', *IEE Proc. B, Electr. Power Appl.*, 1985, **132**, (3), pp. 157–163
- [23] Williamson, S., Smith, S.: 'Pulsating torque and losses in multiphase induction machines'. IEEE Industry Applications Conf. 36th IAS Annual Meeting (Cat. No.01CH37248), Chicago, IL, USA, USA., 2001, vol. 2, pp. 1155–1162
- [24] Bachir, S., Tnani, S., Trigeassou, J.-C., *et al.*: 'Diagnosis by parameter estimation of stator and rotor faults occurring in induction machines', *IEEE Trans. Ind. Electron.*, 2006, **53**, (3), pp. 963–973
- [25] Wang, L., Jatskevich, J., Pekarek, S.D.: 'Modeling of induction machines using a voltage-behind-reactance formulation', *IEEE Trans. Energy Convers.*, 2008, **23**, (2), pp. 382–392
- [26] Sapena-Bano, A., Martinez-Roman, J., Puche-Panadero, R., *et al.*: 'Induction machine model with space harmonics for fault diagnosis based on the convolution theorem', *Int. J. Electr. Power Energy Syst.*, 2018, **100**, pp. 463–481
- [27] Belahcen, A., Arkkio, A., Martinez, J.: 'Broken bar indicators for cage induction motors and their relationship with the number of consecutive broken bars', *IET Electr. Power Appl.*, 2013, **7**, (8), pp. 633–642
- [28] Faiz, J., Ebrahimi, B.M., Toliyat, H.A., *et al.*: 'Mixed-fault diagnosis in induction motors considering varying load and broken bars location', *Energy Convers. Manage.*, 2010, **51**, (7), pp. 1432–1441
- [29] Song, Z., Yu, Y., Chai, F., *et al.*: 'Radial force and vibration calculation for modular permanent magnet synchronous machine with symmetrical and asymmetrical open-circuit faults', *IEEE Trans. Magn.*, 2018, **54**, (11), pp. 1–5
- [30] Fireteanu, V.: 'Detection of the short-circuit faults in the stator winding of induction motors based on harmonics of the neighboring magnetic field', *J. Phys., Conf. Ser.*, 2013, **450**, pp. 1–7
- [31] Martinez, J., Belahcen, A., Detoni, J., *et al.*: 'A 2D FEM analysis of electromechanical signatures in induction motors under dynamic eccentricity', *Int. J. Numer. Model., Electron. Neww. Devices Fields*, 2014, **27**, (3), pp. 555–571
- [32] Ebrahimi, B.M., Faiz, J., Roshtkhari, M.J.: 'Static-, dynamic-, and mixed-eccentricity fault diagnoses in permanent-magnet synchronous motors', *IEEE Trans. Ind. Electron.*, 2009, **56**, (11), pp. 4727–4739
- [33] Toliyat, H.A., Lipo, T.A., White, J.C.: 'Analysis of a concentrated winding induction machine for adjustable speed drive applications. I. Motor analysis', *IEEE Trans. Energy Convers.*, 1991, **6**, (4), pp. 679–683
- [34] Toliyat, H.A., Lipo, T.A., White, J.C.: 'Analysis of a concentrated winding induction machine for adjustable speed drive applications. II. Motor design and performance', *IEEE Trans. Energy Convers.*, 1991, **6**, (4), pp. 684–692
- [35] El-Refaie, A.M., Jahns, T.M., Novotny, D.W.: 'Analysis of surface permanent magnet machines with fractional-slot concentrated windings', *IEEE Trans. Energy Convers.*, 2006, **21**, (1), pp. 34–43
- [36] Faiz, J., Tabatabaei, I.: 'Extension of winding function theory for nonuniform air gap in electric machinery', *IEEE Trans. Magn.*, 2002, **38**, (6), pp. 3654–3657
- [37] Nandi, S.: 'Modeling of induction machines including stator and rotor slot effects', *IEEE Trans. Ind. Appl.*, 2004, **40**, (4), pp. 1058–1065
- [38] Marfoli, A., Bolognesi, P., Papini, L., *et al.*: 'Mid-complexity circuitual model of induction motor with rotor cage: a numerical resolution'. 2018 XIII Int. Conf. on Electrical Machines (ICEM), Alexandroupoli, Greece, 2018, pp. 277–283
- [39] Pippuri, J., Arkkio, A.: 'Time-harmonic induction-machine model including hysteresis and eddy currents in steel laminations', *IEEE Trans. Magn.*, 2009, **45**, (7), pp. 2981–2989
- [40] Kumar, A., Marwaha, S., Marwaha, A., *et al.*: 'Magnetic field analysis of induction motor for optimal cooling duct design', *Simul. Modell. Pract. Theory*, 2010, **18**, (2), pp. 157–164
- [41] Martinez, J., Belahcen, A., Detoni, J.G.: 'A 2D magnetic and 3D mechanical coupled finite element model for the study of the dynamic vibrations in the stator of induction motors', *Mech. Syst. Signal Process.*, 2016, **66–67**, pp. 640–656
- [42] Lin, R., Arkkio, A.: '3-D finite element analysis of magnetic forces on stator end-windings of an induction machine', *IEEE Trans. Magn.*, 2008, **44**, (11), pp. 4045–4048
- [43] Pyrhonen, J., Jokinen, T., Hrabovcova, V.: 'Design of rotating electrical machines' (John Wiley & Sons, Hoboken, NJ, USA, 2009)

11 Appendix

The broken rotor bars can be simulated by changing the resistance values of the related entries in the resistance matrix. The red elements in the equation shown below represent the values need to be changed to simulate second rotor bar. (see (31)) The conversion of integral based equations into mean functions as in (32)–(35), makes their implementation easier.

$$R_{rr} = \begin{bmatrix} 2(R_b + r_e) & -R_b & 0 & 0 & \cdots & 0 & \cdots & 0 & -R_b & -r_e \\ -R_b & 2(R_b + r_e) & -R_b & 0 & \cdots & 0 & \cdots & 0 & 0 & -r_e \\ 0 & -R_b & 2(R_b + r_e) & -R_b & \cdots & 0 & \cdots & 0 & 0 & -r_e \\ \vdots & \vdots & \vdots & \vdots & \vdots & \vdots & \vdots & \vdots & \vdots & \vdots \\ 0 & 0 & 0 & 0 & \cdots & 0 & \cdots & 2(R_b + r_e) & -R_b & -r_e \\ -R_b & 0 & 0 & 0 & \cdots & 0 & \cdots & -R_b & 2(R_b + r_e) & -r_e \\ -r_e & -r_e & -r_e & -r_e & \cdots & -r_e & \cdots & -r_e & -r_e & n_b r_e \end{bmatrix} \quad (31)$$

$$L_{ij}(\theta) = \mu_0 r l \int_0^{2\pi} P(\theta, \alpha) N_i(\theta, \alpha) n_j(\theta, \alpha) d\theta \quad (32)$$

$$L_{ij}(\theta) = 2\pi\mu_0 r l \frac{1}{2\pi} \int_0^{2\pi} P(\theta, \alpha) N_i(\theta, \alpha) n_j(\theta, \alpha) d\theta \quad (33)$$

Since the definition of mean function is

$$\langle f \rangle = \frac{1}{2\pi} \int_0^{2\pi} f(\alpha) \cdot d\theta \quad (34)$$

Therefore,

$$L_{ij}(\theta) = 2\pi\mu_0 r l \langle P(\theta, \alpha) N_i(\theta, \alpha) n_j(\theta, \alpha) \rangle \quad (35)$$

$$f_{BR} = f_s \pm 2ksf_s, \quad k = 1, 2, 3, \dots \quad (36)$$

where f_{BR} , f_s and s are the broken rotor bars based frequencies, supply fundamental frequency and the slip, respectively.

The leakage inductance of end winding can be calculated as [43]

$$L_{ew} = \frac{Q_s}{m} q \left(\frac{Z_q}{a} \right)^2 \mu_0 l_w \lambda_w \quad (37)$$

where Q_s is the number of slots, Z_q is the number of conductors per slot, m is the number of stator phases, a are the number of parallel

paths per phase, q is number of slots per pole and phase, μ_0 is the permeability of free space, l_w is the average length of winding outside of the stator and λ_w is the permeance factor which is 0.20 for motor under investigation.

The stator and the rotor turn functions can be defined as

$$n_{as}(\theta) = \begin{cases} Z_q * i, & i = 1:1:Q_{pp} \\ Z_q * Q_{pp}, & i = (Q_{pp} + 1):1:3 * Q_{pp} \\ Z_q(Q_{pp} - i), & i = (3 * Q_{pp} + 1):1:4 * Q_{pp} \\ 0, & i = (4 * Q_{pp} + 1):1:2 * Q_s/p \end{cases} \quad (38)$$

$$n_r(\alpha) = \begin{cases} 1, & \theta_i \leq \alpha_c \leq \theta_i + \alpha_r \\ 0, & \theta_i > \alpha_c > \theta_i + \alpha_r \end{cases} \quad (39)$$

where Z_q is the number of conductors per stator slot, Q_{pp} is the number of slots per pole and phase, Q_s is the total number of stator slots and i is the integer. This conditional analytical function can be used to generate the turn function of stator phase winding. The remaining two turn functions can be produced by shifting it to $(2\pi/3)$ and $(4\pi/3)$, respectively. While, the rotor turn function can be represented as in (39), where θ_i is the starting angle of rotor bar from a reference point and α_r is the angular displacement between two consecutive bars.

Publication V

B. Asad, T. Vaimann, A. Belahcen, A. Kallaste, A. Rassõlkin, M. Naveed Iqbal. Broken rotor bar fault detection of the grid and inverter fed induction motor by effective attenuation of the fundamental component. IET Electric Power Applications, vol. 13 (12), pp. 2005–2014, Dec. 2019.

Broken rotor bar fault detection of the grid and inverter-fed induction motor by effective attenuation of the fundamental component

ISSN 1751-8660
 Received on 15th May 2019
 Revised 7th July 2019
 Accepted on 17th July 2019
 E-First on 6th August 2019
 doi: 10.1049/iet-epa.2019.0350
 www.ietdl.org

Bilal Asad¹ ✉, Toomas Vaimann¹, Anouar Belahcen², Ants Kallaste¹, Anton Rassõlkin¹, Muhammad Naveed Iqbal¹

¹Department of Electrical Power Engineering and Mechatronics, Tallinn University of Technology, Ehitajate tee 5, Tallinn, Estonia

²Department of Electrical Engineering and Automation, Aalto University, 02150 Espoo, Finland

✉ E-mail: biasad@taltech.ee

Abstract: Since electrical machines are the largest consumer of electricity worldwide, their fault diagnostic at the incipient stage and condition monitoring is essential for better reliability, economy, and safety of operation. Out of several condition monitoring techniques, motor current signature analysis is gaining heightened popularity because of its non-invasive nature, the least number of sensors required and versatility of compatible algorithms. In this study, the best characteristics of infinite impulse response (IIR) filter are exploited to observe the broken rotor bar (BRB) frequencies with good legibility in current and voltage spectrum of the grid and inverter-fed motor, respectively. The causes of various harmonics in the stator current spectrum are first investigated for better understanding. The results are taken based on simulation and measurements taken from the laboratory setup. It is observed that a better tuning of IIR filters can make diagnostic algorithms capable of detecting the frequencies of interest by effectively attenuating the fundamental component and reducing its spectral leakage. Moreover, in case of direct torque control-based industrial inverter-fed motors, the current cannot be a good candidate for fault diagnostics rather the phase voltage can be effectively used for the detection of BRBs.

1 Introduction

The indispensable role of electrical machines in modern day society can be witnessed everywhere ranging from domestic to industrial applications. They are the key elements of the conventional power generating stations in the form of synchronous generators and doubly-fed induction generators in case of wind energy generating systems. As a load, electrical machines particularly induction motors are consuming more than 50% of total generated energy worldwide. Electrical machines especially induction motors are being used as a workhorse in domestic and industrial applications, such as water pumps, fans, ship propulsion, conveyor belt movers, cranes, and electric vehicles etc.

Squirrel cage induction motors (SQIM) are the most popular among various types of electrical machines because of their simple and rugged structure, easy maintenance, low cost and high torque per weight ratio. On account of their prolonged duty hours and associated moving parts, these machines remain at risk of failure. The faults can be classified into stator and rotor associated faults. The stator faults are mainly related to electrical domain, such as inter-turn short circuit, phase drop, voltage unbalance and earth faults. The mechanical faults make the biggest proportion of overall faults in the form of damaged bearings, broken rotor bars (BRBs), static and dynamic eccentricity and cracked end rings etc. These faults are degenerative in nature, making diagnostic algorithms important for their detection at the incipient stage to avoid any catastrophic situation, to improve the reliability of operation and to get economic benefits of reconditioning over replacing with a new machine. A detailed cost comparison of rewind versus recondition of different size motors is presented in [1].

In sophisticated industrial control systems, the need of better controllability and the requirement of multiphase motors to exploit their benefits such as reduced torque ripples, high power density, high efficiency, and reliability is increasing day by day. The different power rating of machines, their versatile structures, the safety of operation and machine itself, different nature of applications and reliability of operation increase the need for power inverters as the input source.

These inverters are accountable for the conversion of a standard three-phase grid supply system into the desired number of phases with different amplitude, and frequency. There are a variety of inverter-based drive systems with a control system ranging from simple scalar (v/f , v/f^2 , v/\sqrt{f}) to complex control systems such as direct torque control (DTC), field-oriented control (FOC), model predictive control, and sliding mode observer etc. The presence of inverter and various control methods as an integral part of the drive system can lead to the failure of the diagnostic algorithms due to the inverter induced frequency components.

A variety of condition monitoring techniques are available in literature, such as, electromagnetic field monitoring, noise and vibration monitoring, infrared recognition, temperature measurements, radio frequency emission monitoring, chemical analysis, acoustic noise measurement, motor current signature analysis (MCSA) and most advanced artificial intelligence-based techniques, such as fuzzy logic and neural networks etc. [2]

The MCSA is gaining increasing popularity among all the above-mentioned techniques because of its non-invasive nature, the least number of sensors required and a variety of compatible diagnostic algorithms. In simple words, the measurement of either voltage or current profile of the machine opens the entire field of signal processing for its analysis to detect the cause and severity of the fault.

It has been observed that each kind of fault leaves certain specific frequency components in the current or voltage spectrum. The detection of those components can be used as a potential indicator of fault nature and its severity [3]. In case of the electrical machine, there are three main sources of generated harmonics; (i) motor itself, (ii) input supply, (iii) fault if any. The motor generated harmonics are dependent on non-sinusoidal winding distribution, non-uniform air gaps permeance associated with stator and rotor and non-linear materials. The stator and rotor anisotropies such as the slot openings and non-uniform air gap because of small eccentricity even under healthy condition lead to the principal slot harmonics (PSH) or rotor slot harmonics [4].

The supply harmonics are small in number in case of grid fed motors, but they are much more in case of inverter fed machines.

The amplitude and frequency of inverter fed harmonics depend upon the switching frequency and modulation technique used by its control algorithm. The switching frequency of inverter solid-state switches makes a tradeoff between efficiency and amplitude of low order harmonics.

The increase in switching frequency attenuates the low order harmonics but at the cost of an increase in the losses of the inverter. The strong low order harmonics increase torque ripples, torsional vibrations, and consequent mechanical deformation that tend to increase with time. Since the BRBs-based lower and upper side band (LSB, USB) frequencies are very close to the fundamental component, the low order harmonics are highly likely to bury them by an increase in the spectral leakage with resultant failure of diagnostic algorithms. For the sake of efficiency, the maximum switching frequency in the range of one-kilo hertz to generate a voltage supply of 50–60 Hz are reported in [5–8], although in case of DTC it can range up to 40 kHz for power up to 100 kW.

Various kind of control algorithms to reduce both switching frequency and losses can be found in literature such as [9, 10] used discontinuous pulse width modulation (DPWM) which reduces switching frequency (f_{sw}) up to two-thirds of f_{sw} of continuous PWM strategies, sine-triangle PWM-based DPWM can be found in [11]. The authors in [12, 13] used space vector-based DPWM and modified DPWM can be found in [14] while space vector-based synchronised DPWM is presented in [5].

The Fourier analysis and its variants, responsible to segregate a signal into its component sinusoids, has revolutionised the field of signal processing. Having different types for various kinds of periodic, aperiodic, stationary, and non-stationary signals, it is being extensively used in literature to find out the frequencies of interest. The production of specific frequency components by different electrical equipment and faults in current and voltage spectrum makes Fourier analysis inevitable for condition monitoring, power quality estimation, and fault diagnostics. In the case of electrical machines, the fault representing frequencies can be traced in current, voltage, speed, torque, and flux profiles. For grid fed machines, the frequency spectrum analysis of line current is comparatively easy because only a few frequencies are being injected from the grid side. The rest of the frequencies are either machine-generated itself or because of the fault, making them easy to segregate. In the case of inverter fed machines, there are several frequency components coming from the inverter side. It makes it challenging for the diagnostic algorithm to detect the frequencies of interest particularly when they are weak enough as compared to the low order harmonics. Moreover, with the growing complexity of inverter control algorithms and modulation techniques, the inverter fed frequencies become difficult to define using some specific rules and mathematical equations. For example, in the case of stochastic control algorithms and machines working in closed loop control systems, the frequencies become load-dependent. So, it becomes highly likely that the faulty components will be either attenuated by drive controller or they will be buried under the inverter-based nearby frequencies. Owing to this fact, the diagnostic algorithm should not rely on the same signal for all cases as it is proved in the results that, in case of DTC controlled motor current is not a reliable diagnostic signal.

Being the most powerful frequency, the fundamental component is the profound cause of the spectral leakage problem. Moreover, in case of low switching to fundamental frequency ratio of the inverter, the low order harmonics are powerful enough to make the spectral leakage problem worst.

The majority of MCSA-based techniques rely on fast Fourier transform (FFT) of signal, e.g. in [15], the authors used the FFT on active and reactive currents of a motor to investigate the BRBs and load oscillations. Authors of [16] used the FFT in conjunction with Park's vector to make artificial ants clustering technique for the fault diagnostics of induction motor. In [17], the autoregressive method is relying on discrete-time Fourier transform (DTFT) and Notch filter. Researchers in [18] used the FFT to prove that the slot harmonics can be used as potential indicators to detect the BRBs. However, this technique has a drawback that the principle slot harmonics (PSH) are not present in the motor for all combinations of pole pairs and number of rotor bars. In [19], the authors used an

adaptive notch filter and FFT for BRB fault diagnostics of induction motor. Authors of [20] used the FFT on simulations and practical results to investigate the BRBs and mechanical vibrations. In [2], the authors used the FFT extensively to study the frequency spectrum of the stator current for different fault conditions.

Since the measured signal has a finite duration and FFT algorithm is designed for an infinitely long-time period, the spectral leakage due to signal truncation is a major complication. This problem becomes worst for the fundamental frequency component because it carries most of the power as compared to the rest of the harmonics. It also invites the logarithmic scale to make low amplitude spatial and fault frequencies visible in the spectrum. Moreover, at low slip conditions, the left-hand side (LHS) and right-hand side (RHS) frequencies are very near to the supply frequency, making them nearly buried under the fundamental component.

In this paper, an infinite impulse response (IIR) filter is used for the attenuation of the fundamental component for its better transition band, low passband ripples, and low order needed. The effective tuning of this filter can improve the legibility of the frequency spectrum and makes the detection of BRB frequencies easy. The technical portion of this paper can be divided into three sections. In the first section, the SQIM is simulated using a finite element model (FEM) and line currents are calculated. The frequency spectrum gives a very good picture to understand the harmonics due to non-sinusoidal winding distribution, non-uniform air gap permeance function due to slot openings and BRBs. In the second section, the results measured form a grid fed motor are investigated to validate the simulation results and the additional grid fed harmonics. Finally, the machine is fed with industrial inverter under healthy and BRB conditions. Unlike [21, 22] where authors have used FOC-based close loop system, the measurements are taken from industrial inverter working under DTC mode. To decrease the torque ripples, it tends to smooth the currents making them unsuitable for fault detection. The change in current is produced by a change in the phase voltage which can be tracked for fault detection.

2 Mathematical background

Majority of MCSA-based techniques exploit the fact that every fault in electrical machines leaves certain specific frequency components in the current spectrum. The effective detection of those harmonics can lead to a good diagnostic algorithm, capable to detect the fault even at the incipient stage. The machine anisotropies such as constructional unbalances can produce PSH in stator current spectrum. Moreover, the irregularities in rotor such as high resistance connections, broken end rings, BRBs can be discovered by detecting the following frequencies:

$$f_{BR} = f_s \pm 2ksf_s, \quad k = 1, 2, 3, \dots \quad (1)$$

where f_s is the supply frequency, s is the motor slip, and k is an integer representing the order of harmonics. With growing k , the frequency of harmonics increases but amplitude decreases. The first harmonic is the strongest and the most important to detect the BRBs. This harmonic has two sideband frequencies, the lower sideband (LSB) or left-hand side (LHS) and upper sideband (USB) or RHS having frequencies ($f_{lsb} = f_s - 2sf_s$) and ($f_{usb} = f_s + 2sf_s$), respectively. The LSB is generated due to unbalanced flux distribution caused by BRBs and RSB is because of resultant speed oscillations [23].

Similarly, some other prominent rotor associated faults such as eccentricity, damaged bearings, and inter-turn short circuit faults can be discovered by segregating following frequencies respectively [24]:

$$f_{ecc} = \left[(kn_{br} + n_d) \left(\frac{1-s}{p} \right) \pm \nu \right] f_s \quad (2)$$

$$f_{bearing} = \left| f_s \pm \left(\frac{mn_b f_r}{2} \right) \left(1 \pm \frac{b_d}{p_d} \cos \theta \right) \right| \quad (3)$$

$$f_{st} = f_s \left[\frac{m}{p} (1-s) \pm k \right], \quad k = 1, 2, 3, \dots \quad (4)$$

where k is an integer, n_{br} is the number of rotor bars, ($n_d=0$) for static eccentricity and $n_d=1, 2, 3, \dots$ in case of dynamic eccentricity, s is the slip, $v=1, 2, 3, \dots$ represents the supply harmonics and p is the number of pole pairs, n_b is the number of bearing balls, f_r is the rotor's mechanical frequency, m is a positive integer, p_d is the bearing pitch diameter, b_d is the bearing ball's diameter, and θ is the angle between ball and races.

The harmonics presented in (4) are the inter-turn short circuit in case of wound rotor, which is converted to BRB frequencies in case of a cage rotor as described in (1). Since the rotor is circular and any fault such as BRB changes its mechanical symmetry, the fault modulating signal can be described by a cosine function as follows:

$$i_{af}(t) = [1 + m(t)]i_a(t) \quad (5)$$

$$m(t) = M \cos(4\pi s f_s t + \phi) \quad (6)$$

$$i_{af}(t) = [1 + M \cos(4\pi s f_s t + \phi)]i_a(t) \quad (7)$$

$$i_{af}(t) = [1 + M \cos(4\pi s f_s t + \phi)]i_m \sin(\omega t) \quad (8)$$

$$i_{af}(t) = I_m \sin(2\pi f_s t) + \left(\frac{MI_m}{2} \right) [\sin(2\pi f_s (1+2s)t + \phi) + \sin(2\pi f_s (1-2s)t + \phi)] \quad (9)$$

where M is the modulation index, depending upon the number of BRBs (N_b) and a total number of rotor bars (N_t) and $\omega_o = 2\pi f_o$, is the fault characteristic frequency and depends upon the nature of the fault and the slip of the machine. The modulation index M can be approximated as a ratio of the number of BRBs and the total number of bars as in [25]

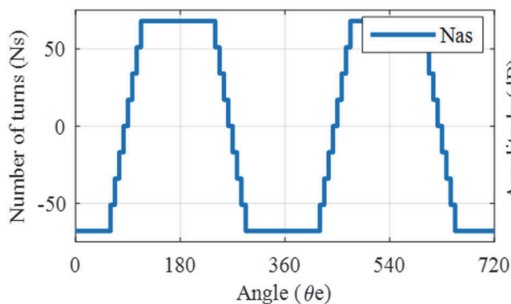
$$M \simeq \frac{N_b}{N_t} \quad (10)$$

The need for harmonics detection for fault diagnostics based on the FFT algorithm need the increase of their segregation according to the cause of their production. A quick review of the harmonics presents in the current spectrum of an induction machine is given below.

3 Harmonic description

3.1 Winding and slot harmonics

Unlike the ideal machine, where the winding is assumed to be sinusoidally distributed, in practical machines it is a stair-cased approximation. Moreover, the air gap permanence is not smooth but becomes a function of stator and rotor slots opening. Owing to these factors, the stator-to-stator inductances are not constant but



change with the change in rotor position as shown in the following equation:

$$L_{ij}(\theta) = \mu_o r l \int_0^{2\pi} P(\phi, \theta) N_i(\phi, \theta) N_j(\phi, \theta) d\theta \quad (11)$$

where $L_{ij}(\theta)$ is the inductance, μ_o is the permeability of free space, r is the radius of motor, l is the effective length, $P(\theta, \phi)$ is the air gap permeance function, and $N(\theta, \phi)$ is the winding function for any phase as shown in Fig. 1 along with its spectrum.

Similarly, the stator to rotor inductances are not pure sinusoid, but act like a trapezoidal function. These changing inductances produce high-frequency components in the current spectrum called the winding harmonics and PSH or RSH, respectively. The PSH harmonics are important in the way that, they can be used for sensorless speed estimation, eccentricity, and BRB fault diagnostics. It is shown in the results that the BRB fault frequencies also appear around fundamental PSH just as they appear around fundamental supply frequency component. The fact that the PSH is not strong enough as compared to the fundamental supply component, leads to the less spectral leakage making the detection of BRB frequencies easier. The eccentricity and PSH frequency can be represented by (2) as described previously.

However, the only flux having pole pairs equal to the pole pairs of the stator winding itself can induce a voltage in a balanced three-phase stator. In other words, the PSH spectrum will be produced if the pole pair number ($n_b \pm n_p$) is equal to that produced by the stator winding-based space harmonics. The authors of [4], made a rule that if a number of rotor slots will satisfy the (11), the PSH will appear otherwise not

$$n_b = 2p[3(m \pm q) \pm r] \quad (12)$$

where $m \pm q = 0, 1, 2, \dots$ and $r = 0$ or 1 .

3.2 Supply harmonics

The harmonics coming from the supply side range from simple odd multiples of fundamental components in case of grid fed system to a high bandwidth of frequencies coming from the inverter side. For better controllability, precision, accuracy, reliability, efficiency, and versatile nature of the load, the inverter becomes an integral part of modern-day drive systems. Along with the mentioned advantages, these inverters are also responsible for increasing cost, switching losses, iron losses, torque ripple, and radiated electromagnetic field interference [26], acoustics noise [27], and high-frequency components for which the machine is not designed for. These drawbacks persuade researchers to find out good drive control algorithms and switching techniques [27–30] but at a cost of random distribution of harmonics in current spectrum.

The measured grid and industrial inverter-based line voltage along with their corresponding spectrum containing some powerful harmonics are shown in Fig. 2. For better resolution, the sampling frequencies in case of the grid and inverter are 10 and 100 kHz, respectively. To improve the legibility of the spectrum, the fundamental component is attenuated using the IIR filter. The total

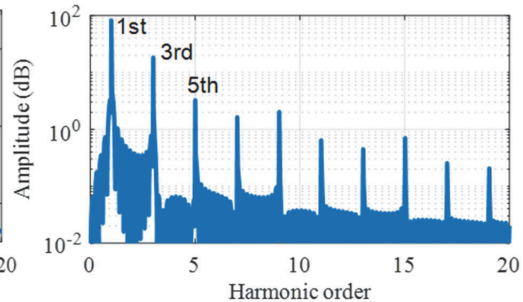


Fig. 1 Per phase stator winding distribution function and corresponding frequency spectrum

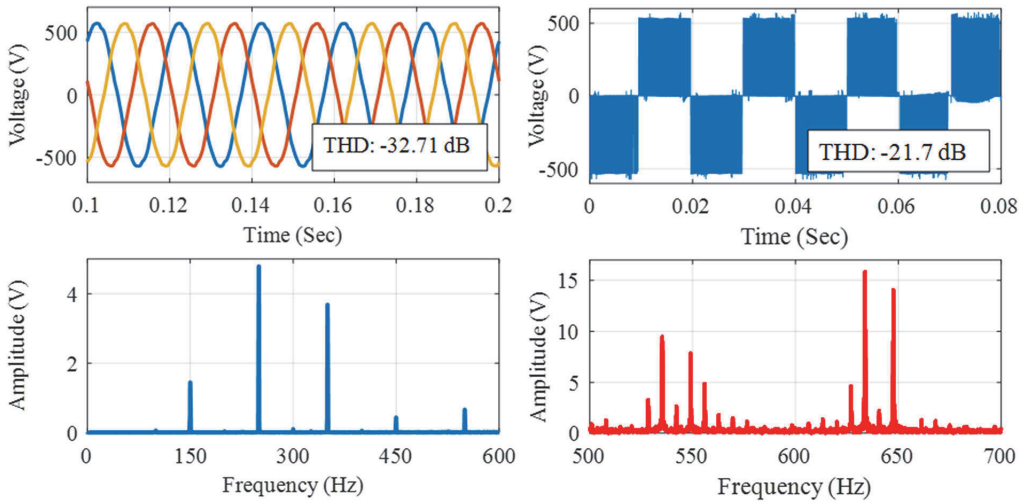


Fig. 2 Grid and inverter-based line voltage and corresponding frequency spectra showing some powerful harmonics with attenuated fundamental component

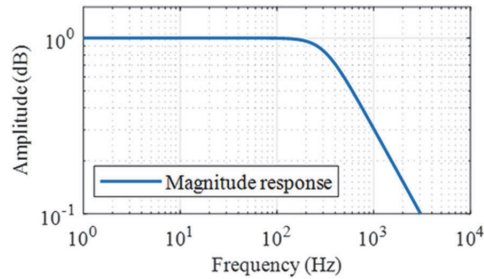


Fig. 3 Current magnitude frequency response of motor

harmonic distortion (THD) for the grid is calculated using a rectangular window and considering the first 70 harmonics. It is -32.7 dB which is equivalent to 2.31%, however, it changes with the change in power quality. For inverter produced line voltage the THD of -21.7 dB which is equivalent to 8.2% is calculated using the Kaiser window while considering first 700 harmonics. This value changes with a change in switching frequency and control strategy being used.

3.3 Motor as a filter

The inverter fed harmonics are highly likely to bury the fault frequency components, particularly the higher-order harmonics because of their small amplitude. Since the inverter is feeding a number of frequencies, it is necessary to investigate the bandwidth of importance. The motor frequency magnitude response is helpful in this regard, which can be approximated by taking equivalent per phase current transfer function as given in the following equations:

$$\frac{i_{as}}{v_{as}} = \frac{1}{\sqrt{(R_s + (R_r/s))^2 + \omega_c^2(L_{ls} + L_{lr})^2}} \quad (13)$$

where R_s (0.15 Ω) is the stator per phase resistance, R_r (0.63 Ω) is the rotor per phase resistance as referred to stator side, s (0.067) is the slip, ω_c is the synchronous speed, L_{ls} (0.003 H) is the stator leakage inductance, L_{lr} (0.002 H) is the rotor leakage inductance as referred to stator side, i_{as} and v_{as} are per phase current and voltage, respectively.

The natural frequency magnitude response is shown in Fig. 3, where it is evident that the motor attenuates the harmonics having a frequency higher than 1 kHz. This magnitude response changes with change in the motor design parameters. This frequency

response has less significance in case of grid fed machines because the high-frequency components are due to either the slotting effects or faulty condition, however, the most significant components remain within a bandwidth of 2 kHz.

4 Fourier transform and its resolution

The effective tuning of the FFT becomes essential in case of an inverter-based signal where there are a number of minima, maxima points, and discontinuities in the signal. The famous formula of DTFT can be represented as

$$X_n = \sum_{n=0}^{N-1} x_n e^{-j2\pi kn/N}, \quad k = 0, 1, 2, 3, \dots, (N-1) \quad (14)$$

where x_n is the discrete sampled signal and N is the number of samples, which should be a number in power of 2, i.e. $N = 2^x$ for less computational time with acceptable resolution.

For FFT of converter-based signal, the phenomena like spectral leakage and resolution are really necessary depending upon the parameter shown in the following equations and FFT windowing function:

$$t_{\text{sig}} = t_s \times N = N/f_s \quad (15)$$

$$df = 1/t_{\text{sig}} = f_s/N = \text{BW}/SL \quad (16)$$

$$SL = N/2 \quad (17)$$

where t_{sig} is the measurement or acquisition time of the signal, t_s and f_s represent the sampling frequency, N is the total number of data samples, BW is the bandwidth, df is the frequency resolution

Table 1 Motor specifications

Parameters	Symbol	Value
rated speed	N_r	1400 rpm @ 50 Hz
rated power	P_r	18 kW @ 50 Hz
connection	—	Star (Y)
power factor	$\cos \phi$	0.860
number of poles	p	4
number of rotor bars	N_{br}	40
number of stator slots	N_s	48

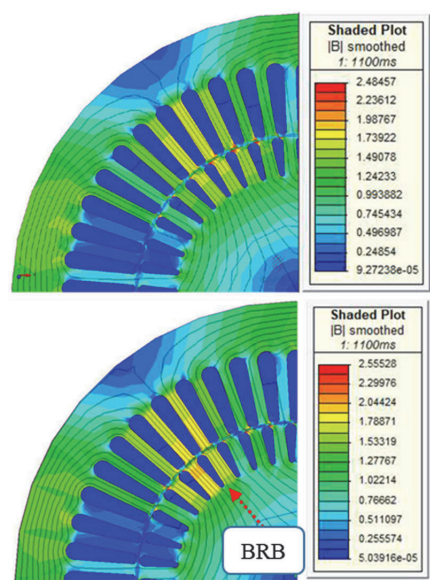


Fig. 4 Magnetic flux distribution and density for healthy (upper) and faulty (lower) motor

or frequency difference between two adjacent frequency bins and SL is the total number of spectral lines.

Owing to their better transition band the low pass band ripples and low order required, the IIR filter can be preferred over finite impulse response (FIR) filter. Out of a number of windows available in the literature, the Hamming window is used which has less spectral leakage making less impact on supply neighbouring, fault frequencies even in the case of the inverter fed machine.

5 Case study

For better understanding and performance analysis, the FEM-based simulation is performed for SCIM having parameters given in Table 1. The cage is made up of typical cast-aluminium rotor slots without skew. As compared to the analytical models, the FEM modelling is preferred for its better accuracy and ability to handle various constraints such as non-linearity and material characteristic etc. To reduce the computational time, only 2D field analysis is performed for the calculation of various performance parameters. Addition series resistances and reactance help to compensate for the neglected end windings. The coils are made up of parallel stranded conductors for uniform distribution of current density. The simulation is performed under rated load conditions with constant speed. After simulating it under healthy condition, one and two BRBs cases are taken into consideration. For accuracy and better resolution, a good number of mesh elements of 5328 are taken into account and simulation is done for 2 s with a sampling rate of 0.033 ms at stator and rotor temperatures of 120 and 140°C, respectively.

It is clear in Fig. 4 that flux density function does not remain the same for all bars under faulty condition but increases across broken bars which increases induced current in adjacent bars

putting them under increased magnetic stress. This makes the motor to break more bars in time if the fault is not diagnosed and repaired at an incipient stage. Owing to this change in flux distribution, the total flux linkage with bars do not remain zero and starts modulating stator current with a frequency dependent on the slip as shown in previous equations.

It is worth mentioning here that all specifications of the motor under simulation are the same as that of the practical motor. The 2D FEM calculation is done for the complete geometry of motor as it is no longer symmetrical because of the faulty condition. However, in Fig. 4 only one sector containing broken bar is shown for better visibility of flux distribution.

6 Practical setup

For practical measurements, two similar machines are connected back to back on a common mechanical foundation as shown in Fig. 5. One motor acts as a loading machine, which is being fed with industrial inverter for better accuracy and controllability of slip. The load side inverter is working under scalar mode to have less impact as in the case of DTC mode. The motor under investigation is first fed with the grid while using the star connection scheme. The phase currents are measured with a sampling frequency of 10 kHz for good resolution. In the second case, the test motor is fed with industrial inverter working under DTC mode while both line currents and phase voltages are measured at a sampling frequency of 100 kHz. All these measurements are taken under healthy, one, two, and three BRB cases.

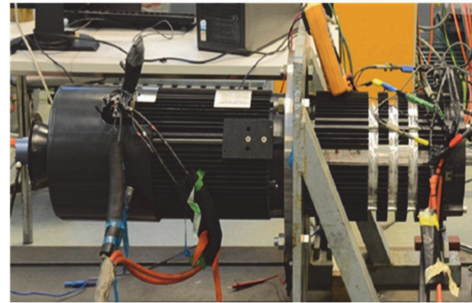
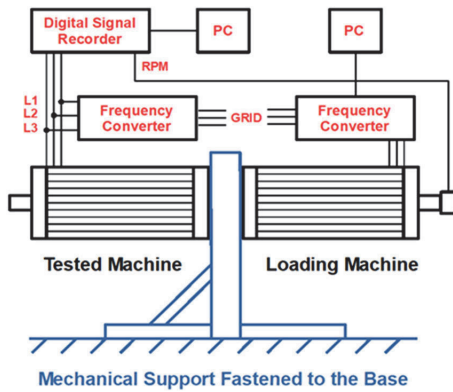


Fig. 5 Practical setup, block diagram (left) and lab measurement setup (right)

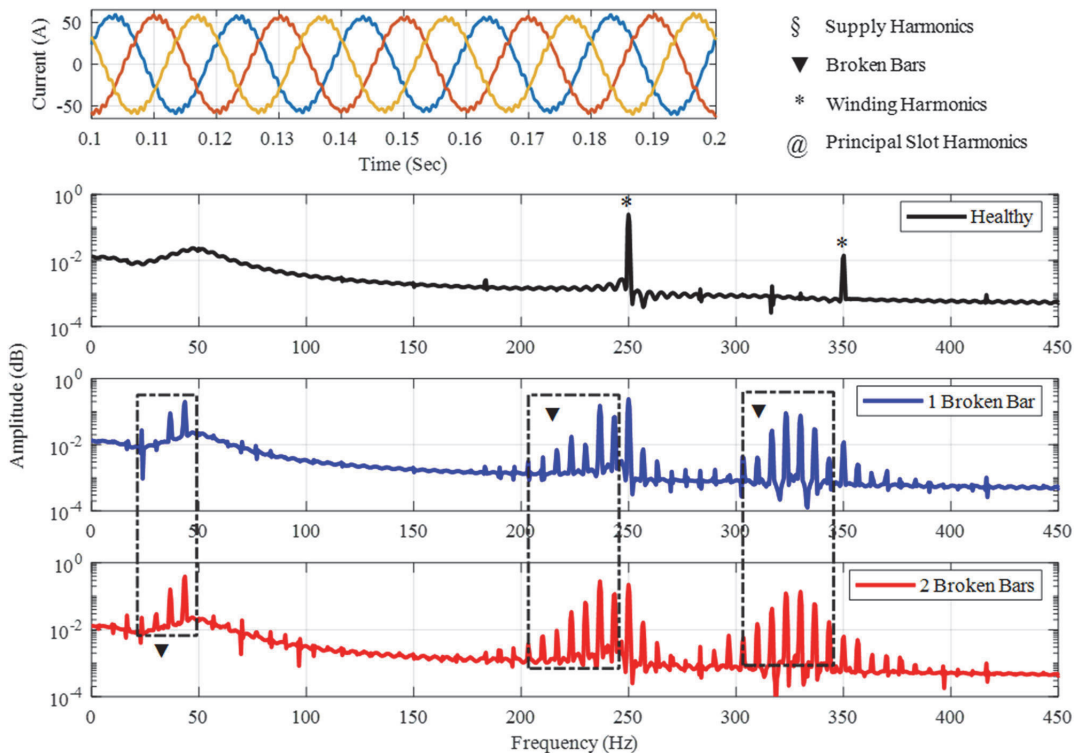


Fig. 6 Simulated line currents and corresponding spectrum with attenuated fundamental component for healthy and BRB cases from top to bottom

7 Results and discussion

7.1 Simulation results

The FEM-based line currents and their corresponding spectrum for healthy and BRBs are shown in Fig. 6. The calculations are done at rated load condition with a step size of 0.033 ms which corresponds to a sampling frequency of 30.3 kHz. The windings are balanced and connected in star scheme being fed with pure sinusoidal line voltage. To investigate the causes and the position of the harmonics, the fundamental component is attenuated using IIR band stop filter of order 2. Since the input does not have any harmonics, the frequency spectrum contains odd multiples of fundamental frequency induced by the stepped distributed winding function and PSH as the number of rotor bars (40) satisfies (12). At rated slip (0.066), the PSHs are present at 883 and 1083 Hz. The BRB frequencies are strong enough around the fundamental component where the left side harmonic (LSH) 46.7 Hz gets

powerful with an increase in the number of broken bars. The RSH develops due to the resultant speed oscillations which are not present in the spectrum because those oscillations are not taken into account. It is evident in Fig. 7 that the BRB frequencies are spread in the complete spectrum making their contribution around winding and PSHs.

7.2 Experimental results

Fig. 8 shows the measured currents and their respective spectrum in case of a grid fed machine. Both RSH and LSH are clearly visible around fundamental component while its attenuation improves their legibility such that the fault is easily detectable even in case of one BRB. The results are in good agreement with the simulation results in a way that the BRB harmonics are present around the odd multiples of the fundamental frequency. The PSH is shown in Fig. 9 for both healthy and faulty cases where its slight

movement on the frequency axis is due to the change in slip because of the change in the average generated torque and change in the rotor itself for different measurements.

In the case of DTC-based inverter-fed motor, the current cannot be a reliable signal for fault detection. This is because of the fact that BRBs increase current distortion with a resultant increase in torque and speed ripples. While, the controller of the DTC drive is designed to change the reference control signals to decrease the

torque and speed ripples by making current smoother. This is achieved by changing applied voltage as a function of load and fault, making it a potential candidate for BRB detection. Fig. 10 shows the current envelope of the grid fed healthy and faulty machines being fed with grid and inverter, respectively. For better clarity and similarity with grid-based current, the inverter-based current is passed through a low pass IIR filter and only frequency components till 1500 Hz are considered.

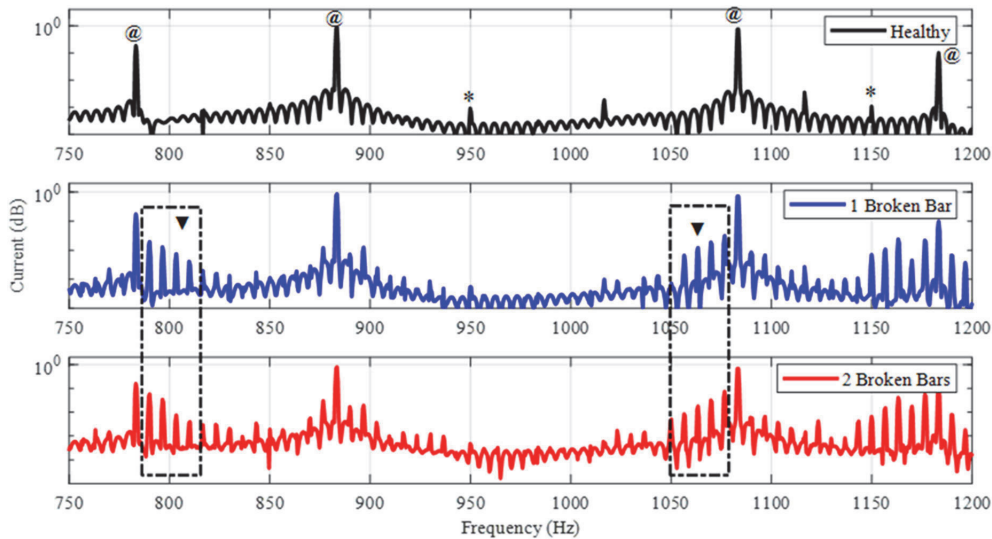


Fig. 7 PSH and subsequent BRB fault frequencies

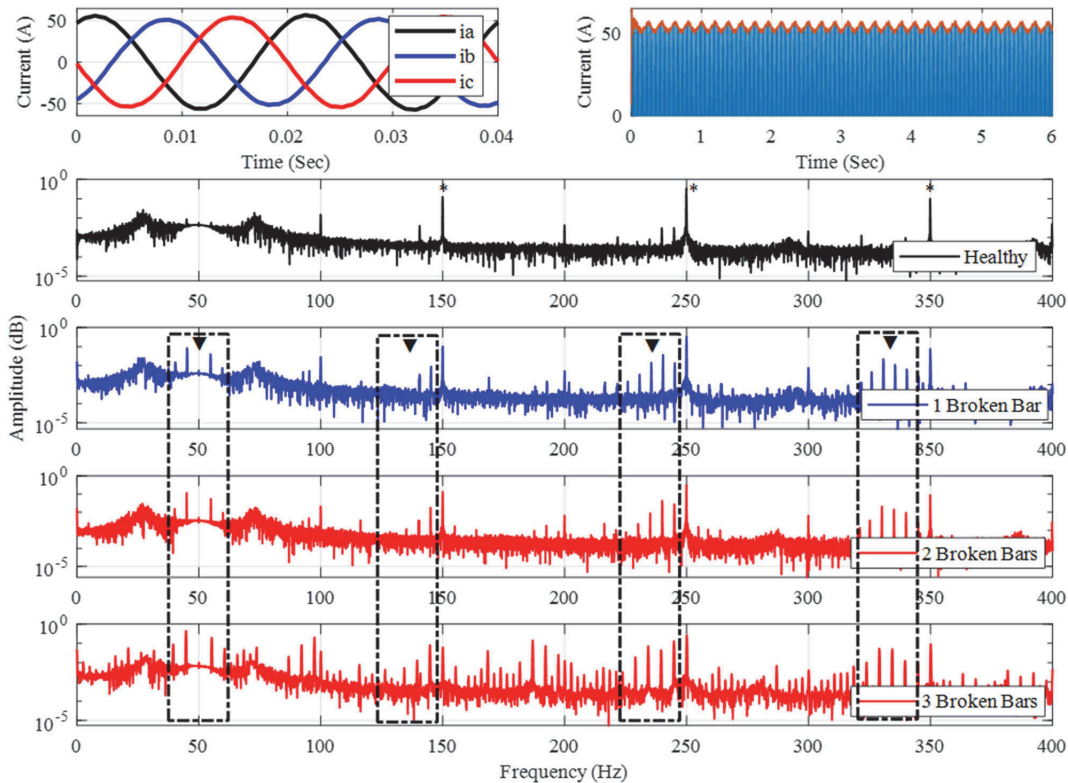


Fig. 8 Measured line currents (top left) with distorted envelope (top right) and corresponding spectrum with attenuated fundamental component, for healthy and BRB cases from top to bottom in case of grid fed motor

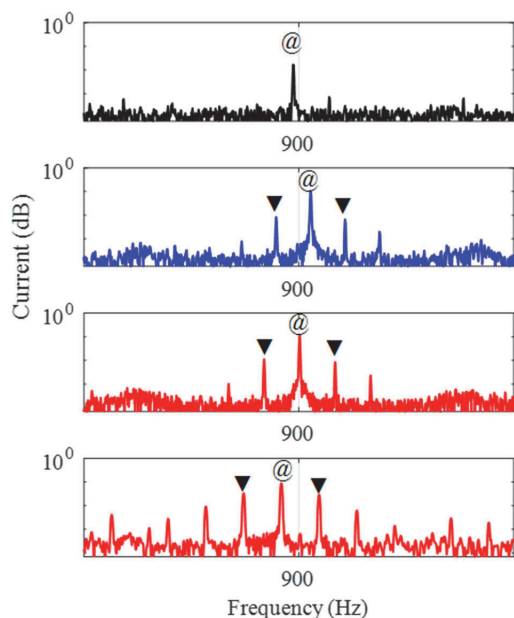


Fig. 9 PSH and subsequent fault frequencies for healthy, one, two, and three BRBs, respectively

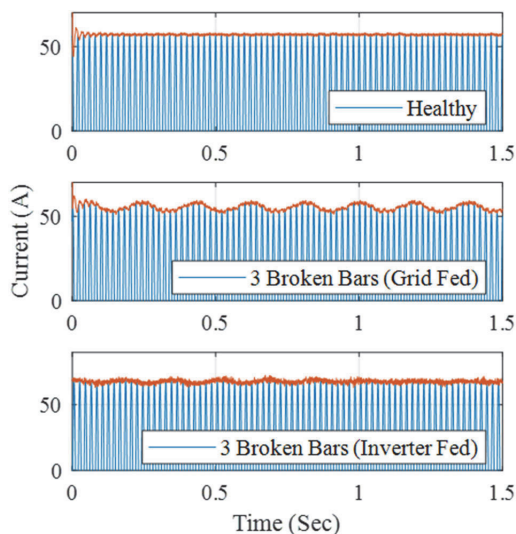


Fig. 10 Current envelope for grid and DTC-based inverter fed motor with three BRBs

Still, the change in the envelope for inverter-fed current is barely visible as compared to the grid-based system. The slight change is visible because of low order harmonics until 1500 Hz. As shown in Fig. 11, the current spectrum is not changing with BRBs. The fault frequencies are so small that the controller of DTC drive system easily attenuates them to reduce resultant torque and speed ripples. The impact of the controller is so strong that even the side band frequencies are no longer present in the spectrum. This makes a correlation between current and voltage in a way that if the machine is no longer symmetric and current is approximately constant then certainly voltage changes with the change in fault. This change in applied voltage is shown in Fig. 12 with the corresponding frequency spectrum in Fig. 13. It is observable that

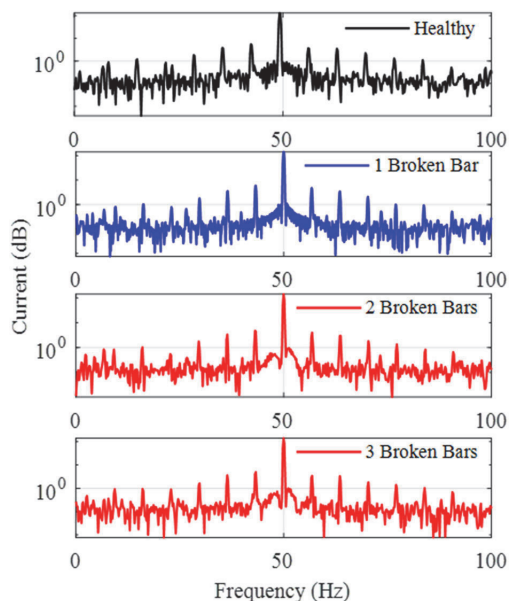


Fig. 11 Frequency spectrum of DTC controlled inverter-based measured currents which shows no significant change under healthy and BRB conditions

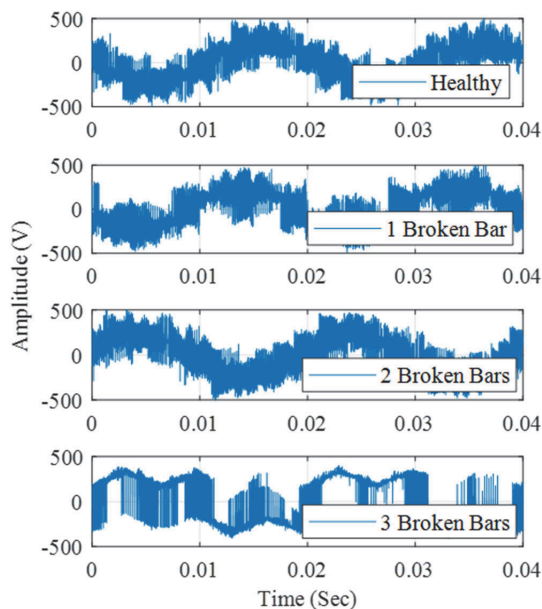


Fig. 12 DTC controlled inverter-based generated phase voltage for motor under healthy and BRB conditions

with BRBs the supply starts injecting odd third multiples of fundamental frequency such as (150, 450, 750, and 1050 Hz) etc.

8 Conclusions

The fact that the BRB increases the magnetic flux density and magnetic forces on the subsequent bars making them vulnerable to break as well increases the need for its detection at the incipient stage. Out of several fault diagnostic techniques, MCSA is gaining more popularity because of its non-invasive nature and compatibility with many diagnostic techniques. In this paper, the

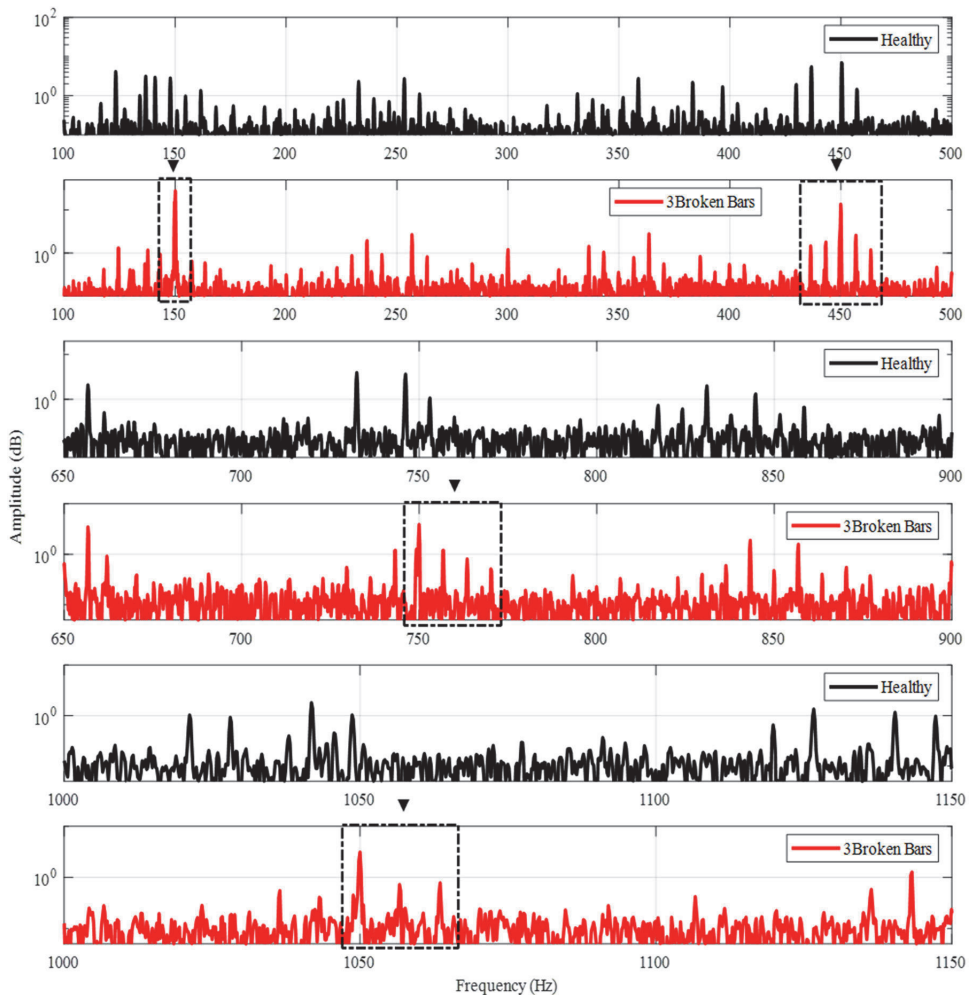


Fig. 13 The generation of odd third multiples of fundamental frequency in spectrum of phase voltage for DTC based inverter fed healthy and faulty motor

complete current spectrum of a three-phase induction motor is investigated under healthy and faulty conditions and the following conclusions can be made.

The generation of odd third multiples of fundamental frequency in spectrum of phase voltage for DTC-based inverter fed healthy and faulty motor.

- The IIR filter is a good choice over FIR and Hilbert filter for the attenuation of the fundamental component because it requires low order and possesses good transition band.
- The second-order IIR filter along with Hamming window have improved the legibility of frequency spectrum to a good extent.
- The total harmonics can be divided into three categories such as, the winding distribution based, non-uniform air gap because of stator and rotor slot openings, the non-symmetries due to fault and supply fed. In simulation results, the faulty frequencies appear near fundamental supply component and PSH. These results can be taken as a benchmark for the segregation of frequency components of the practical motor.
- The results taken from grid-based measurements are in good agreement with the simulation results. Since the faulty frequencies are very close to the fundamental and PSH, they can be detected effectively by attenuating the fundamental component and can be verified by their presence around PSH.

- The day-by-day increase in the need for industrial inverter makes the supply fed harmonics a big issue for the fault diagnostic algorithms. The harmonics coming from the supply side depend upon the inverter control strategy and switching frequency. However, due to the low pass nature of the motor itself, the currents are much smoother. The drive control methods such as DTC work to change the current according to the demand from the load side. These feedback control methods potentially hide the faulty frequency components in the current spectrum by changing the voltage accordingly.
- The BRB fault increases the torque ripples and distorts the envelope of the stator current. The drive system tends to decrease those ripples by changing the phase voltage and maintaining the current smooth. Hence, in the case of inverter fed machines, the current spectrum can mislead the diagnostic algorithm. So, the phase voltage can be used as a potential signal for diagnostic rather than the current in this case.
- In case of inverter fed system, it is noticed that with the increase in the number of broken bars, the odd third multiples of fundamental component become stronger which can be a potential indicator to detect them.
- All the results are taken in an offline environment, however, the practicality of this method in real-time environment is not a challenging task and can be performed easily. For this purpose, an updated algorithm could enable the processor to take the measurement after specific intervals of time and perform

analysis. The time required to perform the analysis is quite manageable for the real-time requirements.

- ix. For a better understanding of the frequency spectrum, the current and voltage signals are measured in a steady-state condition. However, the method can be extended for non-stationary signals measured under variable load conditions using short-time Fourier transform or wavelet approach.
- x. The method works well for all kind of control strategies such as scalar, FOC or DTC. However, for DTC controlled motor the signals such as currents, torque, or speed can mislead making phase voltage as a potential candidate for diagnostics.

9 References

- [1] Penrose, H.W.: 'Test methods for determining the impact of motor condition on motor efficiency and reliability'. Old Saybrook, CT: ALL-TEST Pro, LLC, March 2007, pp. 1–8
- [2] Nandi, S., Toliyat, H.A., Li, X.: 'Condition monitoring and fault diagnosis of electrical motors: a review', *IEEE Trans. Energy Convers.*, 2005, **20**, (4), pp. 719–729
- [3] Hassan, O.E., Amer, M., Abdelsalam, A.K., *et al.*: 'Induction motor broken rotor bar fault detection techniques based on fault signature analysis – a review', *IET Electr. Power Appl.*, 2018, **12**, (7), pp. 895–907
- [4] Nandi, S., Ahmed, S., Toliyat, H.A.: 'Detection of rotor slot and other eccentricity related harmonics in a three phase induction motor with different rotor cages', *IEEE Trans. Energy Convers.*, 2001, **16**, (3), pp. 253–260
- [5] Beig, A.R., Kanukollu, S., Al Hosani, K., *et al.*: 'Space-vector-based synchronized three-level discontinuous PWM for medium-voltage high-power VSI', *IEEE Trans. Ind. Electron.*, 2014, **61**, (8), pp. 3891–3901
- [6] Zhang, Y., Zhao, Z., Zhu, J.: 'A hybrid PWM applied to high-power three-level inverter-fed induction-motor drives', *IEEE Trans. Ind. Electron.*, 2011, **58**, (8), pp. 3409–3420
- [7] Napoles, J., Leon, J.I., Portillo, R., *et al.*: 'Selective harmonic mitigation technique for high-power converters', *IEEE Trans. Ind. Electron.*, 2010, **57**, (7), pp. 2315–2323
- [8] Oikonomou, N., Holtz, J.: 'Closed-loop control of medium-voltage drives operated with synchronous optimal pulsewidth modulation', *IEEE Trans. Ind. Appl.*, 2008, **44**, (1), pp. 115–123
- [9] Holmes, D.G., Lipo, T.A.: 'Pulse width modulation for power converters: principles and practice' (John Wiley, USA, 2003)
- [10] Prieto, J., Jones, M., Barrero, F., *et al.*: 'Comparative analysis of discontinuous and continuous PWM techniques in VSI-fed five-phase induction motor', *IEEE Trans. Ind. Electron.*, 2011, **58**, (12), pp. 5324–5335
- [11] Ojo, O.: 'The generalized discontinuous PWM scheme for three-phase voltage source inverters', *IEEE Trans. Ind. Electron.*, 2004, **51**, (6), pp. 1280–1289
- [12] Nguyen, D., Hobraiche, J., Patin, N., *et al.*: 'A direct digital technique implementation of general discontinuous pulse width modulation strategy', *IEEE Trans. Ind. Electron.*, 2011, **58**, (9), pp. 4445–4454
- [13] Wu, Y., Shafi, M.A., Knight, A.M., *et al.*: 'Comparison of the effects of continuous and discontinuous PWM schemes on power losses of voltage-sourced inverters for induction motor drives', *IEEE Trans. Power Electron.*, 2011, **26**, (1), pp. 182–191
- [14] Nguyen, N.-V., Nguyen, B.-X., Lee, H.-H.: 'An optimized discontinuous PWM method to minimize switching loss for multilevel inverters', *IEEE Trans. Ind. Electron.*, 2011, **58**, (9), pp. 3958–3966
- [15] Bossio, G.R., De Angelo, C.H., Bossio, J.M., *et al.*: 'Separating broken rotor bars and load oscillations on IM fault diagnosis through the instantaneous active and reactive currents', *IEEE Trans. Ind. Electron.*, 2009, **56**, (11), pp. 4571–4580
- [16] Soualhi, A., Clerc, G., Razik, H.: 'Detection and diagnosis of faults in induction motor using an improved artificial ant clustering technique', *IEEE Trans. Ind. Electron.*, 2013, **60**, (9), pp. 4053–4062
- [17] Ayhan, B., Trussell, H. J., Chow, M.-Y., *et al.*: 'On the use of a lower sampling rate for broken rotor bar detection with DTFT and AR-based spectrum methods', *IEEE Trans. Ind. Electron.*, 2008, **55**, (3), pp. 1421–1434
- [18] Khezzar, A., Kaikaa, M.Y., El Kamel Oumaamar, M., *et al.*: 'On the use of slot harmonics as a potential indicator of rotor bar breakage in the induction machine', *IEEE Trans. Ind. Electron.*, 2009, **56**, (11), pp. 4592–4605
- [19] Malekpour, M., Phung, B.T., Ambikairajah, E.: 'Stator current envelope extraction for analysis of broken rotor bar in induction motors'. IEEE 11th Int. Symp. on Diagnostics for Electrical Machines, Power Electronics and Drives (SDEMPED), Tinos, Greece, 2017, pp. 240–246
- [20] Belahcen, A., Martinez, J., Vaimann, T.: 'Comprehensive computations of the response of faulty cage induction machines'. Int. Conf. on Electrical Machines (ICEM), Berlin, Germany, 2014, pp. 1510–1515
- [21] Wang, T., Liu, H., Zhao, L., *et al.*: 'Quantitative broken rotor bar fault detection for closed-loop controlled induction motors', *IET Electr. Power Appl.*, 2016, **10**, (5), pp. 403–410
- [22] Hou, Z., Huang, J., Liu, H., *et al.*: 'Diagnosis of broken rotor bar fault in open- and closed-loop controlled wye-connected induction motors using zero-sequence voltage', *IET Electr. Power Appl.*, 2017, **11**, (7), pp. 1214–1223
- [23] Filippetti, F., Franceschini, G., Tassoni, C., *et al.*: 'AI techniques in induction machines diagnosis including the speed ripple effect', *IEEE Trans. Ind. Appl.*, 1998, **34**, (1), pp. 98–108
- [24] Vas, P.: 'Parameter estimation, condition monitoring, and diagnosis of electrical machines' (Oxford Clarendon Press, USA, 1993)
- [25] Bellini, A., Filippetti, F., Franceschini, G., *et al.*: 'Quantitative evaluation of induction motor broken bars by means of electrical signature analysis', *IEEE Trans. Ind. Appl.*, 2001, **37**, (5), pp. 1248–1255
- [26] Rosales, A., Sarikhani, A., Mohammed, O.A.: 'Evaluation of radiated electromagnetic field interference due to frequency switching in PWM motor drives by 3D finite elements', *IEEE Trans. Magn.*, 2011, **47**, (5), pp. 1474–1477
- [27] Vaimann, T., Sobra, J., Belahcen, A., *et al.*: 'Induction machine fault detection using smartphone recorded audible noise', *IET Sci. Meas. Technol.*, 2018, **12**, (4), pp. 554–560
- [28] Lee, K., Shen, G., Yao, W., *et al.*: 'Performance characterization of random pulse width modulation algorithms in industrial and commercial adjustable-speed drives', *IEEE Trans. Ind. Appl.*, 2017, **53**, (2), pp. 1078–1087
- [29] Kim, T.H., Lee, J.: 'Comparison of the iron loss of a flux-reversal machine under four different PWM modes', *IEEE Trans. Magn.*, 2007, **43**, (4), pp. 1725–1728
- [30] Jung, H.-S., Hwang, C.-E., Kim, H.-S., *et al.*: 'Minimum torque ripple pulse width modulation with reduced switching frequency for medium-voltage motor drive', *IEEE Trans. Ind. Appl.*, 2018, **54**, (4), pp. 3315–3325

Publication VI

B. Asad, T. Vaimann, A. Kallaste, A. Rassõlkin, A. Belahcen, M. Naveed Iqbal. Improving Legibility of Motor Current Spectrum for Broken Rotor Bars Fault Diagnostics. *Electrical, Control, and Communication Engineering*, vol. 15 (1), pp. 1–8, Sep. 2019.

Improving Legibility of Motor Current Spectrum for Broken Rotor Bars Fault Diagnostics

Bilal Asad* (*Ph. D. Student, Tallinn University of Technology, Tallinn, Estonia*),
Toomas Vaimann (*Senior Researcher, Tallinn University of Technology, Tallinn, Estonia*),
Ants Kallaste (*Researcher, Tallinn University of Technology, Tallinn, Estonia*),
Anton Rassõlkin (*Senior Researcher, Tallinn University of Technology, Tallinn, Estonia*),
Anouar Belahcen (*Professor, Aalto University, Espoo, Finland*),
M. Naveed Iqbal (*Ph. D. Student, Tallinn University of Technology, Tallinn, Estonia*)

Abstract – In this paper, the harmonic contribution of the broken rotor bar of an induction machine is investigated using an effective combination of the fast Fourier transform (FFT) and a band stop filter. The winding, spatial, grid fed and fault-based harmonics are investigated. Since the fundamental component is the most powerful component as compared to the other frequencies, it decreases the legibility of spectrum, making logarithmic scale inevitable. It also remains a potential threat of burying the fault representative side band frequencies because of its spectral leakage. In this paper, a band stop Chebyshev filter is used to attenuate the fundamental component, which makes the spectrum clearer and easier to understand even on the linear scale. Its good transition band and low passband ripples make it suitable for attenuating the main supply frequency with low impact on the neighbouring side band frequencies. To study the impact of fault on magnetic flux distribution, simulation is done using finite element method with good number of mesh elements and very small step size. The line current is calculated and frequency spectrum is investigated to segregate the spatial and fault frequencies using the proposed technique. The results are further validated by implementing the algorithm on the data measured in the laboratory environment including the grid fed harmonics.

Keywords – Digital filters; Fault diagnosis; Fourier transform; Induction motors.

I. INTRODUCTION

From the start of the second industrial revolution, induction motors have become the key element of modern-day industry due to variety of their applications ranging from generation to consumer domains. In the form of doubly fed induction generators, they make an integral part of renewable energy resources, such as wind power plants, and in the form electrical to mechanical energy converters, they are driving the cycle of industry making an impact on a nation's economy. They are also being extensively used in commercial and domestic applications, such as electric vehicles, fans, water pumps, etc. There are many machines that can convert electrical energy to mechanical energy, but simple structure, good efficiency and ease of maintenance of induction motors have made them the most common among all. They are the biggest consumer of electricity, consuming about 50 % of the total generated energy worldwide [1].

These machines always remain vulnerable to faults because they contain mechanically moving parts. These faults can be

broadly classified into electrical and mechanical. Electrical faults are mainly associated with the stator, such as voltage imbalance, phase drop, inter-turn short circuits and earthing faults, etc. Mechanical faults make the biggest proportion of overall faults, such as damaged bearings, broken rotor bars, broken end rings and eccentricity faults, etc.

These faults are directly or indirectly related with each other and are degenerative in nature. Hence, it is very important to detect them at an incipient stage in order to avoid extensive economic loss and time-consuming repair processes.

Fig. 1 shows both the energy consumed by induction motors as a percentage of the total used energy and a comparative difference between recondition and rewind costs of different power induction motors as proposed by Penrose in [2]. Due to the above-mentioned facts, the field of fault diagnostics is becoming as important as the field of machine design and control.

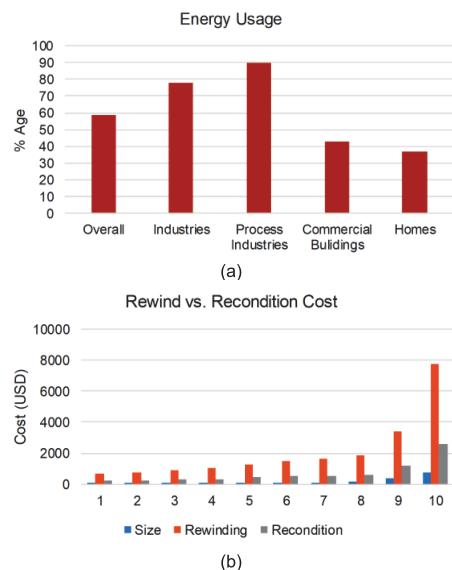


Fig. 1. Worldwide energy usage by electrical machines (a), and a comparison of rewind vs. recondition costs (b).

* Corresponding author.
E-mail: biasad@ttu.ee

Motor current signature analysis (MCSA) based fault diagnostic techniques are extensively used in research, because these techniques are mostly non-invasive in nature and require simple measurements. After the current measurement, an entire domain of signal processing techniques may be used to estimate the nature and the severity of the fault.

Fourier series has laid the foundation for almost all kinds of modern signal processing techniques. The majority of signal processing-based fault diagnostic techniques depend on Fourier analysis due to the need to investigate the frequency spectrum. This is so, because every kind of fault leaves some specific harmonics in the frequency spectrum of the stator current. The majority of MCSA based techniques depend on the fast Fourier transform (FFT) of the signal, e.g. in [3], the authors used the FFT on active and reactive currents of a motor to investigate the broken rotor bars and load oscillations. The authors of [4] used the FFT in conjunction with Park's vector to develop artificial ants clustering technique for the fault diagnostics of induction motor. In [5], the autoregressive method relies on discrete time Fourier transform (DTFT) and notch filter. Researchers in [6] used the FFT to prove that the slot harmonics can be used as potential indicators to detect the broken rotor bars. In [7], the authors used an adaptive notch filter and FFT for broken rotor bar fault diagnostics of the induction motor. The authors of [8] used the FFT to analyse simulations and practical results to investigate the broken rotor bars and mechanical vibrations. In [9], Nandi used the FFT extensively to study the frequency spectrum of the stator current for different fault conditions. [10] used the FFT along with the band stop filter for detection of broken rotor bar frequencies.

The spectral leakage of the fundamental component is the most profound problem associated with the FFT. The fundamental component contains more power than the other higher order harmonics, such as the spatial and the fault bar harmonics. Therefore, the logarithmic scale is usually preferred for better legibility of the spectrum, but spectral leakage remains and is likely to hide the frequency components near the fundamental component. In addition, at low slip conditions, spectral leakage problem becomes severe, because in case of most of the rotor-associated faults the frequencies depend on the slip. Some techniques can be found in literature, in which the researchers have tried to reduce the problem of the spectral leakage. The authors of [11] have used the Hilbert transform to get the envelope of the signal containing potential information about the faults. The authors in [12] used the fractional Fourier transform to recover the faulty frequencies from a non-stationary signal. In [13], the authors used the sliding discrete Fourier transform for detection of broken rotor bars. [14], [15], [16] used wavelet technique to improve the accuracy, but it led to complexity of algorithm.

In this paper, the Chebyshev filter is used due to its better brick wall characteristics compared to other filters, such as Butterworth, Hilbert, etc. In contrast to most of the papers, which focus mainly on the frequency spectrum containing faulty frequency harmonics on the logarithmic scale, while neglecting the supply fed harmonics, in this paper the entire frequency spectrum on the linear scale is studied, using the motor currents taken from both finite element-based simulations and experiments. Moreover, the grid fed harmonics are also tracked to make the picture clearer. It is shown that the proposed filter

makes the spectrum much more legible and effectively removes the fundamental component without disturbing all other harmonics.

II. MATHEMATICAL BACKGROUND

A. Slots and Broken Bar Harmonics

In case of a healthy motor, the frequency spectrum of the stator and rotor current contains a number of harmonics because of the distributed nature of rotor and stator windings, even if the supply is taken as ideal. These harmonics can be represented with the help of stator current linkage and the winding factor by the following equation [1]:

$$MMF(t, \alpha) = \frac{3}{\pi} \left(\frac{k_{wf} N_s}{v p} \right) (I e^{j(\omega t - v \alpha)}), \quad (1)$$

$$k_{wf} = \frac{\sin \frac{N \pi}{2}}{N} \sum_{p=1}^N \cos \alpha_p, \quad (2)$$

where N_s is the number of conductors per phase, k_{wf} is the winding factor, p is the number of pole pairs, v is the harmonic number, N is the total number of slots and α is the angle of the corresponding slot.

Every fault modulates the stator current with a specific frequency and modulation index, depending on the severity of the fault. These fault frequencies can be described mathematically as a function of the geometrical and electrical parameters of the rotor and stator. Extensive mathematics representing these faults can be found in [9], [11]–[19] and the simplified version – in [20]. The detection of the broken bar at an incipient stage is necessary, because when one bar breaks, its consecutive bars come under more thermal stress that leads to their breakage. These faults produce the following harmonics in the frequency spectrum [21]:

$$f_{BR} = f_s \pm 2k s f_s \quad (3)$$

$$f_{BR} = \left[\left(\frac{k}{p} \right) (1 - s) \pm s \right] f_s \quad (4)$$

where $k = 1, 2, 3, \dots, f_s$ is the supply frequency, p is the number of pole pairs and s is the slip of the machine. The lower sideband appears due to the broken rotor bar and the upper sideband due to the resultant speed oscillations. The dependency of these harmonic frequencies on the slip makes them more likely to be buried under the spectrum of the fundamental component. This problem becomes most severe under small and no-load conditions. In addition, the amplitude of these frequencies depends on the number of broken bars and is relatively small compared to the amplitude of the supply frequency.

B. Fourier Transform

The FFT is used in almost every field of science, as it provides the possibility to segregate a non-periodic random signal into sinusoids having specific frequency and amplitude called the harmonics. The amplitude of these harmonics usually attenuates as they travel along the frequency axis, making the fundamental component the most significant one. The discrete Fourier transform (DFT) and its inverse can be represented by the following formulas:

$$X_k = \sum_{n=0}^{N-1} x_n e^{-i2\pi kn/N}, \quad k = 0, 1, 2, \dots, (N-1); \quad (5)$$

$$x_n = \frac{1}{N} \sum_{k=0}^{N-1} X_k e^{-i2\pi kn/N}, \quad k = 0, 1, 2, \dots, (N-1), \quad (6)$$

where N is the number of samples, n is the current sample, x_n is the value of the signal at time n , k is the current frequency and X_k is the resultant bin of the DFT. Frequency resolution is very important for a complete and accurate frequency spectrum, which depends upon the measurement time of the signal and the sampling frequency, as shown in the following equation:

$$\Delta f = 1/T_m = f_s/N = BW/SL = 2 \cdot BW/N, \quad (7)$$

where Δf is the frequency difference between two consecutive frequency bins, N is the number of samples, BW is the bandwidth and SL is the number of spectral lines.

Since the taken signal is of a finite length and the length of the signal may not be an integer multiple of all frequency components, this will lead to a problem of spectral leakage. Being the most significant component, fundamental component can have a larger tendency of spectral leakage, amplifying the need of an attenuation filter.

C. Chebyshev Filters

Digital filters are mathematical algorithms, which are capable to reduce or enhance certain parameters of a signal. Because of their diversified nature, they may be of many types and are extensively used in almost every signal processing-based application.

The Chebyshev filters are well known for their better step response as compared to the Butterworth filter. Its gain response as a function of frequency ω can be represented as:

$$G_n(\omega) = 1/\sqrt{1 + \varepsilon^2 T_n^2(\omega/\omega_0)}, \quad (8)$$

where ε is ripple factor, ω_0 is cutoff frequency and T_n is its polynomial of n^{th} order.

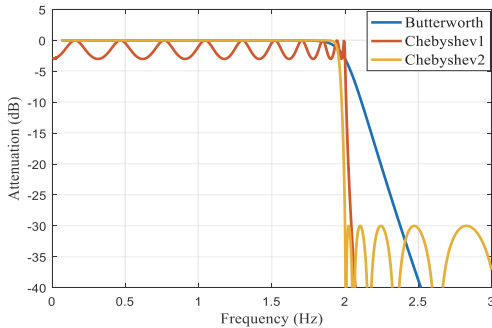


Fig. 2. Step response of the Butterworth and Chebyshev filters.

Fig. 2 shows a comparative analysis of the Butterworth and Chebyshev type I and type II filters for the same tuning parameters. It is evident that the Butterworth filter is flat in its passband interval but has a bad roll-off, which can be fatal for

fault frequencies lying very close to the fundamental component in case of a broken rotor bar. The Chebyshev filters have a very good transition band but have ripples in the passband in case of type I, and stopband in case of type II.

D. Finite Element Method for Motor Simulation

The mathematical modelling and simulations of induction motors are extremely important, as they provide the basis for design and control procedures. The more accurate the mathematical model of the machine is, the more accurate its practical design and control would be. The analytical method is the most common method of modelling found in literature. This method consists in describing the system with the help of integra-differential equations. Analytical models usually neglect the complex nonlinear behaviour of the system to make it simpler. With the increase in computational power, the numerical models such as FEM are gaining more popularity in the field of modelling and simulations. These models are good approximations of an actual system, as they consider all possible parameters, but at the cost of complexity and long computational time. The numerical model of the induction motor relies on the Maxwell's equations:

$$\nabla \times E = -\frac{\partial B}{\partial t}; \quad (9)$$

$$\nabla \times H = J + \frac{\partial D}{\partial t}; \quad (10)$$

$$H = \nu B; \quad (11)$$

$$J = \sigma E, \quad (12)$$

where E is the electric field strength, B is the magnetic flux density, D is displacement current, D is electric flux density, H is the magnetic field strength, J is the current density, ν is the magnetic reluctivity of material and σ is its electric conductivity.

By assuming that the magnetic field lies in an x - y plane, varies sinusoidally in time and induces currents in the z -direction, the vector potential A distributes in the machine according to the following equation [22]:

$$\frac{\partial}{\partial x} \left(\frac{1}{\mu} \right) \frac{\partial A}{\partial x} + \frac{\partial}{\partial y} \left(\frac{1}{\mu} \right) \frac{\partial A}{\partial y} - s \frac{\partial}{\partial t} (\sigma A) + J = 0. \quad (13)$$

If the conductivity of the rotor and stator laminations is taken as zero, and the reluctivity of conducting regions as that of the vacuum, the electric scalar potential and voltage equation of a conductor can be represented as [8]:

$$\nabla \varphi = -\frac{u}{l} e_z, \quad (14)$$

$$u = iR + R \oint \sigma \frac{\partial A_z}{\partial t} \cdot ds. \quad (15)$$

III. SIMULATION RESULTS AND DISCUSSION

The FEM-based simulation of a three-phase induction motor with the parameters shown in Table I is performed under healthy, one, and two broken rotor bar conditions. Since the simulation is performed using 2D field analysis, the ignored end windings are compensated by adding additional resistances and inductances in the series with coils. The per phase stator coils

are series and parallel connections of copper strands making current density uniformly distributed.

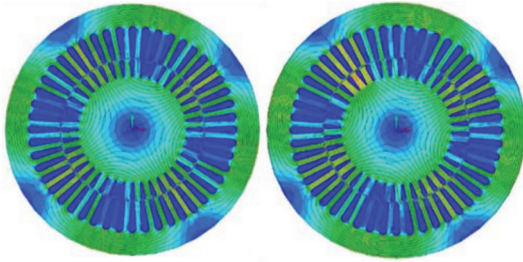


Fig. 3. Normalized magnetic field density of healthy and broken rotor bar motors.

The simulation is performed at rated load under constant speed. The flux distribution under healthy and two broken rotor bar conditions is shown in Fig. 3. It is evident that the flux

density increases across broken bars, putting the adjacent bars under increased magnetic stress. The increase in the current of the neighbouring bars makes the machine vulnerable to breakage of more bars in time, if the fault is not timely diagnosed and repaired.

Fig. 4 shows the motor simulation results for stator currents and frequency spectrum under healthy and broken rotor bar conditions from top to bottom. In the first graph, zoomed stator current is shown, which is calculated using a step size of 0.033 ms at the rated load condition using FEM. The simulation is performed for two seconds with 5328 mesh elements at stator and rotor temperatures of 120 °C and 140 °C, respectively. The current seems distorted because of time and slot harmonics. The second graph represents the positive side of the current and its envelope under two broken bar condition.

The envelope clearly represents the effect of the broken rotor bars and the modulation of the motor current. The ripples in the envelope of the current increase with the increase in the

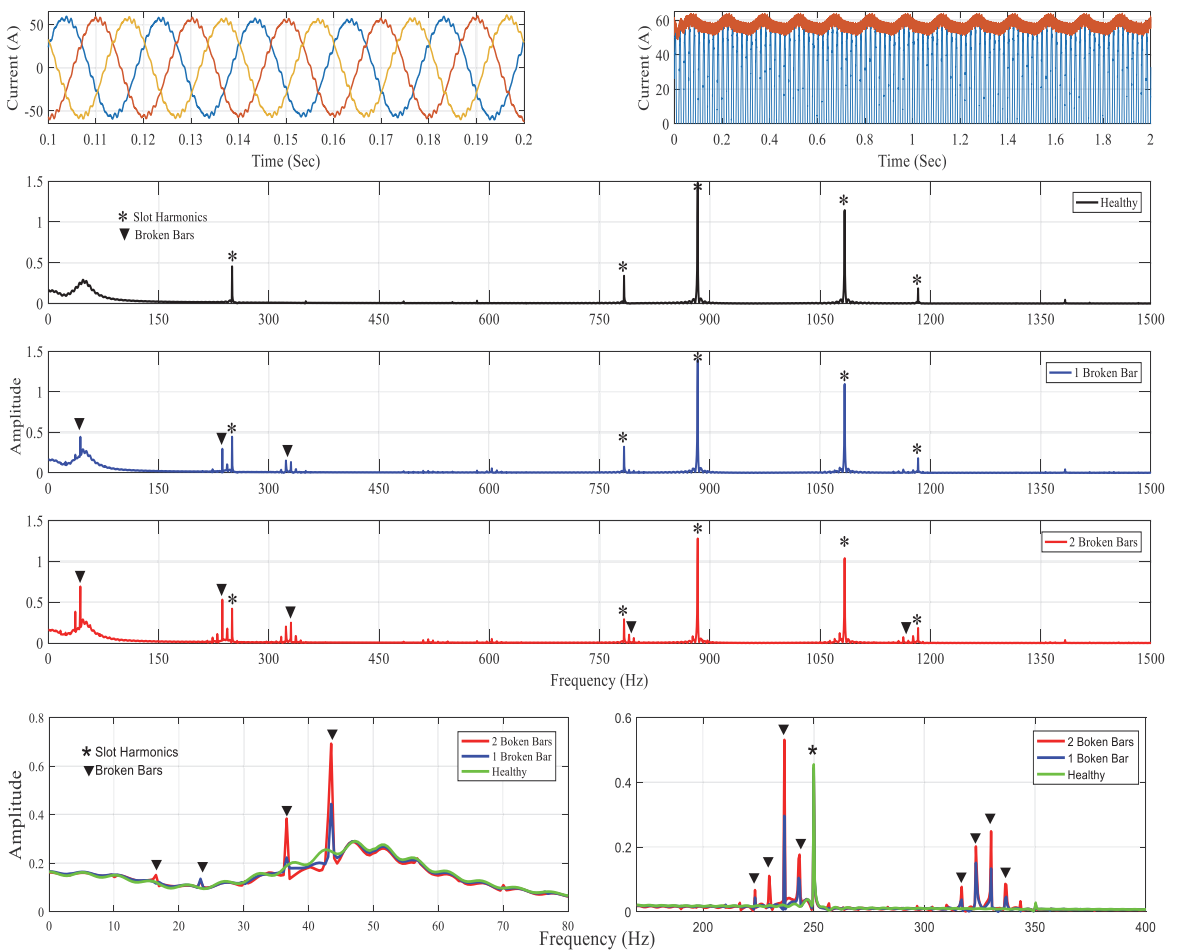


Fig. 4. Simulation results; three phase current in top left, per phase current and its envelope for three broken bars in top right, frequency spectrum for healthy, 1 broken and 2 broken bar cases from top to down; zoomed comparison of harmonics for healthy and faulty motors in bottom two graphs.

modulation index, which depends on the number of broken bars. The distribution of the harmonics in the frequency spectrum of the stator current is shown in the next three graphs for healthy, one broken bar, and two broken bar cases, respectively. The fundamental component of the supply voltage is attenuated, making the spectrum legible on the linear axis. The frequency components can be easily differentiated due to the spatial and broken rotor bar harmonics. In the last two graphs, the frequency spectrums in the range of 0–80 Hz and 170–400 Hz are plotted on the same window for healthy and faulty cases for a comparative analysis. It is clear that the faulty frequencies increase in amplitude with the increase in the number of broken bars.

IV. EXPERIMENTAL SETUP

The measurement setup consists of two same type motors with the parameters shown in Table I. One machine is under investigation and the other one is acting as load. Both machines are mounted on the same mechanical base and coupled through their shafts, as shown in Fig. 5(a). The loading machine is fed through the inverters to improve its controllability for various load levels and the machine under investigation is fed by grid supply containing some harmonics as discussed in results section. The stator currents and voltages are measured using the Dewetron transient recorder. The sampling frequency of the measured signals is 10 000 samples per second and the measurement time is 70 seconds, giving a very good resolution of the frequency spectrum. Fig. 5(b) shows the block diagram of the test setup.

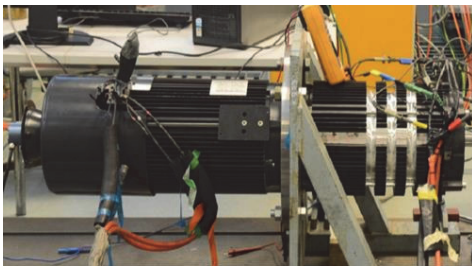
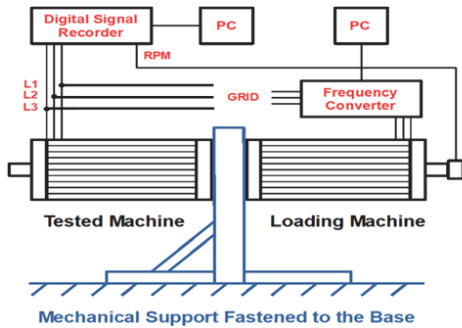


Fig. 5. (a) Experimental setup; (b) Schematic of the experimental setup.

TABLE I
MOTOR PARAMETERS

Parameter	Symbol	Value
Number of poles	P	4
Number of phases	φ	3
Connection	Y- Δ	Star
Stator slots	N_s	48; non-skewed
Rotor slots	N_r	40; non-skewed
Terminal voltage	V	333 V @ 50 Hz
Rated slip	S	0.0667
Rated power	P_r	18 kW @ 50 Hz

V. RESULTS AND DISCUSSION

Fig. 6 shows the cycles of the input phase voltage and the corresponding spectrum. For better visibility of the grid fed harmonics, the fundamental component is attenuated using the proposed filter which removes it effectively without having any influence on the rest of the harmonics.

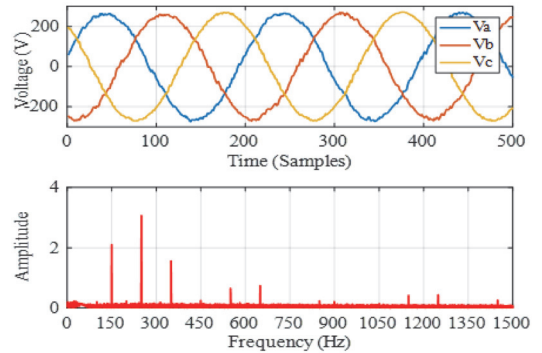


Fig. 6. Grid fed voltage and respective frequency spectrum.

The supply harmonics are mainly odd harmonics and can be represented by the following equation:

$$f_{SH} = k f_s, \quad k = 1, 3, 5, \dots \quad (16)$$

Fig. 7 presents the experimental results. The top two graphs represent the stator three-phase and single-phase currents. The envelope of current is also represented using the Hilbert transform to show the impact of the broken rotor bars. The current is smoother than the current taken from simulation, because the skewness of rotor bars has suppressed the slot harmonics considerably. The next graphs show the frequency spectra for healthy, one, two, and three broken bars, respectively. The fundamental component has been attenuated successfully, making the harmonics discoverable without using the logarithmic scale. It is evident in the results that under healthy condition the only prominent harmonics are supply harmonics, which will be many in case of inverter fed machines. These harmonics can be a misleading factor in diagnostic algorithms if not addressed properly. The last two graphs provide a comparative analysis of all four cases in the same window,

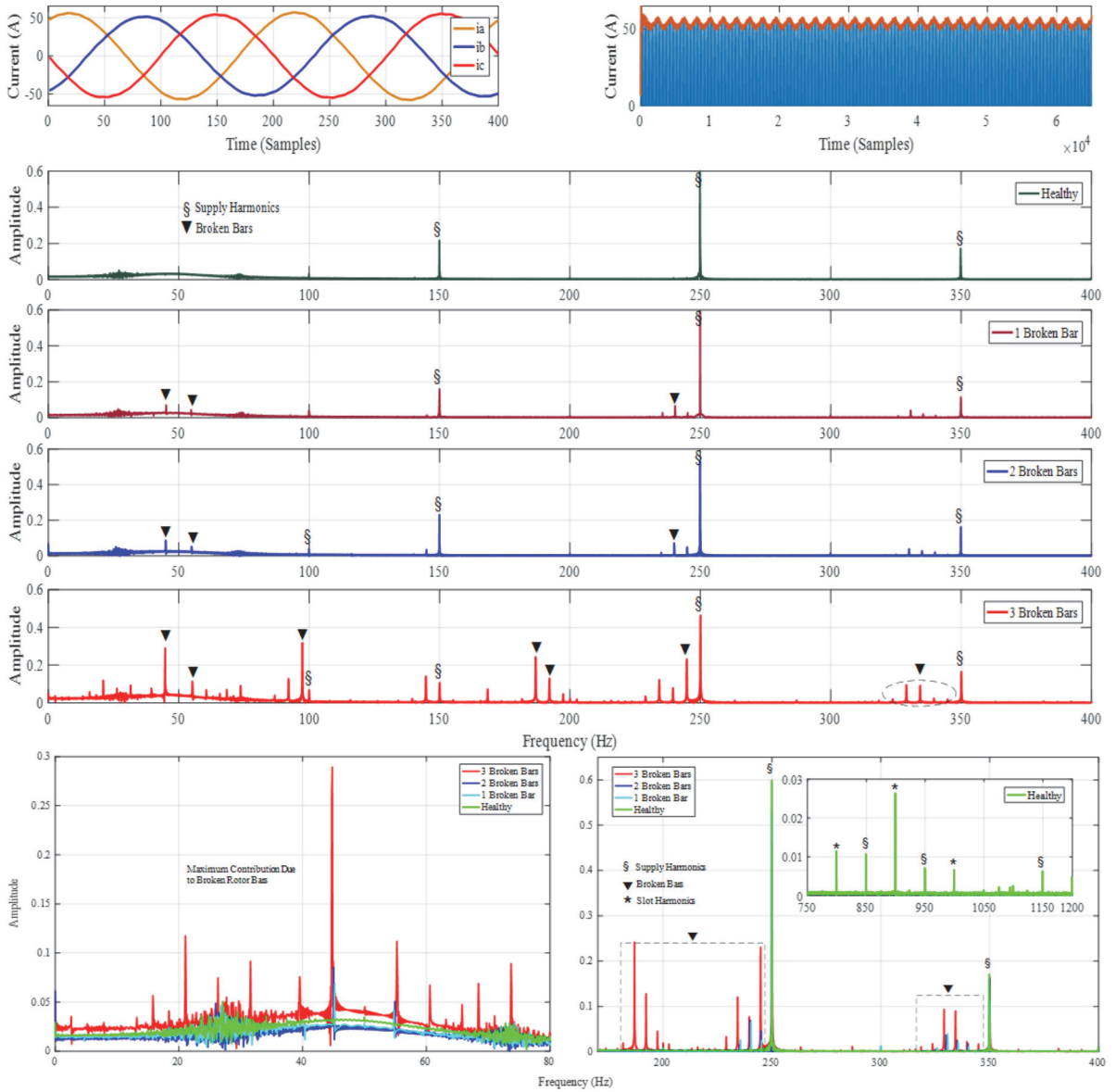


Fig. 7. Experimental results: three phase current – top left, per phase current and its envelope for three broken bars – top right, frequency spectrum for healthy, one, two, and three broken bars cases from top down; zoomed comparison of harmonics for healthy and faulty motors at the bottom.

where it can be seen that the amplitude of the fault harmonics is increasing with the increase in the number of broken bars.

VI. CONCLUSIONS

The MCSA is the most common technique used for fault diagnostics of induction motors, due to its simplicity and non-invasive nature. In this paper, harmonic spectrum of an induction motor for healthy and broken rotor bar cases using signals from the simulation and experiments has been studied.

The FEM based simulations reveal that the rotor bars next to the broken one come under more magnetic and thermal stress making them vulnerable to breakage, increasing the severity of fault with the passage of time. Hence, it is very important for diagnostic algorithm to be able to detect the fault at the incipient stage. The accurate attenuation of the fundamental component can lead to very accurate results.

The use of the Chebyshev filter for the attenuation of the fundamental component reduces its spectral leakage

considerably. This filter has a good transition band and makes less impact on the upper and lower sidebands of the broken rotor bar frequencies. Also, the fewer pass band ripples in case of type II filter reduce the impact of filter on the frequency spectrum.

Since the most powerful component is filtered out, it improves the legibility of the spectrum even at the linear scale. From the simulation results, the broken rotor bar and high frequency slot harmonics are easily readable on the same graph. In case of the experimental setup, since the load motor is supplied from an inverter, hence the slip of test motor is carefully controlled to investigate the location of fault frequencies.

The supply harmonics should be treated carefully, particularly in case of inverter fed machines in order to avoid false fault indications. It can be noticed that the slot harmonics are considerably suppressed by the skewing factor of the rotor.

REFERENCES

- [1] J. Pyrhönen, T. Jokinen, and V. Hrabovcová, *Design of rotating electrical machines*. John Wiley & Sons, Inc., Witshire, 2008.
- [2] H. W. Penrose, "Test Methods for Determining the Impact of Motor Condition on Motor Efficiency and Reliability," PhD Diss., vol. ALL-TEST P, no. LLC, Old Saybrook, CT, pp. 1–8.
- [3] G. R. Bossio, C. H. De Angelo, J. M. Bossio, C. M. Pezzani, and G. O. Garcia, "Separating Broken Rotor Bars and Load Oscillations on IM Fault Diagnosis Through the Instantaneous Active and Reactive Currents," *IEEE Trans. Ind. Electron.*, vol. 56, no. 11, pp. 4571–4580, Nov. 2009. <https://doi.org/10.1109/TIE.2009.2024656>
- [4] A. Soualhi, G. Clerc, and H. Razik, "Detection and Diagnosis of Faults in Induction Motor Using an Improved Artificial Ant Clustering Technique," *IEEE Trans. Ind. Electron.*, vol. 60, no. 9, pp. 4053–4062, Sep. 2013. <https://doi.org/10.1109/TIE.2012.2230598>
- [5] B. Ayhan, H. J. Trussell, Mo-Yuen Chow, and Myung-Hyun Song, "On the Use of a Lower Sampling Rate for Broken Rotor Bar Detection With DTFT and AR-Based Spectrum Methods," *IEEE Trans. Ind. Electron.*, vol. 55, no. 3, pp. 1421–1434, Mar. 2008. <https://doi.org/10.1109/TIE.2007.896522>
- [6] A. Khezgar, M. Y. Kaikaa, M. El Kamel Oumaamar, M. Boucherma, and H. Razik, "On the Use of Slot Harmonics as a Potential Indicator of Rotor Bar Breakage in the Induction Machine," *IEEE Trans. Ind. Electron.*, vol. 56, no. 11, pp. 4592–4605, Nov. 2009. <https://doi.org/10.1109/TIE.2009.2030819>
- [7] M. Malekpour, B. T. Phung, and E. Ambikairajah, "Stator current envelope extraction for analysis of broken rotor bar in induction motors," in *2017 IEEE 11th International Symposium on Diagnostics for Electrical Machines, Power Electronics and Drives (SDEMPED)*, 2017, pp. 240–246. <https://doi.org/10.1109/DEMPED.2017.8062362>
- [8] A. Belahcen, J. Martinez, and T. Vaimann, "Comprehensive computations of the response of faulty cage induction machines," in *2014 International Conference on Electrical Machines (ICEM)*, 2014, pp. 1510–1515. <https://doi.org/10.1109/ICELMACH.2014.6960382>
- [9] S. Nandi, H. A. Toliyat, and X. Li, "Condition Monitoring and Fault Diagnosis of Electrical Motors—A Review," *IEEE Trans. Energy Convers.*, vol. 20, no. 4, pp. 719–729, Dec. 2005. <https://doi.org/10.1109/TEC.2005.847955>
- [10] B. Asad, T. Vaimann, A. Kallaste, and A. Belahcen, "Harmonic Spectrum Analysis of Induction Motor With Broken Rotor Bar Fault," in *2018 IEEE 59th International Scientific Conference on Power and Electrical Engineering of Riga Technical University (RTUCON)*, 2018, pp. 1–7. <https://doi.org/10.1109/RTUCON.2018.8659842>
- [11] R. Puche-Panadero, M. Pineda-Sanchez, M. Riera-Guasp, J. Roger-Folch, E. Hurtado-Perez, and J. Perez-Cruz, "Improved Resolution of the MCSA Method Via Hilbert Transform, Enabling the Diagnosis of Rotor Asymmetries at Very Low Slip," *IEEE Trans. Energy Convers.*, vol. 24, no. 1, pp. 52–59, Mar. 2009. <https://doi.org/10.1109/TEC.2008.2003207>
- [12] M. Pineda-Sanchez, M. Riera-Guasp, J. A. Antonino-Daviu, J. Roger-Folch, J. Perez-Cruz, and R. Puche-Panadero, "Diagnosis of Induction Motor Faults in the Fractional Fourier Domain," *IEEE Trans. Instrum. Meas.*, vol. 59, no. 8, pp. 2065–2075, Aug. 2010. <https://doi.org/10.1109/TIM.2009.2031835>
- [13] M. A. Moussa, M. Boucherma, and A. Khezgar, "A Detection Method for Induction Motor Bar Fault Using Sidelobes Leakage Phenomenon of the Sliding Discrete Fourier Transform," *IEEE Trans. Power Electron.*, vol. 32, no. 7, pp. 5560–5572, Jul. 2017. <https://doi.org/10.1109/TPEL.2016.2605821>
- [14] S. H. Kia, H. Henao, and G.-A. Capolino, "Diagnosis of Broken-Bar Fault in Induction Machines Using Discrete Wavelet Transform Without Slip Estimation," *IEEE Trans. Ind. Appl.*, vol. 45, no. 4, pp. 1395–1404, Jul. 2009. <https://doi.org/10.1109/TIA.2009.2018975>
- [15] S. Singh and N. Kumar, "Detection of Bearing Faults in Mechanical Systems Using Stator Current Monitoring," *IEEE Trans. Ind. Informatics*, vol. 13, no. 3, pp. 1341–1349, Jun. 2017. <https://doi.org/10.1109/TII.2016.2641470>
- [16] M. Kang and J.-M. Kim, "Reliable Fault Diagnosis of Multiple Induction Motor Defects Using a 2-D Representation of Shannon Wavelets," *IEEE Trans. Magn.*, vol. 50, no. 10, pp. 1–13, Oct. 2014. <https://doi.org/10.1109/TMAG.2014.2316474>
- [17] J. R. Cameron, W. T. Thomson, and A. B. Dow, "Vibration and current monitoring for detecting airgap eccentricity in large induction motors," *IEE Proc. B Electr. Power Appl.*, vol. 133, no. 3, p. 155, 1986. <https://doi.org/10.1049/ip-b.1986.0022>
- [18] R. R. Schoen and T. G. Habetler, "Effects of time-varying loads on rotor fault detection in induction machines," *IEEE Trans. Ind. Appl.*, vol. 31, no. 4, pp. 900–906, 1995. <https://doi.org/10.1109/28.395302>
- [19] H. Henao, C. Demian, and G.-A. Capolino, "A frequency-domain detection of stator winding faults in induction machines using an external flux sensor," *IEEE Trans. Ind. Appl.*, vol. 39, no. 5, pp. 1272–1279, Sep. 2003. <https://doi.org/10.1109/TIA.2003.816531>
- [20] A. Sapena-Bano, J. Burriel-Valencia, M. Pineda-Sanchez, R. Puche-Panadero, and M. Riera-Guasp, "The Harmonic Order Tracking Analysis Method for the Fault Diagnosis in Induction Motors Under Time-Varying Conditions," *IEEE Trans. Energy Convers.*, vol. 32, no. 1, pp. 244–256, Mar. 2017. <https://doi.org/10.1109/TEC.2016.2626008>
- [21] J. Milimonfared, H. M. Kelk, S. Nandi, A. D. Minassians, and H. A. Toliyat, "A novel approach for broken-rotor-bar detection in cage induction motors," *IEEE Trans. Ind. Appl.*, vol. 35, no. 5, pp. 1000–1006, 1999. <https://doi.org/10.1109/28.793359>
- [22] N. M. Elkasabgy, A. R. Eastham, and G. E. Dawson, "Detection of broken bars in the cage rotor on an induction machine," *IEEE Trans. Ind. Appl.*, vol. 28, no. 1, pp. 165–171, 1992. <https://doi.org/10.1109/28.120226>



Bilal Asad was born in 1986 in Pakistan. He received his B.Sc. in Electronics Engineering from The Islamia University of Bahawalpur and M.Sc. in Electrical Engineering from the University of Engineering and Technology (UET) Lahore, Pakistan, in 2007 and 2011 respectively. Currently he is a Ph.D. student at the Department of Electrical Power Engineering and Mechatronics, Tallinn University of Technology, Estonia. His area of interest includes design, modelling and fault diagnostics of electrical machines. E-mail: biasad@ttu.ee



Toomas Vaimann received his B.Sc., M.Sc. and Ph.D. degrees in electrical engineering from Tallinn University of Technology, Estonia, in 2007, 2009 and 2014 respectively. He is currently a senior researcher at Tallinn University of Technology, Department of Electrical Power Engineering and Mechatronics. He has been working in several companies as an electrical engineer. He is a member of IEEE, Estonian Society of Moritz Hermann Jacobi and Estonian Society for Electrical Power Engineering. His main research interest is the diagnostics of electrical machines.

E-mail: Toomas.Vaimann@taltech.ee

ORCID iD: <https://orcid.org/0000-0003-0481-5066>



Ants Kallaste received his B.Sc., M.Sc. and Ph.D. degrees in electrical engineering from Tallinn University of Technology, Estonia, in 2004, 2006 and 2013 respectively. He is currently a senior researcher at Tallinn University of Technology, Department of Electrical Power Engineering and Mechatronics. He is holding the position of the Head of Electrical Machines Research Group. He is a member of IEEE and Estonian Society of Moritz Hermann Jacobi. His main research interest is design of electrical machines.

E-mail: Ants.Kallaste@taltech.ee

ORCID iD: <https://orcid.org/0000-0001-6126-1878>



Anton Rassõlkin received Ph.D. degree in electric drives and power electronics from Tallinn University of Technology in 2014. His main research interests are in the field of electric drives and their control systems as well as in the fields of electrical machines and electric transportation. He works as a Research Scientist at the Department of Electrical Power Engineering and Mechatronics at Tallinn University of Technology, Department of Electrical Power Engineering and Mechatronics, Tallinn University of Technology, Ehitajate tee 5, 19086 Tallinn, Estonia.

E-mail: Anton.Rassolkin@taltech.ee

ORCID iD: <https://orcid.org/0000-0001-8035-3970>



Anouar Belahcen received B.Sc. degree in physics from the University Sidi Mohamed Ben Abdellah, Fes, Morocco, in 1988 and M.Sc. (Tech.) and Doctor (Tech.) degrees from Helsinki University of Technology, Finland, in 1998, and 2004, respectively.

He is the professor of electrical machines at Tallinn University of Technology, Estonia and the professor of Energy and Power at Aalto University, Finland.

His research interests are modelling of electrical machines, magnetic materials, coupled magnetic and mechanical problems and magnetostriction.

E-mail: Anouar.Belahcen@taltech.ee

ORCID iD: <https://orcid.org/0000-0003-2154-8692>



M. Naveed Iqbal was born in 1988 in Pakistan. He received his B.Sc. in Electronics Engineering in 2008 from Islamia University of Bahawalpur and M.Sc. degree from University of New South Wales, Australia. He is currently a doctoral student at Tallinn University of Technology. His area of interest includes energy consumption modelling and power quality.

Email: miqbal@ttu.ee

Publication VII

B. Asad, T. Vaimann, A. Kallaste, A. Rassõlkin, A. Belahcen. A Survey of Broken Rotor Bar Fault Diagnostic Methods of Induction Motor. *Electrical, Control and Communication Engineering*, vol. 14 (2), pp. 117–124, Mar. 2019.

A Survey of Broken Rotor Bar Fault Diagnostic Methods of Induction Motor

Bilal Asad (*Ph. D. Student, Tallinn University of Technology, Tallinn, Estonia*),
Toomas Vaimann (*Senior Researcher, Tallinn University of Technology, Tallinn, Estonia*),
Anton Rassõlkin* (*Researcher, Tallinn University of Technology, Tallinn, Estonia*),
Ants Kallaste (*Senior Researcher, Tallinn University of Technology, Tallinn, Estonia*),
Anouar Belahcen (*Professor, Tallinn University of Technology, Tallinn, Estonia*)

Abstract – Electrical machines, induction motors in particular, play a key role in domestic and industrial applications. They act as a work horse in almost every industry and are responsible for a big proportion of total generated electricity consumption worldwide. The faults in induction motors are degenerative in nature and can lead to a catastrophic situation if not diagnosed earlier. The failures can cause considerable financial loss in the form of unexpected downtime. Broken rotor bar is a very common and frequently occurring fault in most of industrial induction motors. To select a better, more accurate and reliable fault diagnostic technique, this paper presents a comprehensive literature survey on the existing motor current signature analysis (MCSA) based fault diagnostic techniques. Different well-known MCSA based fault diagnostic techniques are summarized in the form of basic theories, considering complexity of their implementation, merits and demerits.

Keywords – Fault diagnosis; Induction motors; Rotors.

I. INTRODUCTION

Induction motors are acting as a work horse in domestic and industrial applications because of their high power to weight ratio, rugged structure, low price, easy maintenance and reliability [1]. They play a significant role in about 80% of industries such as transportation, petroleum industries, mining industries, ship propulsion, aerospace, nuclear plants and many other [2].

Because of mechanically moving parts and rough industrial environment, induction machines are always vulnerable to faults. These faults are usually degenerative in nature, i.e. they tend to increase with time. Hence, it is very important to detect them at their early stages to avoid any catastrophic situations like shut down of the entire process [3]. In addition, detection of faults at the early stages gives a lot of advantages like reliability of operation, increased motor life and economic benefits [1]. When motor starts becoming faulty it tends to change some of its parameters, such as mechanical vibrations [4], [5], electromagnetic field distributions [6], [7], temperature [8], stator's current [9]–[11]. Since induction motors are proportionally among the biggest energy consumers worldwide, their proper maintenance and early fault diagnostics will increase efficiency as well. The bar charts in Fig. 1 show energy usage by induction motors in different sectors per hour downtime cost and comparison of rewinding versus recondition

of motors as investigated by [12]. In this paper, the author analyzed a paperboard plan with 485 motors having two operating production lines with an average downtime cost of \$6375 per hour and concluded that preventive maintenance program costs \$73 900 per year and gives a total saving of \$569 360 per year having a payback period of as short as 1.6 months. It is evident considering the figure that induction motors are a major consumer of total generated electricity and can lead to a major economic loss if faults are not timely diagnosed and repaired effectively.

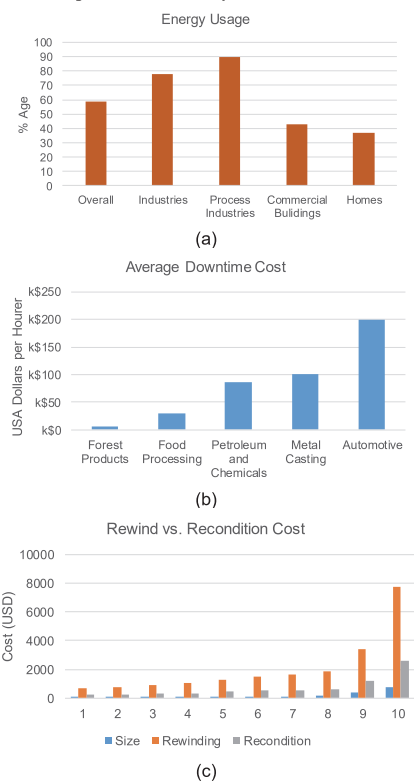


Fig. 1. Worldwide energy usage by electrical machines (a), an average loss due to failures (b) and a comparison of rewind vs. recondition cost (c).

* Corresponding author.
E-mail: Anton.Rassolkin@ttu.ee

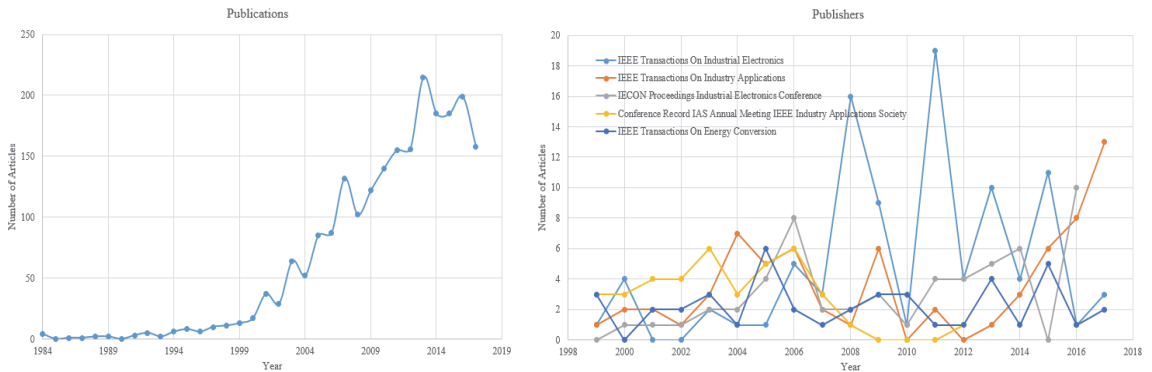


Fig. 2. Importance of fault diagnostics as reflected in the annual scientific research and publications.

It is also claimed in [12] that with preventive maintenance programs total motor rewinds reduced from 85 % to 20 % of the total motor repairs. A lot of research is being done on earlier fault diagnostics of induction motors with regard to the above-mentioned advantages. The graphs shown in Fig. 2 as taken from Scopus describe annual trends in scientific research published each year on fault diagnostics of induction machines.

II. TYPES OF FAULTS AND DIAGNOSTIC TECHNIQUES

A variety of faults found in literature can be divided mainly into three categories as shown in [13] and presented in Table I. Faults in electrical machines can be broadly divided into three categories: electrical, mechanical and external or environmental. Electrical faults are mainly associated with stator side and can be easily detected and controlled using some simple protective devices which can monitor the condition of supply voltage and loading conditions. Moreover, some flexible

AC transmission systems (FACTS) device-based control of various parameters like voltage balancing, reactive power control can also be found in literature [14]. Mechanical faults make a big proportion of overall faults and they are degenerative in nature, i.e. they tend to increase with time. The early diagnosis of these faults is very important in order to avoid any catastrophic situations like shutdown of the entire industry or some portion of industry leading to a major economic loss [15]. These faults are difficult to detect at the early stages, but it is equally important. The main fault diagnosis technique found in literature is mainly associated with signal processing and pattern recognition using motor stator current signal or mechanical vibration signal.

In this paper, some commonly used techniques used for broken rotor bar fault diagnostic of induction machines are reviewed and comparison is done to consider advantages and drawbacks of each technique.

TABLE I
CATEGORIES OF MOST COMMON FAULTS, TYPES AND THEIR DIAGNOSTIC METHODS

Sr. No.	Category	Types	Location of the faults	Common diagnostic methods
1	Electrical	<ul style="list-style-type: none"> Unbalanced supply voltage Over or under voltage Phase reversal Inter-turn short circuit fault Earth fault 	Mainly stator	<ul style="list-style-type: none"> Relays & Switches MCSA
2	Mechanical	<ul style="list-style-type: none"> Broken rotor bar Broken end rings Eccentricity fault Bearing fault Rotor winding failure 	Mainly rotor	<ul style="list-style-type: none"> Mechanical vibration detection MCSA Finite Element Analysis
3	Environmental	<ul style="list-style-type: none"> Ambient temperature External moisture Vibrations due to bad foundation, etc. 	Both	<ul style="list-style-type: none"> Sensors and protective devices

A. Envelope Detection (Hilbert Transform)

Hilbert transform converts a real valued signal into a complex analytical signal. It can be used to find out the envelope of a signal, which is useful in many respects, e.g. in demodulation of an amplitude modulated (AM) signal. It can be considered as a filter which shifts phases of all frequency components of its input signal by $\pi/2$ radians. Implementation strategy of Hilbert transform to get current envelope is shown in Fig. 3.

Mathematically, it can be defined as the convolution of given signal with not integrable function $1/(\pi t)$, as follows,

$$H(t) = \frac{1}{\pi} \int_{-\infty}^{\infty} \frac{f(x)}{t-x} dx. \quad (1)$$

The analytical signal can be obtained as,

$$A(t) = f(t) + jh(t). \quad (2)$$

This can be expressed in polar coordinates as,

$$A(t) = B(t)e^{j\varphi(t)} \quad (3)$$

where $B(t)$ – envelope of analytical signal and φ – phase of analytical signal.

As discussed earlier, the harmonics produced by broken rotor bar (BRB) in stator current spectrum depends on slip. Under very low slip and no-load conditions the frequency of these harmonics becomes very close to the frequency of the fundamental component. This fact makes it very difficult to detect harmonics because of spectral leakage of fundamental one [16]. In other words, those harmonics are usually buried under the spectrum of the fundamental component.

This problem can be solved by using some filters to remove fundamental component. The filters commonly found in literature are notch filters [17], Hilbert transform [16], etc. Some techniques like Hanning window and Bartlett periodogram [18], shifting to DC level [19], quad demodulation [20], Park's vector [21], air gap torque and swing angle [22], [23], etc. have been proposed to avoid this problem. To overcome this problem some literature suggests a minimum percentage of load for experiment. Also, high frequency resolution is required for successful separation of sideband signals. The same kind of problem has also been reported in cases when load changes during the sampling time.

Speed changing devices such as gear boxes also give the same kind of side band frequencies which can be separated by taking a set of two motor current signature analysis (MCSA) tests at entirely different load references. [16] used a simple Hilbert transform to get analytical signal of stator current, found its envelope and by doing its spectral analysis proved that the main frequency component was successfully eliminated, and fault harmonics were clearly readable.

In [16], the number of samples required to get a minimum spectrum resolution of 0.01 was $(5 \cdot 10^5)$ by using the formula $N = T_{mf}$. But [24] proposed a reduced stator current envelope taking only one sample per cycle rather than using high sampling frequencies to reduce aliasing effects in conventional Fourier analysis based techniques. In this paper, the authors used the points at $\theta(t) = 2k\pi$ ($k = 0, 1, \dots$) of current envelope and found that the number of samples required was reduced to (4997) instead of $(5 \cdot 10^5)$ giving similar results. They used a large industrial and a lab-based machine to validate the results and showed that the proposed method is able to segregate fault harmonics from the overall spectrum very efficiently. The authors also claimed that due to a smaller number of samples required, this technique can be easily implemented on simple available computational hardware like digital signal processor (DSP) or field-programmable gate array (FPGA).

In [25], the authors proposed that any fault, such as broken rotor bar, produces a series of harmonics having frequencies integral multiple of fundamental fault component frequency. These harmonics are distributed in the entire frequency spectrum as shown by the following equation for the broken rotor bar.

$$f_{\text{asym}} = f_1 + 2ksf_1, k = \pm 1, \pm 2, \pm 3, \dots, \quad (4)$$

where, $f_{\text{asym}} = f_1 \pm 2sf_1$ is fundamental harmonic component.

It is proposed that if fault current spectrum is taken by considering harmonic order k as an independent variable rather than frequency, the fault can be detected and analyzed more easily and will require less memory and computational power. In the proposed technique the authors took stator current, shifted it to rotor frame of reference, performed its spectrum analysis and rescaled it on harmonic order axis.

The authors also mentioned some drawbacks of this technique, for example, slip should be accurately measured, high frequency resolution is required, and some mechanical vibrations may damage the result.

Fast Fourier transform (FFT) based MCSA successfully gives fault pattern when machine is in the steady state condition but it has certain drawbacks in transient intervals [26]. Some methods like short term Fourier transform (STFT), wavelet transform (WT), Gabor transform (GT) can be regarded as extension of MCSA suitable for transient conditions.

However, the above-mentioned approaches give very complex time frequency patterns. These complex 3D patterns require a huge amount of hardware memory, computational power and trained staff to deal with. In [26], the authors proposed a simplification technique in which firstly they



Fig. 3. Implementation strategy of Hilbert transform to get current envelope.

transformed stator current to rotor side and then obtained a re-scaled spectrogram using harmonic order tracking analysis.

B. Park's Vector Approach

Induction motor models are complex because of their mutual and varying inductances as a function of rotor position, also three circuits are required to represent a three-phase machine. This three-phase model can be transformed into an equivalent two-phase circuit as shown in figure with d_s - q_s as direct and quadrature axis of stator and d_r - q_r as direct and quadrature axis of rotor. Using this approach, the number of circuits and hence the number of equations is reduced but the problem of varying inductances still exists.

In 1920, R. H. Park proposed a technique to resolve this issue by transforming stator variables to a fictitious winding rotating with rotor at synchronous speed, hence made stator inductances static with respect to rotor. Afterward, some other transformations were also proposed, such as H. C. Stanely transformed rotor variables to a fictitious stationary winding,

G. Krone transformed both rotor and stator windings to a fictitious winding rotating with rotating magnetic field.

Since then these transformed models have made a very significant contribution towards modeling [27], analysis [28], drives [29], fault diagnostics [30], [31] and design of various kinds of electrical machines.

Park's vector is a plot between d and q components of machine's rotor or stator currents, voltages or fluxes. For healthy machine, this plot is a perfect circle distributed uniformly across the center, but for faulty machines this pattern changes depending upon the severity of the fault. The modulus of Park's vector is known as extended Park's vector (EPV) in literature, it can be in continuous time [21] or discrete domain [32]. The analysis of this pattern opened new ways in fault diagnostics of induction and some other machines. This technique can be used for fault diagnostics of rotor faults [33], stator winding faults [21]–[34], winding faults in transformers [35], faults in motor drives [36], wind turbines [37], and power converters [38], etc.

TABLE II
DIFFERENT METHODS TO DETECT BROKEN ROTOR BARS IN INDUCTION MOTORS

Technique	Group and assisting techniques		Speed estimation	Mathematical calculations	Memory required	References	Attributes
Active and reactive currents	MCSA	FFT	No	Medium	Medium	[39]	Noninvasive, can segregate load vibration effects
Ant clustering	MCSA	Park's vector, FFT	No	Large	Large	[40]	Noninvasive, difficult to segregate different faults
Autoregressive method	MCSA	DTFT + Notch	No	Low	Low	[2]	Noninvasive, steady state current
Information entropy and fuzzy inference	MCSA	Fuzzy logic	No	Medium	Large	[41]	Noninvasive, requires steady state current
Homogeneity estimation	MCSA	FPGA	No	Low	Medium	[42]	Noninvasive, transient current, segregation of faults is difficult
Slot harmonics	MCSA	FFT	yes	Large	Large	[43]	Noninvasive, unbalanced power supply, speed ripples, segregation of different faults is difficult
Harmonic order tracking	MCSA	Gabor transform	yes	Low	Medium	[26]	Noninvasive, capable to segregate faults and nonstationary conditions
Envelope detection using Hilbert transform	MCSA	Hilbert transform	Yes	Low	Low	[16]	Noninvasive, steady state analysis, segregation of different faults is difficult, problem of varying load conditions
Reduced envelope	MCSA	Hilbert transform	Yes	Low	Low	[24]	Noninvasive, suitable for diagnostic on low slip, suitable to implement on DSP and FPGA kits, Segregation of different faults is difficult
Adoptive notch filter	MCSA	FFT	Yes	Low	Low	[17]	Noninvasive, suitable for diagnostic on low slip, difficult under varying load conditions, Segregation of different faults is difficult
Parameters estimation	MCSA	Analytical	Yes	High	High	[44], [45]	Noninvasive, can be more accurate, under steady state conditions, can be used to segregate faults
Pendulous oscillation	MCSA	Analytical	No	Medium	Low	[22], [23]	Noninvasive, suitable to implement under low slip conditions, under steady state conditions, can be used to segregate faults
Power spectral density	MCSA	STFT, wavelet	No	Medium	Medium	[46]	Noninvasive, suitable to implement under low slip conditions, cab be applied under varying load conditions, can be used to segregate faults, accurate sampling rate and selection of mother wavelet required

Technique	Group and assisting techniques		Speed estimation	Mathematical calculations	Memory required	References	Attributes
Spectrum synch technique	MCSA	Local band synch, central kurtosis analysis	Yes	Medium	Medium	[47]	Noninvasive, suitable to implement under low slip conditions, difficult to implement under varying load conditions, can be used to segregate faults
Zero sequence voltage	MCSA	Analytical	No	High	High	[3]	Noninvasive, suitable for constant load conditions, segregation of different faults is complicated
Wavelet transform	MCSA	Time frequency analysis		Medium	Medium	[48]	Noninvasive, sampling rate and selection of mother wavelet is important, can be used to segregate faults, can be used for varying load conditions

TABLE III
SOME VARIANTS OF PARK'S VECTOR APPROACH

Park's vector (MCSA)	Extended Park's vector	FFT, Gabor transform	No	Medium	Medium	[34], [49]	Noninvasive, suitable under nonstationary load conditions, high sampling rate required, problems of unbalanced power supply
	Double park's vector	FFT	No	Medium	Medium	[50]	Noninvasive, suitable to study various fault conditions, high sampling rate required.
	Reduced modulus of extended Park's vector	FFT	No	Low	Low	[32]	Sampling rate can be reduced, can be implemented on FPGA and DSP kits
	Multiplier Park's vector	FFT	No	Medium	Medium	[51]	Segregation of different faults is difficult

The drawback of conventional extended Park's vector analysis (EPVA) is that all three phase currents are required for its pattern development and FFT analysis. First, samples of all three phase currents are taken with high sampling rate to avoid aliasing and, second, a long acquisition time is required to improve resolution. This may lead to a huge amount of data for processing and analysis, hence making memory and computational power of hardware questionable [32].

In [21], a technique is proposed to reduce the data required for fault diagnosis. It is claimed and sounds good that if samples are taken of one phase only at points where other phases are zero, the results can be as good as for conventional techniques. The authors called this technique reduced Park's vector analysis (RPVA) and claimed that due to less data required for spectrum analysis it can be easily implemented on simple DSP and FPGA kits.

III. CONCLUSION

Conventional MCSA and Park's vector analysis techniques are suitable for fault diagnosis of induction machines operating under steady state conditions, because these techniques are mainly dependent on slip and require exact measurement of speed. [49] proposed a speed sensorless method for BRB fault diagnostic of wound rotor induction motor (WRIM). The authors used Park's vector of modulus of WRIM's rotor current [52] for time frequency (t - f) analysis and proposed a technique of rescaling frequency axis which makes its free from speed measurement, plots the same frequency spectrum and requires less memory and computational power. Based on above analysis and discussion the following conclusions can be made.

- MCSA is the biggest group of most common diagnostic techniques.
- It is easy to understand and implement.
- It requires less computational power.
- All techniques are directly or indirectly dependent on each other providing ample opportunities to exploit the benefits of each other.
- Mainly they rely on the presence of some specific faulty frequencies in the spectrum.
- These faulty frequencies can be misleading if there are some external factors such as bad power source;
- MCSA usually ensures a trade-off between simplicity of algorithm and accuracy of results.
- It becomes problematic if there is more than one fault in the same machine.
- The complexity level increases in case of inverter fed machines.
- It provides a very good platform for the implementation of more advanced techniques such as inverse problem theory, parameter estimation and intelligent techniques.

REFERENCES

- [1] R. H. C. Palacios, I. N. da Silva, A. Goedtel, W. F. Godoy, and T. D. Lopes, "Diagnosis of Stator Faults Severity in Induction Motors Using Two Intelligent Approaches," *IEEE Trans. Ind. Informatics*, vol. 13, no. 4, pp. 1681–1691, Aug. 2017.
<https://doi.org/10.1109/TII.2017.2696978>

- [2] B. Ayhan, H. J. Trussell, M.-Y. Chow, and M.-H. Song, "On the Use of a Lower Sampling Rate for Broken Rotor Bar Detection With DTFT and AR-Based Spectrum Methods," *IEEE Trans. Ind. Electron.*, vol. 55, no. 3, pp. 1421–1434, Mar. 2008. <https://doi.org/10.1109/TIE.2007.896522>
- [3] Z. Hou, J. Huang, H. Liu, M. Ye, Z. Liu, and J. Yang, "Diagnosis of Broken Rotor Bar Fault in Open- and Closed-Loop Controlled Wye-Connected Induction Motors Using Zero-Sequence Voltage," *IET Electr. Power Appl.*, vol. 11, no. 7, pp. 1214–1223, Aug. 2017. <https://doi.org/10.1049/iet-epa.2016.0505>
- [4] Y. Gritli, A. O. Di Tommaso, R. Miceli, C. Rossi, and F. Filippetti, "Diagnosis of Mechanical Unbalance for Double Cage Induction Motor Load in Time-Varying Conditions Based on Motor Vibration Signature Analysis," in *2013 International Conference on Renewable Energy Research and Applications (ICRERA)*, 2013, pp. 1157–1162. <https://doi.org/10.1109/ICRERA.2013.6749927>
- [5] P. Granjon, "Electromagnetic Vibrations Estimation of an Induction Motor by Nonlinear Optimal Filtering," in *2005 5th IEEE International Symposium on Diagnostics for Electric Machines, Power Electronics and Drives*, 2005, pp. 1–5. <https://doi.org/10.1109/DEMPED.2005.4662508>
- [6] L. Weili, X. Ying, S. Jiafeng, and L. Yingli, "Finite-Element Analysis of Field Distribution and Characteristic Performance of Squirrel-Cage Induction Motor With Broken Bars," *IEEE Trans. Magn.*, vol. 43, no. 4, pp. 1537–1540, Apr. 2007. <https://doi.org/10.1109/TMAG.2006.892086>
- [7] R. Fiser and S. Ferkolj, "Application of a Finite Element Method to Predict Damaged Induction Motor Performance," *IEEE Trans. Magn.*, vol. 37, no. 5, pp. 3635–3639, 2001. <https://doi.org/10.1109/20.952679>
- [8] D. Lopez-Perez and J. Antonino-Daviu, "Application of Infrared Thermography to Failure Detection in Industrial Induction Motors: Case Studies," *IEEE Trans. Ind. Appl.*, vol. 53, no. 3, pp. 1901–1908, May 2017. <https://doi.org/10.1109/TIA.2017.2655008>
- [9] J. Antonino-Daviu, A. Quijano-Lopez, V. Clemente-Alarcon, and C. Garin-Abellan, "Reliable Detection of Rotor Winding Asymmetries in Wound Rotor Induction Motors via Integral Current Analysis," *IEEE Trans. Ind. Appl.*, vol. 53, no. 3, pp. 2040–2048, May 2017. <https://doi.org/10.1109/TIA.2017.2672524>
- [10] Y. Park, M. Jeong, S. Bin Lee, J. A. Antonino-Daviu, and M. Teska, "Influence of Blade Pass Frequency Vibrations on MCSA-Based Rotor Fault Detection of Induction Motors," *IEEE Trans. Ind. Appl.*, vol. 53, no. 3, pp. 2049–2058, May 2017. <https://doi.org/10.1109/TIA.2017.2672526>
- [11] M. Drif, H. Kim, J. Kim, S. Bin Lee, and A. J. M. Cardoso, "Active and Reactive Power Spectra-Based Detection and Separation of Rotor Faults and Low-Frequency Load Torque Oscillations," *IEEE Trans. Ind. Appl.*, vol. 53, no. 3, pp. 2702–2710, May 2017. <https://doi.org/10.1109/TIA.2016.2613508>
- [12] H. W. Penrose, "Test Methods for Determining the Impact of Motor Condition on Motor Efficiency and Reliability," Ph. D. Diss., vol. ALL-TEST P, no. LLC, Old Saybrook, CT, pp. 1–8.
- [13] S. Karmakar, S. Chattopadhyay, M. Mitra, and S. Sengupta, *Induction Motor Fault Diagnosis: Approach Through Current Signature Analysis*, 1st ed.
- [14] M. Heydari and N. Mariun, "Assessment of Different Voltage Sags on Performance of Induction Motors Operated With Shunt FACTS," in *2012 3rd Power Electronics and Drive Systems Technology (PEDSTC)*, 2012, pp. 483–489.
- [15] T. Vaimann, A. Belahcen, and A. Kallaste, "Necessity for Implementation of Inverse Problem Theory in Electric Machine Fault Diagnosis," in *2015 IEEE 10th International Symposium on Diagnostics for Electrical Machines, Power Electronics and Drives (SDEMPED)*, 2015, pp. 380–385. <https://doi.org/10.1109/DEMPED.2015.7303718>
- [16] R. Puche-Panadero, M. Pineda-Sanchez, M. Riera-Guasp, J. Roger-Folch, E. Hurtado-Perez, and J. Perez-Cruz, "Improved Resolution of the MCSA Method via Hilbert Transform, Enabling the Diagnosis of Rotor Asymmetries at Very Low Slip," *IEEE Trans. Energy Convers.*, vol. 24, no. 1, pp. 52–59, Mar. 2009. <https://doi.org/10.1109/TEC.2008.2003207>
- [17] M. Malekpour, B. T. Phung, and E. Ambikairajah, "Stator Current Envelope Extraction for Analysis of Broken Rotor Bar in Induction Motors," in *2017 IEEE 11th International Symposium on Diagnostics for Electrical Machines, Power Electronics and Drives (SDEMPED)*, 2017, pp. 240–246. <https://doi.org/10.1109/DEMPED.2017.8062362>
- [18] G. Didier, H. Razik, O. Caspary, and E. Tarnisien, "Rotor Cage Fault Detection in Induction Motor Using Global Modulation Index on the Instantaneous Power Spectrum," in *4th IEEE International Symposium on Diagnostics for Electric Machines, Power Electronics and Drives (SDEMPED)*, 2003, pp. 104–109. <https://doi.org/10.1109/DEMPED.2003.1234555>
- [19] D. Matić, F. Kulić, M. Pineda-Sánchez, and I. Kamenko, "Support Vector Machine Classifier for Diagnosis in Electrical Machines: Application to Broken Bar," *Expert Syst. Appl.*, vol. 39, no. 10, pp. 8681–8689, Aug. 2012. <https://doi.org/10.1016/j.eswa.2012.01.214>
- [20] A. Bellini, "Quad Demodulation: A Time-Domain Diagnostic Method for Induction Machines," *IEEE Trans. Ind. Appl.*, vol. 45, no. 2, pp. 712–719, 2009. <https://doi.org/10.1109/TIA.2009.2013593>
- [21] S. Das, P. Purkait, C. Koley, and S. Chakravorti, "Performance of a Load-Immune Classifier for Robust Identification of Minor Faults in Induction Motor Stator Winding," *IEEE Trans. Dielectr. Electr. Insul.*, vol. 21, no. 1, pp. 33–44, Feb. 2014. <https://doi.org/10.1109/DEI.2013.003549>
- [22] B. Mirafzal and N. A. O. Demerdash, "Induction Machine Broken-Bar Fault Diagnosis Using the Rotor Magnetic Field Space-Vector Orientation," *IEEE Trans. Ind. Appl.*, vol. 40, no. 2, pp. 534–542, Mar. 2004. <https://doi.org/10.1109/TIA.2004.824433>
- [23] B. Mirafzal and N. A. O. Demerdash, "Effects of Load Magnitude on Diagnosing Broken Bar Faults in Induction Motors Using the Pendulous Oscillation of the Rotor Magnetic Field Orientation," *IEEE Trans. Ind. Appl.*, vol. 41, no. 3, pp. 771–783, 2005. <https://doi.org/10.1109/TIA.2005.847315>
- [24] A. Sapena-Baño, M. Pineda-Sanchez, R. Puche-Panadero, J. Martinez-Roman, and Ž. Kanović, "Low-Cost Diagnosis of Rotor Asymmetries in Induction Machines Working at a Very Low Slip Using the Reduced Envelope of the Stator Current," *IEEE Trans. Energy Convers.*, vol. 30, no. 4, pp. 1409–1419, 2015. <https://doi.org/10.1109/TEC.2015.2445216>
- [25] A. Sapena-Bano et al., "Harmonic Order Tracking Analysis: A Novel Method for Fault Diagnosis in Induction Machines," *IEEE Trans. Energy Convers.*, vol. 30, no. 3, pp. 833–841, Sep. 2015. <https://doi.org/10.1109/TEC.2015.2416973>
- [26] A. Sapena-Bano, J. Burriel-Valencia, M. Pineda-Sanchez, R. Puche-Panadero, and M. Riera-Guasp, "The Harmonic Order Tracking Analysis Method for the Fault Diagnosis in Induction Motors Under Time-Varying Conditions," *IEEE Trans. Energy Convers.*, vol. 32, no. 1, pp. 244–256, Mar. 2017. <https://doi.org/10.1109/TEC.2016.2626008>
- [27] B. K. Bose, *Modern Power Electronics and AC Drives*. Prentice Hall, 2002.
- [28] E. P. Cornell and T. A. Lipo, "Modeling and Design of Controlled Current Induction Motor Drive Systems," *IEEE Trans. Ind. Appl.*, vol. IA-13, no. 4, pp. 321–330, Jul. 1977. <https://doi.org/10.1109/TIA.1977.4503414>
- [29] S. A. Odhano, R. Bojoi, A. Boglietti, S. G. Rosu, and G. Griva, "Maximum Efficiency per Torque Direct Flux Vector Control of Induction Motor Drives," *IEEE Trans. Ind. Appl.*, vol. 51, no. 6, pp. 4415–4424, Nov. 2015. <https://doi.org/10.1109/TIA.2015.2448682>
- [30] A. J. Marques Cardoso and E. S. Saraiva, "On-Line Diagnostics of Three-Phase Induction Motors by Park's Vector.pdf," in *ICEM*, 1988, pp. 231–234.
- [31] A. J. Marques Cardoso and E. S. Saraiva, "On-Line Diagnostics of Current Source Inverter Fed Induction Machines by Park's Vector Approach," in *ICEM*, 1990, pp. 1000–1005.
- [32] J. Perez-Cruz, R. Puche-Panadero, M. Pineda-Sanchez, M. Riera-Guasp, J. Martinez-Roman, and A. Sapena-Bano, "Cost-Effective On-Line Fault Diagnosis of Induction Motors Using the Reduced Modulus of the Current Park's Vector," in *2017 IEEE 11th International Symposium on Diagnostics for Electrical Machines, Power Electronics and Drives (SDEMPED)*, 2017, pp. 427–433. <https://doi.org/10.1109/DEMPED.2017.8062390>
- [33] S. M. A. Cruz, A. J. Marques Cardoso, "Rotor Cage Fault Diagnosis in Three-Phase Induction Motors by Extended Park's Vector Approach," *Electr. Mach. Power Syst.*, vol. 28, no. 4, pp. 289–299, Apr. 2000. <https://doi.org/10.1080/073135600268261>
- [34] S. M. A. Cruz and A. J. M. Cardoso, "Stator Winding Fault Diagnosis in Three-Phase Synchronous and Asynchronous Motors, by the Extended Park's Vector Approach," *IEEE Trans. Ind. Appl.*, vol. 37, no. 5, pp. 1227–1233, 2001. <https://doi.org/10.1109/28.952496>
- [35] F. Haghighi and M. Mostafaei, "Flux-Based Turn-to-Turn Fault Protection for Power Transformers," *IET Gener. Transm. Distrib.*, vol. 10, no. 5, pp. 1154–1163, Apr. 2016. <https://doi.org/10.1049/iet-gtd.2015.0738>

- [36] I. Bandyopadhyay, S. Das, P. Purkait, P. P. Das, and C. Koley, "Application of Wavelet Transform to Identify Faulty IGBTs in 3-Phase Induction Motor Drives," in *proc. 2014 International Conference on Control, Instrumentation, Energy and Communication (CIEC)*, 2014, pp. 296–300. <https://doi.org/10.1109/CIEC.2014.6959097>
- [37] N. M. A. Freire, J. O. Estima, and A. J. Marques Cardoso, "Open-Circuit Fault Diagnosis in PMSG Drives for Wind Turbine Applications," *IEEE Trans. Ind. Electron.*, vol. 60, no. 9, pp. 3957–3967, Sep. 2013. <https://doi.org/10.1109/TIE.2012.2207655>
- [38] S. M. A. Cruz, A. M. S. Mendes, and M. B. Abadi, "Fault Diagnostic Algorithm for Three-Level Neutral Point Clamped AC Motor Drives, Based on the Average Current Park's Vector," *IET Power Electron.*, vol. 7, no. 5, pp. 1127–1137, May 2014. <https://doi.org/10.1049/iet-pel.2013.0416>
- [39] G. R. Bossio, C. H. De Angelo, J. M. Bossio, C. M. Pezzani, and G. O. Garcia, "Separating Broken Rotor Bars and Load Oscillations on IM Fault Diagnosis Through the Instantaneous Active and Reactive Currents," *IEEE Trans. Ind. Electron.*, vol. 56, no. 11, pp. 4571–4580, Nov. 2009. <https://doi.org/10.1109/TIE.2009.2024656>
- [40] A. Soualhi, G. Clerc, and H. Razik, "Detection and Diagnosis of Faults in Induction Motor Using an Improved Artificial Ant Clustering Technique," *IEEE Trans. Ind. Electron.*, vol. 60, no. 9, pp. 4053–4062, Sep. 2013. <https://doi.org/10.1109/TIE.2012.2230598>
- [41] R. J. Romero-Troncoso et al., "FPGA-Based Online Detection of Multiple Combined Faults in Induction Motors Through Information Entropy and Fuzzy Inference," *IEEE Trans. Ind. Electron.*, vol. 58, no. 11, pp. 5263–5270, 2011. <https://doi.org/10.1109/TIE.2011.2123858>
- [42] R. A. Lizarraga-Morales, C. Rodriguez-Donate, E. Cabal-Yepez, M. Lopez-Ramirez, L. M. Ledesma-Carrillo, and E. R. Ferrucho-Alvarez, "Novel FPGA-Based Methodology for Early Broken Rotor Bar Detection and Classification Through Homogeneity Estimation," *IEEE Trans. Instrum. Meas.*, vol. 66, no. 7, pp. 1760–1769, 2017. <https://doi.org/10.1109/TIM.2017.2664520>
- [43] A. Khezziar, M. Y. Kaikaa, M. El Kamel Oumaamar, M. Boucherma, and H. Razik, "On the Use of Slot Harmonics as a Potential Indicator of Rotor Bar Breakage in the Induction Machine," *IEEE Trans. Ind. Electron.*, vol. 56, no. 11, pp. 4592–4605, Nov. 2009. <https://doi.org/10.1109/TIE.2009.2030819>
- [44] S. Bachir, S. Tnani, J.-C. Trigeassou, and G. Champenois, "Diagnosis by Parameter Estimation of Stator and Rotor Faults Occurring in Induction Machines," *IEEE Trans. Ind. Electron.*, vol. 53, no. 3, pp. 963–973, Jun. 2006. <https://doi.org/10.1109/TIE.2006.8742258>
- [45] K. Yong-Hwa, Y. Young-Woo, H. Don-Ha, S. Jong-Ho, and K. Dong-Sik, "High-Resolution Parameter Estimation Method to Identify Broken Rotor Bar Faults in Induction Motors," *Ind. Electron. IEEE Trans.*, vol. 60, no. 9, pp. 4103–4117, 2013. <https://doi.org/10.1109/TIE.2012.2227912>
- [46] J. Cusido Cusido, L. Romeral, J. a. Ortega, J. a. Rosero, and A. Garcia Espinosa, "Fault Detection in Induction Machines Using Power Spectral Density in Wavelet Decomposition," *IEEE Trans. Ind. Electron.*, vol. 55, no. 2, pp. 633–643, 2008. <https://doi.org/10.1109/TIE.2007.911960>
- [47] D. Z. Li, W. Wang, and F. Ismail, "A Spectrum Synch Technique for Induction Motor Health Condition Monitoring," *IEEE Trans. Energy Convers.*, vol. 30, no. 4, pp. 1348–1355, Dec. 2015. <https://doi.org/10.1109/TEC.2015.2454440>
- [48] A. Sapena-Bano, M. Pineda-Sanchez, R. Puche-Panadero, J. Martinez-Roman, and D. Matic, "Fault Diagnosis of Rotating Electrical Machines in Transient Regime Using a Single Stator Current's FFT," *IEEE Trans. Instrum. Meas.*, vol. 64, no. 11, pp. 3137–3146, Nov. 2015. <https://doi.org/10.1109/TIM.2015.2444240>
- [49] A. Sapena-Bano, M. Riera-Guasp, R. Puche-Panadero, J. Martinez-Roman, J. Perez-Cruz, and M. Pineda-Sanchez, "Harmonic Order Tracking Analysis: A Speed-Sensorless Method for Condition Monitoring of Wound Rotor Induction Generators," *IEEE Trans. Ind. Appl.*, vol. 52, no. 6, pp. 4719–4729, Nov. 2016. <https://doi.org/10.1109/TIA.2016.2597134>
- [50] T. G. Vilhakar, M. S. Ballal, and H. M. Suryawanshi, "Application of Double Park's Vector Approach for Detection of Inter-Turn Fault in Induction Motor," in *2015 International Conference on Condition Assessment Techniques in Electrical Systems (CATCON)*, 2015, pp. 173–178. <https://doi.org/10.1109/CATCON.2015.7449529>
- [51] J. Burriel-Valencia, A. Sapena-Bano, M. Pineda-Sanchez, and J. Martinez-Roman, "Multilayer Park's Vector Approach, a Method for Fault Detection on Induction Motors," in *2015 IEEE International Conference on Industrial Technology (ICIT)*, 2015, pp. 775–780. <https://doi.org/10.1109/ICIT.2015.7125192>
- [52] B. Asad, T. Vaimann, A. Belahcen, and A. Kallaste, "Broken Rotor Bar Fault Diagnostic of Inverter Fed Induction Motor Using FFT, Hilbert and Park's Vector Approach," in *2018 XIII International Conference on Electrical Machines (ICEM)*, 2018, pp. 2352–2358. <https://doi.org/10.1109/ICELMACH.2018.8506957>



Bilal Asad was born in 1986 in Pakistan. He received his B.sc. in Electronics Engineering from The Islamia University of Bahawalpur and M. sc. in Electrical Engineering from University of Engineering and Technology (UET) Lahore, Pakistan, in 2007 and 2011 respectively. Currently he is a Ph. D. student in the Department of Electrical Power Engineering and Mechatronics, Tallinn University of Technology, Estonia. His area of interest includes design, modeling and fault diagnostics of electrical machines. E-mail: biasad@ttu.ee



Toomas Vaimann received his B. sc., M. sc. and Ph. D. degrees in electrical engineering from Tallinn University of Technology, Estonia, in 2007, 2009 and 2014 respectively. He is currently a senior researcher in Tallinn University of Technology, Department of Electrical Power Engineering and Mechatronics. He has been working in several companies as an electrical engineer. He is the member of IEEE, Estonian Society of Moritz Hermann Jacobi and Estonian Society for Electrical Power Engineering. His main research interest is the diagnostics of electrical machines.

E-mail: Toomas.Vaimann@taltech.ee

ORCID id: <https://orcid.org/0000-0003-0481-5066>



Anton Rassolkina received Ph. D. degree in electric drives and power electronics from Tallinn University of Technology in 2014. His main research interests are in the field of electric drives and their control systems as well as in the fields of electrical machines and electric transportation. He works as a Research Scientist at the Department of Electrical Power Engineering and Mechatronics at Tallinn University of Technology. Department of Electrical Power Engineering and Mechatronics, Tallinn University of Technology, Ehitajate tee 5, 19086 Tallinn, Estonia.

E-mail: Anton.Rassolkina@taltech.ee

ORCID id: <https://orcid.org/0000-0001-8035-3970>



Ants Kallaste received his B. sc., M. sc. and Ph. D. degrees in electrical engineering from Tallinn University of Technology, Estonia, in 2004, 2006 and 2013 respectively. He is currently a senior researcher at Tallinn University of Technology, Department of Electrical Power Engineering and Mechatronics. He is holding the position of Head of Electrical Machines Research Group. He is the member of IEEE and Estonian Society of Moritz Hermann Jacobi. His main research interest is design of electrical machines.

E-mail: Ants.Kallaste@taltech.ee

ORCID id: <https://orcid.org/0000-0001-6126-1878>



Anouar Belahcen received the B. sc. degree in physics from the University Sidi Mohamed Ben Abdellah, Fes, Morocco, in 1988 and the M. sc. (Tech.) and Doctor (Tech.) degrees from Helsinki University of Technology, Finland, in 1998, and 2004, respectively.

He is the professor of electrical machines at Tallinn University of Technology, Estonia and the professor of Energy and Power at Aalto University, Finland.

His research interests are modeling of electrical machines, magnetic materials, coupled magnetic and mechanical problems and magnetostriction.

E-mail: Anouar.Belahcen@taltech.ee

ORCID iD: <https://orcid.org/0000-0003-2154-8692>

Publication VIII

B. Asad, T. Vaimann, A. Kallaste, A. Rassõlkin, A. Belahcen. Review of Electrical Machine Diagnostic Methods Applicability in the Perspective of Industry 4.0. *Electrical, Control, and Communication Engineering*, vol. 14 (2), pp. 108–116, Mar. 2019.

Review of Electrical Machine Diagnostic Methods Applicability in the Perspective of Industry 4.0

Bilal Asad (*Ph. D. Student, Tallinn University of Technology, Tallinn, Estonia*),
Toomas Vaimann* (*Senior Researcher, Tallinn University of Technology, Tallinn, Estonia*),
Anton Rassõlkin (*Researcher, Tallinn University of Technology, Tallinn, Estonia*),
Ants Kallaste (*Senior Researcher, Tallinn University of Technology, Tallinn, Estonia*),
Anouar Belahcen (*Professor, Tallinn University of Technology, Tallinn, Estonia*)

Abstract – Digitalization of the industrial sector and Industry 4.0 have opened new horizons in many technical fields, including electrical machine diagnostics and operation, as well as machine condition monitoring. This paper addresses a selection of electrical machine diagnostics methods that are applicable for the use in the perspective of Industry 4.0, to be used in hand with cloud environments and the possibilities granted by the Internet of Things. The need for further research and development in the field is pointed out. Some potentially applicable future approaches are presented.

Keywords – Fault diagnosis; Induction motors; Inverse problems.

I. INTRODUCTION

It is claimed that with preventive maintenance programs total motor revinds reduced from 85 % to 20 % of the total motor repairs [1]. Moreover, the proper, reliable, accurate and efficient fault diagnostic techniques are becoming more and more essential as the world is moving towards Industry 4.0 standard. Industry 4.0 is the next industrial revolution, which is taking place. This industrial revolution has been preceded by three other industrial revolutions in the history of mankind [2].

The first revolution was the era of mechanical engineering, it started in the middle of the 18th century and intensified throughout the 19th century. During the second revolution, electrification and scientific management, known as

Taylorism, evolved. The invention and implementation of advanced electronics and information technology initiated the third revolution at around the 1970s, which is now called the Digital Revolution. The term “Industry 4.0” was proposed by the German government in 2011 at the Hannover Fair. The architecture first recommended by the Industry 4.0 Working Group is based on three components: The internet of things (IoT), cyber physical systems (CPS) and smart factories [2]. The detailed description of different industrial revolutions is presented in Fig. 1.

Industry 4.0 standards are promising due to their advantages, which include the increase in industrial efficiency because of the decrease in labor and increase in automation of the processes. It will accelerate industrial processes; deeper understanding of both product and process design will bring more innovation in the industry, and the costumers will get better services due to availability of deep information. After the initial investment, Industry 4.0 will lead to lowering the costs because of fewer human related manufacturing problems and lower operating costs. All these advantages will lead the manufacturer towards increasing revenues.

It goes without saying that with such massive change of the paradigm in the industrial sector, different technical fields also have to change and adapt in order to be applicable within the new concept of industry. The diagnostics and condition monitoring of electrical machines is one of these fields.

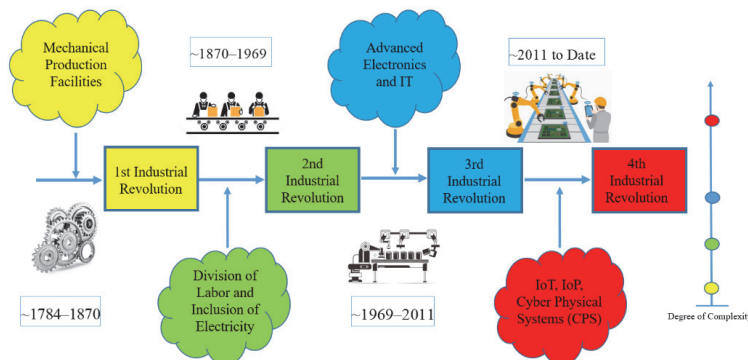


Fig. 1. Trends of industrial revolutions.

* Corresponding author.
E-mail: toomas.vaimann@taltech.ee

II. CONVENTIONAL TECHNIQUES

The key role played by the induction motors in the industry has made its condition monitoring very important. A variety of fault diagnostic techniques can be found in the relevant literature, such as the intelligent techniques, chemical analysis, acoustic measurements, infrared recognition, radio frequency emission, motor current signature analysis (MCSA), mechanical vibration signal analysis, etc. [3] Out of all main diagnostic areas, the MCSA is gaining more and more popularity, because most of its variants require only a clamp meter to detect the stator's current. In addition, almost all MCSA based diagnostic techniques are non-invasive in nature, making them suitable for online fault diagnostics without any disturbance in the process, also requiring less computational cost [4]. However, with the development of Industry 4.0 standards and cloud computing, the benefits of inverse problem theory, parameter estimation and artificial intelligent techniques can be exploited. In the following sections, an overview of some well-known conventional and advanced techniques is presented in the perspective of their pros and cons for fault diagnostics of induction motors.

A. Notch Filter

The notch filter is a band stop filter and can be used to attenuate fundamental component having high energy spectrum as compared to sideband harmonics due to the broken rotor bar. A general second order band pass filter (BPS) can be represented by the following transfer function [5],

$$BPF(s) = \frac{k\omega_0 s}{s^2 + k\omega_0 s + \omega_0^2} \quad (1)$$

and

$$NF(s) = 1 - BPF(s). \quad (2)$$

The authors of [5] proposed a modified adaptive notch filter, named the second order generalized integrator adoptive notch filter (SOGI-ANF), which is capable of rejecting DC offset from the quadrature signal. This DC offset can result in the errors in drives and phase lock loop used for synchronization purposes, etc. The proposed filter can be represented by the following equations:

$$\dot{x}_0 = k_0 \omega e, \quad (3)$$

$$\dot{x}_1 = -\omega x_2 + k \omega e, \quad (4)$$

$$\dot{x}_2 = \omega x_1, \quad (5)$$

$$\dot{\omega} = -\gamma e x_2, \quad (6)$$

where e is the error between actual and estimated signal, x_0 is the DC offset signal, k and γ are the positive valued constants controlling different performance parameters, such as accuracy and convergence speed. A complete analysis of the improved second order generalized integrator-based quadrature signal generator (SOGI-QSG) can be found in [6].

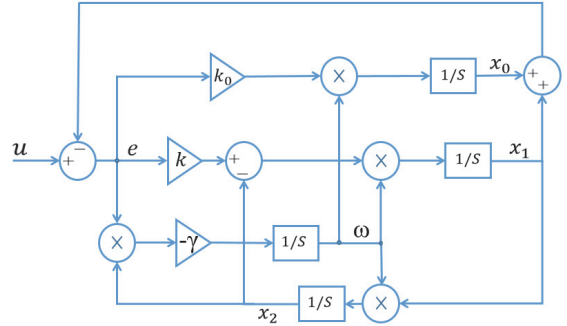


Fig. 2. Schematic diagram of the notch filter.

The authors of [7] used the second order generalized integrator-adaptive notch filter (SOGI-ANF) for envelope detection of stator currents both in the steady state and transient intervals. The author claimed the SOGI-ANF to be more accurate than Hilbert transform because of its adaptive nature. In [8] it is proposed that the sampling rate can be reduced by using digital notch filter with discrete time Fourier transform (DTFT) along with auto regressive spectrum analysis method.

B. ESPRIT and MUSIC

Estimation of signal parameters via rotational invariant technique (ESPRIT) was first proposed by R. Roy *et al.* [9]–[12]. It is a technique to estimate the parameters of cisoids (complex sinusoids) observed in noise. As opposed to Pisarenko's algorithm, which was designed to deal with uniformly sampled data [13], ESPRIT is equally applicable to non-uniformly sampled data. Later on, the multiple signal classification (MUSIC) [14] algorithm generalized Pisarenko's method by relaxing the uniform sampling restriction.

The authors of [15] used ESPRIT for the analysis of the modulus of the analytical signal (envelope signal). The authors claimed that the frequency domain and frequency-time domain analysis techniques, such as FFT, subdivision FFT, zoom FFT and discrete wavelet approach (DWT), are inefficient for fault diagnosis because of limitations like spectral leakage of fundamental component. Moreover, to get high resolution, measurement time needs to be increased, which means that the steady state condition required for FFT analysis will not exist in reality. This spectral leakage problem can be removed by using Hilbert transform as in [16], but the conflict between measurement time and resolution becomes a problem. For high resolution, a long measurement time (100 s in [16]) is required, which may lead to speed and slip variations. To eliminate the above-mentioned problems, [15] used Hilbert transform in conjunction with estimation of signal parameters via rotational invariance technique (ESPRIT) rather than FFT.

The main objective of many signal processing techniques is to find out the set of parameters upon which the signal depends, such as the maximum likelihood (ML) [17] proposed by Capon, and maximum entropy [18] proposed by Burg. Pisarenko extended these techniques to get further benefits by removing some limitations, such as sensitivity. Later, Schmidt developed a complete model to obtain a reasonable solution in the

presence of noise. The resulting algorithm is known as MUSIC and is used in literature extensively for signal processing. More precisely, MUSIC is an extension of Pisarenko's algorithm and it can estimate frequency contents of a signal using the eigenspace method.

The authors in [19] used the MUSIC algorithm along with the discrete resampling method to compute the time frequency response of motor's stator current having one broken rotor bar (BRB) at different load conditions. They claimed that this approach can give a better resolution and is feasible to detect BRB at a very low slip, under transient conditions and in inverter fed machines.

The authors of [20] used high resolution spectral analysis techniques, also known as subspace techniques, i.e. MUSIC and ESPRIT, for detection of bearing and BRB related faults of the induction motor. The proposed method was accomplished in four steps: model order selection, frequency estimation, amplitude estimation and fault severity criterion. In [1], the authors proposed Spectral-MUSIC or Root-Music for frequency estimation of a faulty machine. In [21] spectral MUSIC and finite impulse response filter bank were used to separate the original current and vibration signals into different fault related bandwidths. This technique can be used for BRB and bearing fault detection of the induction motor. The author of [22] used the short time MUSIC algorithm to get high resolution time-frequency pseudo representation for BRB detection. A modified version of MUSIC algorithm, based on fault characteristic frequencies, has been proposed in [23], as well as amplitude estimator and fault indicator has been derived for fault severity measurement.

C. Speed Sensorless Methods (Magnetic Field Space Vector Orientation)

In the majority of MCSA based fault diagnosis schemes of induction motors, speed or slip estimation is a fundamental element of diagnostics, because the fault harmonic frequencies are directly related to the slip. The accurate measurement of slip or speed may produce errors whether it is sensors-based measurement or mathematical equations-based estimation.

The authors of [8] proposed a method to diagnose rotor broken bars based on rotor magnetic field space vector orientation. The authors used the stator current and voltage to compute and observe the rotor magnetic field orientation and showed that with BRB, the rotor's magnetic field orientation shifts at some angle from its actual position at any particular time. The magnitude of this angle depends on the number of broken rotor bars. Moreover, they proved that as time t progresses, the rotor's MMF will be continuously changing and its magnetic field orientation vector will start swinging around the actual magnetic axis of the healthy machine. The authors claimed that it is a good method to detect BRB faults even at very low slip conditions.

In [24], the authors have investigated the effect of load changes on pendulous oscillations of the rotor magnetic field orientation. In [25] slip independent BRB fault diagnostic technique using discrete wavelet approach was proposed and the authors claimed that the squared stator current magnitude and the squared stator current space vector magnitude are good indicators of fault in low frequency bandwidth. The authors of [26] proposed a novel differential magnetic field measurement

(DMFM) method by placing two measurement coils in the stator of a motor and calculating the potential difference between both. In a healthy machine, the potential difference was found to be zero, because the same voltage is generated in both coils, but under faulty conditions, the induced voltages are different, which gives a value of some potential difference. Stator transient current was used in [27] and the authors studied its homogeneity as the classification index. The author used the field programmable gate array (FPGA) for online homogeneity estimation, because of its suitability for rapid prototyping, high performance and low cost as claimed.

D. Wavelet Approach

Fourier transform converts a signal from time domain to the frequency domain, or, in other words, it decomposes the signal into sine and cosine functions having different frequencies and extending till infinity. This leads to a problem of resolution just like Heisenberg's uncertainty principle, that is, when one tries to be sure about time, s/he will increase uncertainty in the frequency and vice versa. Unlike the Fourier transform, wavelet transform decomposes a signal into wavelets of the same shape but different in scale being added together and gives the time frequency analysis of the signal. The wavelets are short waves, which quickly die after appearance unlike sine and cosines of the Fourier transform. There are many types of wavelets used for the signal decomposition but most common are Haar, Shannon, Gaussian, Biorthogonal and Mexican Hat, etc. Due to the problems of poor resolution and spectral leakage in the Fourier transform, wavelet approach is used extensively in literature for fault diagnostics of the induction motors. A continuous wavelet transform can be represented by the following formula;

$$x_w(\alpha, \beta) = \frac{1}{\sqrt{a}} \int_{-\infty}^{\infty} x(t) \varphi\left(\frac{t-b}{a}\right) dt, \quad (7)$$

where b is the shift of the mother wavelet in time, a is the scaling factor, $\frac{1}{\sqrt{a}}$ ensures energy normalization and $\varphi(t)$ is called the mother wavelet, its purpose is to generate daughter wavelets, which are simply translated and shifted versions of the mother wavelet.

Discrete wavelet transform can be represented as,

$$i[n] = A_k[n] + \sum_{j=1}^k D_j[n] = \sum_{i=1}^{N/2^k} a_i^k \varphi_i^k[n] + \sum_{j=1}^k \sum_{i=1}^{N/2^j} d_i^j \psi_i^j[n], \quad (8)$$

where φ^k and ψ^k are the scaling factor and the mother wavelet at level k and j , respectively.

Paper [28] proposed a method to detect BRB by doing transient analysis of the motor startup currents using the wavelet approach. In [29], BRB diagnostics using wavelet under varying load conditions is proposed in a specific frequency band. The authors of [30] applied the discrete wavelet transform on instantaneous reactive power of BRB fault baring induction motor, operating under the time varying load conditions. In [31], stationary wavelet transform (SWT) was used and the authors claimed that the drawback of the invariant translation as mentioned in [32] can be avoided using SWT, rather than the discrete wavelet transform (DWT). The authors further used three modular neural networks (MNN) for fault classifications. The first MNN is used to detect the supply unbalances, sudden load changes, under voltage and stator

phase faults, etc. The second one is used to identify the stator winding phase faults and the third one is used to classify stator inter-turn faults.

In [33], a 2-D wavelet transformation based on Shannon mother wavelet is used and it is claimed that this approach is more efficient for analysis of non-stationary and non-deterministic vibration signals. The created 2-D gray level images are used to generate global neighborhood structure maps to extract global image features. The authors compared the proposed approach with five conventional algorithms, proposed by [34]–[38], and proved that the proposed technique is better in terms of accuracy. The authors claimed that the proposed technique is equally accurate in noiseless and noisy environment.

The authors in [39] proposed a model based fault diagnostic system, in which the measured stator current is compared with the estimated current using actual speed and voltage. The model uses recurrent dynamic neural networks for transient response prediction. The estimated and actual current signals are then analyzed using the wavelet transform to segregate different harmonic frequencies. The accuracy of the model is very much dependent on the accuracy of the healthy machine model.

In [28], DWT was used for transient analysis of motor startup current to get the characteristic component. This continuous valued signal is then converted into discrete signal and an intelligent icon-like approach is applied to condense the relative information into a representation that can be easily manipulated by the nearest neighbor classifier. The tests are carried out for perfectly broken bar case only where there is no contribution of other faults or some external factors. [40] proposed a technique called the discrete harmonic wavelet transform (DHWWT) to perform analysis of stator current in the transient regime with the cost of a single FFT. The author claimed that this technique is capable to eliminate the inherent drawbacks of DWT, such as dependency of sampling rate and frequency bands, spectral leakage due to non-ideal nature of filters, and computation cost.

III. ADVANCED TECHNIQUES

As the computational power of computers is increasing day by day, the researchers are focusing on the implementation of advanced fault diagnostic techniques. These techniques may contain some artificial intelligence-based algorithms, such as neural networks [41], [42] and Fuzzy Logic [43], etc., or some analytical algorithms, such as the finite element analysis [44]–[47] and the inverse problem theory [48]. Unlike conventional forward model-based fault diagnostic techniques, these advanced algorithms can lead to more precise and accurate results, but at the same time they require more sophisticated hardware for implementation.

The authors of [46] used the time-stepping coupled finite element state space (TSCFE-SS) model for predictive non-invasive BRB fault diagnosis of the induction motor. The authors used the model to predict characteristic frequency

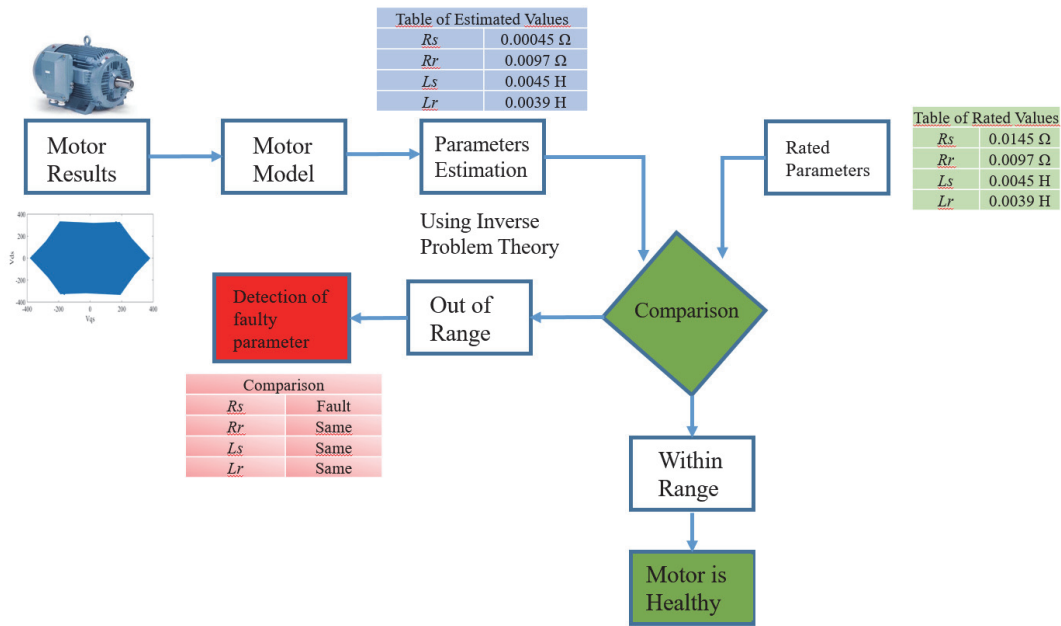
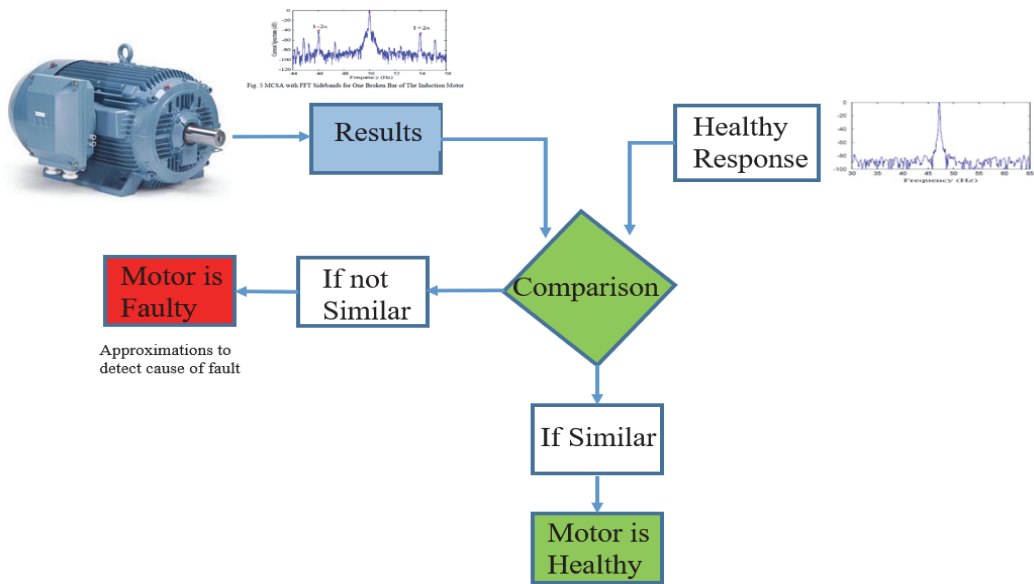
component, which can be used to diagnose rotor bar and connector breakages. [44] used TSCFE-SS model and time series data mining technique for detection and categorization of dynamic/static eccentricities and bar/end-ring connector breakages in squirrel-cage induction motors. In [49], the author used a commercial finite element package to simulate the BRB faults. The simulation results were then compared with the experimental results to validate the model. In [50], the author used time-stepping coupled finite-element approach for BRB fault diagnostics. [51] presented a study on the feature signatures for the induction motor internal faults by utilizing coupled circuit-FEM and DWT. The motor behavior was investigated under both sinusoidal and non-sinusoidal voltage supplies.

Artificial neural networks (ANN) are computing systems mimicking the brain to analyze and learn a specific task without *a priori* knowledge and task specific programming. In the field of machine fault diagnostics, the researchers are trying to implement ANN as artificial intelligent technique to get better and more precise results. In [52] the authors use ANN to prove the possibility of fault detection through smartphone recorded sound files. [41] proposed ANN along with wavelet packet decomposition (WPD) for detection of BRB and claimed that this method is better in accuracy, exact measurement of slip is not required, and diagnostics can be performed with reduced load conditions.

In [42] the authors claimed that multiple discriminant analysis (MDA) and artificial neural networks (ANNs) provide appropriate environments to develop BRB fault-detection schemes because of their multi-input processing capabilities. The authors have proposed that multiple signature processing is more efficient than single signature processing. In [53], the authors proposed a novel approach to detect and classify the comprehensive fault conditions of induction motors using a hybrid fuzzy min-max (FMM) neural network and classification and regression tree (CART) and claimed that the hybrid model, known as FMM-CART, exploits the advantages of both FMM and CART for data classification and rule extraction problems. Successful implementation of these advanced schemes can offer a promising solution for fault diagnostics but at the cost of the required high computational power and storage memory.

IV. INVERSE PROBLEM THEORY

In almost all fault diagnostics techniques mentioned above, the forward problem is used. In the forward problem theory, one usually moves from the input towards the output as shown in Fig. 3. In conventional techniques of fault diagnostics, the current signature of machine is compared with the current signature of the healthy machine using some signal processing techniques or algorithms, as discussed earlier. Since there are many types of faults and every fault can change the pattern of the current signature, the conventional techniques are not good enough to get to the root cause of the fault.



The process of parameter estimation using the system model and data from a set of observations (output in case of forward model) is called the inverse problem theory [48]. Successful implementation of this approach can lead us to the approximation of the faulty parameter of motor, as shown in Fig. 4.

Inverse problem theory has been implemented in various fields like medical sciences [54], geosciences [55], disaster preparedness of infrastructure, signal processing [56] and electrical machine design. [57]–[62] used the inverse problem theory to determine the magnetic induction in the air gap of a machine by measuring the external magnetic field. In [63], inverse problem theory is used to determine the magnetic material characteristics of a wound field synchronous machine. It was shown that the magnetization characteristic can be constructed using core loss and no-load curve measurements.

The author claimed that this method is applicable even without any prior knowledge of magnetization curves, if parameter ranges can be defined by some other means. In [64] the inverse problem theory is used in conjunction with neural networks for optimal design of the switched reluctance motor. The authors of [65] used the inverse problem approach to evaluate the homogenized electromagnetic and thermal characteristics of stator winding of asynchronous motor.

In Table I, a comparison of some advanced fault diagnostic techniques is presented and the main attributes are highlighted.

V. CONCLUSIONS

Below, the authors of the given paper propose some solutions for electrical machine diagnostics in the context of Industry 4.0. In the light of above-presented discussion, the following key points can be highlighted.

- The main objective of almost all fault diagnostic techniques available in literature is the reduction of computational cost in terms of hardware.
- This leads to a trade-off between simplicity of the algorithm and the accuracy of results.
- The conventional, so-called harmonic analysis techniques fail to give a complete picture of the faults in the presence of some other harmonics due to some secondary internal or external factors.
- The picture becomes even more blurred when there are more than one kind of faults or there are some external noise factors, i.e. the segregation of faults is almost impossible.
- Most of techniques are always vulnerable to wrong fault alarms.
- The coming trends of cloud computing and IoT in Industry 4.0 have considerably contributed to solving the problems related to hardware.
- The algorithms are no longer needed to be implemented in DSP kits or just in drives besides the motor.
- The diagnostic algorithms can be placed and solved in some powerful hardware anywhere in the world using cloud computing.
- Unlike forward diagnostic techniques, inverse problem theory can give a very good picture of faults in terms of parametric values rather than harmonics, etc.
- Almost every kind of complicated diagnostic algorithms can be implemented without any need for simplification.

TABLE I
SOME ADVANCED FAULT DIAGNOSTIC TECHNIQUES

Technique	Group and Assisting Techniques		Speed Estimation	Mathematical Calculations	Memory Required	References	Attributes
Sliding mode observer	MCSA + analytical	FFT	No	High	High	[66]–[68]	Noninvasive. Can be used for faults segregation. Difficult to implement under varying load conditions
Datamining	MCSA	Wavelet	No	High	High	[69], [70]	Noninvasive. Can be used for faults segregation
Fuzzy Logic, Neuro-Fuzzy	MCSA	FFT + ANFIS	Yes	High	High	[71], [72]	Noninvasive. Can be used for faults segregation. Sophisticated hardware required
Neural Network	MCSA	WPD	Yes	High	High	[41], [42]	Noninvasive. No need for exact measurement of slip, high accuracy, can be problematic under increasing fault situations and segregation of various faults.
Kalman Filter	MCSA + analytical	State estimation	Yes	High	High	[68]	Noninvasive, dependent on accuracy of the system model, the complexity of states estimation increases with the increase in different types of faults.

REFERENCES

- [1] M. E. H. Benbouzid, M. Vieira, and C. Theys, "Induction Motors' Faults Detection and Localization Using Stator Current Advanced Signal Processing Techniques," *IEEE Trans. Power Electron.*, vol. 14, no. 1, pp. 14–22, 1999. <https://doi.org/10.1109/63.737588>
- [2] M. Hermann, T. Pentek, and B. Otto, "Design Principles for Industrie 4.0 Scenarios," in *2016 49th Hawaii International Conference on System Sciences (HICSS)*, 2016, pp. 3928–3937. <https://doi.org/10.1109/hicss.2016.488>
- [3] S. Nandi, H. A. Toliyat, and X. Li, "Condition Monitoring and Fault Diagnosis of Electrical Motors—A Review," *IEEE Trans. Energy Convers.*, vol. 20, no. 4, pp. 719–729, Dec. 2005. <https://doi.org/10.1109/tec.2005.847955>
- [4] B. Asad, T. Vaimann, A. Belahcen, and A. Kallaste, "Broken Rotor Bar Fault Diagnostic of Inverter Fed Induction Motor Using FFT, Hilbert and Park's Vector Approach," in *2018 XIII International Conference on Electrical Machines (ICEM)*, 2018, pp. 2352–2358.
- [5] M. Karimi-Ghartemani, S. A. Khajehoddin, P. K. Jain, A. Bakhshai, and M. Mojiri, "Addressing DC Component in PLL and Notch Filter Algorithms," *IEEE Trans. Power Electron.*, vol. 27, no. 1, pp. 78–86, Jan. 2012. <https://doi.org/10.1109/tpe.2011.2158238>
- [6] Z. Xin, X. Wang, Z. Qin, M. L. Lu, P. C. Loh, and F. Blaabjerg, "An Improved Second-Order Generalized Integrator Based Quadrature Signal Generator," *IEEE Trans. Power Electron.*, vol. 31, no. 12, pp. 8068–8073, Dec. 2016. <https://doi.org/10.1109/tpe.2016.2576644>
- [7] M. Malekpour, B. T. Phung, and E. Ambikairajah, "Stator Current Envelope Extraction for Analysis of Broken Rotor Bar in Induction Motors," in *2017 IEEE 11th International Symposium on Diagnostics for Electrical Machines, Power Electronics and Drives (SDMPED)*, 2017, pp. 240–246. <https://doi.org/10.1109/sdmped.2017.8062393>
- [8] B. Mirafzal and N. A. O. Demerdash, "Induction Machine Broken-Bar Fault Diagnosis Using the Rotor Magnetic Field Space-Vector Orientation," *IEEE Trans. Ind. Appl.*, vol. 40, no. 2, pp. 534–542, Mar. 2004. <https://doi.org/10.1109/tia.2004.824433>
- [9] R. Roy, A. Paulraj, and T. Kailath, "ESPRIT—A Subspace Rotation Approach to Estimation of Parameters of Cissoids in Noise," *IEEE Trans. Acoust.*, vol. 34, no. 5, pp. 1340–1342, Oct. 1986. <https://doi.org/10.1109/tassp.1986.1164935>
- [10] R. Roy and T. Kailath, "ESPRIT-Estimation of Signal Parameters via Rotational Invariance Techniques," *IEEE Trans. Acoust.*, vol. 37, no. 7, pp. 984–995, Jul. 1989. <https://doi.org/10.1109/29.32276>
- [11] B. Ottersten, M. Viberg, and T. Kailath, "Performance Analysis of the Total Least Squares ESPRIT Algorithm," *IEEE Trans. Signal Process.*, vol. 39, no. 5, pp. 1122–1135, May 1991. <https://doi.org/10.1109/9.78.80967>
- [12] X.-D. Zhang and Y.-C. Liang, "Pre-filtering-Based ESPRIT for Estimating Sinusoidal Parameters in Non-Gaussian ARMA Noise," *IEEE Trans. Signal Process.*, vol. 43, no. 1, pp. 349–353, 1995. <https://doi.org/10.1109/78.365327>
- [13] V. F. Pisarenko, "The Retrieval of Harmonics from a Covariance Function," *Geophys. J. Int.*, vol. 33, no. 3, pp. 347–366, Sep. 1973. <https://doi.org/10.1111/j.1365-246X.1973.tb03424.x>
- [14] R. Schmidt, "Multiple Emitter Location and Signal Parameter Estimation," *IEEE Trans. Antennas Propag.*, vol. 34, no. 3, pp. 276–280, Mar. 1986. <https://doi.org/10.1109/TAP.1986.1143830>
- [15] B. Xu, L. Sun, L. Xu, and G. Xu, "Improvement of the Hilbert Method via ESPRIT for Detecting Rotor Fault in Induction Motors at Low Slip," *IEEE Trans. Energy Convers.*, vol. 28, no. 1, pp. 225–233, Mar. 2013. <https://doi.org/10.1109/tec.2012.2236557>
- [16] R. Puche-Panadero, M. Pineda-Sanchez, M. Riera-Guaspa, J. Roger-Folch, E. Hurtado-Perez, and J. Perez-Cruz, "Improved Resolution of the MCSA Method via Hilbert Transform, Enabling the Diagnosis of Rotor Asymmetries at Very Low Slip," *IEEE Trans. Energy Convers.*, vol. 24, no. 1, pp. 52–59, Mar. 2009. <https://doi.org/10.1109/tec.2008.2003207>
- [17] E. Elbouchikhi, V. Choqueuse, and M. Benbouzid, "Induction Machine Bearing Faults Detection Based on a Multi-Dimensional MUSIC Algorithm and Maximum Likelihood Estimation," *ISA Trans.*, vol. 63, pp. 413–424, 2016. <https://doi.org/10.1016/j.isatra.2016.03.007>
- [18] S. Pan, T. Han, A. C. C. Tan, and T. R. Lin, "Fault Diagnosis System of Induction Motors Based on Multiscale Entropy and Support Vector Machine with Mutual Information Algorithm," *Shock Vib.*, vol. 2016, no. January, 2016. <https://doi.org/10.1155/2016/5836717>
- [19] T. A. Garcia-Calva, D. Morinigo-Sotelo, and R. De Jesus Romero-Troncoso, "Non-Uniform Time Resampling for Diagnosing Broken Rotor Bars in Inverter-Fed Induction Motors," *IEEE Trans. Ind. Electron.*, vol. 64, no. 3, pp. 2306–2315, 2017. <https://doi.org/10.1109/TIE.2016.2619318>
- [20] Y. Trachi, E. Elbouchikhi, V. Choqueuse, and M. E. H. Benbouzid, "Induction Machines Fault Detection Based on Subspace Spectral Estimation," *IEEE Trans. Ind. Electron.*, vol. 63, no. 9, pp. 5641–5651, Sep. 2016. <https://doi.org/10.1109/TIE.2016.2570741>
- [21] A. Garcia-Perez, R. de J. Romero-Troncoso, E. Cabal-Yepez, and R. A. Osornio-Rios, "The Application of High-Resolution Spectral Analysis for Identifying Multiple Combined Faults in Induction Motors," *IEEE Trans. Ind. Electron.*, vol. 58, no. 5, pp. 2002–2010, May 2011. <https://doi.org/10.1109/TIE.2010.2051398>
- [22] A. Garcia-Perez, R. J. Romero-Troncoso, E. Cabal-Yepez, R. A. Osornio-Rios, J. de J. Rangel-Magdaleno, and H. Miranda, "Startup Current Analysis of Incipient Broken Rotor Bar in Induction Motors Using High-Resolution Spectral Analysis," in *8th IEEE Symposium on Diagnostics for Electrical Machines, Power Electronics & Drives*, 2011, pp. 657–663. <https://doi.org/10.1109/DEMPED.2011.6063694>
- [23] E. H. El Bouchikhi, V. Choqueuse, M. Benbouzid, and J. F. Charpentier, "Induction Machine Fault Detection Enhancement Using a Stator Current High Resolution Spectrum," in *38th Annual Conference on IEEE Industrial Electronics Society (IECON 2012)*, 2012, pp. 3913–3918. <https://doi.org/10.1109/IECON.2012.6389267>
- [24] B. Mirafzal and N. A. O. Demerdash, "Effects of Load Magnitude on Diagnosing Broken Bar Faults in Induction Motors Using the Pendulous Oscillation of the Rotor Magnetic Field Orientation," *IEEE Trans. Ind. Appl.*, vol. 41, no. 3, pp. 771–783, 2005. <https://doi.org/10.1109/TIA.2005.847315>
- [25] S. H. Kia, H. Henao, and G.-A. Capolino, "Diagnosis of Broken-Bar Fault in Induction Machines Using Discrete Wavelet Transform Without Slip Estimation," *IEEE Trans. Ind. Appl.*, vol. 45, no. 4, pp. 1395–1404, Jul. 2009. <https://doi.org/10.1109/TIA.2009.2018975>
- [26] A. Elez, S. Car, S. Tvoric, and B. Vaseghi, "Rotor Cage and Winding Fault Detection Based on Machine Differential Magnetic Field Measurement (DMFM)," *IEEE Trans. Ind. Appl.*, vol. 53, no. 3, pp. 3156–3163, May 2017. <https://doi.org/10.1109/TIA.2016.2636800>
- [27] R. A. Lizarraga-Morales, C. Rodriguez-Donate, E. Cabal-Yepez, M. Lopez-Ramirez, L. M. Ledesma-Carrillo, and E. R. Ferrucho-Alvarez, "Novel FPGA-Based Methodology for Early Broken Rotor Bar Detection and Classification Through Homogeneity Estimation," *IEEE Trans. Instrum. Meas.*, vol. 66, no. 7, pp. 1760–1769, Jul. 2017. <https://doi.org/10.1109/TIM.2017.2664520>
- [28] P. Karvelis, G. Georgoulas, I. P. Tsoumas, J. A. Antonino-Daviu, V. Climente-Alarcon, and C. D. Stylios, "A Symbolic Representation Approach for the Diagnosis of Broken Rotor Bars in Induction Motors," *IEEE Trans. Ind. Informatics*, vol. 11, no. 5, pp. 1028–1037, Oct. 2015. <https://doi.org/10.1109/TII.2015.2463680>
- [29] P. Shi, Z. Chen, Y. Vagapov, and Z. Zouaoui, "A New Diagnosis of Broken Rotor Bar Fault Extent in Three Phase Squirrel Cage Induction Motor," *Mech. Syst. Signal Process.*, vol. 42, no. 1–2, pp. 388–403, Jan. 2014. <https://doi.org/10.1016/j.ymssp.2013.09.002>
- [30] K. Yahia, A. J. Marques Cardoso, A. Ghoggal, and S.-E. Zouzou, "Induction Motors Broken Rotor Bars Diagnosis Through the Discrete Wavelet Transform of the Instantaneous Reactive Power Signal under Time-Varying Load Conditions," *Electr. Power Components Syst.*, vol. 42, no. 7, pp. 682–692, May 2014. <https://doi.org/10.1080/15325008.2014.890966>
- [31] N. R. Devi, D. V. S. S. Siva Sarma, and P. V. Ramana Rao, "Diagnosis and Classification of Stator Winding Insulation Faults on a Three-Phase Induction Motor Using Wavelet and MNN," *IEEE Trans. Dielectr. Electr. Insul.*, vol. 23, no. 5, pp. 2543–2555, Oct. 2016. <https://doi.org/10.1109/TDEI.2016.7736811>
- [32] T. Hong, M. T. C. Fang, and D. Hilder, "PD Classification by a Modular Neural Network Based on Task Decomposition," *IEEE Trans. Dielectr. Electr. Insul.*, vol. 3, no. 2, pp. 207–212, Apr. 1996. <https://doi.org/10.1109/94.486772>
- [33] M. Kang and J.-M. Kim, "Reliable Fault Diagnosis of Multiple Induction Motor Defects Using a 2-D Representation of Shannon Wavelets," *IEEE Trans. Magn.*, vol. 50, no. 10, pp. 1–13, Oct. 2014. <https://doi.org/10.1109/TMAG.2014.2316474>

- [34] J. Zarei, "Induction Motors Bearing Fault Detection Using Pattern Recognition Techniques," *Expert Syst. Appl.*, vol. 39, no. 1, pp. 68–73, Jan. 2012. <https://doi.org/10.1016/j.eswa.2011.06.042>
- [35] C. Rodriguez-Donate, R. Romero-Troncoso, E. Cabal-Yepez, A. Garcia-Perez, and R. Osornio-Rios, "Wavelet-Based General Methodology for Multiple Fault Detection on Induction Motors at the Startup Vibration Transient," *J. Vib. Control*, vol. 17, no. 9, pp. 1299–1309, Aug. 2011. <https://doi.org/10.1177/1077546310379141>
- [36] Y. Lei, Z. He, and Y. Zi, "Application of an Intelligent Classification Method to Mechanical Fault Diagnosis," *Expert Syst. Appl.*, vol. 36, no. 6, pp. 9941–9948, Aug. 2009. <https://doi.org/10.1016/j.eswa.2009.01.065>
- [37] V. T. Do and U.-P. Chong, "Signal Model-Based Fault Detection and Diagnosis for Induction Motors Using Features of Vibration Signal in Two-Dimension Domain," *Strojniški Vestn. – J. Mech. Eng.*, vol. 57, no. 09, pp. 655–666, Sep. 2011. <https://doi.org/10.5545/sv-jme.2010.162>
- [38] P. E. William and M. W. Hoffman, "Identification of Bearing Faults Using Time Domain Zero-Crossings," *Mech. Syst. Signal Process.*, vol. 25, no. 8, pp. 3078–3088, Nov. 2011. <https://doi.org/10.1016/j.ymssp.2011.06.001>
- [39] Kyusung Kim and A. G. Parlos, "Induction Motor Fault Diagnosis Based on Neuropredictors and Wavelet Signal Processing," *IEEE/ASME Trans. Mechatronics*, vol. 7, no. 2, pp. 201–219, Jun. 2002. <https://doi.org/10.1109/TMECH.2002.1011258>
- [40] A. Sapena-Bano, M. Pineda-Sanchez, R. Puche-Panadero, J. Martinez-Roman, and D. Matic, "Fault Diagnosis of Rotating Electrical Machines in Transient Regime Using a Single Stator Current's FFT," *IEEE Trans. Instrum. Meas.*, vol. 64, no. 11, pp. 3137–3146, Nov. 2015. <https://doi.org/10.1109/TIM.2015.2444240>
- [41] A. Sadeghian, Zhongming Ye, and Bin Wu, "Online Detection of Broken Rotor Bars in Induction Motors by Wavelet Packet Decomposition and Artificial Neural Networks," *IEEE Trans. Instrum. Meas.*, vol. 58, no. 7, pp. 2253–2263, Jul. 2009. <https://doi.org/10.1109/TIM.2009.2013743>
- [42] B. Ayhan, M.-Y. Chow, and M.-H. Song, "Multiple Discriminant Analysis and Neural-Network-Based Monolith and Partition Fault-Detection Schemes for Broken Rotor Bar in Induction Motors," *IEEE Trans. Ind. Electron.*, vol. 53, no. 4, pp. 1298–1308, Jun. 2006. <https://doi.org/10.1109/TIE.2006.878301>
- [43] V. P. Mini, S. Setty, and S. Ushakumari, "Fault Detection and Diagnosis of an Induction Motor Using Fuzzy Logic," in *2010 IEEE Region 8 International Conference on Computational Technologies in Electrical and Electronics Engineering (SIBIRCON)*, 2010, pp. 459–464. <https://doi.org/10.1109/SIBIRCON.2010.5555123>
- [44] J. F. Bangura, R. J. Povinelli, N. A. O. Demerdash, and R. H. Brown, "Diagnostics of Eccentricities and Bar/End-Ring Connector Breakages in Polyphase Induction Motors Through a Combination Of Time-Series Data Mining and Time-Stepping Coupled FE-State Space Techniques," *IEEE Trans. Ind. Appl.*, vol. 39, no. 4, pp. 1005–1013, Jul. 2003. <https://doi.org/10.1109/TIA.2003.814582>
- [45] S. Abdellatif, S. Tahar, and Z. Boubakeur, "Diagnostic of the simultaneous of Dynamic Eccentricity and Broken Rotor Bars Using the Magnetic Field Spectrum of the Air-Gap for an Induction Machine," in *2015 3rd International Conference on Control, Engineering & Information Technology (CEIT)*, 2015, pp. 1–6. <https://doi.org/10.1109/CEIT.2015.7233158>
- [46] J. Subramanian, S. Nandi, and T. Ilamparithi, "Detection and Severity Estimation of Static and Dynamic Eccentricity in Induction Motors Using Finite Element Analysis," in *2015 IEEE 10th International Symposium on Diagnostics for Electrical Machines, Power Electronics and Drives (SDEMPED)*, 2015, pp. 366–372. <https://doi.org/10.1109/SDEMPED.2015.7303716>
- [47] A. Bentounsi and A. Nicolas, "On Line Diagnosis of Defaults on Squirrel Cage Motors Using FEM," *IEEE Trans. Magn.*, vol. 34, no. 5, pp. 3511–3514, 1998. <https://doi.org/10.1109/20.717828>
- [48] T. Vaimann, A. Belahcen, and A. Kallaste, "Necessity for Implementation of Inverse Problem Theory in Electric Machine Fault Diagnosis," in *2015 IEEE 10th International Symposium on Diagnostics for Electrical Machines, Power Electronics and Drives (SDEMPED)*, 2015, pp. 380–385. <https://doi.org/10.1109/SDEMPED.2015.7303718>
- [49] J. F. Watson and D. G. Dorrell, "The Use of Finite Element Methods to Improve Techniques for the Early Detection of Faults in 3-Phase Induction Motors," *IEEE Trans. Energy Convers.*, vol. 14, no. 3, pp. 655–660, 1999. <https://doi.org/10.1109/60.790931>
- [50] L. Weili, X. Ying, S. Jiafeng, and L. Yingli, "Finite-Element Analysis of Field Distribution and Characteristic Performance of Squirrel-Cage Induction Motor With Broken Bars," *IEEE Trans. Magn.*, vol. 43, no. 4, pp. 1537–1540, Apr. 2007. <https://doi.org/10.1109/TMAG.2006.892086>
- [51] O. A. Mohammed, N. Y. Abed, and S. Ganu, "Modeling and Characterization of Induction Motor Internal Faults Using Finite-Element and Discrete Wavelet Transforms," *IEEE Trans. Magn.*, vol. 42, no. 10, pp. 3434–3436, Oct. 2006. <https://doi.org/10.1109/TMAG.2006.879091>
- [52] T. Vaimann, J. Sobra, A. Belahcen, A. Rassõlkin, M. Rolak, and A. Kallaste, "Induction Machine Fault Detection Using Smartphone Recorded Audible Noise," *IET Sci. Meas. Technol.*, 2018.
- [53] M. Seera, Chee Peng Lim, D. Ishak, and H. Singh, "Fault Detection and Diagnosis of Induction Motors Using Motor Current Signature Analysis and a Hybrid FMM–CART Model," *IEEE Trans. Neural Networks Learn. Syst.*, vol. 23, no. 1, pp. 97–108, Jan. 2012. <https://doi.org/10.1109/TNNLS.2011.2178443>
- [54] M. Mneimneh and R. Povinelli, "An Electrophysiological Cardiac Model With Applications to Ischemia Detection and Infarction Localization," in *2009 36th Annual Computers in Cardiology Conference (CinC)*, 2009.
- [55] J. Wang, Z. Zhao, Z. Nie, and Q.-H. Liu, "Electromagnetic Inverse Scattering Series Method for Positioning Three-Dimensional Targets in Near-Surface Two-Layer Medium With Unknown Dielectric Properties," *IEEE Geosci. Remote Sens. Lett.*, vol. 12, no. 2, pp. 299–303, Feb. 2015. <https://doi.org/10.1109/LGRS.2014.2336983>
- [56] C. Gilavert, S. Moussaoui, and J. Idier, "Efficient Gaussian Sampling for Solving Large-Scale Inverse Problems Using MCMC," *IEEE Trans. Signal Process.*, vol. 63, no. 1, pp. 70–80, Jan. 2015. <https://doi.org/10.1109/TSP.2014.2367457>
- [57] A. Mohamed Abouelyazied Abdallah, "An Inverse Problem Based Methodology With Uncertainty Analysis for the Identification of Magnetic Material Characteristics of Electromagnetic Devices," Dissertation, Ghent University, Department of Electrical energy, systems and automation, Ghent; Leuven, Belgium, 2012.
- [58] G. Crevecoeur, "Numerical Methods for Low Frequency Electromagnetic Optimization and Inverse Problems Using Multi-Level Techniques," Ph. D. Dissertation, Ghent University, Ghent, Belgium, 2009.
- [59] A. Abou-Elyazied Abdallah, P. Sergeant, and L. Dupre, "A Non-Destructive Methodology for Estimating the Magnetic Material Properties of an Asynchronous Motor," *IEEE Trans. Magn.*, vol. 48, no. 4, pp. 1621–1624, Apr. 2012. <https://doi.org/10.1109/TMAG.2011.2173171>
- [60] A. A.-E. Abdallah, P. Sergeant, G. Crevecoeur, and L. Dupre, "An Inverse Approach for Magnetic Material Characterization of an EI Core Electromagnetic Inductor," *IEEE Trans. Magn.*, vol. 46, no. 2, pp. 622–625, Feb. 2010. <https://doi.org/10.1109/TMAG.2009.2033353>
- [61] A. A.-E. Abdallah, G. Crevecoeur, and L. Dupre, "Selection of Measurement Modality for Magnetic Material Characterization of an Electromagnetic Device Using Stochastic Uncertainty Analysis," *IEEE Trans. Magn.*, vol. 47, no. 11, pp. 4564–4573, Nov. 2011. <https://doi.org/10.1109/TMAG.2011.2151870>
- [62] V. P. Bui, O. Chadebec, L.-L. Rouve, and J.-L. Coulomb, "Noninvasive Fault Monitoring of Electrical Machines by Solving the Steady-State Magnetic Inverse Problem," *IEEE Trans. Magn.*, vol. 44, no. 6, pp. 1050–1053, Jun. 2008. <https://doi.org/10.1109/TMAG.2007.916593>
- [63] P. Rasilo, A. A.-E. Abdallah, A. Belahcen, A. Arkkio, and L. Dupre, "Identification of Synchronous Machine Magnetization Characteristics From Calorimetric Core-Loss and No-Load Curve Measurements," *IEEE Trans. Magn.*, vol. 51, no. 3, pp. 1–4, Mar. 2015. <https://doi.org/10.1109/TMAG.2014.2354055>
- [64] A. Kechroud, J. J. H. Paulides, and E. A. Lomonova, "B-Spline Neural Network Approach to Inverse Problems in Switched Reluctance Motor Optimal Design," *IEEE Trans. Magn.*, vol. 47, no. 10, pp. 4179–4182, Oct. 2011. <https://doi.org/10.1109/TMAG.2011.2151183>
- [65] J. Fouladgar and E. Chauveau, "The Influence of the Harmonics on the Temperature of Electrical Machines," *IEEE Trans. Magn.*, vol. 41, no. 5, pp. 1644–1647, May 2005. <https://doi.org/10.1109/TMAG.2005.846113>
- [66] M. Saif and W. Chen, "Observer-Based Strategies for Actuator Fault Detection, Isolation and Estimation for Certain Class of Uncertain Nonlinear Systems," *IET Control Theory Appl.*, vol. 1, no. 6, pp. 1672–1680, Nov. 2007. <https://doi.org/10.1049/iet-cta:20060408>
- [67] Q. Shen, B. Jiang, and V. Cocquemot, "Fault-Tolerant Control for T-S Fuzzy Systems With Application to Near-Space Hypersonic Vehicle With Actuator Faults," *IEEE Trans. Fuzzy Syst.*, vol. 20, no. 4, pp. 652–665, Aug. 2012. <https://doi.org/10.1109/TFUZZ.2011.2181181>

- [68] L. M. Capisani, A. Ferrara, A. Ferreira de Loza, and L. M. Fridman, "Manipulator Fault Diagnosis via Higher Order Sliding-Mode Observers," *IEEE Trans. Ind. Electron.*, vol. 59, no. 10, pp. 3979–3986, Oct. 2012. <https://doi.org/10.1109/TIE.2012.2189534>
- [69] M. N. Nguyen, C. Bao, K. L. Tew, S. D. Teddy, and X.-L. Li, "Ensemble Based Real-Time Adaptive Classification System for Intelligent Sensing Machine Diagnostics," *IEEE Trans. Reliab.*, vol. 61, no. 2, pp. 303–313, Jun. 2012. <https://doi.org/10.1109/TR.2012.2194352>
- [70] D. He, R. Li, and J. Zhu, "Plastic Bearing Fault Diagnosis Based on a Two-Step Data Mining Approach," *IEEE Trans. Ind. Electron.*, pp. 1–1, 2012. <https://doi.org/10.1109/TIE.2012.2192894>
- [71] M. N. Uddin, W. Wang, and Z. R. Huang, "Modeling and Minimization of Speed Ripple of a Faulty Induction Motor With Broken Rotor Bars," *IEEE Trans. Ind. Appl.*, vol. 46, no. 6, pp. 2243–2250, Nov. 2010. <https://doi.org/10.1109/TIA.2010.2070476>
- [72] W. W. Tan and H. Huo, "A Generic Neurofuzzy Model-Based Approach for Detecting Faults in Induction Motors," *IEEE Trans. Ind. Electron.*, vol. 52, no. 5, pp. 1420–1427, Oct. 2005. <https://doi.org/10.1109/TIE.2005.855654>



Bilal Asad was born in 1986 in Pakistan. He received his B. sc. in Electronics Engineering from The Islamia University of Bahawalpur and M. sc. in Electrical Engineering from the University of Engineering and Technology (UET), Lahore, Pakistan, in 2007 and 2011, respectively. Currently, he is a Ph. D. student at the Department of Electrical Power Engineering and Mechatronics, Tallinn University of Technology, Estonia. His areas of interest include design, modeling and fault diagnostics of electrical machines. E-mail: biasad@ttu.ee



Toomas Vaimann received his B. sc., M. sc. and Ph. D. degrees in electrical engineering from Tallinn University of Technology, Estonia, in 2007, 2009 and 2014, respectively. He is currently a senior researcher at Tallinn University of Technology, Department of Electrical Power Engineering and Mechatronics. He has been working in several companies as an electrical engineer. He is the member of IEEE, Estonian Society of Moritz Hermann Jacobi and Estonian Society for Electrical Power Engineering. His main research interest is the diagnostics of electrical machines.

E-mail: Toomas.Vaimann@taltech.ee
ORCID iD: <https://orcid.org/0000-0003-0481-5066>



Anton Rassolkin received the Ph. D. degree in electric drives and power electronics from Tallinn University of Technology in 2014. His main research interests are in the field of electric drives and their control systems, as well as in the fields of electrical machines and electric transportation. He works as a Research Scientist at the Department of Electrical Power Engineering and Mechatronics at Tallinn University of Technology. Department of Electrical Power Engineering and Mechatronics, Tallinn University of Technology, Ehitaajate tee 5, 19086 Tallinn, Estonia.

E-mail: Anton.Rassolkin@taltech.ee
ORCID iD: <https://orcid.org/0000-0001-8035-3970>



Ants Kallaste received his B. sc., M. sc. and Ph. D. degrees in electrical engineering from Tallinn University of Technology, Estonia, in 2004, 2006 and 2013, respectively. He is currently a senior researcher at Tallinn University of Technology, Department of Electrical Power Engineering and Mechatronics. He is holding the position of Head of Electrical Machines Research Group. He is the member of IEEE and Estonian Society of Moritz Hermann Jacobi. His main research interest is the design of electrical machines.

E-mail: Ants.Kallaste@taltech.ee
ORCID iD: <https://orcid.org/0000-0001-6126-1878>



Anouar Belahcen received the B. sc. degree in physics from the University Sidi Mohamed Ben Abdellah, Fes, Morocco, in 1988 and the M. sc. (Tech.) and Doctor (Tech.) degrees from Helsinki University of Technology, Finland, in 1998, and 2004, respectively. He is the professor of Electrical Machines at Tallinn University of Technology, Estonia, and the professor of Energy and Power at Aalto University, Finland. His research interests include modeling of electrical machines, magnetic materials, coupled magnetic and mechanical problems and magnetostriction.

E-mail: Anouar.Belahcen@taltech.ee
ORCID iD: <https://orcid.org/0000-0003-2154-8692>

Publication IX

B. Asad, T. Vaimann, A. Belahcen, A. Kallaste, A. Rassõlkin. Rotor Fault Diagnostic of Inverter Fed Induction Motor Using Frequency Analysis. 12th IEEE International Symposium on Diagnostics for Electric Machines, Power Electronics and Drives (SDEMPED) Toulouse, France, 2019, pp. 127–133.

Rotor Fault Diagnostic of Inverter Fed Induction Motor Using Frequency Analysis

Bilal Asad, Toomas Vaimann, *Member, IEEE*, Anouar Belahcen, *Senior Member, IEEE*, Ants Kallaste, *Member, IEEE*, Anton Rassõlkin, *Member, IEEE*

Abstract -- Condition monitoring of electrical machines is essential in industrial operations for improving workplace safety and ensuring reliable and economical exploitation of the machines. Motor current signature analysis (MCSA) monitoring technique is gaining heightened popularity due to the simplicity of its algorithms and the least number of sensors required. In this paper, the harmonic spectrum of industrial inverter fed induction motor is investigated for the detection of broken rotor bars. To improve the legibility of the spectrum, the fundamental component is attenuated using infinite impulse response (IIR) filter because of its good transition band, less passband ripples and low order. The results are first taken from finite element method (FEM) based simulation, where the motor is fed with pure sinusoidal current and only faulty and spatial frequencies are investigated and used as a benchmark. The practical results are based on the measurements taken from the laboratory setup, where the motor under investigation is fed through an industrial inverter working under scalar control mode. The data acquisition is done with a good sampling rate of 100 kHz for better resolution.

Index Terms--Fast Fourier transform, fault diagnosis, harmonic analysis, induction motors.

I. INTRODUCTION

INDUCTION motors are playing a vital role in our domestic and industrial life. Since the second industrial revolution, their presence can be witnessed everywhere in the form of generators such as doubly fed induction generators and in the form of electrical to mechanical energy converters such as in electrical vehicles, ship propulsion, fans and pumps, etc. As a load, they are responsible of consuming about 60% of total generated energy worldwide [1]. This fact makes their control, efficiency and health, to have a direct impact on reliability of operation and economy.

Although three phase induction motors are acting as the workhorse for industry, researchers are working on multiphase motors to exploit their advantages, such as high efficiency, reduced torque ripples high power density and reliability, etc. Their versatile structures, power ratings, different nature of applications, reliability and safety of both operation and machine itself, increases the need of inverters as

an input source [2]. These inverters are purposely designed to control the motor according to the load requirements and responsible to convert standard grid AC-to-AC supply with the desired number of phases, amplitudes and frequencies. While working as a closed loop control system, these drives can better control machine ranging from simple scalar (v/f , v/\sqrt{f} , $v/\sqrt[3]{f}$) to complex vector control, such as field-oriented control (FOC), direct torque control (DTC), model predictive control (MPC) and sliding mode observers (SMO), etc.

Although these drives improve the safety and reliability of operation, they also inject many harmonics into the motor. The amplitude and frequency of these harmonics depend on the modulation technique and the switching frequency of the solid-state switches of the inverter, making a tradeoff between efficiency and amplitude of low order harmonics. The increase in modulation frequency increases the inverter losses but attenuates low order harmonics. The low order harmonics are dangerous in the sense that they produce more torsional oscillations, pulsating torques and consequent deformations such as damaged shaft and broken rotor bars. For the sake of efficiency, the maximum switching frequency in the range of less than 1 kHz for a maximum stator frequency of 50 or 60 Hz is reported in [3][4][5][6]. For high speed motors having modulation frequencies in the range of 167-1500 Hz, the switching frequencies in the range of few kilo hertz (up to 16 kHz) can be found in [7][8].

The researchers are trying to reduce the required switching frequency and switching losses with different control strategies, such as [9], [10] used discontinuous pulse width modulation (DPWM) which reduces the switching frequency (f_{sw}) up to two-third of f_{sw} of continuous PWM strategies, sine-triangle PWM based DPWM can be found in [11]. The authors in [12], [13] used space vector based DPWM and modified DPWM can be found in [14], while space vector based synchronized DPWM is presented in [3].

In the field of fault diagnostics, the most common approach to detect the nature and severity of the fault is through the detection of faulty frequency components in the frequency spectrum of the stator current, etc. This detection is simple in case of grid fed machines, as there are only few frequency components based on grid supply and motor itself, which are easy to segregate. However, in case of inverter fed machines, there is always a mess of frequency components, making a challenging task for diagnostic algorithms to detect frequencies of interest. These inverter fed frequencies sometimes cannot be defined using some specific rule, such as in case of inverters, being controlled by stochastic control

B. Asad, T. Vaimann, A. Kallaste and A. Rassõlkin are with the Department of Electrical Power Engineering and Mechatronics, Tallinn University of Technology, Estonia (e-mail: biasad@ttu.ee)

A. Belahcen is with Department of Electrical Engineering and Automation, Aalto University, Espoo, Finland and with the Department of Electrical Power Engineering and Mechatronics, Tallinn University of Technology, Estonia (e-mail: anouar.belahcen@aalto.fi)

algorithms and working in a feedback control manner, making frequencies dependent on load. Also, in case of low switching to fundamental frequency ratio of the inverter, the low order faulty frequencies are highly likely to be buried under the frequencies coming from the inverter side. Moreover, as most of the drives work in closed loop control system, the influence of drive controller on harmonics is inevitable.

In this paper the frequency spectrum of an industrial inverter fed three phase induction motor is investigated and broken rotor bar components are tried to recover using infinite impulse response (IIR), band stop filters. The fundamental component being the strongest frequency is first attenuated to improve the legibility of the spectrum and then the rest of frequencies are studied on the linear scale. This paper is the extension of [15], where the spectrum of a grid fed motor was investigated under healthy and broken rotor bar conditions. The motor harmonics are studied using finite element-based simulation and used as a benchmark for the comparison with actual spectrum.

II. HARMONICS DESCRIPTION

A. Slots and Broken Rotor Bars

The harmonics in line current of the motor are due to three factors: 1) the harmonics coming from supply side, 2) the harmonics generated by the motor itself and 3) the harmonics produced by faults in the motor. The motor generated harmonics are called rotor slot harmonics (RSH) or principal slot harmonics (PSH). These harmonics are present due to the non-sinusoidal nature of the stator and the rotor winding functions and continuous change in air gap due to their slot permeance. This change in the air gap changes all stator and rotor self and mutual inductances, as shown by the modified winding function formula:

$$L_{ij}(\theta) = \mu_o r l \int_0^{2\pi} P(\varphi, \theta) N_i(\varphi, \theta) N_j(\varphi, \theta) d\theta \quad (1)$$

where r is the average radius of the air gap, l is the effective length of the stator core, P is the inverse air gap distribution, N_i and N_j are the winding functions of i th and j th phase of the motor.

The power of PSHs depends upon the saturation of the core, which changes the effective air gap, skewing of stator and the rotor slots, which tend to reduce them. Moreover, machine asymmetries and unbalanced power supplies can also produce some of them. The RSHs or PSHs can be described by following analytical expression as in [16].

$$f_{sh} = \left[(kn_{br} \pm n_d) \left(\frac{1-s}{p} \right) \pm v \right] \quad (2)$$

where n_{br} are the number of rotor slots, n_d is for the dynamic eccentricity, s is the slip, p is the number of the fundamental pole pairs and v is the order of slot time harmonics. The first two harmonics are the most powerful components as compared to the rest of them and can be used for sensor less speed estimation if n_{br} and p are known.

It is well known that each kind of fault modulates the motor line current with some specific frequencies, which can be

detected for fault diagnostics. Deformations in the rotor, such as the broken end rings, broken rotor bars or high resistance connections can be detected by the following frequencies in the spectrum:

$$f_{BR} = f_s \pm 2ksf_s, \quad k = 1, 2, 3, \dots \quad (3)$$

where f_s is the supply frequency, s is the slip of the machine and k is the order of harmonics. These harmonics decrease in amplitude and increase in frequency as their order increases in the spectrum. The first two harmonics at ($f_{lsb} = f_s - 2sf_s$) and ($f_{usb} = f_s + 2sf_s$) are called the upper side band (USB) and the lower side band (LSB) respectively. The LSB is emerging due to broken rotor bars, while USB is present due to the subsequent oscillations in the speed. The fundamental fault frequencies are more powerful components than the rest of the fault harmonics and are highly likely to be buried under the supply frequency due to its spectral leakage, if the resolution of FFT is not appropriate, particularly under the low slip conditions.

B. Inverter Supply

The presence of inverters in the drive systems cannot be neglected in modern day industries. Along with various advantages, such as precision, accuracy and safety of operation, inverters bring various drawbacks, such as increase in cost, torque ripples, switching losses, increase in iron losses, radiated electromagnetic field interference [17], acoustic noise and high frequency harmonics, for which most of machines are not designed. Moreover, as it is previously mentioned that there is a tradeoff between power of low order harmonics and efficiency as switching frequency increases. Out of various control strategies of inverter switches, pulse width modulation (PWM) is the most common because of its simplicity and many types as well as having different advantages. For example, authors in [18] used random PWM (RPWM) to reduce the acoustic noise in motor drive systems. Authors of [19] have used four different PWM modes to investigate the iron losses of a salient stator permanent magnet machine. The authors in [20] used minimum torque ripple PWM technique with reduced switching frequency for medium voltage motor drive systems, while [21] tested an induction motor for its efficiency, powered from three different PWM drive systems. The radiated electromagnetic field interference due to the switching frequency in PWM motor drives is investigated in [17].

The output line and phase voltage measured from ABB industrial drive system with a sampling rate of 100 kHz is shown in Fig. 1.

C. Motor's Behavior as a Filter

Since the inverter fed motors are subjected to many high frequency components, it is important to discuss its frequency magnitude response. Using equivalent circuit model, the per phase transfer function of the three phase induction motor can be approximated as:

$$\frac{i_{as}}{v_{as}} = \frac{1}{\sqrt{(R_s + \frac{R_r}{s})^2 + \omega_e^2 (L_{ls} + L_{lr})^2}} \quad (3)$$

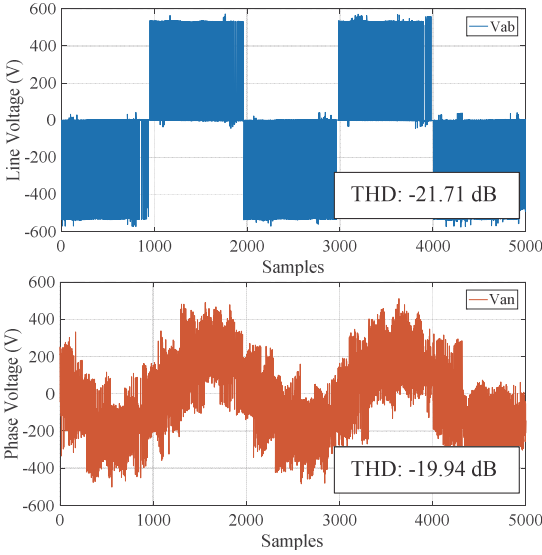


Fig. 1. Inverter's output line and phase voltage respectively.

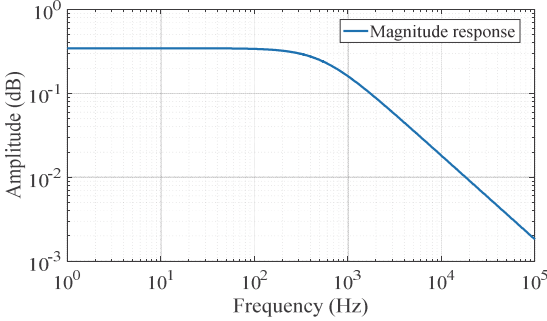


Fig. 2. Motor's current gain magnitude response.

where i_{as} , v_{as} , R_s , R_r , ω_c , L_{ls} and L_{lr} are the motor phase current, voltage, stator per phase resistance, rotor's equivalent per phase resistance, synchronous speed, stator's and rotor's leakage inductances respectively.

The natural frequency response is shown in Fig. 2 from where the low pass nature of the induction motor is evident. Hence, for fault diagnostic, the low frequency components are very important and the performance of machine will improve when low order harmonics are less powerful, because the high frequency components will be attenuated by the motor itself.

D. Fourier Transform and its Resolution

Fourier transform has proven its importance in almost every field of engineering and is the tool to understand the nature of a signal. It was invented as Fourier series, responsible to convert a single time domain signal to n time domain sinusoids, having different amplitudes and frequencies. However, the need of the analysis of aperiodic and non-stationary signals led us towards its variants such as continuous time Fourier transform (CTFT), discrete time

Fourier transform (DTFT) and short time Fourier transform (STFT), etc. The fast Fourier transform (FFT) is an efficient algorithm to solve DFT represented by the following formula:

$$X_n = \sum_{k=0}^{N-1} x_n e^{-i2\pi kn/N}, \quad k = 0, 1, 2, \dots, (N-1) \quad (4)$$

where x_n is the discrete sampled signal and N is the number of samples, which should be a number in power of 2, i.e. $N = 2^x$.

The frequency resolution is very important for signal analysis, particularly in case of inverter fed machines, where there are a number of frequencies and it is important to segregate fault frequencies. It is the difference between two adjacent frequency bins and can be described by the following equation [22].

$$t_{sig} = t_s \times N = N/f_s \quad (5)$$

$$df = 1/t_{sig} = f_s/N = BW/SL \quad (6)$$

$$SL = N/2 \quad (7)$$

where, t_{sig} is the measurement or acquisition time of the signal, t_s and f_s are representing the sampling frequency, N is the total number of data samples, BW is the bandwidth, df is the frequency resolution or frequency difference between two adjacent frequency bins and SL is the total number of spectral lines. It is obvious that the frequency resolution depends upon the length of measured signal, also called acquisition or frame time of the signal. Since the measured signal is of finite duration, the frequency resolution can also be improved by a technique called zero padding or spectral interpolation. In this technique, the length of the signal is artificially increased by adding zeros before and after it.

E. Infinite Impulse Response Filters

Filters have many applications in data acquisition and analysis. They can be used to remove or amplify certain frequency components, anti-aliasing, noise reduction and offset removal, etc. They can be broadly classified into two types, called the finite impulse response (FIR) and the infinite impulse response (IIR) filters. Unlike FIR, IIR filters use some of their outputs as inputs, making them recursive functions. This fact reduces their computational time, filter order and accuracy, as compared to the corresponding FIR filters. However, their closed loop nature makes them more unstable than the FIR filters. In this paper, a low order IIR filter is tuned to attenuate the fundamental component, which is more powerful as compared to the rest of the harmonics. This attenuation increases the legibility of the spectrum on linear scale and makes the faulty frequencies easily detectable.

III. CASE STUDY

The modeling, simulation and analysis is always been very important for design, control and diagnostics of electrical machines. The most common types of modeling found in literature are analytical and numerical such as finite element

TABLE I
MOTOR SPECIFICATIONS

Sr. No.	Parameter	Symbol	Value
1	Rated speed	N_r	1400 rpm@50 Hz
2	Rated power	P_r	18 kW@50 Hz
3	Connection	Y, Δ	Star (Y)
4	Power factor	$\cos\phi$	0.860
5	Number of poles	P	4
6	Number of rotor bars	N_{rb}	40
7	Number of stator slots	N_s	48

method (FEM) based models. Out of these techniques, FEM based models give good approximation of actual systems but at the cost of complexity and long computational time.

The FEM-based simulation of a three-phase induction motor, with the parameters shown in Table I, is performed under healthy, one, and two broken rotor bar conditions. Since the simulation is performed using 2D field analysis, the ignored end windings are compensated by adding additional resistances and inductances in series with coils. The per phase stator coils are series and parallel connections of copper strands, making the current density uniformly distributed. The simulation is performed at rated load under constant speed. The flux distribution under healthy and two broken rotor bar conditions is shown in Fig. 3. It is evident that the flux density increases across the broken bars, putting the adjacent bars under increased magnetic stress. The increase in the current of the neighboring bars makes the machine vulnerable to break more bars in time, if the fault is not timely diagnosed and repaired. The obtained results can be used as a benchmark to differentiate between harmonics due to motor itself (slot harmonics), due to a fault, such as broken rotor bars, and due to inverter. In Fig. 4, simulated three phase currents for the healthy case and frequency spectra for the healthy and the broken rotor bars is presented. The attenuation of the fundamental component with the help of IIR filter improves the legibility of the spectrum and makes the segregation of various harmonics easy. The simulation is performed for two seconds with 5328 mesh elements at stator and rotor temperatures of 120°C and 140°C respectively.

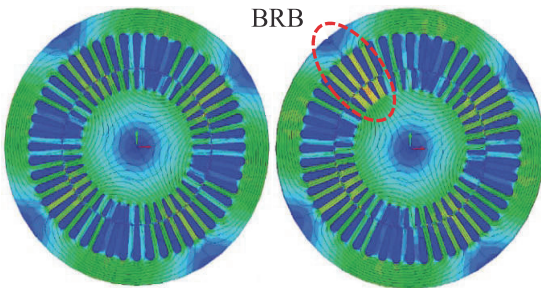


Fig. 3. Motor's flux distribution under healthy and broken rotor bar conditions.

The detailed description of these specific harmonics can be found in [15], where the harmonic spectrum analysis is done for a grid fed induction motor with broken rotor bars.

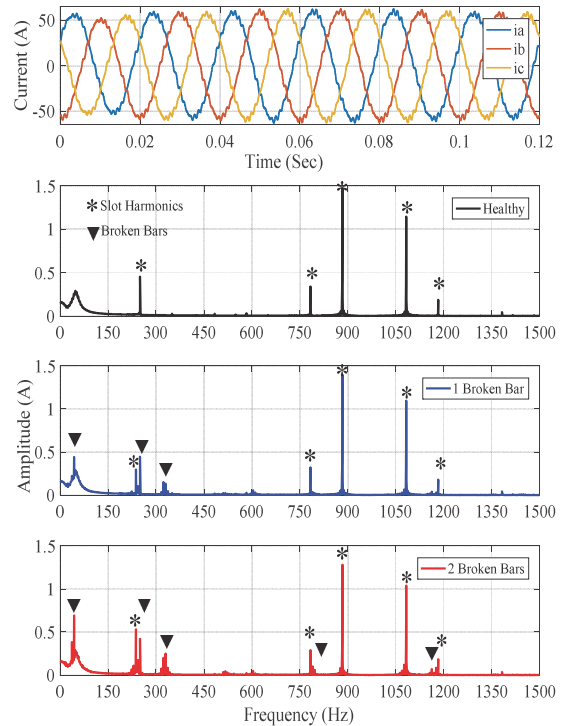
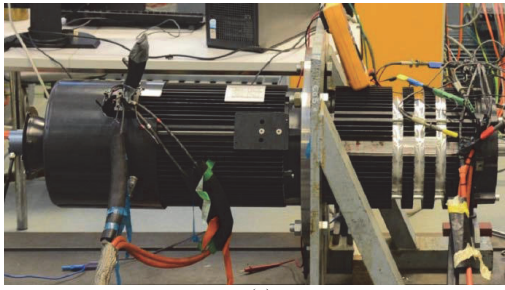


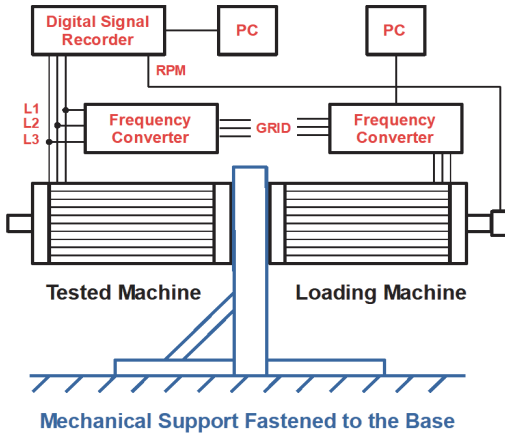
Fig. 4. Simulated stator currents and corresponding frequency spectrum for healthy, one, and two broken rotor bars respectively from top to bottom.

IV. PRACTICAL SETUP

The measurement setup consists of two same type motors with the parameters shown in Table 1. One machine is under investigation and the other one is acting as the load. Both machines are mounted on the same mechanical base and coupled through their shafts as shown in Fig. 5(a). Both machines are fed through the inverters to improve the controllability of the loading motor and investigate the harmonic spectrum of the machine under investigation. The stator currents and voltages are measured using the Dewetron transient recorder. The sampling frequency of the measured signals is 100000 samples per second and the measurement time is 70 seconds, giving a very good resolution of the frequency spectrum. Fig. 5(b) shows the block diagram of the test setup. The ABB industrial frequency converters is used in scalar control mode, preferable for the smaller size motors. Moreover, the modulation scheme is simple sinusoidal pulse width modulation (SPWM), as it can directly control the inverter output voltage and output frequency according to the sine functions. The modulation frequency is in the range from 2 kHz to 16 kHz and can be tuned manually for selected models.



(a)



(b)

Fig. 5. (a) Hardware setup, (b) block diagram.

It is important to know that the motor under investigation is working under scalar control mode, because in DTC the faulty frequencies are highly likely to be attenuated by the drive controller.

V. RESULTS AND DISCUSSION

Fig. 6 shows a few cycles of the inverter fed phase voltage with the corresponding frequency spectrum up to 400 Hz and 25 kHz respectively. The fundamental component is effectively attenuated with the second order IIR filter with stopband attenuation of 45 dB and sampling frequency of 100 kHz.

In Fig. 7, the experimental results are presented. The topmost graph is representing the actual three phase currents drawn by motor from the inverter, which are much smoother than their corresponding supply voltages, because of the motor filtering effects. In the rest of graphs, the spectrum for healthy, one, two and three broken rotor bars are shown. The elimination of 50 Hz component by proper tuning of IIR bandstop filter makes faulty frequencies discoverable even when only one out of 48 rotor bars is broken. The motor under this test is working under rated load conditions and the total harmonic distortion is calculated before attenuation of the fundamental component.

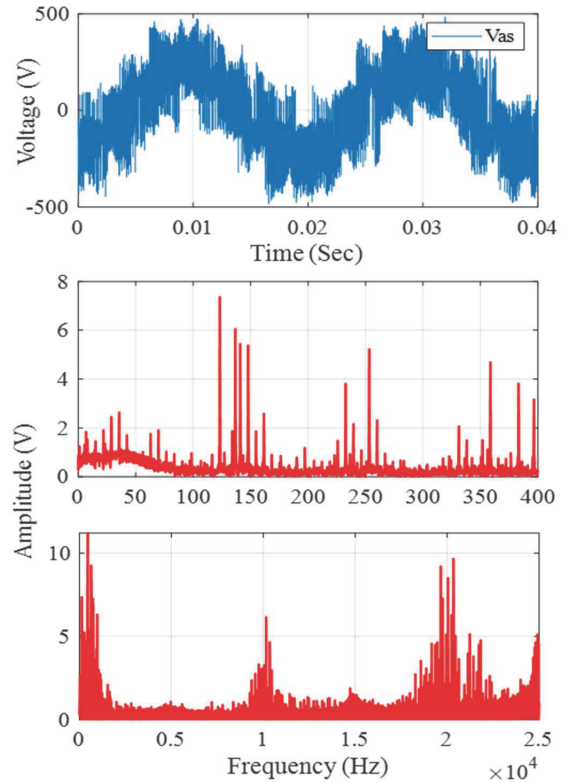


Fig. 6. Inverter's generated phase voltage and corresponding frequency spectrum up to 400 Hz and 25 kHz respectively with attenuated fundamental component.

VI. CONCLUSIONS

The MCSA is the most common technique used for the fault diagnostics of induction motors, because of its simplicity and noninvasive nature. As an extension of [15], in this paper harmonic spectrum of an inverter fed induction motor for the healthy and broken rotor bar cases using signals from the simulation and experiments is studied.

FEM-based simulations reveal that the rotor bars next to the broken one come under more magnetic and thermal stresses making them vulnerable to break, increasing the severity of the fault with the passage of time. Hence, it is very important for diagnostic algorithm to be able to detect fault at incipient stage. The accurate attenuation of the fundamental component can improve the legibility of spectrum for detection of the frequencies representing broken rotor bars.

The use of the IIR filter for the attenuation of the fundamental component reduces its spectral leakage considerably. This filter has a good transition band and makes less impact on the upper and lower sidebands of the broken rotor bar frequencies. Less passband ripples reduces the impact of filter on frequency spectrum. Moreover, the low order IIR filters can give more accurate results as compared to the correspondent finite response (FIR) filters.

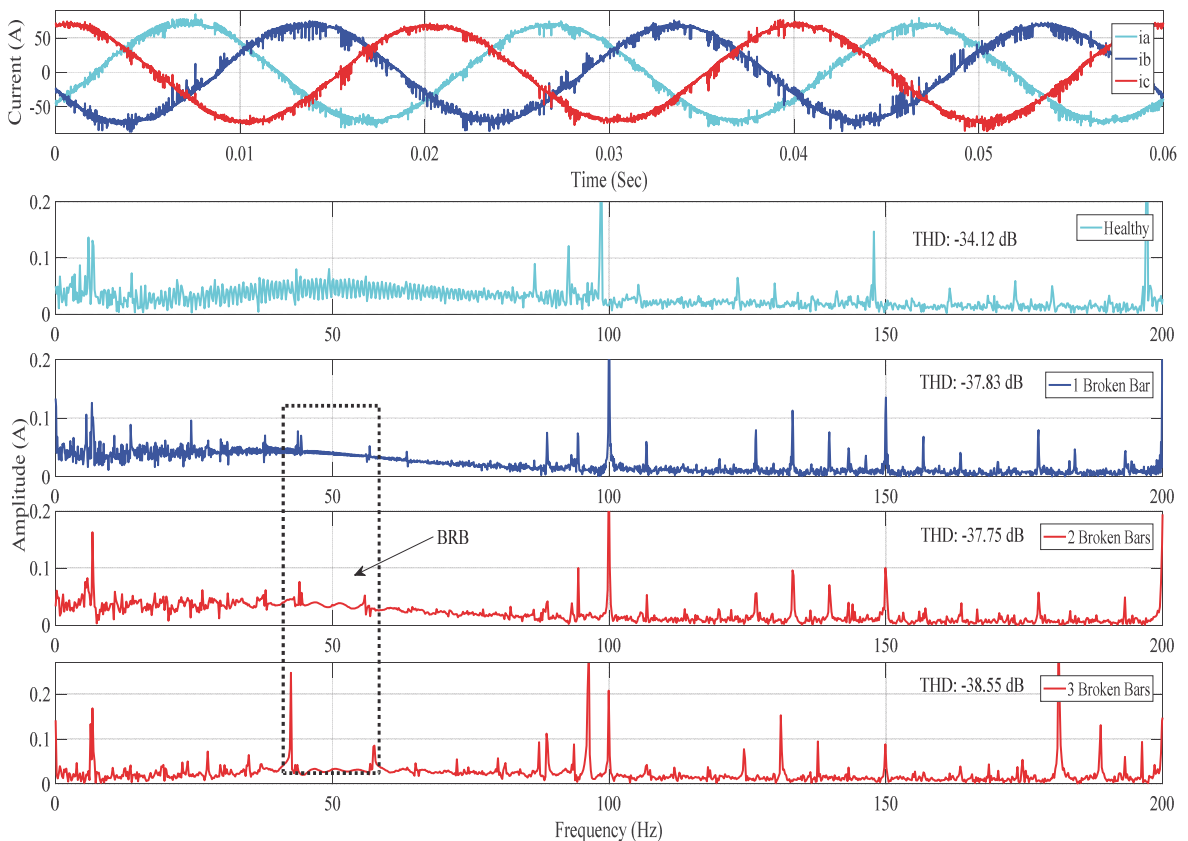


Fig. 7. Measured phase currents and corresponding frequency spectra for health, one, two and three broken rotor bars respectively.

Since the most powerful component is filtered out, it improves the legibility of the spectrum even at the linear scale. From the simulation results, the broken rotor bar and high frequency slot harmonics are easily readable on the same graph. In case of the experimental setup, since the load motor is supplied from an inverter, the slip of the test motor is carefully controlled to investigate the location of the fault frequencies.

The proposed filter works good to attenuate the 50 Hz component without having major impact of sideband frequencies emerging because of broken rotor bars. The frequencies of interest are clearly detectable, even when one out of 48 bars is broken. The method gives promising results for scalar control, but in case of DTC, some extra care is needed to avoid the impact of the drive controller on these frequencies.

VII. REFERENCES

- [1] H. W. Penrose and A. Pro, "The impact of condition on motor efficiency and reliability," *Production*, no. February, pp. 1–8, 2001.
- [2] U. S. and K. Sivakumar, "Multilevel Inverter Scheme for Performance Improvement of Pole Phase Modulated Multiphase Induction Motor Drive," *IEEE Trans. Ind. Electron.*, vol. 63, no. 4, pp. 2036–2043, 2015.
- [3] A. R. Beig, S. Kanukollu, K. Al Hosani, and A. Dekka, "Space-Vector-Based Synchronized Three-Level Discontinuous PWM for Medium-Voltage High-Power VSI," *IEEE Trans. Ind. Electron.*, vol. 61, no. 8, pp. 3891–3901, Aug. 2014.
- [4] Y. Zhang, Z. Zhao, and J. Zhu, "A Hybrid PWM Applied to High-Power Three-Level Inverter-Fed Induction-Motor Drives," *IEEE Trans. Ind. Electron.*, vol. 58, no. 8, pp. 3409–3420, Aug. 2011.
- [5] J. Napoles, J. I. Leon, R. Portillo, L. G. Franquelo, and M. A. Aguirre, "Selective Harmonic Mitigation Technique for High-Power Converters," *IEEE Trans. Ind. Electron.*, vol. 57, no. 7, pp. 2315–2323, Jul. 2010.
- [6] N. Oikonomou and J. Holtz, "Closed-Loop Control of Medium-Voltage Drives Operated With Synchronous Optimal Pulsewidth Modulation," *IEEE Trans. Ind. Appl.*, vol. 44, no. 1, pp. 115–123, 2008.
- [7] R. K. Jordan, P. Stumpf, P. Barta, Z. Varga, and I. Nagy, "A Novel Approach in Studying the Effects of Subharmonics on Ultrahigh-Speed AC Motor Drives," *IEEE Trans. Ind. Electron.*, vol. 58, no. 4, pp. 1274–1281, Apr. 2011.
- [8] D. P. Marcetic, I. R. Krcmar, M. A. Gecic, and P. R. Matic, "Discrete Rotor Flux and Speed Estimators for High-Speed Shaft-Sensorless IM Drives," *IEEE Trans. Ind. Electron.*, vol. 61, no. 6, pp. 3099–3108, Jun. 2014.
- [9] D. G. Holmes and T. A. Lipo, *Pulse width modulation for power converters : principles and practice*. John Wiley, 2003.
- [10] J. Prieto, M. Jones, F. Barrero, E. Levi, and S. Toral, "Comparative Analysis of Discontinuous and Continuous PWM Techniques in VSI-Fed Five-Phase Induction Motor," *IEEE Trans. Ind. Electron.*, vol. 58, no. 12, pp. 5324–5335, Dec. 2011.
- [11] O. Ojo, "The generalized discontinuous PWM scheme for three-

phase voltage source inverters,” IEEE Trans. Ind. Electron., vol. 51, no. 6, pp. 1280–1289, Dec. 2004.

- [12] The Dung Nguyen, J. Hobraiche, N. Patin, G. Friedrich, and J. Vilain, “A Direct Digital Technique Implementation of General Discontinuous Pulse Width Modulation Strategy,” IEEE Trans. Ind. Electron., vol. 58, no. 9, pp. 4445–4454, Sep. 2011.
- [13] Y. Wu, M. A. Shafi, A. M. Knight, and R. A. McMahon, “Comparison of the Effects of Continuous and Discontinuous PWM Schemes on Power Losses of Voltage-Sourced Inverters for Induction Motor Drives,” IEEE Trans. Power Electron., vol. 26, no. 1, pp. 182–191, Jan. 2011.
- [14] Nho-Van Nguyen, Bac-Xuan Nguyen, and Hong-Hee Lee, “An Optimized Discontinuous PWM Method to Minimize Switching Loss for Multilevel Inverters,” IEEE Trans. Ind. Electron., vol. 58, no. 9, pp. 3958–3966, Sep. 2011.
- [15] B. Asad, T. Vaimann, A. Belahcen, and A. Kallaste, “Harmonic Spectrum Analysis of Induction Motor With Broken Rotor Bar Fault,” in IEEE 59th International Scientific Conference on Power and Electrical Engineering of Riga Technical University (RTUCon), 2018, pp. 1–7.
- [16] S. Nandi, “Modeling of Induction Machines Including Stator and Rotor Slot Effects,” IEEE Trans. Ind. Appl., vol. 40, no. 4, pp. 1058–1065, Jul. 2004.
- [17] A. Rosales, A. Sarikhani, and O. A. Mohammed, “Evaluation of Radiated Electromagnetic Field Interference Due to Frequency Switching in PWM Motor Drives by 3D Finite Elements,” IEEE Trans. Magn., vol. 47, no. 5, pp. 1474–1477, May 2011.
- [18] K. Lee, G. Shen, W. Yao, and Z. Lu, “Performance Characterization of Random Pulse Width Modulation Algorithms in Industrial and Commercial Adjustable-Speed Drives,” IEEE Trans. Ind. Appl., vol. 53, no. 2, pp. 1078–1087, Mar. 2017.
- [19] T. H. Kim and J. Lee, “Comparison of the Iron Loss of a Flux-Reversal Machine Under Four Different PWM Modes,” IEEE Trans. Magn., vol. 43, no. 4, pp. 1725–1728, Apr. 2007.
- [20] H.-S. Jung, C.-E. Hwang, H.-S. Kim, S.-K. Sul, A. Hee-Won, and H. Yoo, “Minimum Torque Ripple Pulse Width Modulation With Reduced Switching Frequency for Medium-Voltage Motor Drive,” IEEE Trans. Ind. Appl., vol. 54, no. 4, pp. 3315–3325, Jul. 2018.
- [21] D. A. Casada, J. D. Kueck, H. Staunton, and M. C. Webb, “Efficiency testing of motors powered from pulse-width modulated adjustable speed drives,” IEEE Trans. Energy Convers., vol. 15, no. 3, pp. 240–244, 2000.
- [22] B. Asad, T. Vaimann, A. Belahcen, and A. Kallaste, “Broken Rotor Bar Fault Diagnostic of Inverter Fed Induction Motor Using FFT, Hilbert and Park’s Vector Approach,” in 2018 XIII International Conference on Electrical Machines (ICEM), 2018, pp. 2352–2358.

VIII. BIOGRAPHIES



Bilal Asad was born in 1986 in Pakistan. He received his BSc in Electronics Engineering from The Islamia University of Bahawalpur and MSc in Electrical Engineering from University of Engineering and Technology (UET) Lahore, Pakistan in 2007 and 2011 respectively. Currently he is a PhD student in the Department of Electrical Power Engineering and Mechatronics, Tallinn University of Technology, Estonia. His area of interest includes design, modeling and fault diagnostics of electrical machines

E-mail: biasad@ttu.ee



Toomas Vaimann and received his BSc, MSc and PhD degrees in electrical engineering from Tallinn University of Technology, Estonia, in 2007, 2009 and 2014 respectively. He is currently a senior researcher in Tallinn University of Technology, Department of Electrical Power Engineering and Mechatronics. He has been working in several companies as an electrical engineer. He is the member of IEEE, Estonian Society of Moritz Hermann Jacobi and Estonian Society for Electrical Power Engineering. His main research interest is the diagnostics of electrical machines.

E-mail: Toomas.Vaimann@taltech.ee

ORCID iD: <https://orcid.org/0000-0003-0481-5066>



Estonia.

E-mail: Anton.Rassolkin@taltech.ee

ORCID iD: <https://orcid.org/0000-0001-8035-3970>



Ants Kallaste received his BSc, MSc and PhD degrees in electrical engineering from Tallinn University of Technology, Estonia, in 2004, 2006 and 2013 respectively. He is currently a senior researcher in Tallinn University of Technology, Department of Electrical Power Engineering and Mechatronics. He is holding the position of Head of Electrical Machines Research Group. He is the member of IEEE and Estonian Society of Moritz Hermann Jacobi. His main research interest is the design of electrical machines.

E-mail: Ants.Kallaste@taltech.ee

ORCID iD: <https://orcid.org/0000-0001-6126-1878>



Anouar Belahcen received the BSc degree in physics from the University Sidi Mohamed Ben Abdellah, Fes, Morocco, in 1988 and the MSc (Tech.) and Doctor (Tech.) degrees from Helsinki University of Technology, Finland, in 1998, and 2004, respectively. He is the professor of electrical machines at Tallinn University of Technology, Estonia and in the professor of Energy and Power at Aalto University, Finland. His research interest are modeling of electrical machines, magnetic materials, coupled magnetic and mechanical problems and magnetostriction.

E-mail: anouar.belahcen@aalto.fi

ORCID iD: <https://orcid.org/0000-0003-2154-8692>

Publication X

B. Asad, T. Vaimann, A. Belahcen, A. Kallaste, A. Rassõlkin. Winding Function-Based Analytical Model of Squirrel Cage Induction Motor for Fault Diagnostics. 26th International Workshop on Electric Drives: Improvement in Efficiency of Electric Drives (IWED), Mar. 2019, pp. 1–6.

Winding Function Based Analytical Model of Squirrel Cage Induction Motor for Fault Diagnostics

Bilal Asad, Toomas Vaimann, Ants Kallaste, Anton
Rassõlkin
Dept. of Electrical Power Engineering and Mechatronics
Tallinn University of Technology
Tallinn, Estonia
biasad@ttu.ee

Anouar Belahcen
Dept. of Electrical Engineering and Automation
Aalto University
Espoo, Finland

Abstract— In this paper, a detailed analytical model of a three-phase squirrel cage induction motor is derived. The geometrical parameters of the motor are considered and couple magnetic circuit theory is used for the calculation of inductances, resistances and other performance parameters. Although analytical models are not as accurate as numerical models, their lower calculation time makes them important in the field of performance analysis and fault diagnostics, particularly in hardware-in-the-loop environment and inverse problem theory implementation. The model is made general for any number of rotor bars even if they are not integral number per pole and stator geometry considering the end ring parameters, leakage inductances, slotting and end winding effects.

Keywords— Analytical model, induction motors, fault diagnosis

I. INTRODUCTION

Electrical machines, particularly induction motors, are playing a key role in modern day society. This argument can be supported by the fact that they are consuming more than 60% of total generated energy worldwide [1]. The induction machines are dominating all other types of electrical machines, working as motors such as squirrel cage induction motors and as generators such as doubly fed induction generator [2]. This is because of their simple structure, high efficiency, easy maintenance, efficient controllability, high torque and ability to work in rough industrial environment. This increasing importance of the induction motors make their fast and accurate mathematical models equally important. These models are very important for performance analysis [3], fault simulations under transient and steady state conditions [4], parameters estimations [5], hardware-in-the-loop environment [6], design of electrical machine drives [7], etc.

Since these motors are associated with mechanically moving parts, they are always subject to failures [8]. The faults in electrical machines are degenerative in nature, inviting fast and accurate diagnostic algorithms, to avoid any catastrophic situation. Although finite element analysis based numerical models are more accurate, they are not suitable for diagnostic algorithms, where the mathematical model of the system is necessary. This is so because numerical models

require more computational time and memory as compared to analytical models. Moreover, the conventional d-q models are not always suitable to be used in diagnostic algorithms, because they neglect the effect of spatial harmonics. The time and space harmonics have impact on speed, torque, currents and other performance parameters of electrical machines. The faults at the incipient stage are so small that any approximation can lead to failure in their detection.

In this paper, a detailed analytical model of squirrel cage induction motor is derived. Unlike the conventional mathematical models, as presented in [9][10][11][12], the stator slots opening effect on the air gap is considered, the stator and rotor electrical parameters are computed using their geometrical dimensions, the stator end winding and rotor end ring parameters are calculated using analytical functions. The model is presented in a systematic manner for ease of understanding and implementation.

II. FLOW CHART DIAGRAM

Induction motor is a complex system where a number of parameters are interrelated with each other. It is recommended to follow a systematic way while making its mathematical model. To avoid complexity the entire parameters can be divided into rotor, stator and mutual parameters as shown in fig. 1.

On the stator side the electrical parameters such as number of phases, voltage, connection scheme, frequency and the mechanical parameters such as number of slots, dimensions of slot and winding configuration are taken as input and stator per phase resistances and leakage inductances are calculated. The stator self and mutual inductances are calculated using winding function approach as discussed in subsequent section.

Similarly, on the rotor side, the bar and end ring resistances and the leakage inductances are calculated based on the geometry of rotor slots. The self and mutual inductance among various rotor loops are calculated using winding function approach.

In order to consider the slotting effect the air gap is taken as a function of rotor and stator angles and their mutual inductances are calculated using winding function approach.

All inductances and resistances are calculated in the form of matrices for ease of implementation. At the end, the performance parameters like torque, currents, speed and rotor position is calculated. The calculated rotor position is used in feedback manner to calculate air gap and mutual inductances.

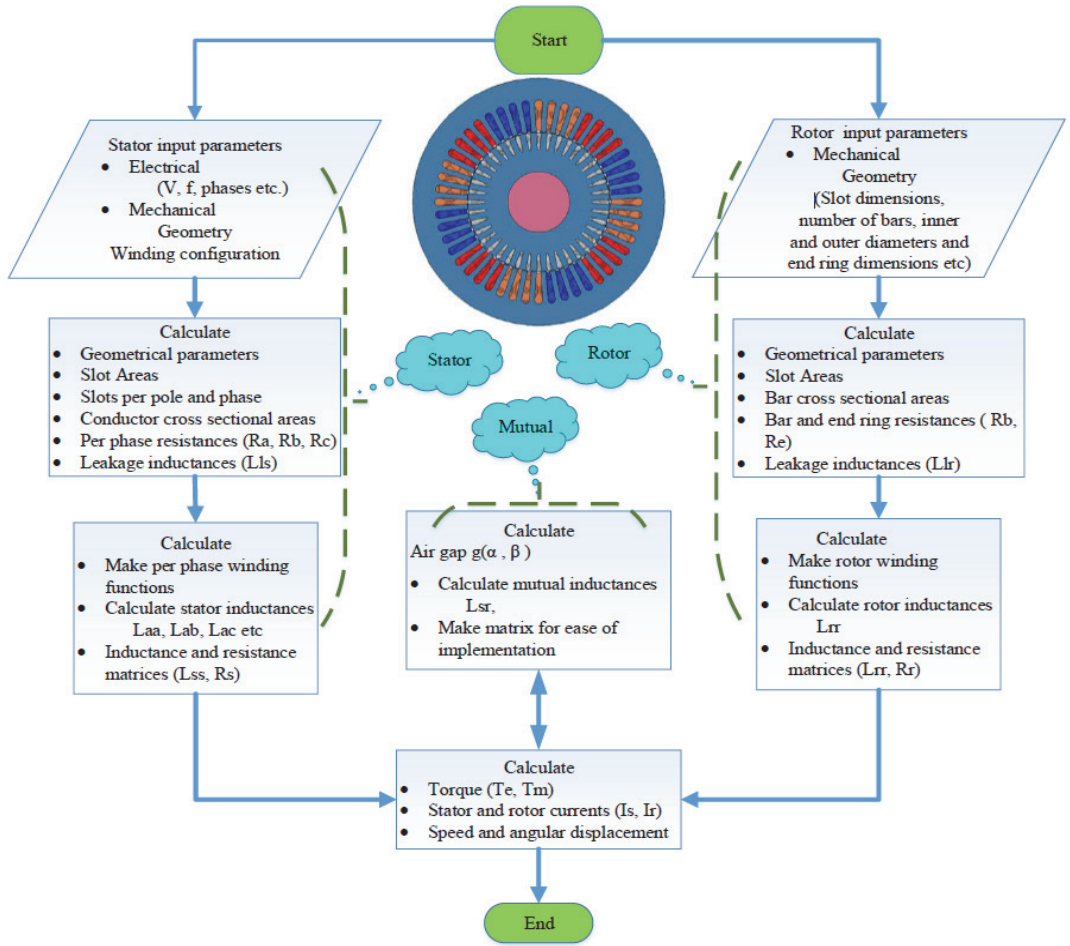


Fig. 1. Flow chart diagram of mathematical model

III. MATHEMATICAL MODELING

A. Air gap

Because of the fact that stator and rotor slot openings generate frequencies in current spectrum called spatial harmonics, the careful calculation and implementation of air gap is very important. If these slot frequencies are not considered effectively, they can become a potential candidate for errors in diagnostic algorithms. The total effective flux crosses the air gap to generate air gap flux linkage and connects different parts of machine. It means that the air gap and slot openings of stator and rotor have an impact on total flux linkage, torque, radial and tangential forces, speed and current. The total air gap of motor can be divided into two parts, the constant air gap g_c and slot air gaps variable with stator and rotor geometry (φ) and relative position (θ) as shown in equation 1.

$$g = g_c + g(\varphi, \theta) \quad (1)$$

The calculation procedure is shown in fig. 2, where distance between rotor outer and stator inner surface is taken as constant g_c . The stator slots based air gap, shown by solid line, is calculated from geometry of stator and slots. Since the motor is squirrel cage, its rotor surface is smooth having no effect on physical air gap.

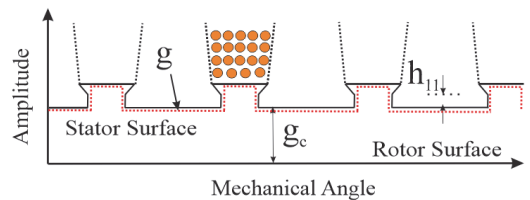


Fig. 2. Physical air gap

B. Leakage Inductance

In electrical machines, total flux can be divided into two parts, the magnetization and leakage flux. The magnetization flux (φ_m) is responsible to generate air gap flux linkage (Ψ_m) between rotor and stator and participates in energy conversion. The leakage flux (φ_l) creates leakage flux

linkage (Ψ_l) and is associated with both stator and rotor as stator leakage flux (φ_{sl}) and rotor leakage flux (φ_{rl}). This is a common perception about leakage flux that it has a negative role in electrical machines due to increase in losses which is not always true. This argument can be justified by the fact that the transient inductance of induction motors depends mainly on leakage inductances as shown by following equation.

$$L'_s \cong L_{sl} + L_{rl} \quad (2)$$

These leakage inductances should be calculated carefully because any error in their calculation can lead to wrong transient analysis of motor.

The leakage induction of a machine can be divided into air gap leakage inductance L_g , slot leakage inductance L_q , tooth tip leakage inductance L_t , end winding leakage inductance L_{ew} and skew leakage inductance L_{sq} as shown by the following equation.

$$L_l = L_g + L_q + L_t + L_{ew} + L_{sq} \quad (3)$$

In case of asynchronous machines

$$L_{ew} > L_g > L_q > L_t > L_{sq} \quad (4)$$

The detailed analytical formulas of these inductances can be found in [13].

C. Resistance Calculation

The per phase stator resistance is calculated by counting the number of turns per phase, the resistance and length of a single turn along with the number of parallel paths. The effective slot area A_s can be calculated by multiplying the actual area of slot A_A with filling factor K_f as shown in equation below.

$$A_s = A_A \times K_f \quad (5)$$

The cross sectional area of conductor can be calculated by dividing effective slot area with number of conductors (N_c) in it as given by following equation.

$$A_c = A_s / N_c \quad (6)$$

The average length of a single turn can be calculated using analytical expression as discussed in [13].

$$l_{av} \approx (2l + 2.4W + 0.1)m \quad (7)$$

Where l is the effective length of the machine and W is the average coil span. The per phase stator resistance can be calculated as,

$$R_s = N_s(\rho l_{av}/aAc) \quad (8)$$

Where, a is the number of parallel paths and N_s is effective number of series turns per phase, which is the function of total number of series turns per phase (N_t) and winding factor K_w as described by following equations.

$$N_s = K_p K_d K_s N_t \quad (9)$$

Where K_p , K_d and K_s are pitch, distribution and skewing factors respectively.

The rotor bar resistance is also calculated in a conventional way by calculating the slot area whereas, the end ring resistance is calculated and divided by number of rotor bars (n_b) to calculate the resistance of a sector between two consecutive rotor bars.

$$r_s = R_e/n_b \quad (10)$$

D. Inductance Calculation

The self and mutual inductances associated with various coils are calculated using conventional winding function approach [14].

$$L_{ij}(\theta) = \mu_0 r l \int_0^{2\pi} g^{-1}(\varphi, \theta) N_i(\varphi, \theta) N_j(\varphi, \theta) d\theta \quad (11)$$

Where θ is rotor's angular position with respect to some reference point, φ is some point along air gap, $g^{-1}(\varphi, \theta)$ is the inverse air gap, $N_i(\varphi, \theta)$ is the winding function of i th coil and can be calculated by using following formula,

$$N_i(\varphi, \theta) = n_i(\varphi, \theta) - \langle n_i(\varphi, \theta) \rangle \quad (12)$$

Where $n_i(\varphi, \theta)$ is turn function of coil, which is spatially distributed along stator or rotor surface and $\langle n_i(\varphi, \theta) \rangle$ is the average of this turn function. Since the shape of the turn function depends upon the reference point, hence it is advisable to make it in such a way that it fulfills following conditions,

$$N_i(\theta^*) = N_i(-\theta^*) \quad (13)$$

$$\int_0^{2\pi} N_i(\theta^*) d\theta^* = 0 \quad (14)$$

Where $\theta^* = 0$ is the unique angle for which $N_i(0)$ has a maximum value and condition shown by equation (13) ensures even symmetry of function.

i. Stator Inductances

For a full pitch sinusoidal distributed stator winding shown in fig. 3, the winding function can be calculated using equation (12) as given below.

$$N_i(\theta_e) = \frac{N_s}{p} \cos(\theta_e) \quad (15)$$

For constant air gap the magnetization inductance can be calculated using equation (11) as,

$$L_m = \frac{\mu_0 r l}{g} \int_0^{2\pi} \left(\frac{N_s}{p} \cos(\theta_e) \right)^2 d\theta_e \quad (16)$$

Upon integrating,

$$L_m = \frac{\mu_0 r l}{g} \left(\frac{N_s}{p} \right)^2 \pi \quad (17)$$

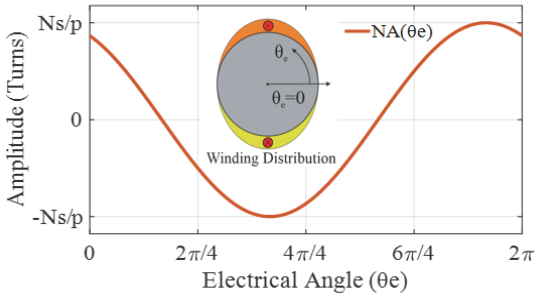


Fig. 3. Winding function of single phase sinusoidally distributed winding in stator of p poles machine

In addition, the self-inductances can be calculated by adding magnetization inductance (16) and leakage inductance (3).

$$L_{AA} = L_{BB} = L_{CC} = (L_m + L_{ls}) \quad (18)$$

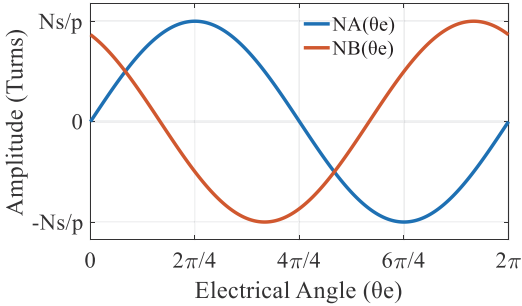


Fig. 4. Winding function of two phases for sinusoidally distributed winding in stator of p poles machine

Since phase windings are α ($2\pi/3$) electrical radians apart from each other as shown in fig. 4, the mutual inductance can be calculated as follows.

$$L_{AB} = \frac{\mu_0 r l}{g} \int_0^{2\pi} \left(\frac{N_A}{p} \cos(\theta_e) \right) \left(\frac{N_B}{p} \cos(\theta_e + \alpha) \right) d\theta_e \quad (19)$$

After integration and simplification

$$L_{AB} = \frac{\mu_0 r l}{g} \frac{N_A N_B}{p^2} \pi \cos(\theta_e) \quad (20)$$

$$L_{AB} = -\frac{\mu_0 r l}{g} \frac{N_A N_B}{p^2} \frac{\pi}{2} = -\frac{L_m}{2} \quad (21)$$

So far a symmetrical three phase system

$$L_{AB} = L_{BC} = L_{CA} = -\frac{L_m}{2} \quad (22)$$

ii. Rotor Inductances

The turn function of one rotor loop can be represented by an analytical function given below.

$$n(\theta) = \begin{cases} 1, & \theta_i \leq \theta_e \leq \theta_i + \alpha_r \\ 0, & \theta_i > \theta_e > \theta_i + \alpha_r \end{cases} \quad (23)$$

$$\begin{aligned} \langle n(\theta) \rangle &= \frac{1}{2\pi} \int_{\theta_i}^{\theta_i + \alpha_r} 1 \cdot d\theta_e \\ &= \frac{\alpha_r}{2\pi} \end{aligned} \quad (24)$$

Where $\alpha_r = \frac{2\pi}{nb}$, is the angle span between two consecutive rotor bars. The following equation shows the winding function of single loop analytically shown in fig. 5.

$$N_r(\theta_e) = \begin{cases} -\frac{\alpha_r}{2\pi}, & 0 \leq \theta_e < \theta_i \\ 1 - \frac{\alpha_r}{2\pi}, & \theta_i \leq \theta_e \leq \theta_i + \alpha_r \\ -\frac{\alpha_r}{2\pi}, & \theta_i + \alpha_r < \theta_e \leq 2\pi \end{cases} \quad (25)$$

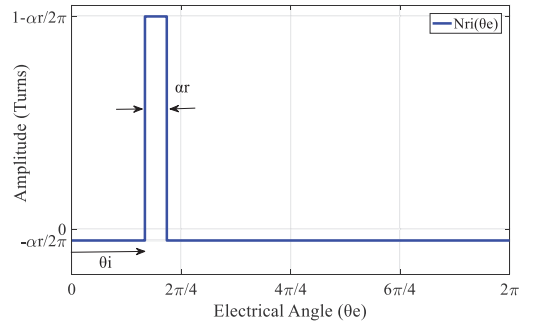


Fig. 5. Winding function of a single rotor loop

The following equation shows how to calculate self-inductance of rotor's k th loop.

$$L_{rkk} = \frac{\mu_0 r l}{g} \int_0^{2\pi} (N_r(\theta_e))^2 d\theta_e \quad (26)$$

$$\begin{aligned} &= \frac{\mu_0 r l}{g} \left[\int_0^{\theta_i} \left(-\frac{\alpha_r}{2\pi} \right)^2 d\theta_e + \int_{\theta_i}^{\theta_i + \alpha_r} \left(1 - \frac{\alpha_r}{2\pi} \right)^2 d\theta_e + \int_{\theta_i + \alpha_r}^{2\pi} \left(-\frac{\alpha_r}{2\pi} \right)^2 d\theta_e \right] \end{aligned} \quad (27)$$

$$L_{rkk} = \frac{\mu_0 r l}{g} \alpha_r \left[1 - \frac{\alpha_r}{2\pi} \right] \quad (28)$$

The equation (28) can be modified as a function of magnetization inductance (17) as follows.

$$L_{rkk} = \frac{\mu_0 r l}{g} N_s^2 N_r \frac{\pi}{4} \alpha_r \left[1 - \frac{\alpha_r}{2\pi} \right] \frac{1}{N_s^2 \pi} \quad (29)$$

$$L_{rkk} = \frac{4}{\pi} \left(\frac{N_r}{N_s} \right)^2 L_m \alpha_r \left[1 - \frac{\alpha_r}{2\pi} \right] \quad (30)$$

Fig. 6, shows the winding function of any two rotor-loops i and j . While the mutual inductance can be calculated using following equations.

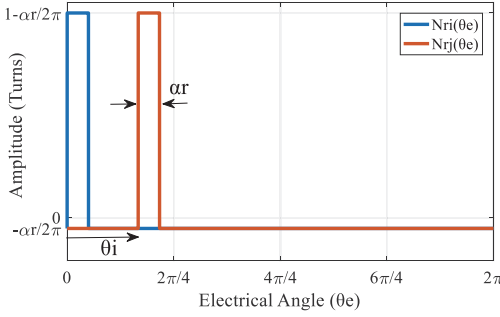


Fig. 6. Winding function of two rotor loops placed at arbitrary locations.

$$L_{rni} = \frac{\mu_o r l}{g} \int_0^{2\pi} (N_{rn}(\theta_e))(N_{ri}(\theta_e)) d\theta_e \quad (31)$$

$$= \frac{\mu_o r l}{g} \left[\int_0^{\alpha_r} \left(1 - \frac{\alpha_r}{2\pi}\right) \left(-\frac{\alpha_r}{2\pi}\right) d\theta_e + \int_{\alpha_r}^{\theta_i} \left(-\frac{\alpha_r}{2\pi}\right)^2 d\theta_e + \int_{\theta_i}^{\theta_i + \alpha_r} \left(1 - \frac{\alpha_r}{2\pi}\right) \left(-\frac{\alpha_r}{2\pi}\right) d\theta_e + \int_{\theta_i + \alpha_r}^{2\pi} \left(-\frac{\alpha_r}{2\pi}\right)^2 d\theta_e \right] \quad (32)$$

$$L_{rni} = \frac{\mu_o r l}{g} \left[-\frac{\alpha_r^2}{2\pi} \right] \quad (33)$$

After modification as a function of magnetization inductance (17), equation (33) can be represented as.

$$L_{rni} = \frac{4}{\pi} \left(\frac{N_r}{N_s} \right)^2 L_m \left[-\frac{\alpha_r^2}{2\pi} \right] \quad (34)$$

This equation shows that the mutual inductance between any two rotor loops does not depend on the angle between them.

iii. Rotor and Stator Mutual Inductances

The mutual inductance between rotor and stator is the function of rotor's angle and can be calculated as follows. The graphical representation of mutual inductance using winding functions is shown in fig. 7.

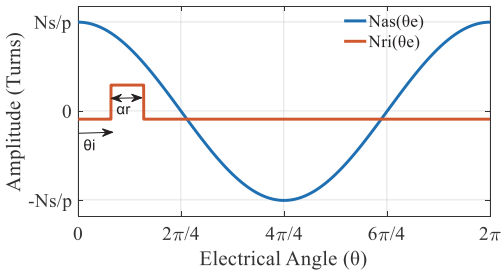


Fig. 7. Winding function of a stator winding and ith rotor loop

$$L_{asri} = \frac{\mu_o r l}{g} \int_0^{2\pi} (N_{as}(\theta_e))(N_{ri}(\theta_e)) d\theta_e \quad (35)$$

$$= \frac{\mu_o r l N_s}{g p} \left[\int_0^{\theta_i} \left(-\frac{\alpha_r}{2\pi}\right) \cos(\theta_e) d\theta_e + \int_{\theta_i}^{\theta_i + \alpha_r} \left(1 - \frac{\alpha_r}{2\pi}\right) \cos(\theta_e) d\theta_e + \int_{\theta_i + \alpha_r}^{\frac{\pi}{2}} \left(-\frac{\alpha_r}{2\pi}\right) \cos(\theta_e) d\theta_e + \int_{\frac{\pi}{2}}^{\frac{3\pi}{2}} \left(-\frac{\alpha_r}{2\pi}\right) \cos(\theta_e) d\theta_e + \int_{\frac{3\pi}{2}}^{2\pi} \left(-\frac{\alpha_r}{2\pi}\right) \cos(\theta_e) d\theta_e \right] \quad (36)$$

$$= \frac{\mu_o r l N_s}{g p} [-\sin \theta_i + \sin(\theta_i + \alpha_r)] \quad (37)$$

$$= \frac{\mu_o r l N_s}{g p} [\sin \alpha_r \cos \theta_i - \sin \theta_i (1 - \cos \alpha_r)] \quad (38)$$

For a two-pole machine, this equation can be simplified using trigonometric identities as in [15].

$$L_{sri} = \frac{\sin(\frac{\alpha_r}{2})}{N_s} \frac{4}{\pi} L_m \cos(\theta_r + (i-1)\alpha_r + \frac{\alpha_r}{2}) \quad (39)$$

The mutual induction between i th rotor loop and phases b and c can be calculated in same way by shifting phase a by ± 120 degrees.

E. Speed and Torque

The final equations in matrices form can be shown as;

$$\begin{bmatrix} V_s \\ 0 \end{bmatrix} = \begin{bmatrix} R_s & 0 \\ 0 & R_r \end{bmatrix} \begin{bmatrix} I_s \\ I_r \end{bmatrix} + \frac{d}{dt} \begin{bmatrix} L_{ss} & L_{sr} \\ L_{rs} & L_{rr} \end{bmatrix} \begin{bmatrix} I_s \\ I_r \end{bmatrix} \quad (40)$$

From where currents can be calculated as

$$\begin{bmatrix} I_s \\ I_r \end{bmatrix} = \frac{1}{\begin{bmatrix} L_{ss} & L_{sr} \\ L_{rs} & L_{rr} \end{bmatrix}} \int \left[\begin{bmatrix} V_s \\ 0 \end{bmatrix} - \begin{bmatrix} R_s & 0 \\ 0 & R_r \end{bmatrix} \begin{bmatrix} I_s \\ I_r \end{bmatrix} \right] dt \quad (41)$$

$$T_e = I_s^T \left(\frac{d}{d\theta} L_{rs} \right) I_r \quad (42)$$

In matrices form it is very easy to implement the model in Matlab environment.

$$T_{e1} = \begin{bmatrix} I_s \\ I_r \end{bmatrix}^T \frac{d}{d\theta} \begin{bmatrix} L_{ss} & L_{sr} \\ L_{rs} & L_{rr} \end{bmatrix} \begin{bmatrix} I_s \\ I_r \end{bmatrix} \quad (43)$$

$$= \begin{bmatrix} I_s^T & I_r^T \end{bmatrix} \begin{bmatrix} 0 & \frac{d}{d\theta} L_{sr} \\ \frac{d}{d\theta} L_{rs} & 0 \end{bmatrix} \begin{bmatrix} I_s \\ I_r \end{bmatrix} \\ = I_r^T \frac{d}{d\theta} L_{rs} I_s + I_s^T \frac{d}{d\theta} L_{sr} I_r \\ = 2T_e \quad (44)$$

The generated torque becomes double using the matrices approach hence it should be divided by two to get actual result.

$$T_e = \frac{T_{e1}}{2} \quad (45)$$

Finally the speed and angular displacement of motor can be calculated using following equation where T_e is generated torque, T_L is load torque, B is friction coefficient J is moment of inertia of rotor and ω_m is motor's electrical speed.

$$J \frac{d}{dt} \omega_m = T_e - T_L - B \omega_m \quad (46)$$

CONCLUSIONS

A detailed systematic approach to make the mathematical model of squirrel cage induction motor is presented in this paper. Unlike pre-calculated values of resistances, leakage and magnetization inductances; the motor's geometry and winding configurations are used to calculate all performance parameters analytically.

The air gap of motor is proposed as a function of rotor position and stator angle. The inclusion of slots opening effect is very important for mathematical models designed for fault diagnostics. This is so because slot openings produce high frequency components in current spectrum, which should be handled carefully. Although for the sake of simplicity, it is taken as constant for various inductances calculations however, it can be easily handled using Taylor and Fourier series. This is a general model for any number of rotor bars regardless to the integral number of bars per pole. Moreover, this model can be used for any number of poles, parallel paths and number of conductors per slot.

It is good to study transient and steady state response of system and simulate common types of faults such as broken rotor bar, stator short circuit and eccentricity. The equations are compiled in the form of matrices, which reduces the complexity while implementing them in computer program.

The non-sinusoidal distribution of rotor circuits improves the accuracy of model. The equations work good for two pole machine while they can be updated for general p pole machine by multiplying L_m with $(p/2)$ and changing L_{sr} and L_{rr} correspondingly.

REFERENCES

- [1] H. W. Penrose, "Test Methods for Determining the Impact of Motor Condition on Motor Efficiency and Reliability," PhD Diss., vol. ALL-TEST P, no. LLC, Old Saybrook, CT, pp. 1–8.

- [2] J. Ma, D. Zhao, L. Yao, M. Qian, K. Yamashita, and L. Zhu, "Analysis on application of a current-source based DFIG wind generator model," *CSEE J. Power Energy Syst.*, vol. 4, no. 3, pp. 352–361, Sep. 2018.
- [3] B. Asad, T. Vaimann, A. Rassolkina, and A. Belahcen, "Dynamic state space model based analysis of a three-phase induction motor using nonlinear magnetization inductance," in 2018 19th International Scientific Conference on Electric Power Engineering (EPE), 2018, pp. 1–6.
- [4] H. A. Toliyat and T. A. Lipo, "Transient analysis of cage induction machines under stator, rotor bar and end ring faults," *IEEE Trans. Energy Convers.*, vol. 10, no. 2, pp. 241–247, Jun. 1995.
- [5] S. Bachir, S. Tnani, J.-C. Trigeassou, and G. Champenois, "Diagnosis by parameter estimation of stator and rotor faults occurring in induction machines," *IEEE Trans. Ind. Electron.*, vol. 53, no. 3, pp. 963–973, Jun. 2006.
- [6] A. Saleem, R. Issa, and T. Tutunji, "Hardware-In-the-Loop for on-line identification and control of three-phase squirrel cage induction motors," *Simul. Model. Pract. Theory*, vol. 18, no. 3, pp. 277–290, Mar. 2010.
- [7] M. Mengoni, L. Zarri, A. Tani, G. Serra, and D. Casadei, "Stator Flux Vector Control of Induction Motor Drive in the Field Weakening Region," *IEEE Trans. Power Electron.*, vol. 23, no. 2, pp. 941–949, Mar. 2008.
- [8] B. Asad, T. Vaimann, A. Belahcen, and A. Kallaste, "Broken Rotor Bar Fault Diagnostic of Inverter Fed Induction Motor Using FFT, Hilbert and Park's Vector Approach," in 2018 XIII International Conference on Electrical Machines (ICEM), 2018, pp. 2352–2358.
- [9] Zhongming Ye, Bin Wu, and N. Zargari, "Modeling and simulation of induction motor with mechanical fault based on winding function method," in 2000 26th Annual Conference of the IEEE Industrial Electronics Society. IECON 2000., vol. 4, pp. 2334–2339.
- [10] A. K. Ibrahim, M. I. Marei, H. S. El-Gohary, and S. A. M. Shehata, "Modeling of Induction Motor Based on Winding Function Theory to Study Motor under Stator/Rotor Internal Faults."
- [11] H. A. Toliyat, M. S. Arefeen, and A. G. Parlos, "A method for dynamic simulation of air-gap eccentricity in induction machines," *IEEE Trans. Ind. Appl.*, vol. 32, no. 4, pp. 910–918, 1996.
- [12] R. M. Tallam, T. G. Habetler, and R. G. Harley, "Transient model for induction machines with stator winding turn faults," *IEEE Trans. Ind. Appl.*, vol. 38, no. 3, pp. 632–637, 2002.
- [13] J. Pyrhönen, T. Jokinen, and V. Hrabovcová, Design of rotating electrical machines. .
- [14] Xiaogang Luo, Yuefeng Liao, H. A. Toliyat, A. El-Antably, and T. A. Lipo, "Multiple coupled circuit modeling of induction machines," *IEEE Trans. Ind. Appl.*, vol. 31, no. 2, pp. 311–318, 1995.
- [15] A. R. Munoz and T. A. Lipo, "Complex vector model of the squirrel-cage induction machine including instantaneous rotor bar currents," *IEEE Trans. Ind. Appl.*, vol. 35, no. 6, pp. 1332–1340, 1999.

Publication XI

B. Asad, T. Vaimann, A. Belahcen, A. Kallaste. Broken Rotor Bar Fault Diagnostic of Inverter Fed Induction Motor Using FFT, Hilbert and Park's Vector Approach. IEEE XXIIIrd International Conference on Electrical Machines (ICEM'2018) Alexandroupoli - Greece September 3-6, 2018, pp. 2352–2358.

Broken Rotor Bar Fault Diagnostic of Inverter Fed Induction Motor Using FFT, Hilbert and Park's Vector Approach

Bilal Asad, Toomas Vaimann, Anouar Belahcen, Ants Kallaste

Abstract --In this paper, fast Fourier transform, Hilbert transform and extended Park's vector algorithms are implemented for broken rotor bar fault diagnostics of a 22 kW inverter fed induction motor. The mentioned algorithms are initially explained in their mathematical point of view with the help of simulations and then implemented on the phase currents taken from laboratory setup of inverter fed healthy and faulty machines containing one, two and three broken rotor bars. The effects of faults and inverter-based harmonics are studied and a comparison of the techniques in some major attributes is presented.

Index Terms--Fast Fourier transforms, fault diagnosis, harmonic analysis, induction motors.

I. INTRODUCTION

IN almost every domain of industrial and domestic life, induction motors are playing a vital role. They are acting as the working horse in almost every sector, such as fans, water pumps, washing machines, traction, textile mills, process industries, ship thrust systems, robots, conveyor belts etc. In a survey done by Penrose [1], it is claimed that induction motors are the major consumers of electricity, consuming about 60% of the total generated electric energy distributed between different sectors as shown in Fig. 1.

The popularity of induction motors is due to their simple and rugged structure, low cost, high torque per weight ratio and easy maintenance. Since these machines are associated with mechanically moving parts, they are always subject to failures. The faults in the induction motors are usually degenerative in nature; hence, their detection at incipient stage is very important to avoid any catastrophic situation. No doubt, the failure of the motor will affect the reliability of operation, economy and motor's life itself. The rotor and bearing associated faults always make a big proportion of the total faults because of the mechanical and magnetic stresses acting on them. The percentage contribution of different types of faults is shown in Fig. 2 [2], where other faults may consist of supply related or external faults.

The key role of the induction motors in industry has made its condition monitoring very important. A variety of fault

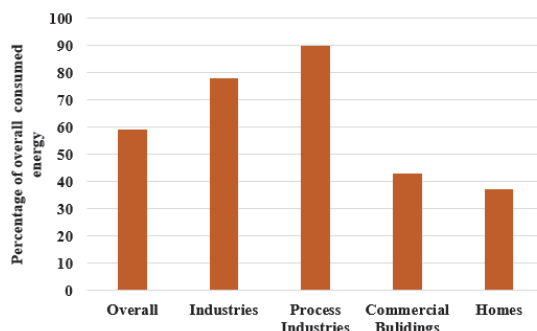


Fig. 1. Overall electric energy consumption by induction motor and percentage of it in different sectors.

diagnostic techniques can be found in the literature, such as the motor current signature analysis (MCSA), the mechanical vibration signal analysis, etc. Out of all main diagnostic areas, the MCSA is gaining more and more popularity, because most of its variants require only a current sensor to detect the stator's current. In addition, almost all MCSA based diagnostic techniques are non-invasive in nature, making them suitable for online fault diagnostics without any disturbance in the process.

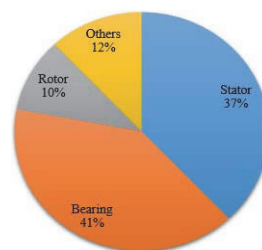


Fig. 2. Types and percentage contribution of various faults in an induction motor.

These techniques also require low computational power and memory to save the intermediate and final results, making them suitable to be implemented on a digital signal processing (DSP) system or a field programmable gate array (FPGA) kits, as compared to some advanced techniques like neural networks, fuzzy logic, etc.

Researchers are struggling to make diagnostic algorithms more accurate, fast, reliable and cheap in the sense of hardware cost. The research presented in [3] proposed a

This work was supported by the European Regional Development Fund under Mobilias Plus programme returning researcher grant MOBTP13.

B. Asad, T. Vaimann and A. Kallaste are with the Department of Electrical Power Engineering and Mechatronics, Tallinn University of Technology, Estonia (e-mail: biasad@ttu.ee)

A. Belahcen is with Department of Electrical Engineering and Automation, Aalto University, Espoo, Finland and with the Department of Electrical Power Engineering and Mechatronics, Tallinn University of Technology, Estonia (e-mail: anouar.belahcen@aalto.fi)

Hilbert transform to reduce the problem of spectral leakage and frequency resolution, without considerable increase in the sampling rate or data acquisition time. In [4], a reduced envelope of the stator current is introduced, to decrease the size of data, making it suitable to implement in embedded devices. The harmonic order tracking analysis is proposed in [5], giving a high frequency resolution in time-frequency domain. In parallel with these harmonic analysis based techniques, Park's vector is also gaining popularity. It was proposed by Cardoso *et. al.* in [6], [7] and is a potential candidate in the field of diagnostics. Many variations of Park's vector based diagnostic algorithms can be found in the literature, such as the extended Park's vector approach (EPVA) [8], [9], the reduced modulus of Park's vector (RMPV) [10], etc. The researchers in [11] have introduced faults diagnostics using the finite element analysis and [12] proposed diagnostic in some remote location using cloud computation, both of which can be paired for better results with any of the above mentioned technique.

In this paper, three common diagnostic techniques, called the discrete Fourier transform, Hilbert transform and Park's vector are implemented to detect broken rotor bars of a 22 kW inverter fed induction motor. These techniques are extensively used in literature but have not been very much used in conjunction with frequency converter supplied motors. In this paper, we have implemented the above-mentioned algorithms on real data taken from laboratory where both drive and load motors are fed with frequency converters with a switching frequency of 10kHz and working under the state vector control (SVC) based direct torque control (DTC) mode.

II. ROTOR ASYMMETRIES AND FREQUENCY SPECTRUM

Most of the MCSA based techniques are related with the detection of harmonics in the motor's current spectrum. It has been shown that each kind of fault modulates the stator current in a specific manner resulting in specific harmonics. The detection of these harmonic components can lead to the cause of the fault even at incipient stage. Irregularities in the rotor, such as broken rotor bar, broken end rings and high resistance connections, can be detected by detecting the following modulating frequencies [13]:

$$f_{BR} = f_s \pm 2ksf_s, \quad k = 1, 2, 3, \dots \quad (1)$$

where, f_s is the supply frequency and s is the slip of the machine. With an increase in the order k , the frequency of harmonics increases but the amplitude decreases. Hence, for simplicity, only the first harmonic can be taken as fault indicator, because it contains more energy than the rest of the higher order harmonics. This first harmonic will have two frequencies around the supply frequency component, called the lower side band (LSB) and the upper side band (USB), having frequencies ($f_{lsb} = f_s - 2sf_s$) and ($f_{usb} = f_s + 2sf_s$) respectively. Since these fault frequencies depend on the slip, the spectral leakage of the supply frequency becomes a major problem under small and no load conditions. This problem can be solved by filtering out the fundamental component using signal-processing tools.

The eccentricity fault can be detected with the help of

harmonic frequencies, described by the formula [14]:

$$f_{ecce} = \left[(kn_{br} + n_d) \left(\frac{1-s}{p} \right) \pm v \right] f_s \quad (2)$$

where k is any integer, n_{br} is the number of rotor bars, ($n_d = 0$) for static eccentricity and $n_d = 1, 2, 3, \dots$ in case of dynamic eccentricity, s is the slip, $v = 1, 2, 3, \dots$ represents the supply harmonics and p is the number of pole pairs. More precisely, mixed eccentricity faults harmonics can be represented as [5].

$$f_{ecce} = f_1 \pm kf_r, \quad k = 1, 2, 3, \dots \quad (3)$$

Broken bearings can be diagnosed by detecting the harmonic frequencies as shown in the following equation [14]:

$$f_{ecce} = \left| f_s \pm \left(\frac{mn_b f_r}{2} \right) \left(1 \pm \frac{b_d}{p_d} \cos \theta \right) \right| \quad (4)$$

where n_b is the number of bearing balls, f_r is the rotor's mechanical frequency, m is a positive integer, p_d is the bearing pitch diameter, b_d is the bearing ball's diameter and θ is the angle between ball and races. For n_b between 6 and 9, the above equation can be simplified as in [5]:

$$f_{bbo} = f_s \pm 0.4kn_b f_r, \quad k = 1, 2, 3, \dots \quad (5)$$

$$f_{bbi} = f_s \pm 0.6kn_b f_r, \quad k = 1, 2, 3, \dots \quad (6)$$

where f_{bbo} and f_{bbi} are the harmonic frequencies in case of outer race and inner race defect respectively.

In case of short turn faults, the emerging harmonics can be found according to the following equation:

$$f_{st} = f_s \left[\frac{m}{p} (1-s) \pm k \right], \quad k = 0, 1, 3, 5, \dots \quad (7)$$

These harmonics also appear in the spectrum under the unbalanced rotor conditions, hence they can also be used as a general fault diagnostic indicator when precision is not required [14]. In subsequent sections only broken rotor bar cases are emphasized.

III. MATHEMATICAL BACKGROUND AND SIMULATIONS

A. Broken Rotor Bars Current Amplitude Modulation

The phase currents of an ideal healthy machine can be described as follows:

$$i_a(t) = I_m \sin(\omega t) \quad (8)$$

$$i_b(t) = I_m \sin\left(\omega t + \frac{2\pi}{3}\right) \quad (9)$$

$$i_c(t) = I_m \sin\left(\omega t - \frac{2\pi}{3}\right) \quad (10)$$

where I_m is the peak current and ω is its angular frequency. When a rotor bar breaks, it starts modulating the healthy current to generate a faulty signal:

$$i_{af}(t) = [1 + m(t)]i_a(t) \quad (11)$$

where $m(t)$ is the modulating signal, having a modulation index M , which depends on the number of broken bars (N_b) and the total number of rotor bars (N_r). Since the rotor is circular and symmetrical, the modulating signal is also sinusoidal, i.e.:

$$m(t) = M \cos(\omega_o t + \varphi) \quad (12)$$

where $\omega_o = 2\pi f_o$ is the fault characteristic frequency and depends upon the nature of the fault and the slip of the machine. In case of broken rotor bars, the characteristic fault frequency is at $2sf_s$:

$$f_o = 2sf_s \quad \text{and} \quad \omega_o = 2\pi(2sf_s) \quad (13)$$

$$m(t) = M \cos(4\pi sf_s t + \varphi) \quad (14)$$

$$i_{af}(t) = [1 + M \cos(4\pi sf_s t + \varphi)] i_a(t) \quad (15)$$

$$i_{af}(t) = [1 + M \cos(4\pi sf_s t + \varphi)] I_m \sin(\omega t) \quad (16)$$

$$i_{af}(t) = I_m \sin(2\pi f_s t) + \left(\frac{MI_m}{2}\right) [\sin(2\pi f_s(1 + 2s)t + \varphi) + \sin(2\pi f_s(1 - 2s)t + \varphi)] \quad (17)$$

where the modulation index M can be approximated as a ratio of the number of broken rotor bars and the total number of bars as in [15]:

$$M \approx N_b / N_t \quad (18)$$

B. Discrete Fourier Transform

Fourier series is a very powerful tool to convert a signal from the time domain to the frequency domain. Fourier series deals with periodic signals but non-periodic signals can be segregated into its frequency components using the Fourier transform. A very good overview and history of Fourier transform can be found in [16]. Fast Fourier transform (FFT) is an algorithm to solve the discrete Fourier transform (DFT) represented by the formula:

$$X_n = \sum_{k=0}^{N-1} x_n e^{-i2\pi kn/N}, \quad k = 0, 1, 2, \dots, (N-1) \quad (19)$$

where x_n is the discrete sampled signal and N is the number of samples, which should be a number in power of 2, i.e. $N = 2^x$. For better understanding, a very simple Hann window based FFT analysis of faulty machine current given in (17) is shown in Fig. 3. The results are representing at three different load conditions with five broken bars out of a total of 40 bars. It is evident that the sideband frequencies are moving away from the fundamental supply frequency with the increase in the load or slip. In addition, the amplitude of the harmonic frequencies depends on the number of broken bars.

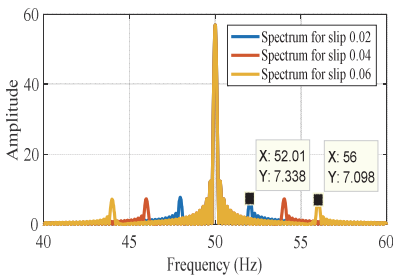


Fig. 3. Frequency spectrum of a faulty signal with five broken bars at the slip of 0.02 (blue), 0.04 (red), 0.06 (yellow).

Almost every kind of signal processing technique depends on the frequency resolution when the knowledge of harmonics becomes essential. It is a separation between two adjacent data points of DFT and can be defined using the following equations:

$$t_{sig} = t_s \times N = N / f_s \quad (20)$$

$$df = 1/t_{sig} = f_s / N = BW / SL \quad (21)$$

$$SL = N / 2 \quad (22)$$

where df is the frequency resolution, f_s is the sampling frequency, BW is the bandwidth, SL is the number of spectral lines, t_{sig} is the measurement or acquisition time of the signal and N is the number of data points used in FFT or the total number of samples. It is evident that frequency resolution can only be increased by increasing the measurement time, also called the acquisition or frame time, of the signal. Frequency resolution can also be increased by zero paddings of the signal called the spectral interpolation.

C. Hilbert Transform

Hilbert transform converts a real valued signal into a complex analytical signal. It can be used to find an envelope of a signal, which is useful in many ways, such as the demodulation of an amplitude modulated (AM) signal. It can be considered as a filter, which shifts the phases of all frequency components of its input signal by $-\pi/2$ radians. Mathematically, it can be defined as the convolution of a given signal with a non-integrable function $(1/\pi t)$ as follows:

$$H(t) = \frac{1}{\pi} \int_{-\infty}^{\infty} \frac{f(x)}{t - x} dx, \quad (23)$$

Fig. 4 (a) is representing the envelope of a faulty motor current carrying the information of a faulty harmonic modulating stator's current. The frequency spectrum of this envelope for three different load conditions is shown in Fig. 4 (b), where it does not contain a fundamental component, reducing the problem of spectral leakage.

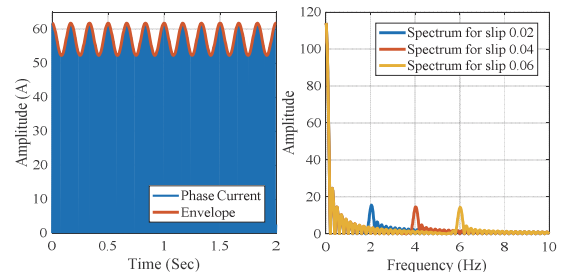


Fig. 4. Envelope detection of phase current using Hilbert transform and its frequency spectrum at different slips.

D. Modulus of Park's Vector

Park's vector is a complex analytical representation of three phase currents into two phases proposed by R.H. Park in 1929 [17]. The transformation of abc phases to equivalent $d-q$

phases reduces the number of equations and mutual inductances, making it a very popular tool in the field of electrical machines modeling [18], control [19] and diagnostics [20]. Researchers in [7] used the Park's vector of current, voltage and flux for diagnostic purposes on a current source inverter fed induction motor. Park's space vector can be constructed by adding vectors to the corresponding single phases as:

$$\vec{i}_s(t) = \frac{2}{3} (\vec{i}_{as}(t) + a\vec{i}_{bs}(t) + a^2\vec{i}_{cs}(t)) \quad (24)$$

$$\vec{i}_s(t) = \frac{2}{3} \left(\vec{i}_{as}(t) + \left(-\frac{1}{2} + j\frac{\sqrt{3}}{2}\right) \vec{i}_{bs}(t) + \left(-\frac{1}{2} - j\frac{\sqrt{3}}{2}\right) \vec{i}_{cs}(t) \right) \quad (25)$$

$$\vec{i}_s(t) = \vec{i}_{ds}(t) + j\vec{i}_{qs}(t) \quad (26)$$

$$PVM_h = \sqrt{i_{ds}^2 + i_{qs}^2} = I_m \quad (27)$$

Similarly, the modulus of the faulty machine with broken rotor bars can be calculated as shown below. It is evident that Park's vector modulus of the faulty machine is no longer a constant number, but becomes a sinusoidal function of time.

$$PVM_f(t) = \sqrt{i_{dsf}^2 + i_{qsf}^2} = I_m[1 + M \cos(4\pi s f_s t + \varphi)] \quad (28)$$

where $a = e^{j\frac{2\pi}{3}} = -\frac{1}{2} + j\frac{\sqrt{3}}{2}$ and $a^2 = e^{j\frac{4\pi}{3}} = -\frac{1}{2} - j\frac{\sqrt{3}}{2}$. As proposed by [21], the modulus of Park's vector can be very useful to diagnose the faults. With the increase in the number of broken rotor bars, distortion in the modulus of Park's vector increases, as shown in Fig. 5.

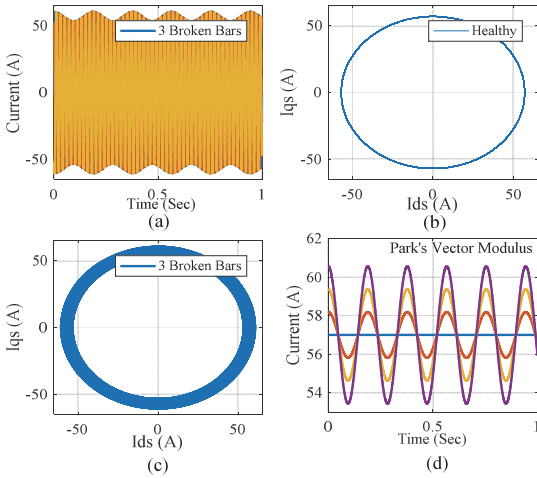


Fig. 5. (a) Motor current with three broken bars, (b) Park's vector of the healthy motor, (c) Park's vector of the faulty motor with three broken bars, (d) Park's vector modulus of healthy (blue), 1 (red), 2 (yellow) and 3 (purple) broken rotor bars motor.

IV. EXPERIMENTAL SETUP

The methods under study are applied to the experimental measurement results of a 22 kW, three-phase squirrel-cage induction motor, the parameters of which are shown in Table 1. The motor is fed with three-phase supply through an industrial frequency converter with a switching frequency of 10kHz and it is mechanically loaded by an identical machine fed from a frequency converter to ensure the correct loading level. The stator currents are measured with the Dewetron data acquisition device, as shown in Fig. 6. The current samples are taken for healthy as well as one, two and three broken rotor bar induction motors under no-load and rated load conditions. The measurement time is 100 sec with the sampling frequency of 1000 Hz.

TABLE I
MOTOR SPECIFICATIONS

Sr. No.	Parameter	Symbol	Value
1	Rated speed	N_r	1680 rpm@60 Hz; 1400 rpm@50 Hz
2	Rated power	P_r	22 kW@60 Hz; 18 kW@50 Hz
3	Connection	Y, Δ	Star (Y)
4	Power factor	$\cos\phi$	0.860
5	Number of poles	P	4
6	Number of rotor bars	N_{rb}	40
7	Number of stator slots	N_s	48

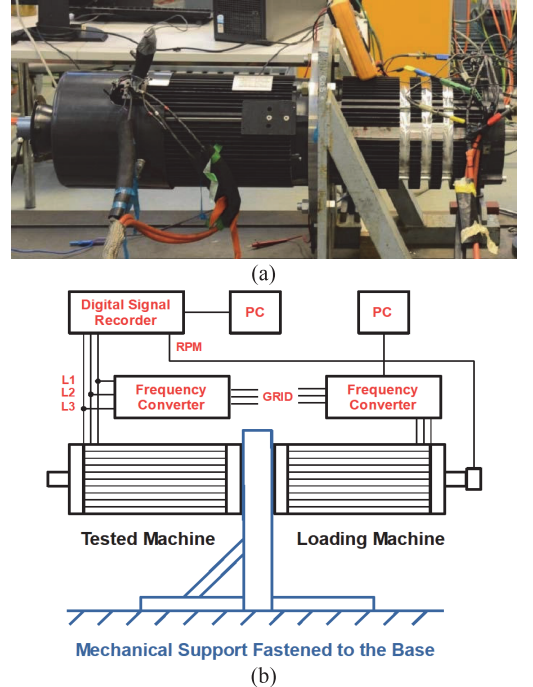


Fig. 6. (a) Hardware setup, (b) block diagram.

V. RESULTS AND DISCUSSION

The motor current signature of a phase A for healthy, one, two, and three broken bar cases taken from laboratory setup is shown in Fig. 7. The effect of broken rotor bars on the envelope of the current signature is clearly visible where the current axis is zoomed in to make signal's variations more legible.

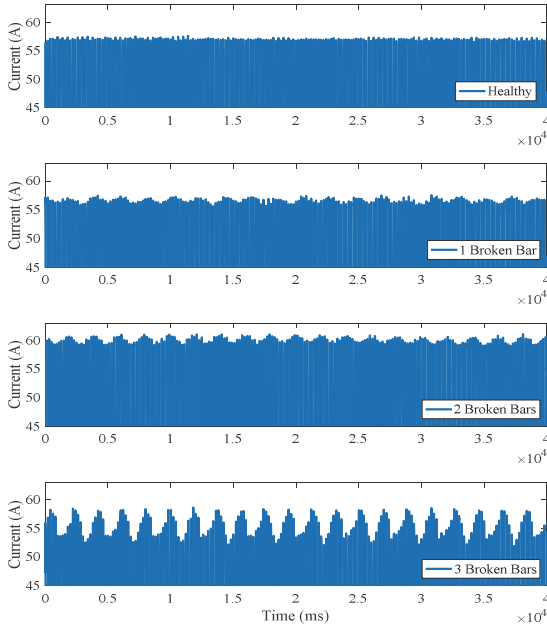


Fig. 7. Motor's phase current for healthy, one broken bar, two broken bars and three broken bars.

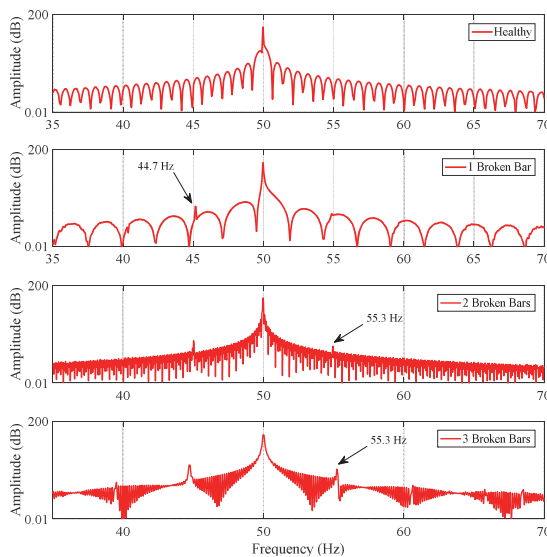


Fig. 8. Frequency spectrum of healthy, two broken bar and three broken bar induction motors.

The frequency spectra of the currents shown in Fig. 7 are presented in Fig. 8. It is clear in the Fig that at rated load corresponding to a slip of 0.053, the faulty harmonic frequency appears at 55.3 Hz, having the lower side band at 44.7 Hz. The amplitude of harmonics is increasing with the increase in the number of broken rotor bars.

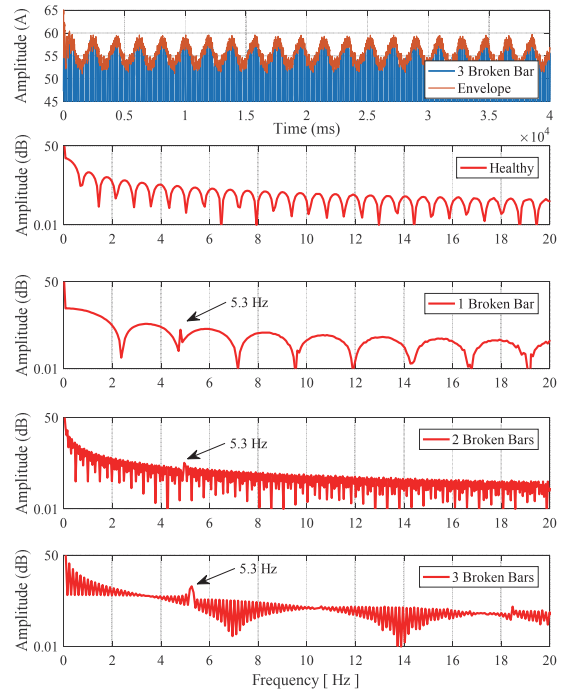


Fig. 9. Current signature and envelope of motor with three broken bars, Frequency spectrum of motor's current envelope for healthy, one broken bar, two broken bars and three broken bars cases respectively from top to bottom.

In Fig. 8, it is evident that most of the power is in the fundamental component, which is the supply frequency and leads to the spectral leakage. Since the power of faulty frequencies is very small as compared to the supply frequency, it is very difficult to detect the faulty harmonics under no load and low slip conditions. This problem can be solved by performing the FFT analysis of the current envelope, taking advantage of the fact that the envelope always contains the modulating frequencies. Fig. 9 shows the detection of the envelope of motor phase current with three broken bars using the Hilbert transform and the frequency spectrum of the detected envelope for one, two and three broken rotor bar cases.

Fig. 10 shows the Park's vector plots of motor currents presented in Fig. 7. It is evident that for healthy case it is not perfectly circular because the supply is from an inverter and the width of the circumferential line is increasing with the increase in the number of broken rotor bars. The modulus of all the above-mentioned Park's vectors is shown in Fig. 11. For better legibility, only oscillating component across zero line are shown by subtracting the mean value. The fluctuations in the case of the healthy motor are due to the harmonics injected by the inverter.

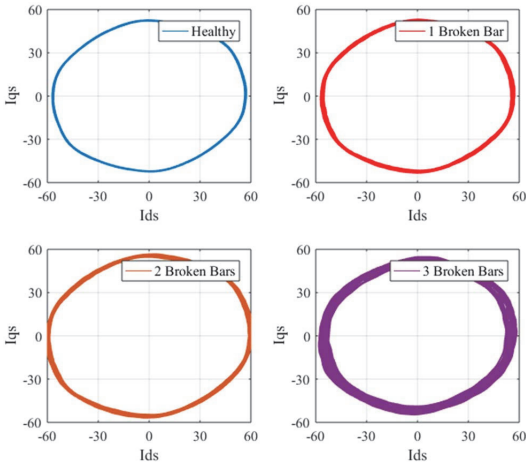


Fig. 10. Park's vector of motor current for healthy and three broken rotor bar cases.

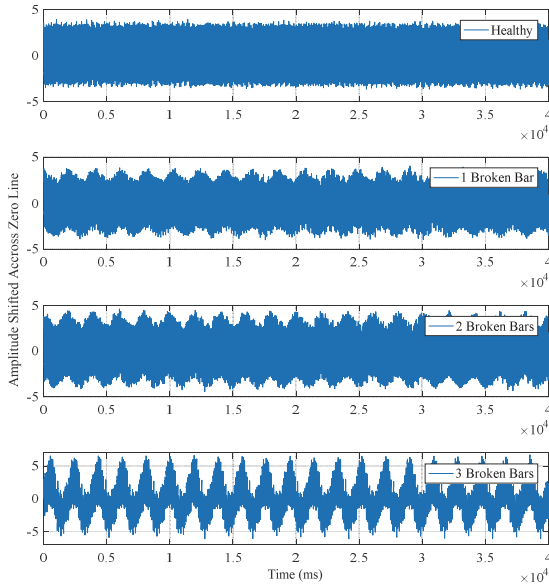


Fig. 11. Oscillating components of the modulus of Park's vector of motor current for healthy and the broken rotor bar cases.

The total harmonic distortion (THD) of Park's vector modulus (PVM) shown in Fig. 11 are -12.6092, -12.3144, -13.8261 and -12.6410 dB respectively. Since these values are not increasing in a specific manner, the THD cannot be used as fault indicator and frequency analysis is inevitable. Fig. 12 presents the FFT analysis of Park's vector modulus, where it is evident that spectral leakage is not a potential problem and faulty harmonics are easy to detect.

Table II gives an insight into different features of techniques under study, where the second column represents the time, elapsed for the computer to solve the algorithm in Matlab, and gives a comparative analysis of techniques in terms of complexity level.

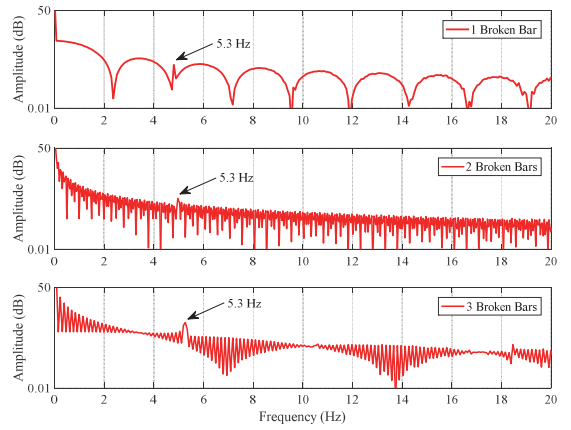


Fig. 12. Frequency spectrum of healthy, one broken bar, two broken bars and three broken bars induction motors using FFT analysis of PVM.

TABLE II
COMPARISON OF TECHNIQUES

Tech.	Time	Attributes
FFT	3.64 mSec	<ul style="list-style-type: none"> Non-invasive Slip estimation required Single phase measurement is enough Simple to implement Spectral leakage Segregation of other faults and noise is difficult Bad results under low slip conditions
		<ul style="list-style-type: none"> Non-invasive Slip estimation required Single phase measurement is enough Simple to implement Spectral leakage is no more a problem Comparative good results under low slip conditions Segregation of other faults and noise is difficult
EPVM	9.266 mSec	<ul style="list-style-type: none"> Non-invasive Slip estimation required Measurement of minimum two phases is required An open platform to try various signal processing tools Segregation is somehow possible as compared to FFT and Hilbert Some techniques like RPVM can reduce sampling rate

VI. CONCLUSIONS

With the growing dependency of industry on induction motors, their fault diagnostic at incipient stage has become very important to avoid any time consuming catastrophic situation. Among a variety of faults diagnostic techniques found in literature, MCSA based methods make the largest portion because of the requirement of the least number of sensors and non-invasive nature. The use of variable frequency converters to control the induction motors is increasing day-by-day, making diagnostic techniques more complicated due to the injected harmonics by power electronics circuits.

In this paper, three fault diagnostic techniques, such as FFT, Hilbert and modulus of Park's vector are applied on the same signals taken from an inverter fed three-phase induction motor running at rated load and broken rotor bar fault conditions. Since all techniques are using FFT for frequency analysis hence computational time gradually increases. However, the Park's vector approach is more informative and can be used as a potential indicator even without doing frequency analysis. Also the effect of inverter fed harmonics is very prominent in Park's vector modulus. Almost all industrial inverters being used as drive of induction motors have built-in closed loop control systems, which causes the suppression of slot harmonics. Hilbert transform can be used to attenuate the fundamental component but still the effect of its spectral leakage is visible in frequency spectrum. A simple comparison of studied techniques is presented in table II.

VII. REFERENCES

- [1] H. W. Penrose, "Test Methods for Determining the Impact of Motor Condition on Motor Efficiency and Reliability," *PhD Diss.*, vol. ALL-TEST P, no. LLC, Old Saybrook, CT, pp. 1–8.
- [2] T. Vaimann, A. Belahcen, and A. Kallaste, "Necessity for implementation of inverse problem theory in electric machine fault diagnosis," in *2015 IEEE 10th International Symposium on Diagnostics for Electrical Machines, Power Electronics and Drives (SDMPED)*, 2015, pp. 380–385.
- [3] R. Puche-Panadero, M. Pineda-Sanchez, M. Riera-Guasp, J. Roger-Folch, E. Hurtado-Perez, and J. Perez-Cruz, "Improved Resolution of the MCSA Method Via Hilbert Transform, Enabling the Diagnosis of Rotor Asymmetries at Very Low Slip," *IEEE Trans. Energy Convers.*, vol. 24, no. 1, pp. 52–59, Mar. 2009.
- [4] A. Sapena-Bano, M. Pineda-Sanchez, R. Puche-Panadero, J. Martinez-Roman, and Z. Kanovic, "Low-Cost Diagnosis of Rotor Asymmetries in Induction Machines Working at a Very Low Slip Using the Reduced Envelope of the Stator Current," *IEEE Trans. Energy Convers.*, vol. 30, no. 4, pp. 1409–1419, Dec. 2015.
- [5] A. Sapena-Bano, J. Burriel-Valencia, M. Pineda-Sanchez, R. Puche-Panadero, and M. Riera-Guasp, "The Harmonic Order Tracking Analysis Method for the Fault Diagnosis in Induction Motors Under Time-Varying Conditions," *IEEE Trans. Energy Convers.*, vol. 32, no. 1, pp. 244–256, Mar. 2017.
- [6] A. J. Marques Cardoso and E. S. Saraiva, "On-line diagnostics of three-phase induction motors by Park's vector," *ICEM*, 1988, pp. 231–234.
- [7] A. J. Marques Cardoso and E. S. Saraiva, "On-line diagnostics of current source inverter fed induction machines by Park's vector approach," *ICEM*, 1990, pp. 1000–1005.
- [8] L. M. R. Oliveira and A. J. M. Cardoso, "Extended Park's vector approach-based differential protection of three-phase power transformers," *IET Electr. Power Appl.*, vol. 6, no. 8, p. 463, 2012.
- [9] S. M. A. Cruz and A. J. M. Cardoso, "Stator winding fault diagnosis in three-phase synchronous and asynchronous motors, by the extended Park's vector approach," *IEEE Trans. Ind. Appl.*, vol. 37, no. 5, pp. 1227–1233, 2001.
- [10] J. Perez-Cruz, R. Puche-Panadero, M. Pineda-Sanchez, M. Riera-Guasp, J. Martinez-Roman, and A. Sapena-Bano, "Cost-effective on-line fault diagnosis of induction motors using the reduced modulus of the current park's vector," in *2017 IEEE 11th International Symposium on Diagnostics for Electrical Machines, Power Electronics and Drives (SDMPED)*, 2017, pp. 427–433.
- [11] A. Belahcen, J. Martinez, and T. Vaimann, "Comprehensive computations of the response of faulty cage induction machines," in *2014 International Conference on Electrical Machines (ICEM)*, 2014, pp. 1510–1515.
- [12] A. Belahcen, K. N. Gyftakis, J. Martinez, V. Clemente-Alarcon, and T. Vaimann, "Condition monitoring of electrical machines and its relation to industrial internet," in *2015 IEEE Workshop on Electrical Machines Design, Control and Diagnosis (WEMDCD)*, 2015, pp. 233–241.

- [13] A. Sapena-Bano *et al.*, "Harmonic Order Tracking Analysis: A Novel Method for Fault Diagnosis in Induction Machines," *IEEE Trans. Energy Convers.*, vol. 30, no. 3, pp. 833–841, Sep. 2015.
- [14] J. Cusido, L. Romeral, J. A. Ortega, J. A. Rosero, and A. Garcia Espinosa, "Fault detection in induction machines using power spectral density on the wavelet decomposition," *IEEE Trans. Ind. Electron.*, vol. 55, no. 2, pp. 633–643, 2008.
- [15] A. Bellini, F. Filippetti, G. Franceschini, C. Tassoni, and G. B. Kliman, "Quantitative evaluation of induction motor broken bars by means of electrical signature analysis," *IEEE Trans. Ind. Appl.*, vol. 37, no. 5, pp. 1248–1255, 2001.
- [16] M. T. Heideman, D. H. Johnson, and C. S. Burrus, "Gauss and the history of the Fast Fourier Transform," *IEEE Acoust. Speech, Signal Process. Mag.*, vol. 1, no. October, pp. 14–21, 1984.
- [17] R. H. Park, "Two-reaction theory of synchronous machines generalized method of analysis-part I," *Trans. Am. Inst. Electr. Eng.*, vol. 48, no. 3, pp. 716–727, Jul. 1929.
- [18] W. Xu *et al.*, "Equivalent Circuits for Single-Sided Linear Induction Motors," *IEEE Trans. Ind. Appl.*, vol. 46, no. 6, pp. 2410–2423, Nov. 2010.
- [19] S. A. Odhano, R. Bojoi, A. Boglietti, S. G. Rosu, and G. Griva, "Maximum Efficiency per Torque Direct Flux Vector Control of Induction Motor Drives," *IEEE Trans. Ind. Appl.*, vol. 51, no. 6, pp. 4415–4424, Nov. 2015.
- [20] S.-K. Kim and J.-K. Seok, "High-Frequency Signal Injection-Based Rotor Bar Fault Detection of Inverter-Fed Induction Motors With Closed Rotor Slots," *IEEE Trans. Ind. Appl.*, vol. 47, no. 4, pp. 1624–1631, Jul. 2011.
- [21] A. J. M. Cardoso and E. S. Saraiva, "Computer-aided detection of airgap eccentricity in operating three-phase induction motors by Park's vector approach," *IEEE Trans. Ind. Appl.*, vol. 29, no. 5, pp. 897–901, 1993.

VIII. BIOGRAPHIES

Bilal Asad was born in 1986 in Pakistan. He received his BSc in Electronics Engineering from The Islamia University of Bahawalpur and MSc in Electrical Engineering from University of Engineering and Technology (UET) Lahore, Pakistan in 2007 and 2011 respectively. Currently he is a PhD student in the Department of Electrical Power Engineering and Mechatronics, Tallinn University of Technology, Estonia. His area of interest includes design, simulations and fault diagnostics of electrical machines.

Toomas Vaimann (S'11-M'14) was born in Pärnu, Estonia, in 1984. He received his BSc, MSc and PhD degrees in Electrical Engineering from Tallinn University of Technology, Estonia in 2007, 2009 and 2014 respectively. He is currently a senior researcher in Tallinn University of Technology, Department of Electrical Power Engineering and Mechatronics. He has been working in several companies as electrical engineer. He is member of IEEE, Estonian society of Moritz Hermann Jacobi and Estonian Society of Electrical Power Engineering.

Anouar Belahcen (M'13-SM'15) was born in Essaouira, Morocco, in 1963. He received the BSc degree in physics from the University Sidi Mohamed Ben Abdellah Fes, Morocco, in 1988 and the MSc (Tech.) and Doctor (Tech.) degrees from Helsinki University of Technology, Finland, in 1998 and 2004 respectively.

From 2008 to 2013, he has been working as Adjunct Professor in the field of coupled problems and material modeling at Aalto University, Finland. Since 2011 he is Professor of electrical machines at Tallinn University of Technology, Estonia and in 2013 he became Professor of Energy and Power at Aalto University.

His research interests are numerical modeling of electrical machines, especially magnetic material modeling, coupled magnetic and mechanical problems, magnetic forces and magnetostriction

Ants Kallaste (M'13) was born in Pärnu, Estonia, in 1980. He received his BSc, MSc and PhD degrees in Electrical Engineering from Tallinn University of Technology, Estonia in 2004, 2006 and 2013 respectively. He is currently a senior researcher in Tallinn University of Technology, Department of Electrical Power Engineering and Mechatronics.

He has been working in several companies as electrical engineer. His main research interests include permanent magnet machine design and wind turbines.

Publication XII

B. Asad, T. Vaimann, A. Rassölkin, A. Belahcen. Dynamic State-Space Model-Based Analysis of a Three-Phase Induction Motor Using Nonlinear Magnetization Inductance. IEEE 19th International Scientific Conference on Electric Power Engineering (EPE) Brno, Czech Republic, June 2018, pp. 260–265.

Dynamic State Space Model Based Analysis of a Three-Phase Induction Motor Using Nonlinear Magnetization Inductance

Bilal Asad, Toomas Vaimann, Anton Rassõlkin
Dept. of Electrical Power Engineering and Mechatronics
Tallinn University of Technology
Tallinn, Estonia
biasad@ttu.ee

Anouar Belahcen
Dept. of Electrical Engineering and Automation
Aalto University
Espoo, Finland

Abstract— In this paper, the dynamic state space model of a three-phase induction motor with the inclusion of magnetic saturation effect is presented. Mathematical modelling is a very important tool for design and analysis of a system. In case of electrical machines, its importance becomes twofold, because of its involvement in design and control algorithms. Since more and more sophisticated control algorithms are coming forward, the accurate mathematical modelling is becoming essential. Unlike the conventional linear magnetization inductance-based models, in this paper, magnetization inductance as a nonlinear function of flux is used. Park's transformation-based equations are prepared and simulated in Matlab/Simulink environment. Different motor parameters in transient and steady state intervals are studied both under on and off load conditions.

Keywords—Mathematical model, saturation magnetization, induction motor, simulation, dynamics.

I. INTRODUCTION

In almost every field of domestic or industrial life, the presence of induction motors cannot be neglected. They have many applications, such as fans, textile mills, water pumps, robotics, computer applications, wind power generation, ship propulsion, etc. Hence, their control, monitoring and protection are very sensitive issues, which should be addressed properly, in order to avoid any kind of time-consuming and catastrophic fault situations. Although their simple and rugged structure make them feasible to work in rough and tough industrial environments, at the same time their design and control becomes difficult, because of the variety of its system variables, which are directly or indirectly dependent on each other.

Currently, majority of induction motors are dependent on power electronics-based switching devices, which are able to convert more power at higher frequencies than previous technologies. However, these advancements are making adverse effects on the performance of induction motors in the form of generated harmonics. A lot of work is being done on power supply based harmonic impact analysis of induction machines as in [1]-[4].

With the invention of more advanced power electronics-based power supplies, mathematical tools, solution

This work was supported by the European Regional Development Fund under Mobilias Plus programme returning researcher grant MOBTPI3.

algorithms, calculating hardware (FPGA, DSP Microprocessors), and hardware in the loop strategy, electrical machines are becoming more and more dependent on their accurate mathematical model. Although mathematical modelling of induction machine has a very old history, there is still a lot of work needed to be done, to model a good replica of the original machine. There is a variety of papers, in which mathematical model of induction machines is proposed and used. For example [5] has used it for the analysis of AC drive systems, [6], [7]-[10] have used the induction machine models to analyze different faults, occurring in induction machines, in [11] author used different equations of induction motor for its flux level control, [12] used extensive mathematical equations to predict the behavior of a system, etc.

A reliable electrical motor depends on its accurate design and perfect control system. The basic engineering design steps to build any system are the schematic diagram, the circuit diagram and the mathematical equations representing that system. Moreover, the control of electrical machines also depends on its perfect mathematical model, because the control equipment uses it, for states estimation and comparison with the actual one in most of sophisticated drives. It means that mathematical modeling is a very basic and key step to get an efficient and reliable electrical machine and its control system. The more accurate the mathematical model is the more efficient and reliable the motor and its control will be.

In this research paper Park's transformation based state-space model of three phase induction motor is made and its critical analysis in MATLAB/Simulink is done. Moreover, unlike linear magnetization inductance based models, L_m as a nonlinear function of flux is used making it more suitable for hardware in the loop like environment.

II. MATHEMATICAL MODELING

A. State Space Model of Induction Motor

The state space model of a physical system is its mathematical representation using first order differential equations in the following format:

$$\begin{aligned} \dot{x} &= Ax + Bu \\ y &= Cx + Du \end{aligned} \quad (1)$$

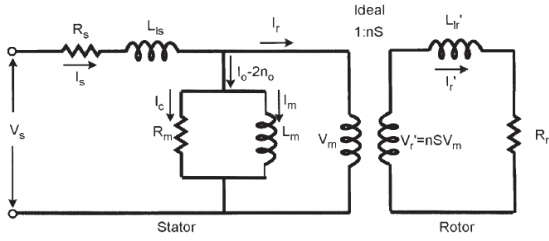


Fig. 1. Per phase equivalent circuit diagram of an induction motor.

As presented in per phase equivalent circuit diagram in Fig. 1, the induction machine is just like a transformer with a rotating secondary winding, where R_s is representing the copper resistance, L_{ls} the leakage inductance, L_m is the magnetization component, I_c and I_m are the working and magnetization components of no load current respectively, and I_r is the rotor current.

Both schematic and mathematical modeling of induction motor starts from basic electromagnetic equations based on Faraday's, Ampere's, Lenz's law and Maxwell equations as discussed in [13] and ends at complex states space model of order 6x6. This mathematical model always has a room for extension, because it can never represent the system in a 100% accurate manner because of non-linear behavior of some parameters. The presence of these nonlinearities has invited many other mathematical tools for modeling and state estimation of electrical machines, such as neural networks as in [14], fuzzy logic [15] predictive controllers and many more intelligent algorithms. However, the base of all these advanced mathematical techniques is the fundamental mathematical model of an induction motor. Hence, the improvements in this model can lead to the improvement of control, operation and protection of induction machines.

Another aspect, towards which the researchers are focusing, is the reduction of the number of equations, as the conventional models need a lot of time to be solved by controllers, introducing a phenomenon of delay time in hardware in the loop environment [16]. In order to reduce the number of equations, a three-phase induction motor can be represented by a two-phase machine as shown on Fig. 2. In 1920, R. H. Park proposed that all stator variables could be associated with imaginary windings rotating with the rotor.

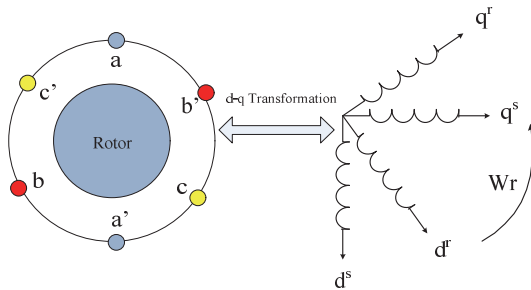


Fig. 2. Three phase to two-phase conversion.

Therefore, he transformed the stator variables from the stationary frame of reference to the rotating frame of reference, hence, eliminating the problem of time varying inductances due to relative motion of stator and rotor. After doing the dynamic d-q modeling and Park's transformation, the equations of stator and rotor voltage in the rotating frame of reference can be described as follows [17]:

$$\begin{bmatrix} v_{qs} \\ v_{ds} \\ v_{qr} \\ v_{dr} \end{bmatrix} = [A] \begin{bmatrix} i_{qs} \\ i_{ds} \\ i_{qr} \\ i_{dr} \end{bmatrix} \quad (2)$$

where

$$[A] = \begin{bmatrix} R_s + sL_s & \omega_e L_s & sL_m & \omega_e L_m \\ -\omega_e L_s & R_s + sL_s & -\omega_e L_m & sL_m \\ sL_m & (\omega_e - \omega_r)L_m & R_r + sL_r & (\omega_e - \omega_r)L_r \\ -(\omega_e - \omega_r)L_m & sL_m & -(\omega_e - \omega_r)L_r & R_r + sL_r \end{bmatrix}$$

Let the states of system under observation be:

$$x = [ids^s \quad iqs^s \quad \phi dr^s \quad \phi qr^s]^T \quad (3)$$

and the inputs:

$$V_s = [vds^s \quad vqs^s \quad 0 \quad 0]^T \quad (4)$$

Then the state space model of a three-phase induction motor can be represented as;

$$\begin{bmatrix} d(ids^s)/dt \\ d(iqs^s)/dt \\ d(\phi dr^s)/dt \\ d(\phi qr^s)/dt \end{bmatrix} = \begin{bmatrix} -\frac{Lm^2Rr + Lr^2Rs}{\sigma LsLr^2} & 0 & \frac{LmRr}{\sigma LsLr^2} & \frac{Lm\omega_r}{\sigma LsLr} \\ 0 & -\frac{Lm^2Rr + Lr^2Rs}{\sigma LsLr^2} & -\frac{Lm\omega_r}{\sigma LsLr} & \frac{LmRr}{\sigma LsLr^2} \\ \frac{LmRr}{Lr} & 0 & -\frac{Rr}{Lr} & -\omega_r \\ 0 & \frac{LmRr}{Lr} & \omega_r & \frac{Rr}{Lr} \end{bmatrix} \begin{bmatrix} ids^s \\ iqs^s \\ \phi dr^s \\ \phi qr^s \end{bmatrix} + \begin{bmatrix} \frac{1}{\sigma Ls} & 0 \\ 0 & \frac{1}{\sigma Ls} \\ 0 & 0 \\ 0 & 0 \end{bmatrix} \begin{bmatrix} Vds^s & 0 & 0 & 0 \\ 0 & Vqs^s & 0 & 0 \end{bmatrix}$$

$$\begin{bmatrix} ids^s \\ iqs^s \\ 0 \\ 0 \end{bmatrix} = \begin{bmatrix} 1 & 0 & 0 & 0 \\ 0 & 1 & 0 & 0 \\ 0 & 0 & 1 & 0 \\ 0 & 0 & 0 & 1 \end{bmatrix} \begin{bmatrix} ids^s \\ iqs^s \\ \phi dr^s \\ \phi qr^s \end{bmatrix} \quad (5)$$

where $\sigma = 1 - \frac{Lm^2}{LrLs}$ and L_m is the magnetization induction, which can be a constant or a nonlinear function of flux. For a 30-kW squirrel-cage induction motor, the values of different parameters are given in Table I.

B. Magnetization Inductance

For the sake of simplicity, conventional mathematical models of induction motors neglect the effect of magnetic saturation by taking a constant value of magnetization inductance L_m . This fact makes the model suitable only for analysis under the fixed load and speed conditions. In actual, magnetization inductance of a motor is a nonlinear function of the flux, which can be used in mathematical models in the form of a look up table or a power function as in [18]:

$$i_m = \left(\frac{1 + \left(\frac{\phi_m}{\beta} \right)^s}{L_{mu}} \right) \phi_m \quad (6)$$

Where L_{mu} is the unsaturated magnetization inductance, ϕ_m the magnetization flux, s and β are the positive constants, which can be calculated by minimizing the function using Matlab function like “*fminsearch*”.

$$i_m - \left(\frac{1 + \left(\frac{\phi_m}{\beta} \right)^s}{L_{mu}} \right) \phi_m = 0 \quad (7)$$

This is a broad general nonlinear relationship between current and flux, where the degree of nonlinearity depends upon the values of s and β . Fig. 3. shows two different types of magnetization curves plotted from the same equation.

TABLE I. PARAMETRIC VALUES

No.	Parameter	Symbol	Value
1	Stator resistance	R_s	0.087 Ω
2	Rotor resistance as referred to primary side	R_r	0.187 Ω
3	Stator inductance	L_s	0.0425 H
4	Magnetization Inductance	L_m	0.04 H
5	Rotor Inductance as referred to stator side	L_r	0.043 H
6	Rotor inertia	J	1.662 Kg-m ²
7	Friction	B	0.01 N-m sec

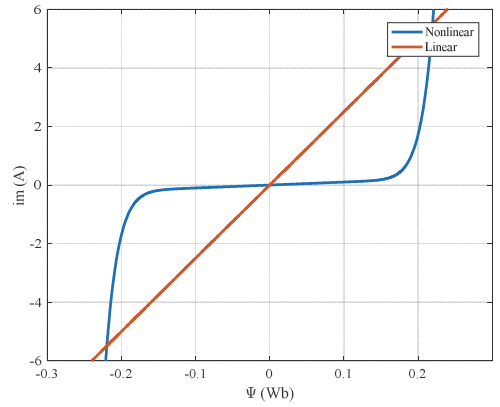


Fig. 3. Linear vs. nonlinear magnetization curve.

III. SIMULATIONS

The equivalent d-q transformation-based T-model with the nonlinear magnetization inductance is shown in Fig. 4, which can be used to construct the mathematical model as shown above. This state space model can be used to study different evaluation parameters like Eigenvalues, Root Locus, Bode Plot and output responses, etc. It can also be easily implemented on MATLAB/Simulink to get a general model for testing different kinds of machine parameters, fault conditions and control algorithms.

In this Simulink model motor three phase voltage is firstly transformed to d-q axis in static frame of reference which are then transformed to d-q voltage in rotating frame of reference. These voltages are then used to compute stator and rotor currents of the induction motor in synchronously rotating frame of reference. The calculated currents and fluxes are used to plot various parameters like the speed, the torque and the actual three phase currents of the stator. A general simulation block diagram can be represented as in Fig. 5.

For the magnetization inductance, the motor's stator voltages and currents are used to calculate the magnetization voltage, which gives the magnetization flux after the integration. The calculated flux is used by nonlinear function to calculate L_m , which is further used in the dynamic model of the induction motor as shown in Fig. 6.

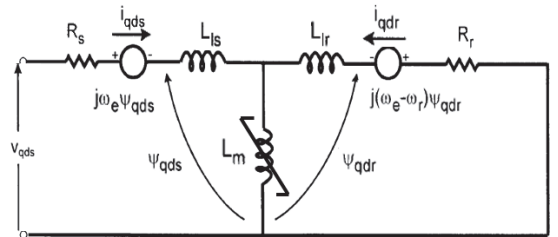


Fig. 4. Equivalent d-q model of induction motor

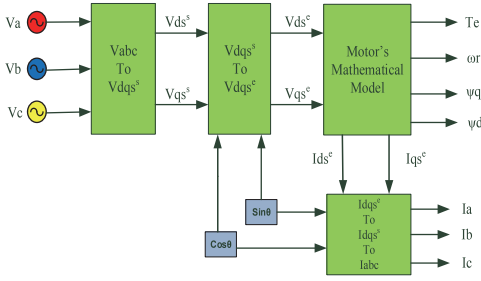


Fig. 5. Block diagram of the Simulink model.

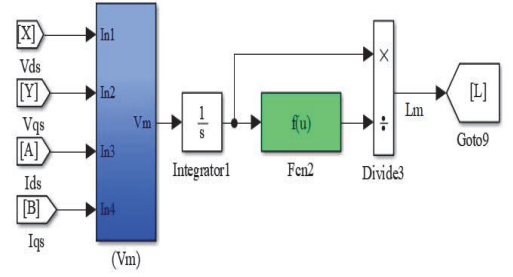


Fig. 6. Measurement and implementation of the nonlinear magnetization inductance.

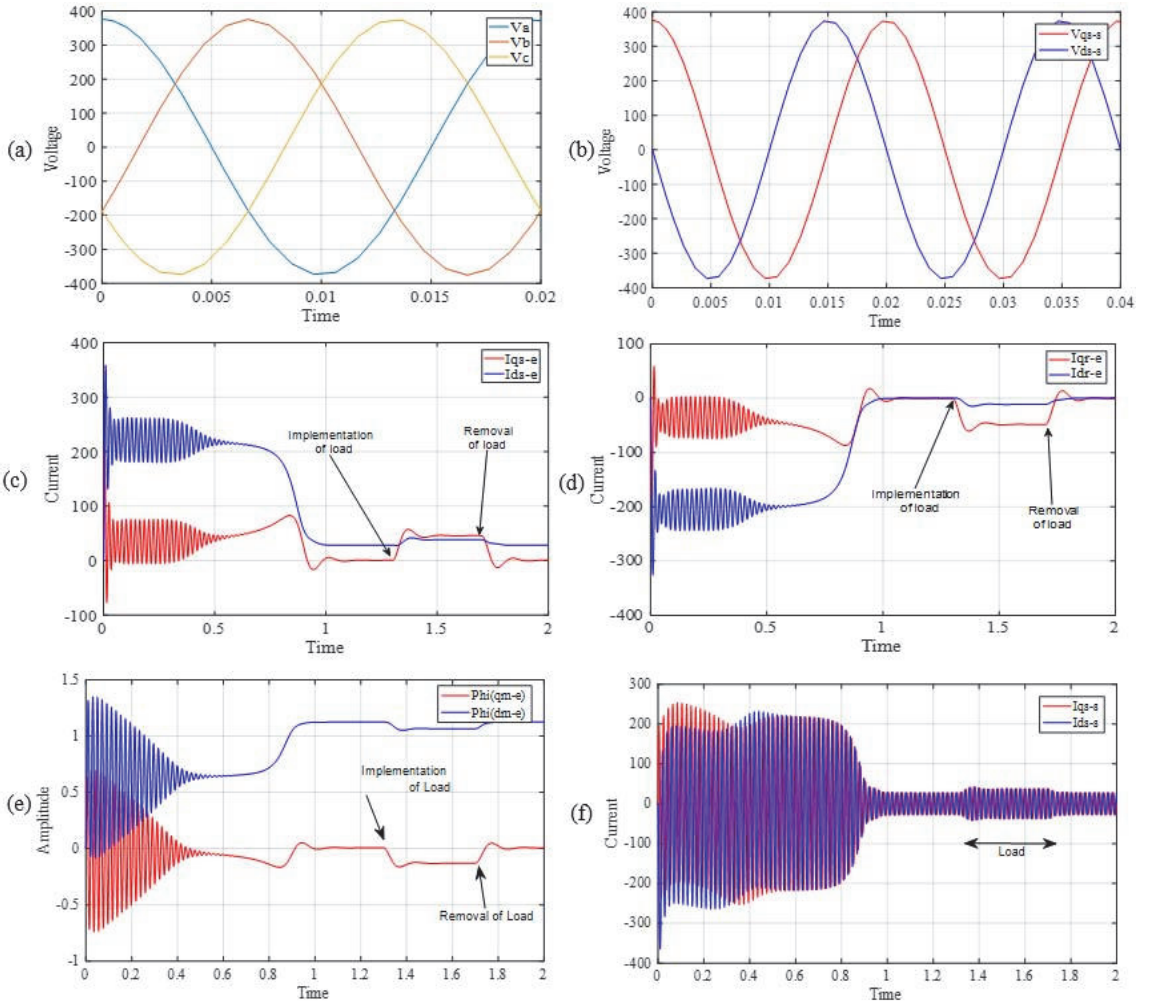


Fig. 7. (a). Three phase supply voltage, (b). Transformed two phase voltage in the stationary frame of reference, (c). Stator's d and q phase currents in the rotating frame of reference, (d). Rotor's d and q phase currents in the rotating frame of reference, (e). d and q components of the magnetization flux, (f). d and q components of stator's current.

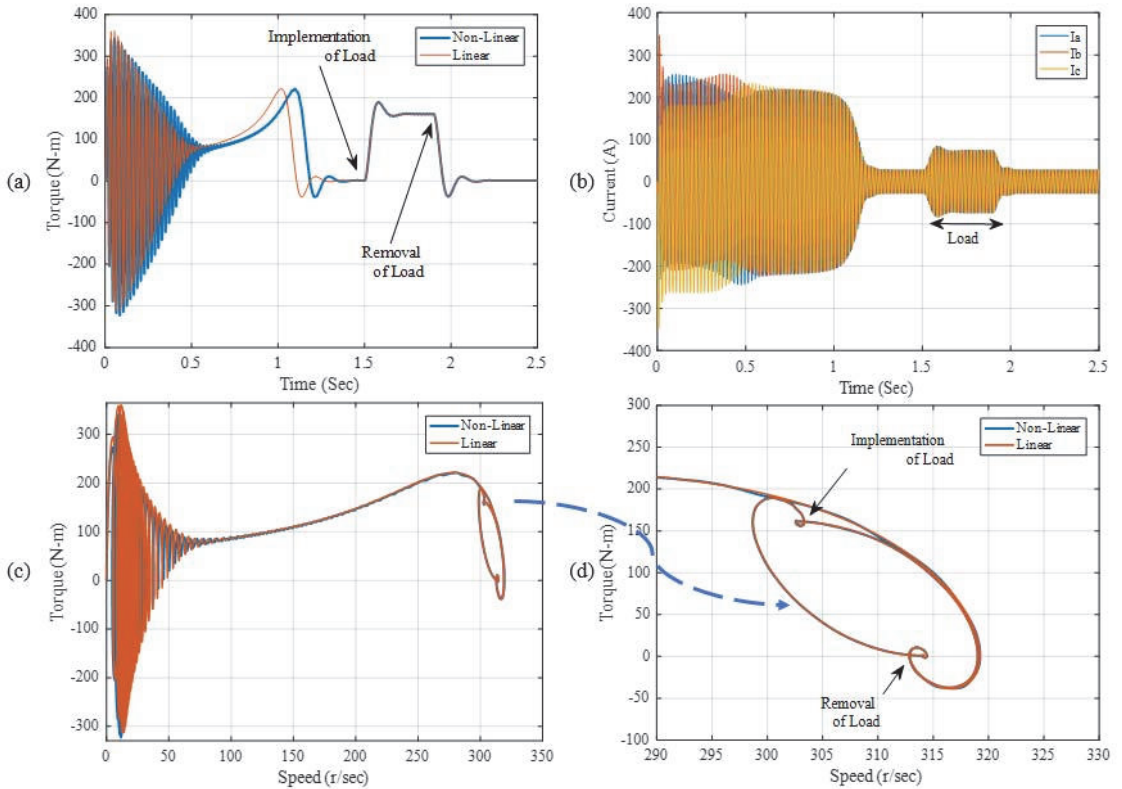


Fig. 8. (a). Generated torque (T_e), (b). Three phase stator's currents, (c). Speed-Torque curve, (d). Zoomed speed-torque curve to show the effect of load.

IV. RESULTS AND DISCUSSION

In this section, the motor behavior for both, transient and steady state intervals, is investigated. Fig. 7(a) shows the three-phase input supply, which is converted to an equivalent two-phase supply as shown in Fig. 7(b). These two-phase voltages are in the stationary frame of reference, which are further transformed into two phases in the rotating frame of reference. This transformation of voltage into the rotating frame of reference is done, because the presented mathematical model follows the Park's transformation and the model is prepared in synchronously rotating frame of reference.

Motor's stator and rotor currents in the synchronously rotating frame of reference are shown in Fig. 7(c) and (d) respectively, where the transient and steady state intervals and the effects of load can be easily studied. Similarly, Figs. 7(e, f) are presenting the magnetization flux in the rotating and the stator's current in the stationary frame of reference respectively.

Fig. 8 is representing the behavior of the motor in the perspective of torque, speed and actual three phase current. Fig. 8(a) is demonstrating the electromagnetically generated torque (T_e) of the motor both for linear and nonlinear models.

The comparison of both results don't show any considerable difference except settling time because nonlinear inductance model is calculating its tuning parameters using flux of Simulink model itself. Since motor is working in linear region hence both results are coincided with each other. This fact reveals that this model can be used in hardware in the loop environment of machine drives. Fig. 8(b) presents the actual three-phase current of the machine that is calculated by converting the stator currents from the rotating frame of reference back to the static frame of reference, which are then transformed to the actual three-phase currents. Fig. 8(c, d) represents the speed (electrical) torque curve of the motor, where the effect of load implementation and removal on speed and torque can be easily studied.

V. CONCLUSIONS

Induction motors are gaining popularity in domestic and industrial applications because of their simple structure, low cost, ability to work in rough industrial environments and easy maintenance. Since industry depends a lot on these machines, their efficient control, instant fault diagnosis and best protection should be emphasized to ensure reliable and safe operation. The importance of accurate mathematical modeling of the induction motor becomes important because of two reasons. First, the mathematical modeling is a very

fundamental step to analyze as system for different operating conditions before its fabrication. Second, most of the intelligent and sophisticated control algorithms of induction machines rely on its mathematical model such as control drives etc. Hence, the more accurate the model is, the more reliable the system and its control will be.

In this paper, a general mathematical model of three-phase squirrel-cage induction machine with the inclusion of nonlinear magnetization characteristic is prepared and studied, the results are then validated on MATLAB/Simulink environment. This model can be used to simulate the effect of different faults and load conditions on the motor under transient and steady state conditions. It can be further improved by including eddy current losses in it. This model gives a very basic insight into mathematics modeling of an induction motor, which can be used in drives and hardware in the loop environment.

REFERENCES

- [1] A. Panchbhavi, N. Prajapati, and S. Parmar, "Harmonic Mitigation in AC Motor Using Multi-pulse Rectifier," 2016 IEEE International WIE Conference on Electrical and Computer Engineering (WIECON-ECE), Pune, pp. 1-4, 19-21 December 2016.
- [2] R. Jyothi, R. Jayapal, and K. Uma Rao, "Severity and Impact of Faults on Current Harmonics in Inverter-Fed AC Drives" IEEE Transactions on Power Electronics, vol. 19, pp. 401-405, March 2004.
- [3] M. Chirindo, M. A. Khan, and P. S. Barendse, "Considerations for Nonintrusive Efficiency Estimation of Inverter-Fed Induction Motors" IEEE Transactions on Industrial Electronics, vol. 63, pp. 741-749, February 2016.
- [4] A. Antonopoulos, G. Mörée, J. Soulard, L. Ängquist, and H.-P. Nee, "Experimental Evaluation of the Impact of Harmonics on Induction Motors Fed by Modular Multilevel Converters" International Conference on Electrical Machines (ICEM), Berlin, Germany, pp. 768-775, 2-5 Sept. 2014.
- [5] Champagne, L. A. Dessaint, H. F. Blanchette, and G. Sybille, "Analysis and Validation of a Real-Time AC Drive Simulator" IEEE Transactions on Power Electronics, vol. 19, pp. 336-345, March 2004.
- [6] H. Mahmoud, A. A. Elyazied Abdallah, N. Bianchi, S. M. El-Hakim, A. Shaltout, and L. Dupré, "An Inverse Approach for Interturn Fault Detection in Asynchronous Machines Using Magnetic Pendulous Oscillation Technique", IEEE Transactions on Industry Applications, vol. 52, pp. 226-233, January/February 2016.
- [7] B. Asad, and K. M. Hasan, "Laguerre Function's Based Model Predictive Control of Three Phase Induction Motor", Applied Mechanics and Materials, vol. 229-231, pp. 961-967, 2012.
- [8] T. Vaimann, A. Belahcen, A. Kallaste, "Changing of magnetic flux density distribution in a squirrel-cage induction motor with broken rotor bars," Electronics and Electrical Engineering, vol. 20, pp. 11-14, 2014.
- [9] A. Rassõlkin, T. Vaimann, A. Belahcen, A. Kallaste, A. Petrov, I. Plokhov, A. Kotelnikov, "Adjusted Electrical Equivalent Circuit Model of Induction Motor With Broken Rotor Bars," Electric Power Quality and Supply Reliability Conference (PQ) proceedings, Tallinn, pp. 213-217, 29-31 Aug. 2016.
- [10] A. Petrov, A. Rassõlkin, T. Vaimann, A. Belahcen, A. Kallaste, I. Plokhov, "Adjusted Electrical Equivalent Circuit Model of Induction Motor with Broken Rotor Bars and Eccentricity Faults," 11th IEEE International Symposium on Diagnostics for Electric Machines, Power Electronics and Drives – SDEMPED, Tinos, Greece, 29 Aug.-1 Sept. 2017.
- [11] Z. Qu, M. Ranta, M. Hinkkanen, and J. Luomi, "Loss-Minimizing Flux Level Control of Induction Motor Drives", IEEE Transactions on Industry Applications, vol. 48, pp. 952-961, May/June 2012.
- [12] E. S. de Santana, E. Bim, and W. Caradori do Amaral, "A Predictive Algorithm for Controlling Speed and Rotor Flux of Induction Motor" IEEE Transactions on Industrial Electronics, vol. 55, pp. 4398 – 4407, December 2008.
- [13] S. L. Vesely, A. A. Vesely, and C. A. Dolci, "Maxwell's Motor Equation and the Mechanical Power", PIERS Proceedings, Maorocco, March 20-23, 2011.
- [14] F. A. Mohamed, and H. Koivo, "Modelling of Induction Motor Using Identification non-Linear Neural Network System," SICE 2004 Annual Conference, Sapporo, Japan, vol. 2, pp. 977-982, 2004.
- [15] M. Zerikat, A. Mechemene and S. Chekroun, "High-Performance Sensorless Vector Control of Induction Motor Drives using Artificial Intelligent Technique", 15th International Conference on Methods and Models in Automation and Robotics, Miedzyzdroje, Poland, pp. 67-75, 23-26 Aug. 2010.
- [16] B. Jandaghi and V. Dinavahi, "Hardware-in-the-Loop Emulation of Linear Induction Motor Drive for MagLev Application" IEEE Transactions on Plasma Science, vol. 44, pp. 689-686, April 2016.
- [17] B. K. Bose "Modern Power Electronics and AC drives" Prentice-Hall Inc., 2nd ed., 2002, pp. 29-96.
- [18] M. Ranta ; M. Hinkkanen ; A. Belahcen ; J. Luomi, "Inclusion of hysteresis and eddy current losses in nonlinear time-domain inductance models", IECON 2011 - 37th Annual Conference on IEEE Industrial Electronics Society, Melbourne, pp. 1897-1902, 7-10 Nov. 2011.

Curriculum vitae

Personal data

Name: Bilal Asad
Date of birth: 03.06.1986
Place of birth: Pakistan
Nationality: Pakistan
E-mail: bilal.asad@taltech.ee/ bilal.asad@aalto.fi

Education

2017–Date Ph.D. studies, Tallinn University of Technology, Estonia / Aalto University, Finland
2009–2011 MSc, Electrical Engineering, University of Engineering and Technology (UET), Lahore, Pakistan
2004–2008 BSc, Electronics Engineering, The Islamia University Bahawalpur, Pakistan

Language competence

English Fluent
Urdu Fluent (Native)

Professional employment

2017–Date Early Stage Researcher, Tallinn University of Technology, Estonia
2013–2017 Senior Lecturer, The Islamia University Bahawalpur, Pakistan
2011–2013 Senior Lecturer, HITECH University Taxila, Pakistan
2010–2011 Lecturer, The University of Faisalabad, Pakistan
2008–2010 Lecturer, Hajvery University Lahore, Pakistan

Honors and Awards

- Keynote speaker at “International Scientific Conference on Electrical Engineering 2021”, ISCEE-2021.
- 2020, Bilal Asad, Best presenter award in the 19th International Symposium “TOPICAL PROBLEMS IN THE FIELD OF ELECTRICAL AND POWER ENGINEERING” and “Doctoral School of Energy and Geo-technology III” January 14 - 17, 2020, Tartu, Estonia.
- 2020, Bilal Asad, 3rd prize of IEEE IES Student and Young Professionals Activity Committee in 19th International Symposium “TOPICAL PROBLEMS IN THE FIELD OF ELECTRICAL AND POWER ENGINEERING” and “Doctoral School of Energy and Geo-technology III” January 14 - 17, 2020, Tartu, Estonia.
- 2019, Bilal Asad, Best presenter award in the 18th International Symposium “TOPICAL PROBLEMS IN THE FIELD OF ELECTRICAL AND POWER ENGINEERING” and “Doctoral School of Energy and Geo-technology III: School of Engineering, Tallinn University of Technology, Toila, Estonia.

Fields of research

- Electrical and Electronics Engineering
- Modeling and analysis of electromechanical devices
- Design, modeling and analysis of electrical machines
- Condition monitoring and fault diagnosis of electrical equipment

Projects

- ETAG21001, “Industrial internet methods for electrical energy conversion systems monitoring and diagnostics”, Tallinn University of Technology, School of Engineering, Department of Electrical Power Engineering and Mechatronics.

- PUTJD134, "Solution for inverse problems in fault detection of electrical machines", Tallinn University of Technology , School of Engineering, Department of Electrical Power Engineering and Mechatronics.
- PSG137, "Additive Manufacturing of Electrical Machines", Tallinn University of Technology, School of Engineering, Department of Electrical Power Engineering and Mechatronics.

Elulookirjeldus

Isikuandmed

Nimi: Bilal Asad
Sünniaeg: 03.06.1986
Sünnikoht: Pakistan
Kodakondsus: Pakistan
E-post: bilal.asad@taltech.ee/ bilal.asad@aalto.fi

Hariduskäik

2017–... Doktoriõpe, Tallinna Tehnikaülikool, Eesti / Aalto Ülikool, Soome
2009–2011 MSc, Electrical Engineering, University of Engineering and Technology (UET), Lahore, Pakistan
2004–2008 BSc, Electronics Engineering, The Islamia University Bahawalpur, Pakistan

Keelteoskus

Inglise keel kõrgtase
Urdu keel emakeel

Teenistuskäik

2017–... Nooremteadur, Tallinna Tehnikaülikool, Eesti
2013–2017 Vanemlektor, The Islamia University Bahawalpur, Pakistan
2011–2013 Vanemlektor, HITECH University Taxila, Pakistan
2010–2011 Lektor, The University of Faisalabad, Pakistan
2008–2010 Lektor, Hajvery University Lahore, Pakistan

Teaduspreemiad ja tunnustused

- Kutsutud esineja "International Scientific Conference on Electrical Engineering 2021", ISCEE-2021.
- 2020, Bilal Asad, Parima ettekande preemia, 19th International Symposium "TOPICAL PROBLEMS IN THE FIELD OF ELECTRICAL AND POWER ENGINEERING" and "Doctoral School of Energy and Geo-technology III", Tartu, Eesti.
- 2020, Bilal Asad, Kolmas preemia, IEEE IES Student and Young Professionals Activity Committee in 19th International Symposium "TOPICAL PROBLEMS IN THE FIELD OF ELECTRICAL AND POWER ENGINEERING" and "Doctoral School of Energy and Geo-technology III", Tartu, Eesti.
- 2019, Bilal Asad, Parima ettekande preemia, 18th International Symposium "TOPICAL PROBLEMS IN THE FIELD OF ELECTRICAL AND POWER ENGINEERING" and "Doctoral School of Energy and Geo-technology III: School of Engineering, Tallinn University of Technology, Toila, Eesti.

Teadustöö põhisuunad

- Elektrotehnika ja elektroonika
- Elektromehaaniliste seadmete modelleerimine ja analüüs
- Elektrimasinate projekteerimine, modelleerimine ja analüüs
- Elektriseadmete seire ja diagnostika

Jooksvad projektid

- ETAG21001, "Tööstuslikul internetil baseeruvad energiamuundussüsteemide seire- ja diagnostikameetodid", Tallinna Tehnikaülikool, Inseneriteaduskond, Elektroenergeetika ja mehhatroonika instituut.

- PUTJD134, "Elektrimasinate rikketuvastuse pöördprobleemide lahendamine", Tallinna Tehnikaülikool, Inseneriteaduskond, Elektroenergeetika ja mehhatroonika instituut.
- PSG137, "3D prinditud elektrimasinad", Tallinna Tehnikaülikool, Inseneriteaduskond, Elektroenergeetika ja mehhatroonika instituut.

ISSN 2585-6901 (PDF)
ISBN 978-9949-83-727-4 (PDF)